

Perylene Dyes Based Dye Sensitized Solar Cells (DSSC)

Basma Basil Ismael Al Khateeb

Submitted to the
Institute of Graduate Studies and Research
in partial fulfillment of the requirements for the degree of

Doctor of Philosophy
in
Chemistry

Eastern Mediterranean University
August 2020
Gazimağusa, North Cyprus

Approval of the Institute of Graduate Studies and Research

Prof. Dr. Ali Hakan Ulusoy
Director

I certify that this thesis satisfies all the requirements as a thesis for the degree of Doctor of Philosophy in Chemistry.

Prof. Dr. İzzet Sakallı
Chair, Department of Chemistry

We certify that we have read this thesis and that in our opinion it is fully adequate in scope and quality as a thesis for the degree of Doctor of Philosophy in Chemistry.

Prof. Dr. Huriye İcil
Supervisor

Examining Committee

1. Prof. Dr. Huriye İcil
2. Prof. Dr. Sermet Koyuncu
3. Prof. Dr. Mahmut Kuş
4. Assoc. Prof. Dr. Nur P. Aydınlık
5. Asst. Prof. Dr. Süleyman Aşır

ABSTRACT

Recently, dye-sensitized solar cells (DSSCs) have received great attention for their simple fabrication process, low production costs and, relatively high conversion efficiency.

DSSCs are a combination of materials, consisting of a transparent electrode coated with a dye-sensitized mesoporous film of nanocrystalline particles of TiO_2 , an electrolyte containing a suitable redox couple and an electrode. DSSCs based on PDI derivatives are attractive because of enhanced light absorption due to their high molar absorption coefficient and good electron transport properties; moreover, high electron mobility through π - π stacking favors intermolecular charge transfer and increase the charge separation.

In this project, we aim to develop materials and manufacturing procedure for Dye sensitized solar cell (DSSC) based on titanium dioxide with long lifetime and high efficiencies. Additionally, the DSSC's based on different PDIs produced in our research group are successfully made. The energy conversion efficiency in different DSSC's are measured and calculated. Furthermore, the DSSC production technology details are optimized in applications. Accordingly, we synthesized a new bay substituted anhydride and diimides in three consecutive steps (1, 7-dibromoperylene-3, 4, 9, 10-tetracarboxylic dianhydride, 1, 7(6)-di (2-decyl-1-tetradecanoyl) perylene-3, 4, 9, 10-tetracarboxylic acid bisanhydride, N, N'-bis-(dodecyl)-1, 7(6) - di (2-decyl-1-tetradecanoyl).

Perylene-3, 4, 9, 10-tetracarboxy bisimide and N,N'-bis-((S)-(-)-1-phenylethyl)-1,7(6)- di(2-decyl-1-tetradecanoyl)perylene-3,4,9,10-tetracarboxy bisimide).

The final compounds were purified and characterized successfully (FTIR, UV-vis, NMR, MS, Emission spectroscopies and elemental analysis. The electrochemical properties of the compounds were investigated by cyclic voltammetry (CV). Additionally, the thermal stability of the compounds was studied by differential scanning calorimetry (DSC) and thermogravimetric analysis (TGA).

The adsorption behavior of dye molecules with various anchoring groups on the surface of TiO₂ were investigated via FT-IR and solid state UV-Vis spectroscopies also in this work.

Keywords: solar cells, dye sensitized solar cells, sensitizers, perylene diimides, TiO₂ film.

ÖZ

Organik boya esaslı güneş pilleri (OGP'ler) basit imalat süreçleri, düşük üretim maliyetleri ve nispeten yüksek dönüşüm verimliliği nedeniyle son dönemlerde büyük ilgi ile araştırılan konulardandırlar.

OGP'ler, TiO₂'nin nanokristalin parçacıklarının boyaya duyarlı gözenekli film ile kaplanmış şeffaf bir elektrot, uygun bir redoks çifti içeren bir elektrolit ve bir elektrottan oluşan malzeme birleşimidir. PDI türevleri, yüksek molar absorpsiyon katsayıları ve elektron transferi yapabilme özellikleri nedeniyle özellikle OGP'lerde denenmektedirler; ayrıca, bu ürünlerde π - π etkileşimiyle oluşan yüksek elektron mobilitesi yük transferini ve ayrışımını desteklemektedir.

Bu projede, uzun ömürlü ve yüksek verimlilikte titanyum dioksit tabanlı organik boya esaslı güneş pilleri (OGP) üretiminde kullanılmak üzere yeni materyal sentezleri amaçlanmıştır. Ayrıca, araştırma grubumuzda sentezlenen bazı farklı PDI türevlerinin OGP'de ışıktan enerjiye dönüşüm performansları ölçülmüş ve ilgili aygıt üretimi ve ölçmelerde teknik detaylar optimize edilmiştir. Bu amaçla, ardışık üç adımla yeni bir körfez/çekirdek (1,7-) pozisyonunda süstitüe edilmiş perilen dianhidrit ve diimidler sentezlendi (1,7(6)-di(2-desil-1-tetradekanoyil)perilen-3,4,9,10-tetrakarboksilik asit dianhidrit, N, N'-bis-(dodesil)-1, 7(6) - di (2-desil-1-tetradekanoyil)-perilen-3, 4, 9, 10-tetrakarboksibisimid ve N,N'-bis-((S)-(-)-1-feniletıl)-1,7(6)- di(2-desil-1-tetradekanoyil)perilen-3,4,9,10-tetrakarboksi bisimid).

Sentezlenen yeni ürünler saflandırılarak karakterize edilmişlerdir (FTIR, UV-vis, NMR, MS ve Emisyon gibi spektroskopik teknikler ve elementel analiz). Ürünlerin

elektrokimyasal özellikleri dönüşümlü voltametri (CV) ile incelenmiştir. Ayrıca, ürünlerin termal kararlılıkları diferansiyel tarama kalorimetresi (DSC) ve termogravimetrik analiz (TGA) ile incelenmiştir.

Tez kapsamında üretilen organik boya esaslı güneş pillerinde boya moleküllerinin şeffaf TiO₂ filmi ile etkileşimi FT-IR spektroskopisi ve UV-vis spektroskopisinde katı halde detaylı biçimde incelenmiş ve yorumlanmıştır.

Anahtar kelimeler: güneş pilleri, organik boya esaslı güneş pilleri, duyarlaştırıcı, perilen diimid, TiO₂ film.

DEDICATION

To

My Family

ACKNOWLEDGEMENT

I would like to say a special thanks to my supervisor Prof. Dr.Huriye İcil. Her support , guidance and overall insights in this field have made this a great and an inspiring experience for me. I am extremely grateful for our friendly chats at the ends of our meetings and for your personal support in my life.

I would like to thank the members of my dissertation committee not only for their time and extreme patience, but for their intellectual contributions to my development as a researcher and for their continued support through this project.

I wish to acknowledge the support that I received from the university and the chemistry department. I would also like to thank Dr. Duygu Uzun for her support and encouragement throughout the process.

I wish to thank Meltem Dinleyici, you simply make everything brighter, thanks for being always by my side. I am also grateful to everyone in the organic research group and all my friends and colleagues.

I wish to acknowledge the support and great love of my family. I am forever indebted to my parents for giving me the opportunities and experiences that have made me who I am. They encouraged me to explore new directions in life and seek my own destiny.

TABLE OF CONTENTS

| | |
|---|------|
| ABSTRACT..... | iii |
| ÖZ | v |
| DEDICATION..... | vii |
| ACKNOWLEDGMENT..... | viii |
| LIST OF TABLES | xiii |
| LIST OF FIGURES..... | xv |
| LIST OF SCHEMES. | xx |
| LIST OF SYMBOLS AND ABBREVIATIONS | xxi |
| 1 INTRODUCTION | 1 |
| 1.1 Solar Cell..... | 1 |
| 1.2 Configuration of Dye Sensitized Solar Cells (DSSC)..... | 3 |
| 1.3 Motivation of the Study..... | 4 |
| 1.3.1 Design and Synthesis of Perylene Diimides | 5 |
| 1.3.2 Rotational Design of DSSCs..... | 9 |
| 1.3.3 Selection of the Dyes (Sensitizers) | 9 |
| 2 THEORETICAL | 13 |
| 2.1 Solar Cells Technology | 13 |
| 2.1.1 Organic Solar Cells | 15 |
| 2.1.1.1 Bulk Hetrojunction Solar Cells | 17 |
| 2.1.1.2 Dye Sensitized Solar Cells (DSSCs)..... | 19 |
| 2.1.2 Organic-Inorganic Hybrid Solar Cell..... | 21 |
| 2.1.2.1 Perovskite Solar Cells (PSCs)..... | 23 |
| 2.2 The Components of DSSC | 25 |

| | |
|---|----|
| 2.2.1 The Working Electrode | 25 |
| 2.2.2 The Sensitizing Dyes..... | 26 |
| 2.2.3 Electrolyte | 33 |
| 2.2.4 The Counter Electrode | 35 |
| 2.3 The Working Principle | 35 |
| 2.4 Electron Transfer Dynamic | 37 |
| 2.5 Perylene Diimide Derivatives for OPV | 39 |
| 2.6 Perylene Diimide Derivatives | 40 |
| 2.7 Photo Induced Electron Transfer..... | 42 |
| 3 EXPERIMENTAL..... | 43 |
| 3.1 Material and Reagents | 43 |
| 3.2 Instrumental Part | 44 |
| 3.3 Synthesis of Bay Substituted Perylene Diimide Derivatives | 45 |
| 3.3.1 Synthesis of 1, 7-Dibromoperylene-3, 4, 9, 10-tetracarboxylic dianhydride (2)..... | 47 |
| 3.3.2 Synthesis of 1, 7-Di (2-decyltetradecanoyl) perylene-3, 4, 9, 10- tetra carboxylic bisanhydride (4)..... | 48 |
| 3.3.3 Synthesis of N, N'-bisdodecyl-1, 7-di (2-decyltetradecanoyl) Perylene -3, 4, 9, 1- tetracarboxylic bisimide (6)..... | 50 |
| 3.3.4 Synthesis of N, N'-bis ((S)-(-)-1-phenylethyl)-1, 7-di (2- decyltetradecanoyl) Perylene-3, 4, 9, 10-tetracarboxylic bisimide (8) | 52 |
| 3.4 DSSC Device Fabrication | 55 |
| 3.4.1 Transparent Conducting Oxide Substrates (TCO) | 55 |
| 3.4.2 Preparation of TiO ₂ Compact Layer..... | 56 |
| 3.4.3 Preparation of Nanocrystalline TiO ₂ Layer | 56 |

| | |
|---|----|
| 3.4.4 Sensitization..... | 57 |
| 3.4.5 Deposition of the Counter Electrode | 59 |
| 3.4.6 Preparation of the Redox Mediator | 59 |
| 3.4.7 Sealing of the Device..... | 60 |
| 3.5 DSSC Device Characterizations..... | 61 |
| 3.5.1 DSSC Parameters | 61 |
| 3.5.1.1 Short-Circuit Current Density (I_{sc})..... | 62 |
| 3.5.1.2 Open-Circuit Voltage (V_{oc})..... | 63 |
| 3.5.1.3 Power Maximum (P_{max}) | 63 |
| 3.5.1.4 The Fill Factor (FF)..... | 63 |
| 3.5.1.5 Power Conversion Efficiency (PCE) | 64 |
| 4 DATA AND CALCULATIONS | 65 |
| 4.1 Calculation of Optical Parameters..... | 65 |
| 4.1.1 Molar Absorption Coefficients... .. | 65 |
| 4.1.2 Fluorescence Quantum Yield | 69 |
| 4.1.3 Half-Width of Selected Absorption..... | 72 |
| 4.1.4 Theoretical Radiative Life Times | 73 |
| 4.1.5 Theoretical Fluorescence Life-Time | 76 |
| 4.1.6 Theoretical Fluorescence Rate Constant | 77 |
| 4.1.7 Radiationless Deactivation Rate Constant | 78 |
| 4.1.8 Oscillator Strength... .. | 79 |
| 4.1.9 Singlet Energies..... | 80 |
| 4.2 Electrochemistry of Synthesized Compounds..... | 83 |
| 4.2.1 Redox Potential/Half-Wave Potential | 83 |
| 4.2.2 LUMO/HOMO Energy Levels | 85 |

| | |
|---|-----|
| 4.2.3 The Optical Band Gap Energy..... | 87 |
| 4.3 Dye Sensitized Solar Cell Characterization | 90 |
| 4.3.1 Short Circuit Current | 90 |
| 4.3.2 Open Circuit Voltage..... | 91 |
| 4.3.3 Power Maximum | 92 |
| 4.3.4 Fill Factor | 94 |
| 4.3.5 Efficiency..... | 95 |
| 5 RESULT AND DISCUSSION | 142 |
| 5.1 Synthesis of (4) and IR Spectra Analysis..... | 142 |
| 5.2 Synthesis of (6) and IR Spectra Analysis..... | 142 |
| 5.3 Synthesis of (8) and IR Spectra Analysis..... | 143 |
| 5.4 NMR Spectra Analysis..... | 144 |
| 5.5 Solubility of 1, 7-Bay-substituted PDIs... .. | 147 |
| 5.6 UV/Vis Spectra Analysis | 148 |
| 5.7 Emission Spectra Analysis | 152 |
| 5.8 Solid State UV/Vis and Emission of the Synthesized Compounds..... | 154 |
| 5.9 Electrochemistry of the Synthesized Compounds..... | 155 |
| 5.10 Thermal Stability of the Synthesized Compounds | 156 |
| 5.11 Photovoltaic Performance | 157 |
| 5.12 FT-IR Spectra of Dyes 9-15 and the Dyes Adsorbed on TiO ₂ | 159 |
| 5.13 UV-Vis Absorption Studies of Dyes 9, 12 and 13..... | 161 |
| 6 CONCLUSION | 162 |
| REFERENCES..... | 166 |

LIST OF TABLES

| | |
|--|----|
| Table 2.1: The structure of organometallic halide MAX ₃ | 23 |
| Table 2.2: Crystalline composition of degussa P25 collected from the same package. | 28 |
| Table 2.3: Organic compounds used for DSSCs last years with their PCE..... | 32 |
| Table 3.1: Materials used for preparing the liquid electrolyte..... | 60 |
| Table 4.1: Concentration,Maximum wavelength and absorbance of 6 in chloroform. | 66 |
| Table 4.2: Maximum extinction coefficients of 4 in various solvents..... | 68 |
| Table 4.3: Maximum extinction coefficients of 6 in various solvents..... | 68 |
| Table 4.4: Maximum extinction coefficients of 8 in various solvents..... | 69 |
| Table 4.5: Fluorescence quantum yields of 4,6 and 8 in different solvent $\lambda_{exc}=485nm$ | 71 |
| Table 4.6: Half width of 4,6 and 8 in various solvents..... | 73 |
| Table 4.7: Theoretical radiative life time (ns) of 4..... | 74 |
| Table 4.8: Theoretical radiative life time (ns) of 6..... | 75 |
| Table 4.9: Theoretical radiative life time (ns) of 8..... | 75 |
| Table 4.10: Theoretical fluorescence life-time of 4,6 and 8 in varios solvents..... | 76 |
| Table 4.11: Theoretical fluorescence rate constant of 4,6 and 8 in varios solvents.... | 77 |
| Table 4.12: Radiationless deactivation rate constant of 4,6and 8 in varios solvents.... | 78 |
| Table 4.13: Oscillator streangth of 4,6 and 8 in various solvents..... | 79 |
| Table 4.14: Singlet energies of 4,6 and 8 in various solvents..... | 81 |
| Table 4.15: Photophysical properties of compounds 4,6 and 8 in various solvents... | 82 |
| Table 4.16: Cyclic voltammetry data, electrochemical and optical band gap energy, HOMO and LUMO energies of compounds 4, 6 and 8..... | 89 |
| Table 4.17: Short circuit current I _{sc} of DSSC using various dyes..... | 91 |

| | |
|---|-----|
| Table 4.18: Open circuit voltage V_{oc} of DSSC using various dyes..... | 92 |
| Table 4.19: V_{max} , I_{max} and P_{max} of DSSC using various dyes..... | 93 |
| Table 4.20: V_{max} , I_{max} , V_{oc} , I_{sc} and FF of DSSC using various dyes..... | 94 |
| Table 4.21: Photovoltaic parameters of the dyes. Solar simulation at $100\text{mW}/\text{cm}^2$... | 95 |
| Table 5.1: Solubility (solubility/color) of 4, 6 and 8 in different organic solvents... | 147 |
| Table 5.2: Ratio of absorption intensities of 4 in various solvents..... | 149 |
| Table 5.3: Ratio of absorption intensities of 6 in various solvents..... | 150 |
| Table 5.4: Ratio of absorption intensities of 8 in various solvents..... | 150 |
| Table 5.5: Absorption, emission wavelengths and calculated stock's shifts of 4 in various solvents..... | 153 |
| Table 5.6: Absorption, emission wavelengths and calculated stock's shifts of 6 in various solvents..... | 153 |
| Table 5.7: Absorption, emission wavelengths and calculated stock's shifts of 8 in various solvents..... | 154 |
| Table 6.1: Structures and optoelectronic properties of dyes 9-15 | 165 |

LIST OF FIGURES

| | |
|--|----|
| Figure 1.1: The configuration of DSSC | 3 |
| Figure 1.2: Design and synthesis of perylene diimides | 7 |
| Figure 1.3: Structures of synthesized compounds 4,6and 8..... | 8 |
| Figure 1.4: Structures of the dyes used for fabrication of DSSCs | 12 |
| Figure 2.1: p-n junction PV under solar radiation..... | 13 |
| Figure 2.2: Classification of photovoltaic technology..... | 14 |
| Figure 2.3: Structure of bulk heterojunction solar cell | 18 |
| Figure 2.4: Inorganic-Organic hybrid solar cells..... | 21 |
| Figure 2.5: SEM and particle size distribution of TiO ₂ anatase at 230°C prepared by Grätzel..... | 27 |
| Figure 2.6: Structure of the ruthenium sensitizers..... | 30 |
| Figure 2.7: Donor- π -bridge-acceptor structure..... | 31 |
| Figure 2.8: Electron transfer dynamic process in DSSC..... | 38 |
| Figure 2.9: Structure of a) perylene diimide (PDI), b) perylene dianhydride (PDA) and c) first industry pigment based on PDI | 40 |
| Figure 2.10: Structure of perylene diimide | 41 |
| Figure 2.11: Photo-induced electron transfer process..... | 42 |
| Figure 3.1: Dyes structures used for fabrication of DSSCs | 57 |
| Figure 3.2: The dyes adsorbed on the TiO ₂ layers..... | 58 |
| Figure 3.3: Pt coated counter electrode..... | 59 |
| Figure 3.4: Fabricated DSSC based on dye14..... | 61 |
| Figure 4.1: Concentration dependent spectra of 6 in chloroform..... | 66 |
| Figure 4.2: Absorbance vs. concentration of 6 in chloroform..... | 67 |

| | |
|---|-----|
| Figure 4.3: Half width estimation of 8 in chloroform..... | 72 |
| Figure 4.4: Cyclic voltammogram for compound 8 in acetonitrile at 100mVs ⁻¹ scan rate showing parameters E _{pc} , E _{pa} , I _{pc} and I _{pa} | 83 |
| Figure 4.5: Cyclic voltammogram for compound 8 in acetonitrile at 100mVs ⁻¹ scan rate showing parameters E _{ox/redonset} and HOMO/LUMO energies..... | 86 |
| Figure 4.6: Absorption spectrum of compound 8 in TCE..... | 88 |
| Figure 4.7: Graphic illustration of I _{sc} on I-V curve of dye 9 in dark and under light illumination at 100 mW/cm ² | 90 |
| Figure 4.8: Graphic illustration of V _{oc} on I-V curve of dye 9 in dark and under light illumination at 100 mW/cm ² | 91 |
| Figure 4.9: I-V curve with the photovoltaic parameters of dye 9 in dark and under light illumination at 100 mW/cm ² | 93 |
| Figure 4.10: FT-IR spectrum of 4..... | 96 |
| Figure 4.11: FT-IR spectrum of 6..... | 97 |
| Figure 4.12: FT-IR spectrum of 8..... | 98 |
| Figure 4.13: FT-IR spectrum of a. dye 9 and b. dye 9 adsorbed on TiO ₂ | 99 |
| Figure 4.14: FT-IR spectrum of a. dye 10 and b. dye 10 adsorbed on TiO ₂ | 100 |
| Figure 4.15: FT-IR spectrum of a. dye 11 and b. dye 11 adsorbed on TiO ₂ | 101 |
| Figure 4.16: FT-IR spectrum of a. dye 12 and b. dye 12 adsorbed on TiO ₂ | 102 |
| Figure 4.17: FT-IR spectrum of a. dye 13 and b. dye 13 adsorbed on TiO ₂ | 103 |
| Figure 4.18: FT-IR spectrum of a. dye 14 and b. dye 14 adsorbed on TiO ₂ | 104 |
| Figure 4.19: FT-IR spectrum of a. dye 15 and b. dye 15 adsorbed on TiO ₂ | 105 |
| Figure 4.20: UV/Vis spectra of 4 in various solvents at (1×10 ⁻⁵ M)..... | 106 |
| Figure 4.21: Emission spectra of 4 in various solvents at λ _{exc.} =485nm..... | 107 |

| | |
|---|-----|
| Figure 4.22: Concentration dependent spectra\ UV/Vis of 4 the solvents of a), b) and c) are: CHL, TCE and TFAc respectively..... | 108 |
| Figure 4.23: Concentration dependent spectra\ UV/Vis of 4 the solvents of a), b) and c) are: NMP, DMF and DMSO respectively..... | 109 |
| Figure 4.24: Concentration dependent spectra\ emission of 4 the solvents of a), b) and c) are: CHL, TCE and TFAc respectively at $\lambda_{exc.} = 485nm$ | 110 |
| Figure 4.25: Concentration dependent spectra\ emission of 4 the solvents of a), b) and c) are: NMP, DMF and DMSO respectively at $\lambda_{exc.} = 485nm$ | 111 |
| Figure 4.26: UV/Vis in solid state spectrum of 4..... | 112 |
| Figure 4.27: UV/Vis spectra of 6 in various solvents at ($1 \times 10^{-5}M$)..... | 113 |
| Figure 4.28: Emission spectra of 6 in various solvents at $\lambda_{exc.} = 485nm$ | 114 |
| Figure 4.29: Concentration dependent spectra\ UV/Vis of 6 the solvents of a), b) and c) are: CHL, TCE and TFAc respectively..... | 115 |
| Figure 4.30: Concentration dependent spectra\ UV/Vis of 6 the solvents of a), b) and c) are: NMP and DMF respectively..... | 116 |
| Figure 4.31: Concentration dependent spectra\ emission of 6 the solvents of a), b) and c) are: CHL, TCE and TFAc respectively at $\lambda_{exc.} = 485nm$ | 117 |
| Figure 4.32: Concentration dependent spectra\ emission of 6 the solvents of a), b) and c) are: NMP and DMF respectively at $\lambda_{exc.} = 485nm$ | 118 |
| Figure 4.33: UV/Vis in solid state spectrum of 6..... | 119 |
| Figure 4.34: UV/Vis spectra of 8 in various solvents at ($1 \times 10^{-5}M$)..... | 120 |
| Figure 4.35: Emission spectra of 8 in various solvents at $\lambda_{exc.} = 485nm$ | 121 |
| Figure 4.36: Concentration dependent spectra\ UV/Vis of 8 the solvents of a), b) and c) are: CHL, TCE and TFAc respectively..... | 122 |

| | |
|---|-----|
| Figure 4.37: Concentration dependent spectra\ UV/Vis of 8 the solvents of a), b) and c) are: NMP, DMF and DMSO respectively..... | 123 |
| Figure 4.38: Concentration dependent spectra\ emission of 8 the solvents of a), b) and c) are: CHL, TCE and TFAc respectively at $\lambda_{exc.} = 485nm$ | 124 |
| Figure 4.39: Concentration dependent spectra\ emission of 8 the solvents of a), b) and c) are: NMP, DMF and DMSO respectively at $\lambda_{exc.} = 485nm$ | 125 |
| Figure 4.40: UV/Vis in solid state spectrum of 8..... | 126 |
| Figure 4.41: UV/Vis spectra of 9 in solid state and 9 adsorbed on TiO ₂ | 127 |
| Figure 4.42: UV/Vis spectra of 12 in solid state and 12 adsorbed on TiO ₂ | 128 |
| Figure 4.43: UV/Vis spectra of 13 in solid state and 13 adsorbed on TiO ₂ | 129 |
| Figure 4.44: Cyclic voltammogram of 4 in acetonitrile solution at 100 mVs ⁻¹ , supporting electrolyte 0.1M TBAPF ₆ | 130 |
| Figure 4.45: Cyclic voltammogram of 6 in acetonitrile solution at 100 mVs ⁻¹ , supporting electrolyte 0.1M TBAPF ₆ | 131 |
| Figure 4.46: Cyclic voltammogram of 8 in acetonitrile solution at 100 mVs ⁻¹ , supporting electrolyte 0.1M TBAPF ₆ | 132 |
| Figure 4.47: TGA curves a. and DSC thermogram b. of 4, 6 and 8 at 10°C min ⁻¹ heating rate..... | 133 |
| Figure 4.48: I-V characteristics of 4 in the dark and under 100 mW/cm ² illumination..... | 134 |
| Figure 4.49: I-V characteristics of 9 in the dark and under 100 mW/cm ² illumination..... | 135 |
| Figure 4.50: I-V characteristics of 10 in the dark and under 100 mW/cm ² illumination..... | 136 |

| | |
|---|-----|
| Figure 4.51: I-V characteristics of 11 in the dark and under 100 mW/cm ² illumination..... | 137 |
| Figure 4.52: I-V characteristics of 12 in the dark and under 100 mW/cm ² illumination..... | 138 |
| Figure 4.53: I-V characteristics of 13 in the dark and under 100 mW/cm ² illumination..... | 139 |
| Figure 4.54: I-V characteristics of 14 in the dark and under 100 mW/cm ² illumination..... | 140 |
| Figure 4.55: I-V characteristics of 15 in the dark and under 100 mW/cm ² illumination..... | 141 |
| Figure 5.1: Structure of compound 4..... | 144 |
| Figure 5.2: Structure of compound 6..... | 145 |
| Figure 5.3: Structure of compound 8..... | 146 |
| Figure 5.4: UV/Vis spectra of compounds a. 4, b. 6 and c. 8 in DMF and upon microfiltration..... | 151 |

LIST OF SCHEMES

| | |
|---|----|
| Scheme 3.1: The Synthetic route of 1, 7- disubstituted perylene diimides..... | 46 |
| Scheme 3.2: Synthesis of compound 2..... | 48 |
| Scheme 3.3: Synthesis of compound 4..... | 49 |
| Scheme 3.4: Synthesis of compound 6..... | 51 |
| Scheme 3.5: Synthesis of compound 8..... | 53 |

LIST OF SYMBOLS AND ABBREVIATIONS

| | |
|---------|---|
| A | Absorption |
| AU | Arbitrary unit |
| C | Concentration |
| Calcd. | Calculated |
| CHL | Chloroform |
| DMF | Dimethylformamide |
| DMSO | Dimethyl sulfoxide |
| DSSC | Dye sensitized solar cells |
| eV | Electron volt |
| Fc | Ferrocene |
| FF | Fill Factor |
| FT – IR | Fourier Transform Infrared Spectroscopy |
| h | Hour |
| HOMO | Highest Occupied Molecular Orbital |
| IR | Infrared Spectrum/ Spectroscopy |
| l | path length |
| LUMO | Lowest Unoccupied Molecular Orbital |
| M | Molar concentration |
| max | Maximum |
| min | Minimum |
| mmol | Millimole |
| mol | Mole |
| NMP | <i>N</i> -methylpyrrolidinone |

| | |
|--------------------|---|
| PDA | Perylene 3, 4, 9, 10-tetracarboxylic dianhydride |
| PDI | Perylene Diimide |
| PV | Photovoltaic |
| Std. | Standard |
| t | Time |
| TBAPF ₆ | Tetrabutylammoniumhexafluorophosphate |
| TCE | 1, 1, 2, 2-tetrachloroethane |
| TFAc | Trifluoroacetic acid |
| TGA | Thermogravimetric analysis |
| UV | Ultraviolet |
| UV-vis | Ultraviolet visible light absorption |
| ν_{\max} | Maximum wavenumber |
| V | Volt |
| V_{oc} | Open circuit voltage |
| Å | Angstrom |
| ϵ | Molar Absorption Coefficient |
| ϵ_{\max} | Maximum Extinction Coefficient / Molar absorptivity |
| $E_{1/2}$ | Half- Wave Potential |
| E_{pa} | Anodic peak potential |
| E_{pc} | Cathodic peak potential |
| E_{red} | Reduction potential |
| E_{oxd} | Oxidation potential |
| f | Oscillator Strength |
| I_{pa} | Cathodic peak current |
| I_{pc} | Anodic peak current |

| | |
|-------------------|---|
| I_{sc} | Short circuit current |
| k_d | Rate Constant of Radiationless Deactivation |
| k_f | Fluorescence Rate Constant |
| Φ_f | Fluorescence quantum yield |
| τ_0 | Theoretical Radiative Lifetime |
| $\bar{\nu}$ | Wavenumber |
| $\Delta\nu_{1/2}$ | Half-width (of the selected absorption) |
| λ | Wavelength |
| λ_{exc} | Excitation wavelength |
| λ_{em} | Emission wavelength |

Chapter 1

INTRODUCTION

1.1 Solar Cells

The world now needs new technologies which provide renewable and environmentally friendly energy resources. The energy provided from the sun in an hour is more than the energy demanded on the earth in one year therefore the sunlight energy is an excellent free, natural and abundant source of energy. The solar radiation as a form of a renewable energy provides a practical, clean and valuable solution to meet the world's global energy consumption and the growing environmental challenges.

At 1839, The French physicist Alexander Edmond first discovered the process of producing electrical energy from the solar radiation and that was the beginning of solar cell technology [1].

The devices that can produce electrical energy from solar energy are called solar cells, over the years, solar cells were classified into 3 main categories the 1st generation represented by the wafer based silicon which includes mono-crystalline or polycrystalline silicone cells, these cells are the oldest and the most commercially used solar cells owing to their high efficiencies however they are relatively expensive to produce [2].

The 2nd generation of solar cells which represented by the thin film cells have been modified to meet the demands of decreasing the material, fabrication and purification costs. This generation of solar cells are consisting of thin layer of different semiconductor materials like amorphous silicon, copper indium gallium (II) selenide and cadmium telluride. The complex production processes of the different combinations of rare materials are expensive and may limit a future large-scale production [3].

Dye sensitized solar cells (DSSCs) are the new emerging technology which represent the 3rd generation solar cells and it is the subject of the present thesis.

1.2 Configuration of Dye Sensitized Solar Cells (DSSC)

DSSC include working electrode (WE) and counter electrode (CE) linked by a redox couple (electrolyte) as shown in figure 1.1. the Working electrode consist of a porous TiO_2 layer attached to a conducting glass substrate, mainly fluorine-doped tin oxide (FTO) and a sensitizer adsorbed on the TiO_2 layer , Counter electrode (CE) which is either platinized or carbon conducting substrate, and Redox system which is usually liquid electrolyte based on iodide/triiodide (I^-/I_3^-) redox couple [3].

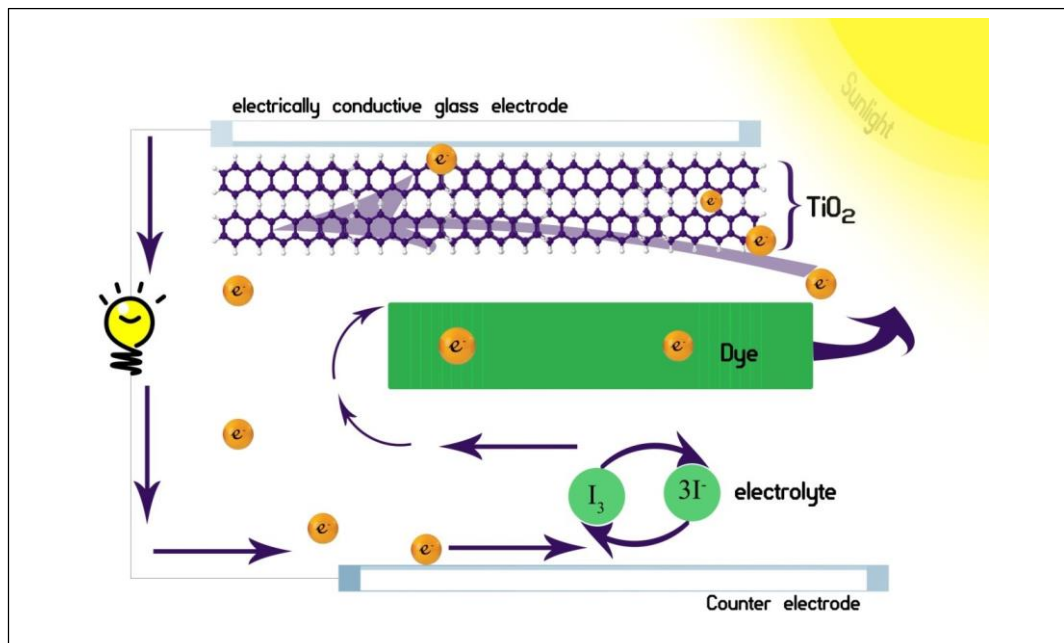


Figure 1.1: The configuration of DSSC

1.3 Motivation of the Study

In this project, we aim to develop materials and manufacturing procedure for DSSC based on titanium dioxide with long lifetime and high efficiencies.

This project has been started with synthesis of novel 1, 7-bay substituted perylene dianhydride and two 1, 7-bay substituted perylene diimides with a large and swallow tail type, 2-decyl-1-tetradecanoyl substituent at 1, 7-bay positions. Absorption, emission and electrochemical properties of the synthesized compounds were comparatively studied and characterized. The second part of this work focused on the fabrication of DSSC based on metal free organic dyes namely, perylene dyes.

In fact the dyes showing better efficiencies in DSSC field of research are Ru-complexes with efficiency of 11-12%, however these dyes were characterized by low stability and low extinction coefficient which might affect the performance and life time of the DSSC devices. Therefore it is the appropriate time to experience other types of organic dyes such as perylene dyes.

In this logic, electrolyte dye sensitized solar cell devices were fabricated using some perylene dyes which had been synthesized and characterized before by Prof. Dr. Huriye İcil's group members [4-8] and their structures are listed in figure 1.4. The effect of these dyes' adsorption mode containing carboxylic acid, phosphonate amino and hydroxyl as anchor groups on the TiO₂ surface. The DSSC devices were examined and characterized and this work was supported by the optical and electrochemical analysis.

1.3.1 Design and Synthesis of Perylene Diimides

During the last decade, synthesis and characterization of soluble PDIs based organic solar cells is an interesting area of research, perylene derivatives have been emerged as the most considerable compounds of the group of polycyclic aromatic hydrocarbons owning their outstanding properties such as high molar extinction coefficient, excellent photophysical and photochemical stability, high fluorescence quantum yield, high electron mobility through π - π stacking, good electron transport properties, ease processing and functionalization of imide or bay positions of perylene core [9].

The solubility and packing arrangement in solid state of perylene compounds can be controlled by the substitution in imide positions of PDIs while enhancing the optical properties and modifying the HOMO and LUMO levels to cover the whole visible-NIR region can be achieved by substitution at 1,6- 1,7 bay positions of PDI [10].

In the present research, we are planning to synthesize novel 1, 7-bay substituted perylene diimides within three steps as shown in figure 1.2. In the first step, 1, 7-dibrominated perylene dianhydride was prepared in sulfuric acid following a known procedure mentioned in section 3.3.1.

Bromine atoms in the second step were substituted by 2-decyl-1-tetradecanoyl substituent to synthesize bay- substituted perylene dianhydride, called 1, 7(6)-di (2-decyl-1-tetradecanoyl) perylene-3, 4, 9, 10-tetracarboxylic acid bisanhydride (4). Finally, N, N'-Imidization of 1, 7-bay substituted perylene dianhydride with various amines in isoquinoline/m-cresol at reflux yielded 1, 7- disubstituted PDIs, called N, N'-bis-(dodecyl)-1, 7(6)-di (2-decyl-1-tetradecanoyl) perylene-3, 4, 9, 10-tetracarboxy bisimide (6) and N,N'-bis-((S)-(-)-1-phenylethyl)-1,7(6)- di(2-decyl-1-

tetradecanoyl) perylene-3,4,9,10-tetracarboxy bisimide (8). The structures of synthesized compounds (4, 6 and 8) were shown in figure 1.4.

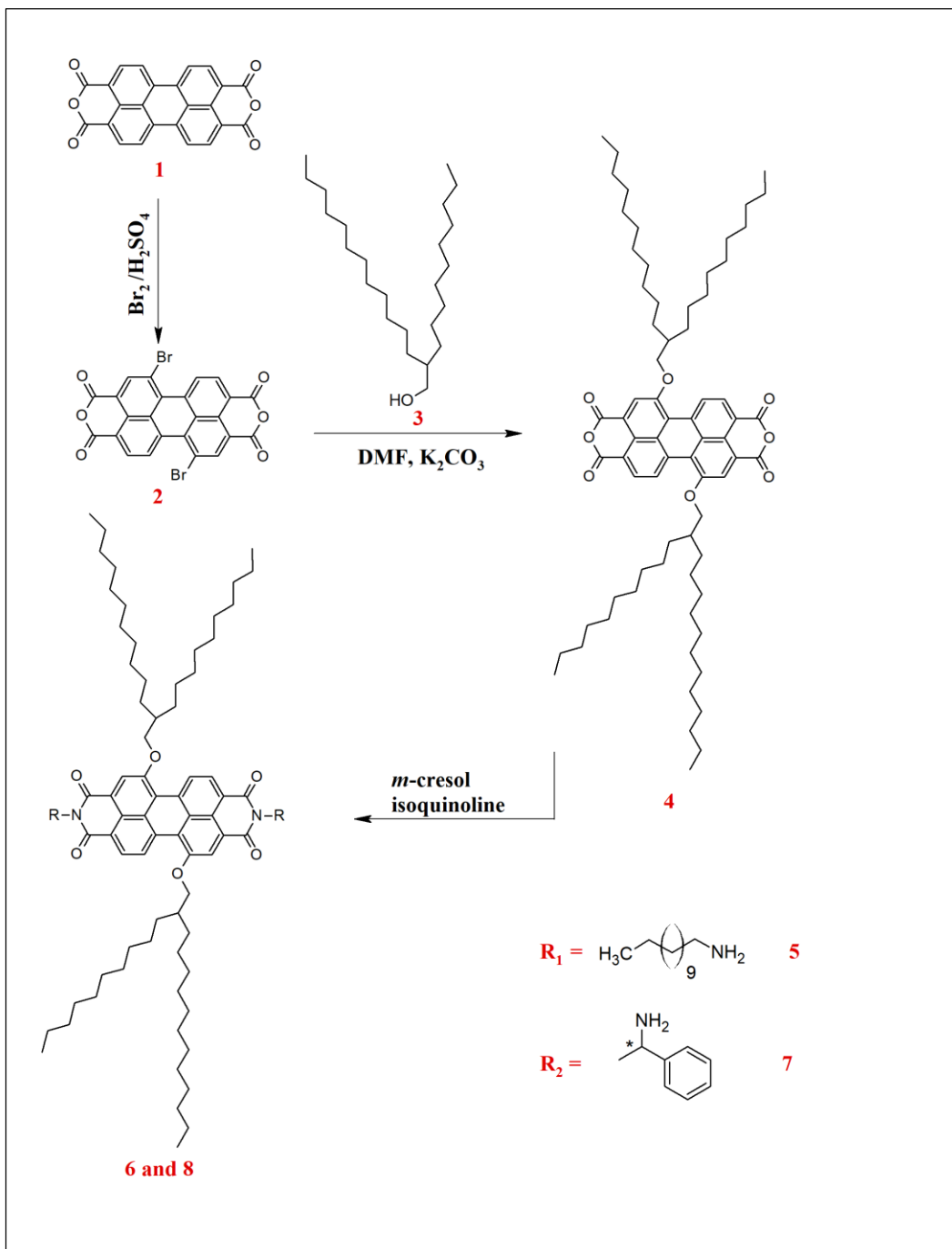


Figure 1.2: Design and synthesis of Perylene diimides

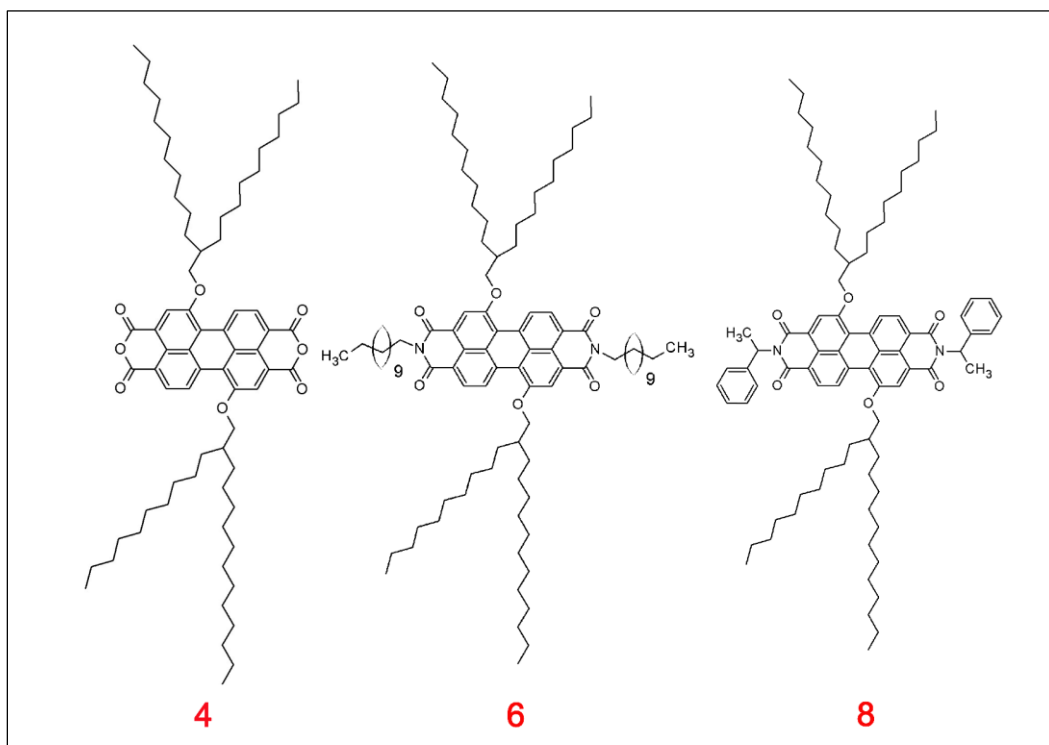


Figure 1.3: Structures of synthesized compounds 4 , 6 and 8

1.3.2 Rotational Design of DSSCs

DSSC devices using various perylene and naphthalene derivatives as shown in figure 1.4 were fabricated using sandwich type structure according to the procedure reported in literature [11]. The FTO glass substrates were pretreated with titanium isopropoxide solution, photo-electrodes were prepared on FTO glass substrates using spin coating technique and sintered at 450-500 °C for 45 min.

For Dye sensitization, TiO₂ photo electrode was immersed in dye solutions overnight. The DSSC devices were then prepared by assembling the photosensitized mesoporous TiO₂ films with platinum coated counter electrodes in sandwich geometry and the liquid electrolyte was injected into the space between the working electrode (WE) and the counter electrode (CE).

DSSC devices using different dyes were characterized by current- voltage (I-V) curves via Keithley 2400-source meter and solar conversion efficiencies of the fabricated DSSCs were calculated accordingly.

1.3.3 Selection of the Dyes (Sensitizers)

The dye structures play a crucial role in the performance of the DSSC devices since they are responsible for capturing the solar radiation, therefore much effort was invested in the synthesis and investigation of new dyes for high efficiency DSSCs.

The dyes for DSSC application need to meet certain requirements for an efficient light absorption and electron transfer to the conduction band of the TiO₂ and hence result in high performance and high power conversion efficiency.

These requirements are: 1) broad absorption spectrum with intense absorption in visible region as well as high molar absorption coefficient, 2) strong adsorption onto the semiconductor surface (strong anchoring group), 3) it should possess several =O or –OH groups capable of chelating to the Ti^{4+} site on the TiO_2 surface 4) efficient electron injection into the conduction band of the semi-conductor surface.

Understanding the structure of various DSSC anchors and the search for new anchors are critical factors for the development of DSSCs. Traditionally, carboxylic acid sulfonic acid, phosphonic acid and cyanoacrylic acid groups are employed as dye anchors in DSSCs.

In this project, we have studied the influence of the large and swallow tail type 2-decyl-1-tetradecanoyl substituent at bay area of the perylene core named 1, 7(6)-di (2-decyl-1-tetradecanoyl) perylene-3, 4, 9, 10-tetracarboxylic acid bisanhydride (4) figure 1.3 on the device performance in DSSCs.

Additionally, we designed DSSCs based on novel perylene diimides (PDIs), naphthalene diimides (NDI) and naphthalene polymer which have been linked to various moieties (anchoring groups) as shown in figure 1.4. We started with a small molecule which is NDI with sulfonic acid group on imide positions (dye 9) since sulfonic acid group provides excellent anchoring stability to the TiO_2 surface through both bidentate and tridentate anchoring modes.

N, N'-bis (4-hydroxyphenyl)-perylene-3, 4, 9, 10-tetracarboxy bisimide (dye 10) was investigated owing to its good solubility, high molar absorption coefficient and also the presence of the –OH chelating group. Since bay substitution improves the

photophysical and electrochemical properties of perylene diimides, N, N'-bis (4-hydroxyphenyl)-1, 7(6)-diphenoxyperylene-3, 4, 9, 10-tetracarboxy bisimide (dye 11) with the same substituents of dye 10 at imide positions was also investigated for comparison.

Asymmetric PDI, N-((2S)-aminohexanoic acid)-N'-(1-dehydroabietyl)-3, 4, 9, 10-perylene tetracarboxydiimide (dye 12) was also examined because of its higher molar absorption coefficient and longer λ_{\max} compared to the previous dyes as well as the presence of the carboxylic acid anchoring group which can bind to the TiO₂ surface through monodentate and bidentate anchoring modes as well as hydrogen bonding modes which can also be seen in perylene 3,4-dicarboxylic-9,10- ((R)-1-phenylethyl) carboxyimide (dye 14).

Perylene dicarboxylic acid anhydride itself can be used as an anchoring group for TiO₂ sensitization without the need of additional anchoring groups on the perylene dicarboxylic acid anhydride, therefore N-(4-Hydroxyphenyl)-3,4,9,10-perylenetetra carboxylic-3,4-anhydride-9,10-imide (dye 13) was selected.

Lastly, naphthalene-1, 4, 5, 8- tetracarboxylic acid-bis (N, N'-bis-6- phenyl-1, 3, 5 triaznyl) polyimide (dye 15) was also investigated as sensitizer for DSSC.

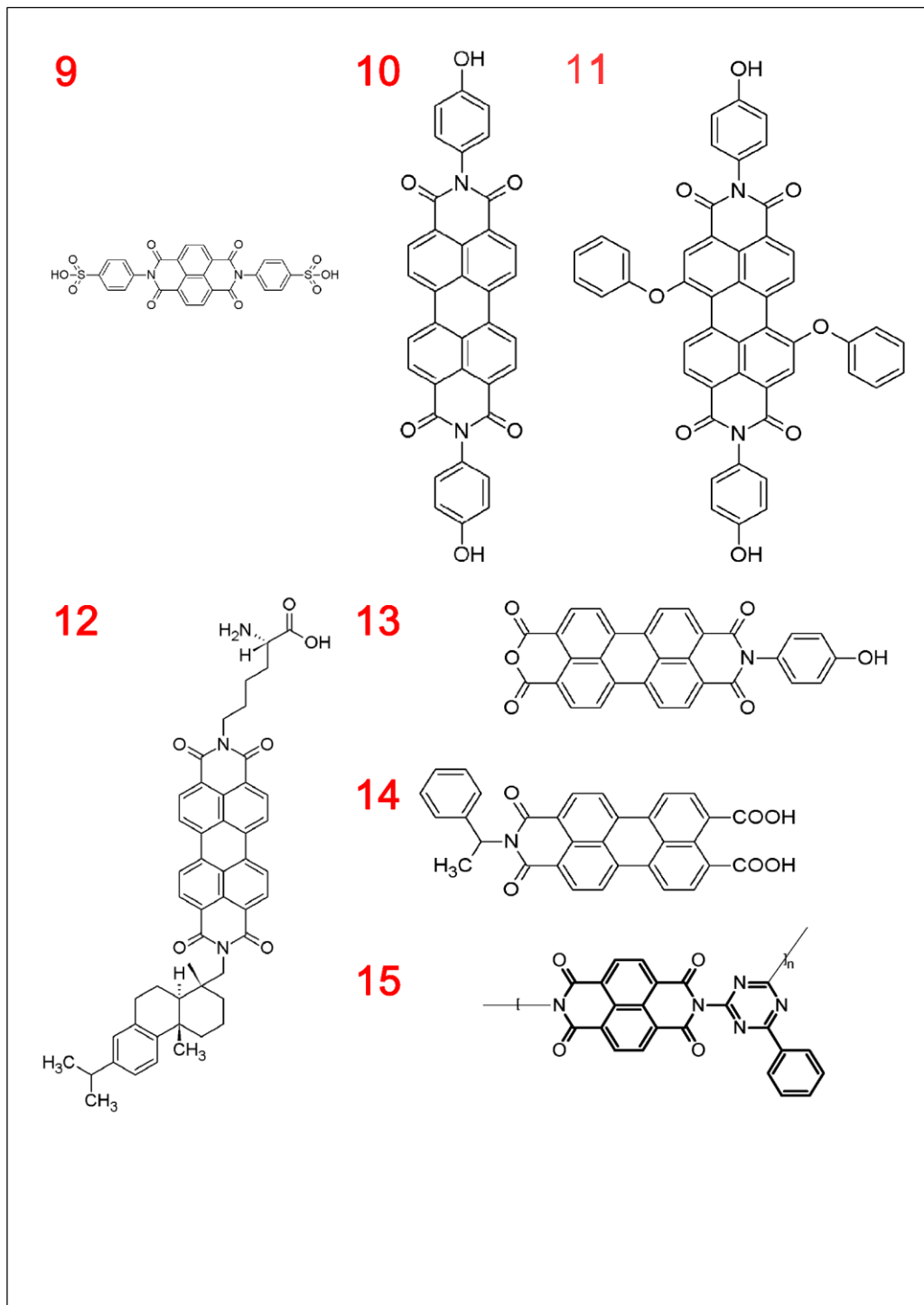


Figure 1.4: Structures of the dyes used for fabrication of DSSCs

Chapter 2

THEORETICAL

2.1 Solar Cells Technology

Solar cells, also known as photovoltaics (PV), are devices converting the solar light into electrical energy, these cells consist of special components called semiconductors. In 1839 Alexandre-Edmond Becquerel first noticed the Photovoltaic influence, then in 1946, the first modified solar cell was invented by Russel Ohl based on silicon as a semiconductor material, up to recent years the most common PV cells are the thin silicon wafers which consist of n-type and p-type semiconductors as two different layers based on electron-hole creation mechanism figure 2.1[12].

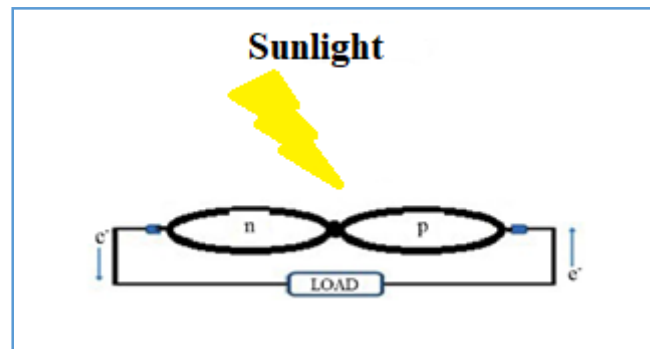


Figure 2.1: p-n junction PV under solar radiation

An electron is transferred by absorbing the photons when the sun light flash on the semiconductor of the solar cell from one layer to another, this electron transfer process produces an electron-hole couple, subsequently electric power is created.

Different materials used for PV cells include inorganic materials such as silicon in different forms like single crystal, multi-crystalline amorphous silicon and copper-indium-gallium sulfide or organic compounds. The PV cells have been classified into different categories based on these materials, the classification of PV technologies is shown in Figure 2.2 [13].

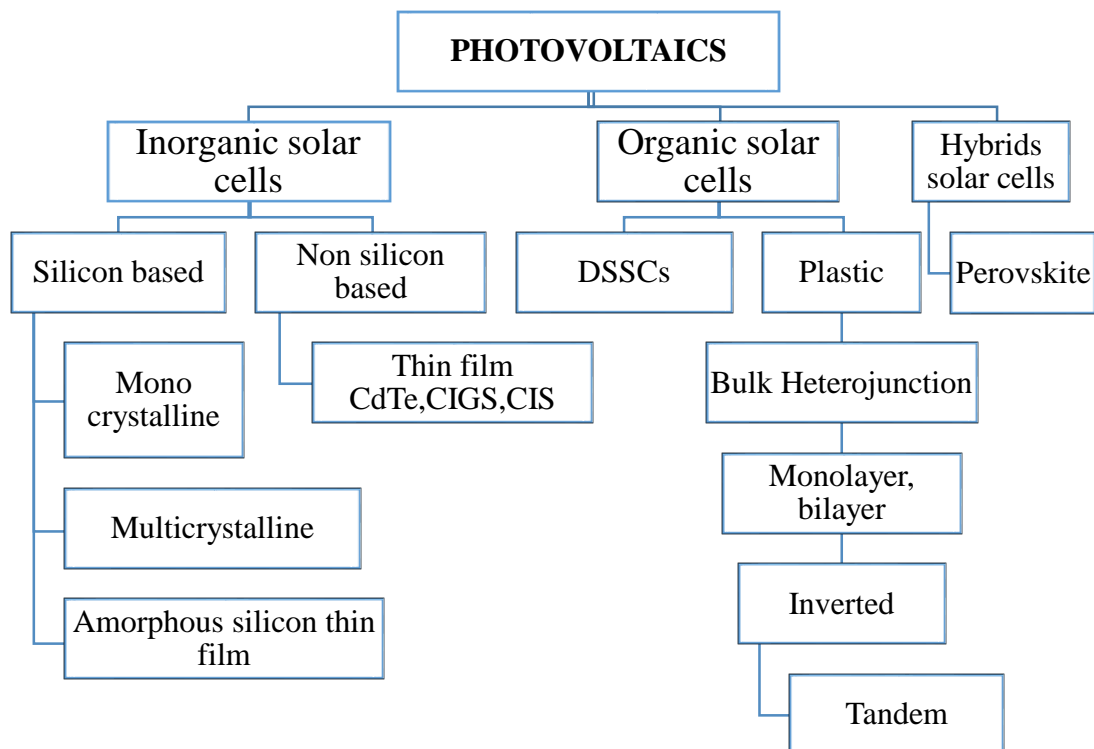


Figure 2.2: Classification of photovoltaic technology

For photovoltaic technology to compete with the traditional fossil fuels technologies there are some challenges to be solved, in terms of power conversion efficiencies, ease and cost of production, availability of the materials and environmental contamination starting from the fabrication process.

2.1.1 Organic Solar Cells

Today the silicon based solar cells are dominated on the solar power industry. Photovoltaic global production and modules of this type have been grew considerably. This technology has influenced the world encouraging the extension of energy sources from coal to green energy. Recently, the PCE of silicon solar cells has exceeded 25%. Nevertheless, the limitation that this type of photovoltaic researcher faces is not only their conversion of efficiency but also the expensive cost of production, both in terms of energy and money. Organic photovoltaics (OPV) is one solution that might overcome these obstacles [14].

During the last few years, considerable attention has been given to overcoming technical and material obstacles to the production and commercial viability of organic solar cells with equivalent cost-efficiency compared to silicone and another inorganic photovoltaic devices.

Major improvements are needed to exploit the low cost of organic solar cells, including efficiency of more than 20%, high environmental stability from degradation, novel optically active organic compounds, and the modification of new manufacturing applications.

One of the problems effecting the efficiency of organic solar cells is the short diffusion length of excitons therefore, this problem should be solved in order to meet the strict requirements to compete inorganic solar cells [15].

Simple and low cost techniques like spray deposition, screen printing and spin coating techniques were used for fabrication of organic solar cells based on thin film polymers and small organic compounds, mainly dyes or pigments, or a mixture of both small compounds and polymers. These materials have been inserted into organic solar cells in recent years, leading to remarkable improvements.

Organic compounds have the capacity to absorb the light in UV-Vis spectral regions because of the sp^2 hybridization of carbon atoms and this can be enhanced by increasing the conjugation in the compounds, as well as their good ability to transfer the electrical current [16]. Unlike inorganic semiconductors, the organic materials have generally poor charge carrier mobility, which affect the performance of organic solar cells, however, they possess relatively high absorption coefficients ($\geq 10^5 \text{cm}^{-1}$), which significantly balance the low charge motilities, resulting in high absorption capacity even in thin-film devices with less than 100 nm [17].

In organic solar cells, the light interaction with the compound (photon absorption) generates an important intermediate called exciton (photo-excitation pair connected by coulomb attraction). Strong electrical field is required to dissociate the excitons into free charge carriers, which are the required outcome for solar energy conversion.

The optical band gaps of organic semiconductors (2 eV) are relatively higher than those of silicon which limit the solar of the solar radiation. Nevertheless, the low cost, large scale production and the chemical versatility of the organic compounds via chemical synthesis have been attracted a great interest in academia and industry [18].

2.1.1.1 Bulk Heterojunction Solar Cells

Organic bulk heterojunction solar cells (BHJ) have been developed starting with the fact that the diffusion length of the excitons is considerably smaller than the thickness of the layer required for sufficient light absorption, during 1990s BHJ designed where a conjugated polymer as a donor was mixed with conjugated small molecules such as fullerenes, thiazoles, and isoindigos as an acceptor. This mixture gives rise for many localized donor/acceptor interfaces across the active layer, regardless to the active layer thickness, and the dissociation rate of the exciton in the donor/acceptor interface is increased Moreover, the charge separation process is increased [19].

In 2013, Ankita Gaur and Ponkaj Kumar reported an approximate 100% efficiency of exciton dissociation in BHJ. With the presence of percolation pathways in photoactive substrate, charge carriers travel from the dissociation area to the corresponding electrodes, and consequently, the power conversion efficiency is exceeding 10 % [20].

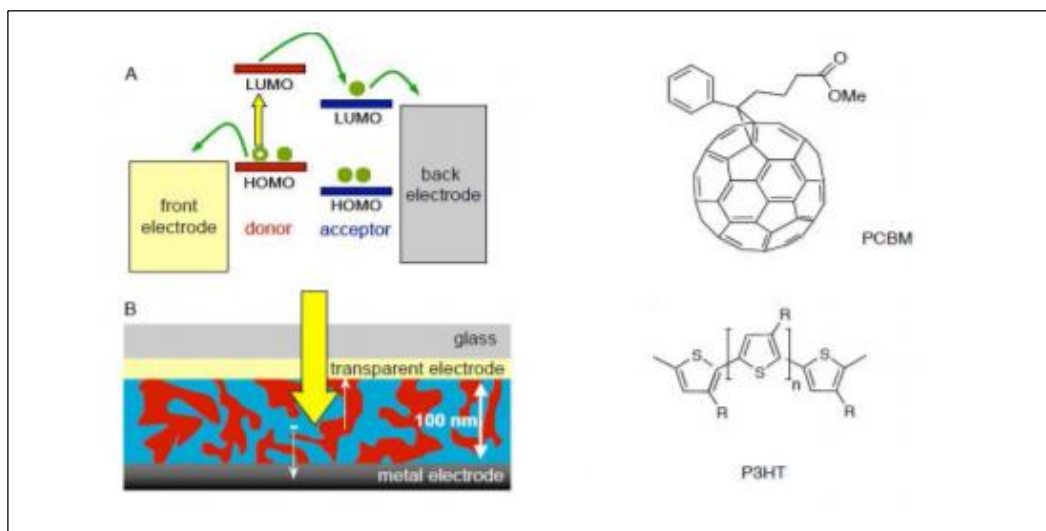


Figure 2.3: Structure of bulk heterojunction solar cell

BHJs are one of the most promising organic photovoltaic devices, they have been substantially studied considering their applications in the market. However, there is a huge work to be done concerning the study of their electric behavior, though the highest power conversion efficiencies have been recorded at approximately 10 percent, these tend to occur on very small laboratory devices which are not practical for a real size scale.

At present, the major research on the organic photovoltaic need to concentrate on general device structure and active layer composition as well as some new organic compounds with enhanced properties and performance [21].

2.1.1.2 Dye Sensitized Solar Cells (DSSCs)

Dye sensitized solar cells have been attracted the attention of the researchers as a new renewable and clean source of energy since they were first introduced by Michael Grätzel at 1990s, DSSCs belong to the 3rd generation (thin film)solar cells. In contrast to conventional organic photovoltaics where the organic semiconductors should have good light-absorbing properties as well as excellent charge carriers mobility which is a difficult task to achieve, these two requirements are separated in DSSC technology as the light is absorbed by the sensitizer (organic dye), the charge is generated at the wide bandgap semiconductor (TiO₂)/dye interface and finally the charge is transported by the TiO₂ semiconductor and the electrolyte (redox couple).

The sensitizer (dye) is the key component effecting the overall performance and efficiency of the DSSC as it is responsible for the light absorption therefore enhancing the photophysical properties can be achieved by modifying the dye molecule through different synthesis pathways, while the charge carriers mobility can be improved by modifying the semiconductor and the electrolyte [22].

A photoelectrode's first sensitization was observed in 1887 by Moser who was researching the field of photography. However, the operational mechanism was clarified and reported by Gerischer and Tributsch at 1960s which states the electrons injection from photo-excited dye molecules (sensitizer) into the n-type semiconductor through its conduction band, then the process was developed in the following years starting at 1976 with the adsorption mechanism of the dye molecules on the semiconductor surface by Dare-Edwards et al., and Tsuboroma et al.,

followed by increasing the semiconductor/dye interface via using dispersed particles at 1984 by Duonghong et al, and Desilvestro et al., [23].

Even though DSSC has a long history, due to weak sunlight absorption, its power conversion efficiency was limited to 1 percent by the 1990s Michael Grätzel described a nano-crystalline Titanium dioxide DSSC with an average size of 15 nm for the anode material and a high turnover ruthenium-complex sensitizer achieving an efficiency of 7 percent and then to 10 percent, Grätzel constructed a basic DSSC.

Transparent conductive oxide, abbreviated as TCO, glass substrate, highly porous wide band gap semiconductors (mainly TiO_2), photosensitizer (organic dye), redox electrolyte couple (I_3^-/I^-) and counter electrode which can be either platinum or active carbon coated on TCO are the main components of DSSC. the cell is normally built in sandwich like structure between the working and counter electrodes [24].

Extensive efforts have been done and still going for further improvement in the performance and efficiency of DSSC in terms of dye structures, semiconductor formulation, thickness of the working and counter electrodes and their annealing process and composition of the electrolyte.

2.1.2 Organic-Inorganic Hybrid Solar Cells

Hybrid solar cells are thin film devices that consist of a photoactive light-absorbing layer between a metal electrode and a conductive electrode which is often highly conductive TCO doped indium tin oxide, abbreviated as ITO, or a flexible plastic as an anode. The photoactive layer contains conjugated polymer as an organic component and a semiconducting nanocrystal as an inorganic part. Metal electrode can be a pure metal such aluminum or a mixture such as lithium fluoride/ aluminum and calcium/ aluminum, metal electrode is ultimately deposited on the photoactive layer. Figure 2.4 shows the typical structure of Hybrid solar cells.

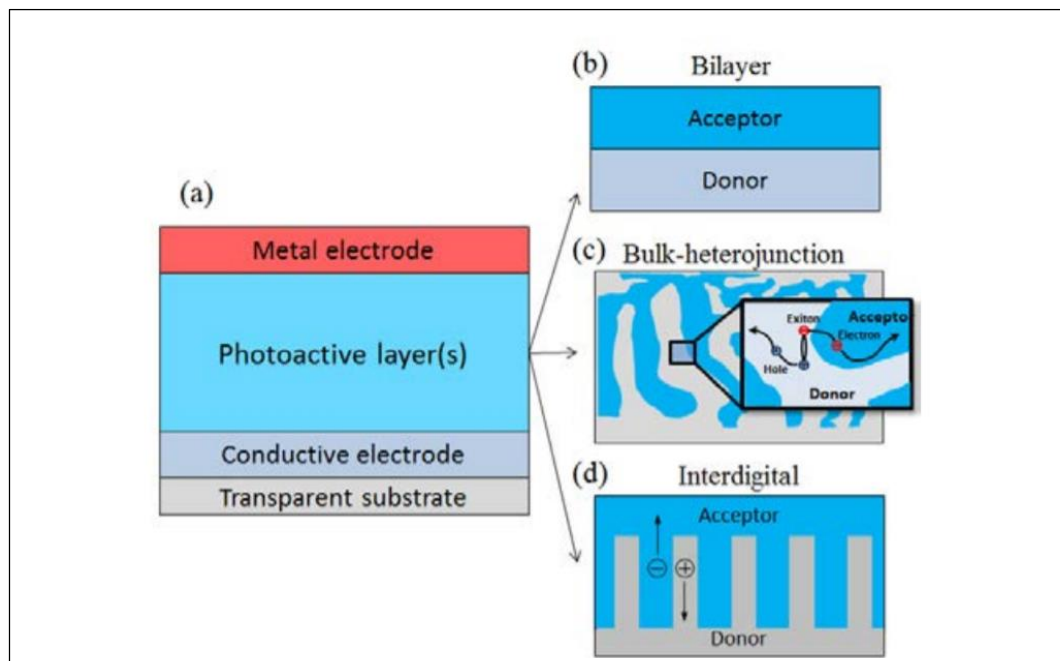


Figure 2.4: Structure of organic-inorganic hybrid solar cell

The photoactive layer of hybrid solar cells can be classified according to the donor-acceptor ratio and mixing process, bilayer and bulk- heterojunction represent the two main types of the photoactive layer figure (2.4 a&b), while the interdigital figure (2.4c) represent the ideal structure which offers an efficient exciton dissociation as well as excellent charge transfer [25].

Light absorption by the organic semiconductors produces electron-hole pairs called excitons. The optimal distance of the exciton to the donor\acceptor interface should be within the same range of the exciton diffusion distance in the conjugated polymer which is approximately between 10-20 nm to allow an efficient exciton dissociation and charge transfer. For this reason, bulk heterojunction type was developed where the donor and acceptor materials have been extensively mixed. Accordingly, the donor\acceptor interfacial area was dramatically increased, the distance of excitons to the the donor\acceptor interface was reduced, and the electron transfer process after exciton dissociation was also improved.

In hybrid solar cells, the photocurrent generation required multistep, mainly four steps, starting with light absorption, followed by exciton diffusion, charge separation and charge transfer. Greenham and saunders reviewed the physics of orgnic-inorganic hybrid solar cells in details [26].

2.1.2.1 Perovskite Solar Cells (PSCs)

The interest in PSCs is rapidly growing in scientific and industrial communities because of their flexibility, high-efficiency ($\geq 20\%$), affordable cost and ease of production. The photoactive layer in PSCs consists of organic-inorganic hybrid compounds in crystalline form of MAX_3 (M and A: two different sizes cations, X = anion) with relatively large absorption coefficient and long carriers diffusion within this structure, organometallic as shown in table 2.1, have attracted much attention for an efficient PSCs [27].

Table 2.1: The structure of organometallic halide MAX_3

| M | CH_3NH_3 | $\text{HC}(\text{NH}_2)_2^+$ |
|---|--------------------------|------------------------------|
| A | Pb | Sn |
| X | I | Br, Cl |

In general, PSCs are classified into two types based on their structures, first type is the planar heterojunction PSC which comprises a thin film of metal oxide layer or conductive polymer layer with a sandwich-like structure, this type is more flexible for device application. The second type which is nonflexible requires high manufacturing temperature includes depositing perovskites on a mesoporous metal oxides scaffold such as TiO_2 and Al_2O_3 that work as electron transfer layer.

Planar heterojunction PSCs require enormous efforts to make a good quality films, the rough and cracked film lowers cell performance and efficiency, also the thickness of that film needs to be less than 400 nm to obtain a sufficient charge collection.

Film morphology and the cell performance have been investigated using different techniques such as spin coating technique, vacuum evaporation, heat treatment and sequential deposition.

The cheapest technique used for formation of thin-film is the one-step spin coating which is commonly used in solution-processed. On the other hand, Vacuum evaporation is one of the most effective methods for controlling the prepared film quality and properties such as uniformity, morphology, and thickness, and numerous precursors can be also utilized to prepare different perovskites by using the co-evaporation technique [28].

Perovskites based on organic-inorganic halides have appeared in recent years as prospective materials for high-efficiency, simple, and environmentally friendly perovskite solar devices. Despite their ease of production, high flexibility and high-efficiency, low stability of the PSCs toward oxygen, solar radiation, humidity and heat limits their applications. Besides, attention must be given to the toxicity issues on the human, plants and animals health related to the high lead content of high efficient perovskites, and to appropriate ways of achieving large-scale production before commercialization [29].

2.2 The Components of DSSC

The main components of DSSC are photoactive working electrode (WE) which consist of highly porous nanostructured TiO₂ layer applied on a transparent conductive oxide substrates mainly a fluorine-doped tin oxide, abbreviated as FTO, sensitizing dye adsorbed on the TiO₂ thin layer as an working electrode (anode) and a counter electrode (CE) as a cathode which is either carbon black counter electrode or platinized electrode and liquid electrolyte containing mainly iodide/triiodide as redox couple [30].

2.2.1 The Working Electrode (WE)

The WE in DSSC comprise a wide bandgap nanostructures semiconductors attached to a transparent conductive mainly FTO or ITO substrates. Transparent conductive oxides are the most suitable glass substrates for DSSCs regarding to their unique properties like low sheet resistance which allows more excited electrons to complete the circuit, high optical properties and transparency at Vis –NIR regions as well as high chemical and thermal stability and durability. however, the glasses weight and inflexibility limit the DSSCs application fields [31].

ITO glass substrate doesn't make good contact with the photoanode layer which generally peeled off on the ITO surface therefore it is not the best option for fabrication of DSSC, additionally the sintering process of the photoanode layer is performed in open atmosphere at around 500 °C, the conductivity of the ITO film drops dramatically above 300 °C due to the presence of oxygen which can fill the vacancies of ITO and the resistivity value of ITO increases after the sintering process to 52 Ω/ sq [32].

Most of the DSSCs are currently fabricated using FTO glasses with 8-20 Ω /square resistance, FTO induced by replacing the oxygen by fluorine this doping improve both the conductivity and transparency of the TCO [33].

Highly porous semiconductors with Wide band gap of ($\sim 3\text{eV}$) are generally favorable for the photo electrode in DSSC. High chemical stability, high adhesion to the TCO and high electron mobility are the requirements for this layer. Tin oxide, zinc oxide, niobium (V) oxide, zirconium (IV) oxide and titanium oxide are the metal oxides which investigated in DSSCs.

Highest power conversion was achieved by using TiO_2 nanoparticles and thus, TiO_2 became the material of choice as a semiconductor for DSSC. TiO_2 is a wide band gap ($\sim 3.2\text{ eV}$), abundant, inexpensive and nontoxic material used widely in paint and food industries [34].

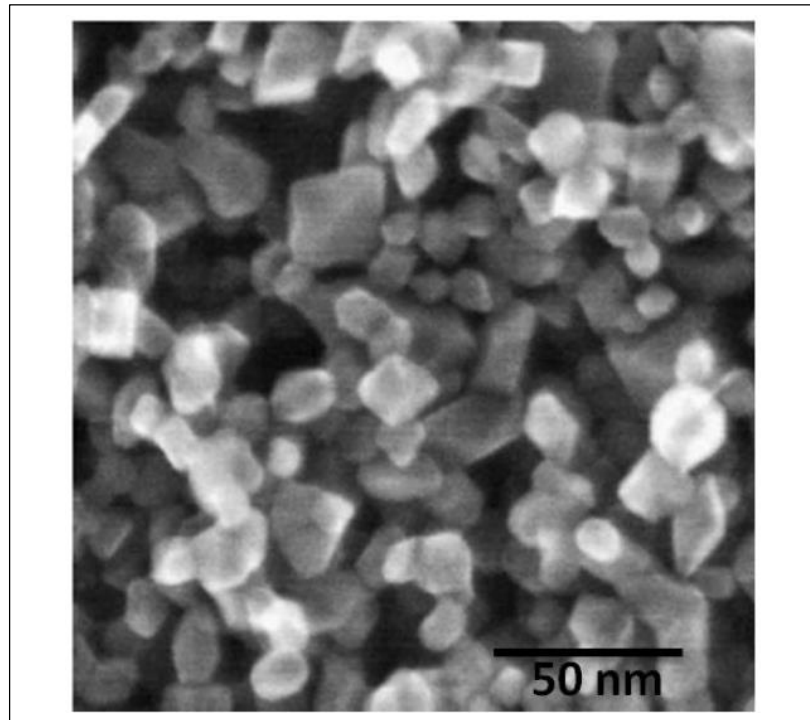


Figure 2.5: SEM and particle size distribution of TiO₂ anatase at 230 °C prepared by Grätzel and it gave the maximum photovoltaic performance so far [34]

Commercial Degussa (P25) TiO₂ (titania photocatalyst) is widely used for the preparation of nanocrystalline TiO₂ films, because of its high photocatalytic activity, its photocatalytic activity has been reported in too many papers since 1990 when Grätzel used first to prepare the photoanode TiO₂ film for DSSC Degussa (P25) TiO₂ consists of anatase and rutile crystallites with a ratio varies from 80:20 to 70:30 and 55 m²/g BET surface area [35].

Table 2.2: Crystalline composition of P25 collected from the same package [35]

| Entry | %Composition | | | Anatase: |
|-------|--------------|--------|-----------|--------------|
| | Anatase | Rutile | Amorphous | Rutile ratio |
| 1 | 78 | 14 | 8 | 5: 6 |
| 2 | 73 | 14 | 13 | 5: 2 |
| 3 | 82 | 16 | 2 | 5: 1 |
| 4 | 83 | 17 | 0 | 4: 9 |
| 5 | 84 | 16 | 0 | 5: 3 |
| 6 | 85 | 15 | 0 | 5: 7 |

The working electrode consists of inter-connected TiO₂ nanoparticles with the mean size of 15-30 nm. TiO₂ colloid form a transparent highly porous film as shown in figure (2.5), with a thickness of about 1-15 μm , higher film thickness increases the dye loading which increases the possibility of charge recombination with the electrolyte or the oxidized dye as a result affects the efficiency of the DSSC.

Doctor blading , screen printing and spin coating are the most common used techniques for the deposition of colloidal TiO₂ on the FTO glass substrate before the annealing process [36].

Annealing is usually performed at a high temperature ranging from 70 - 450 °C for a 45-60 min with the help of furnace or hot plate, enhancing the electrical inter-connection between the TiO₂ particles is achieved at high temperature. The dye

sensitization process is performed by dipping the coated electrode in a dye solution for 12-24h [37].

2.2.2 The Sensitizing Dye

The sensitizing dye plays a central role in performance and efficiency of the DSSCs, since it is responsible for capturing the sun light as well as forming the electron-hole pairs. Therefore much effort has been invested in the synthesis and development of novel dyes for DSSCs [38].

Dyes for DSSC application should have certain important properties for a good electron transfer to the CB of the TiO₂ semiconductor and hence result in high performance and efficiency of the device. These properties are namely: 1) the dye should be a good and stable electron donor compound with strong and broad absorption spectrum from Vis-NIR regions with high molar extinction coefficients, 2) the anchorage of the dye molecule (surface-anchoring groups such as carboxylic acid, hydroxyl, sulfonyl, amino groups) to the TiO₂ surface must be strong and the conduction band (CB) of TiO₂ should be localized lower than the LUMO level of the dye molecule for better electron injection, 3) the oxidation potential of the sensitizer (dye molecule) must be aligned with the electrolyte potential for ensuring an efficient dye regeneration, 4) high photo and chemical stabilities, good solubility, long lifetime and low toxicity are the other common requirements from the dye sensitizers [39].

Generally there are two main groups of the dyes used for DSSCs include: metal based complexes (transition metal coordination compounds) and metal free organic dyes. Ruthenium figure (2.6) and osmium polypyridyl complexes such as N3, N719 and black dye were used as effective metal based complexes for the development of high efficiency DSSCs with PCE of 11-12% [40].

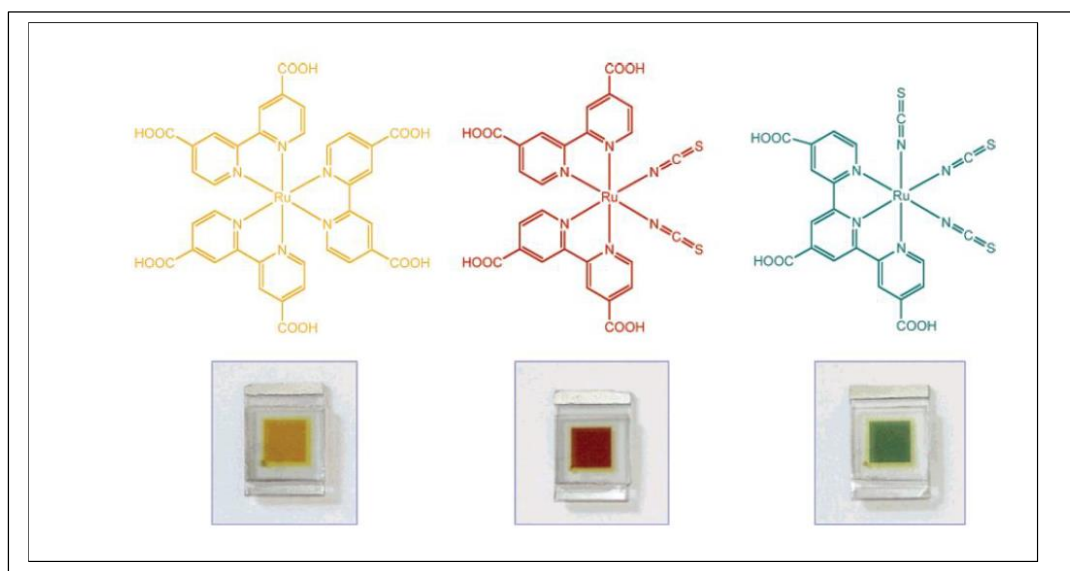


Figure 2.6: Structure of the ruthenium sensitizers: RuL₃(yellow), RuL₂(NCS)₂(red)N₃ and RuL(NCS)₃ (green) with their nanocrystalline TiO₂ film [41]

However, the process of synthesizing Ru and Os based complexes is complicated and these metals are rare occurring and being expensive. Moreover, transition metal coordination complexes contain heavy metals which have harmful environmental effect.

Alternatively, metal free organic dyes can be used as photosensitizers with an acceptable efficiency of about 5-12 %. The advantages of organic dyes include their easy availability, low cost, easy dye structural modifications, high stability (chemically, thermally and electrochemically) in addition to their relatively high molar extinction coefficients compared to the metal based complexes [42].

The common character of these organic dyes is donor- π -bridge-acceptor structure figure 2.7. Regarding to this structure new dyes can be easily designed with broader absorption spectra, well-adjusted HOMO/LUMO levels and enhanced intramolecular charge transfer and separation [43].

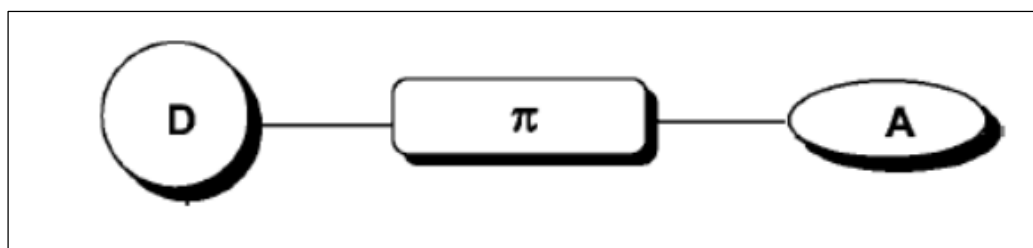
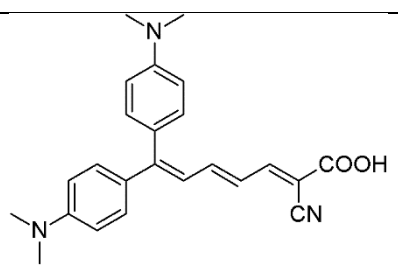
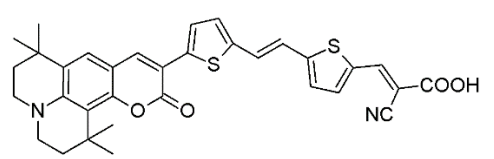
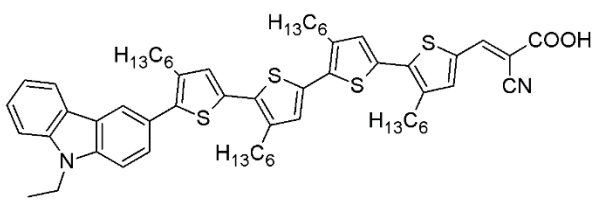
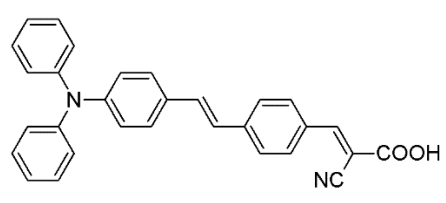
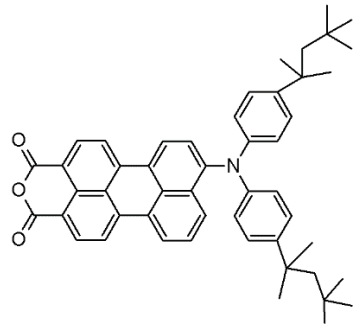
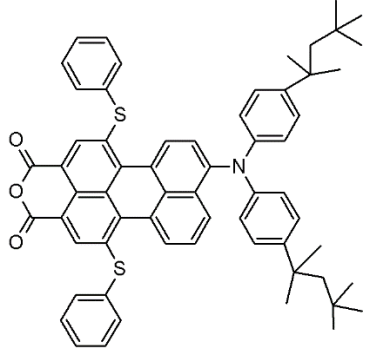
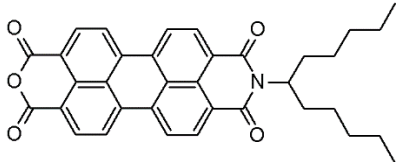
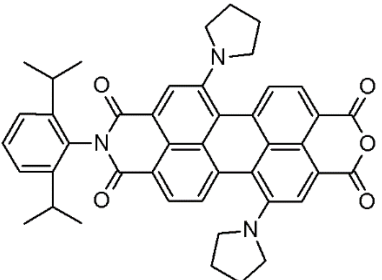


Figure 2.7: Donor- π -bridge-acceptor structure

For the last 10 years Organic compounds such as perylenes, indoline triphenylamine and xanthenes have been widely used as sensitizer for DSSCs. Table (2.3) shows some of the dyes used for DSSCs.

Table 2.3: Organic compounds used for DSSCs last years with their power conversion efficiencies

| NO. | Compound | η % | Reference |
|-----|---|----------|-----------|
| 1 |  | 6.8 | [44] |
| 2 |  | 8.2 | [45] |
| 3 |  | 7.7 | [46] |
| 4 |  | 9.1 | [47] |
| 5 |  | 3.9 | [48] |

| | | | |
|---|--|------|------|
| 6 |  | 6.8 | [49] |
| 7 |  | 1.61 | [11] |
| 8 |  | 2.6 | [50] |

2.2.3 Electrolyte

Liquid electrolyte which contains the redox couple iodide/triiodide is the most commonly used redox mediator for DSSCs. The charge transfer between working and counter electrodes (CE) occurs through the diffusion of I/I_3^- , completing the solar cell device circuit. The electrochemical potential at CE is dictated by the electrolyte redox potential, the oxidized dye is reduced by iodide producing triiodide at the working electrode, and the triiodide ion is reduced producing iodide at the counter electrode [51].

Liquid electrolyte should have some properties like high boiling point, low vapor pressure and high dielectric properties, low viscosity as well as high thermal, chemical and electrochemical stability to reach good performance and high efficiency of the solar cell device and make them reliable for the outside applications [52].

The redox electrolyte mainly consists of iodide such as lithium, sodium and imidazolium iodides which can provide different size cations, iodine and often additional additives like 4-tert-butylpyridine, which have good effect on the energetics of semiconductor (TiO_2), dye /electrolyte interface. Nakale et al. observed that using 4-tert-butylpyridine as an additive in liquid electrolyte with presence of Li^+ increases the open voltage circuit (V_{oc}) and decrease the electron recombination because of the possibility of complex formation between iodine and 4-tert-butylpyridine (i.e. low accessibility to accept electrons) [53].

At present, iodine-triiodide redox in relatively high boiling point solvents (nonvolatile) like ethyleneglycol, acetonitrile and valeronitrile were used to avoid the leakage and instability problems of the liquid electrolyte [54].

2.2.4 The Counter Electrode (CE)

CE consists of FTO glass substrate coated with a catalyst such as platinum (Pt), gold (Au), graphite, carbon black and activated carbon. These catalysts were used to afford reversible and fast electron transfer within the cell. Coating of catalysts on the FTO glass substrate can be deposited by dip coating, spin coating or screen printing techniques [55].

Platinum is the most favored catalyst for CE in DSSC because of its special properties such as high electrical conductivity and electrocatalytic activity toward triiodide reduction as well as high reflecting properties. However, Pt metal is expensive. Platinum coating can be achieved via thermal decomposition of chloroplatinic acid or hydrogen hexachloroplatinate (IV), this method requires low Pt quantities, and thus the cost can be reduced [56].

2.3 The Working Principle

The working principle of DSSC relied on the photo electrochemical processes which include three steps 1) light absorption, 2) charge separation, 3) charge collection.

Upon light irradiation, the dye molecules adsorbed on TiO₂ mesoporous layer absorb light (photons) and excite to higher energy levels (excited state) from their ground state equation (1), then the excited dye molecules either return back to the ground state by relaxation process or electron injection from their excited state to CB of the semiconductor (TiO₂) through the dye anchoring group and thus become oxidized equation (2).



The charge separation where an electron and a hole are located on TiO_2 and the oxidized dye molecule respectively is achieved on the photoanode layer, then the electrons are diffused through the TiO_2 mesoporous layer and reach to the TCO of the working electrode (anode) for extracting the collecting electrons to the counter electrode (cathode) for generating an external circuit.

The oxidized dye molecule is reduced (regenerated) by iodide in redox couple (I^-/I_3^-) equation (3), in return it is regenerated by the electrons released from the cathode equation (4), and subsequently the circuit is completed and the current is generated [57].



2.4 Electron Transfer Dynamic

DSSCs are photo electrochemical devices where competitively several processes of electron transfer occur in parallel as shown in figure (2.8). Unlike convention p-n junction cells, good collection efficiencies do not necessarily involve the presence of a local electrostatic field. The latest studies on the electron injection mechanism of the ruthenium polypyridyl complexes and perylene dyes from their excited state to the CB of the TiO₂ semiconductors have shown that their K_{inj} (electron injection rate constant) are relatively close, K_{inj} of ruthenium complexes and perylene dyes were reported to be $> 4 \times 10^{14} \text{ s}^{-1}$ and $5 \times 10^{13} \text{ s}^{-1}$ respectively. Similar characteristics are expected to be shown by electron injection from the dye molecules in both the electrolyte and the solid-state solar cells.

Upon solar irradiation, the dye molecules are photoexcited in femtoseconds (eq.5), the photoexcitation process is followed by electron injection process from dye excited states (Dye*) to CB of TiO₂ (eq.6) within the subpicosecond time scale, intramolecular relaxation through lattice collisions and photon emission might interfere with the injection process and therefore complicate and change the process time scale. Then relaxation of excited dye (Dye*) takes place in nanoseconds (eq.7) and it is quite slow in comparison with the electron injection process ensured the unity in the injection efficiency, dye's ground state is reduced by I⁻ in redox mediator within microsecond scale (eq.8).

The recombination of the TiO₂ electrons with the oxidized dye (eq.9) occurring within the millisecond time domain. And the back reaction of redox electrolyte (I₃⁻) (eq.10) with the oxidized dye take place within milliseconds or even seconds [58].

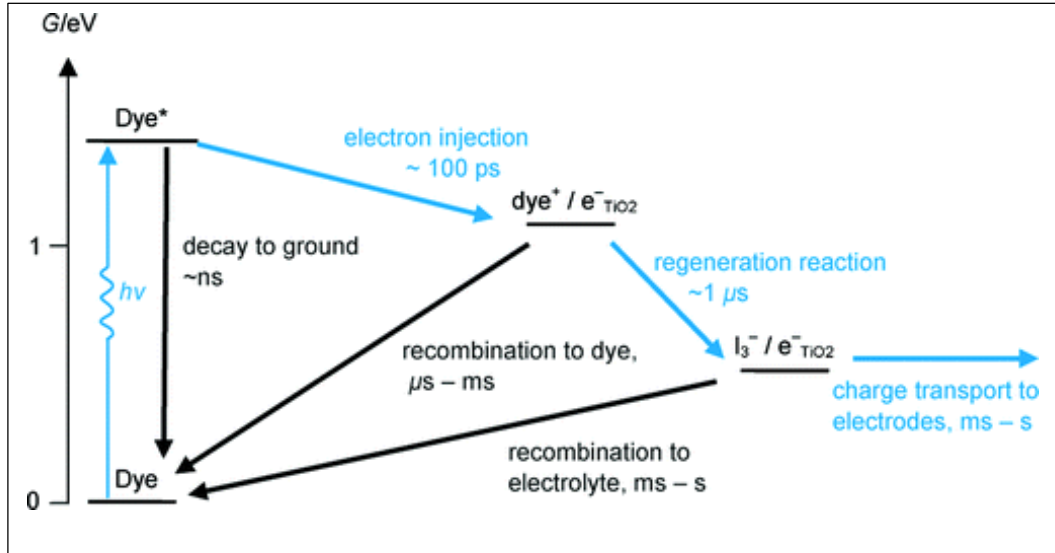
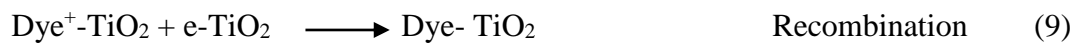
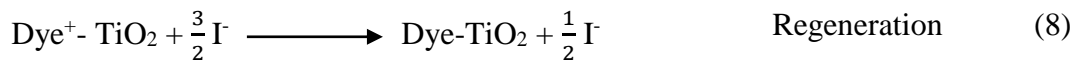
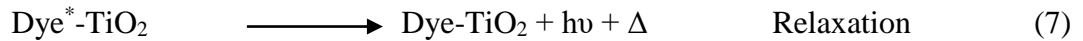
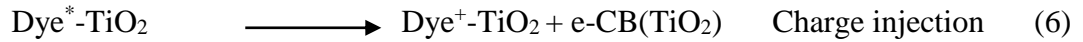
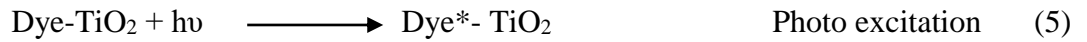


Figure 2.8: Electron transfer dynamic process in DSSC



2.5 Perylene Diimide Derivatives for OPV

Perylene diimides have been used extensively in different solar cell devices as metal free dyes owing to their ease of functionalization, good chemical, photochemical and thermal stability, broad and strong absorption properties, relatively high extinction coefficient ($\geq 10^5 \text{ M}^{-1} \text{ cm}^{-1}$) in the visible region and non-toxicity. Moreover, perylene dyes have high electron affinity and thus can couple to most of the electron donating groups to form donor/acceptor systems. Perylene molecules can also be applied in DSSC by using the anhydride or carboxylic acid groups as anchors [59].

In literatures, perylene derivatives have been investigated in DSSC devices as sensitizers but their PCE was relatively low (0.002-1.9%) compared to the other organic dyes, probably due to their strong electron withdrawing capacity which makes the electron injection to the CB of the TiO_2 more difficult as well as their low solubility and high aggregation possibility.

Recently, perylene derivatives based DSSC devices have reached power conversion efficiencies around 2.6% after a bay substitution of perylene core with strong electron donating substituents which increase the electron density. This continuous development in perylene dyes in term of introducing different substituents have been attracted a great interest dealing with the efficiency issue of DSSC devices based on perylene dyes [50].

2.6 Perylene Diimide Derivatives (PDIs)

Regarding to their outstanding n-type semiconducting, absorption, fluorescence, and electrochemical properties as well as thermal and chemical stabilities perylene derivatives are materials of great scientific and industrial interest among the polycyclic aromatic hydrocarbons during the last decade.

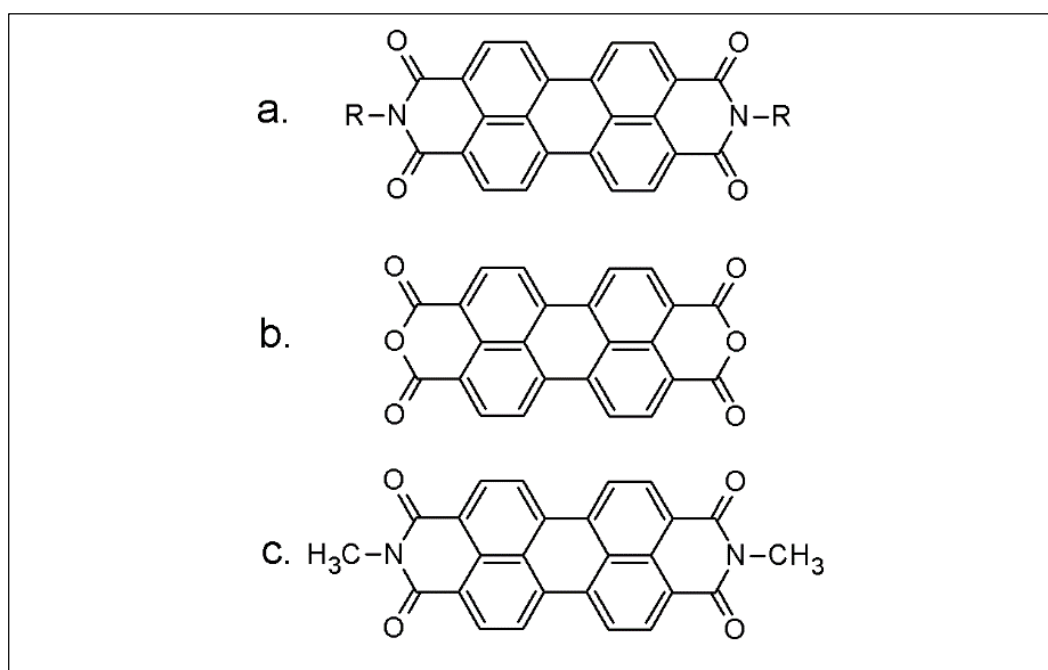


Figure 2.9: Structures of a) perylene diimide (PDI), b) perylene dianhydride (PDA) and c) first industry pigment based on PDI reported by Harmon colour in 1930 known as pigment Red 179

Initially perylene dyes were used exclusively in vat dyeing process as red colorant, nowadays PDIs have been intensively explored in different fields such as organic solar cells, NIR dyes, sensors, optical switches, optical micro cavities and photo-conduction materials [60].

Two strategies were used for modifying the structure of perylene dyes include various imide substitution and/or (1, 6, 7 and 12) bay substitution. Substitution of imide position using sterically hindered imido-substituents mainly controls their solubility, aggregation properties as well as the packing arrangement in solid state. However, imide substitution of perylene dyes doesn't affect the electronic and optical properties such absorption, emission and HOMO/LUMO energies considering the FMO nodes on HOMO/LUMO orbitals at the nitrogen of imide position.

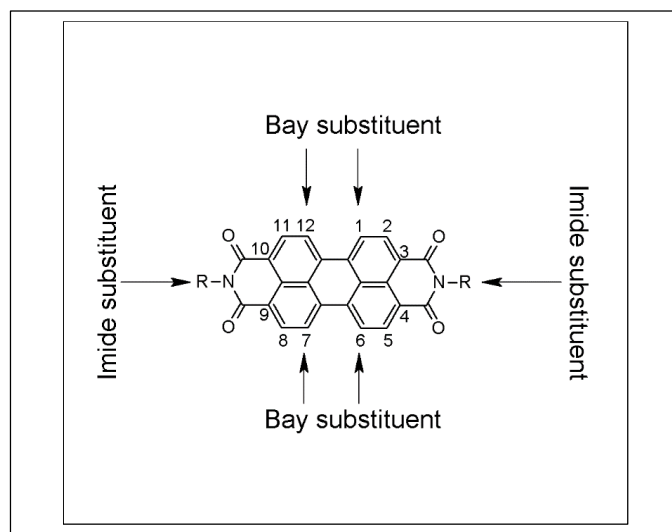


Figure 2.10: Structure of Perylene diimide

The molecular structure of perylene dyes imply a planar rigid aromatic core which exhibit strong π - π molecular interactions. Principally, modifying the opto-electronic properties of the PDIs can be achieved via bay substitution of the electron deficient aromatic perylene core. The solubility of PDIs can be increased significantly by bay substitution due to the twisting in perylene core (disturbing the π - π molecular interactions) as well as affecting the photoinduced charge-transfer of perylene dyes [61].

2.7 Photo-Induced Electron Transfer

It is one of the fluorescence quenching mechanism in which an excited state electron transfer takes place from the donor to the acceptor as a result photo induced charge separation is generated (i.e. redox reaction occur in excited state). Figure 2.11 shows the oxidative-reductive electron transfer process.

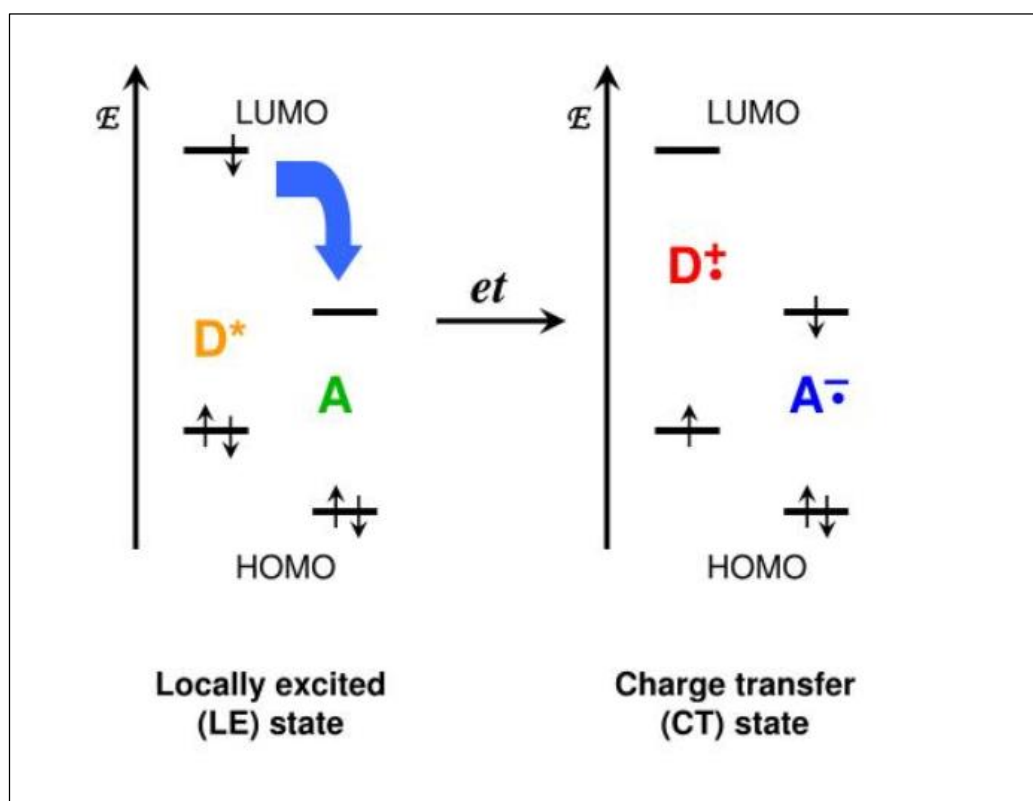


Figure 2.11: Photo-induced electron transfer process

Photo induced electron transfer from a donor to an acceptor is widely studied to mimic the natural photosynthetic reaction center and to investigate the prospect of molecular materials in photovoltaic energy conversion [62].

Chapter 3

EXPERIMENTAL

3.1 Materials and Reagents

All chemicals used in synthesis of perylene derivatives were of commercial grade. Perylene-3, 4, 9, 10-tetracarboxylic dianhydride, dodecyl amine, 1-phenylethylamine, 2-decyl-1-tetradecanol, potassium carbonate, zinc acetate, iodine and bromine were acquired from Aldrich and used without additional purification.

DMF and m-cresol as well as isoquinoline which were used as reaction solvents in this work were obtained from Aldrich. These solvents were dried using activated molecular sieves in size 4 Å and stored under inert atmosphere until use. The solvents for photo physical and electrochemical measurements were of spectroscopic grade.

Sodium tetrafluoroborate (supporting electrolyte) and ferrocene (internal reference) were obtained from Fluka and were put to use without further purification.

Materials used in fabrication of DSSC were FTO (SnO₂: F, Pilkington TEC-15; R_{sheet}: ~ 20 Ω/sq), TiO₂ (Degussa P25, Germany), acetyl acetone (Aldrich), Tritone x-100 (Merck, Germany), Tintanium isopropoxide (Aldrich), 1-Methyl-3-propyl-imidazolium iodide (Aldrich), litium iodide (Aldrich), tetrabutyl prridine (Aldrich) and hydrogen hexachloroplatinate(Fluka).those materials were stored in dry

atmosphere until use and used received. Ethanol, acetonitrile and isopropanol were purchased from Aldrich and used as solvents after drying and degasing.

3.2 Instrumental Part

Thin-Layer Chromatography (aluminum coated films by silica gel, Merk), abbreviated as TLC, and was used to monitor the reactions progress. Mattson (USA) satellite FT-IR spectrophotometer was utilized for recording the FT-IR spectra via KBr pellets. Solution and solid state UV/Vis absorption spectra were measured using Varian-Cary 100 spectrophotometer. Emission, excitation spectra and absolute fluorescence quantum yield data were obtained by Varian-Cary Eclipse spectrophotometer.

Mass spectrometric analysis were performed on Finnigan MAT 311A machine and the data have been reported in m/z %. ^1H and ^{13}C NMR of the synthesized perylene diimides were also characterized with 400 MHz Buker spectrometer using tertamethylsilane as an internal reference. Elemental analysis which used to estimate carbon, hydrogen and nitrogen content was obtained on Carlo-Erba-1106 analyzer.

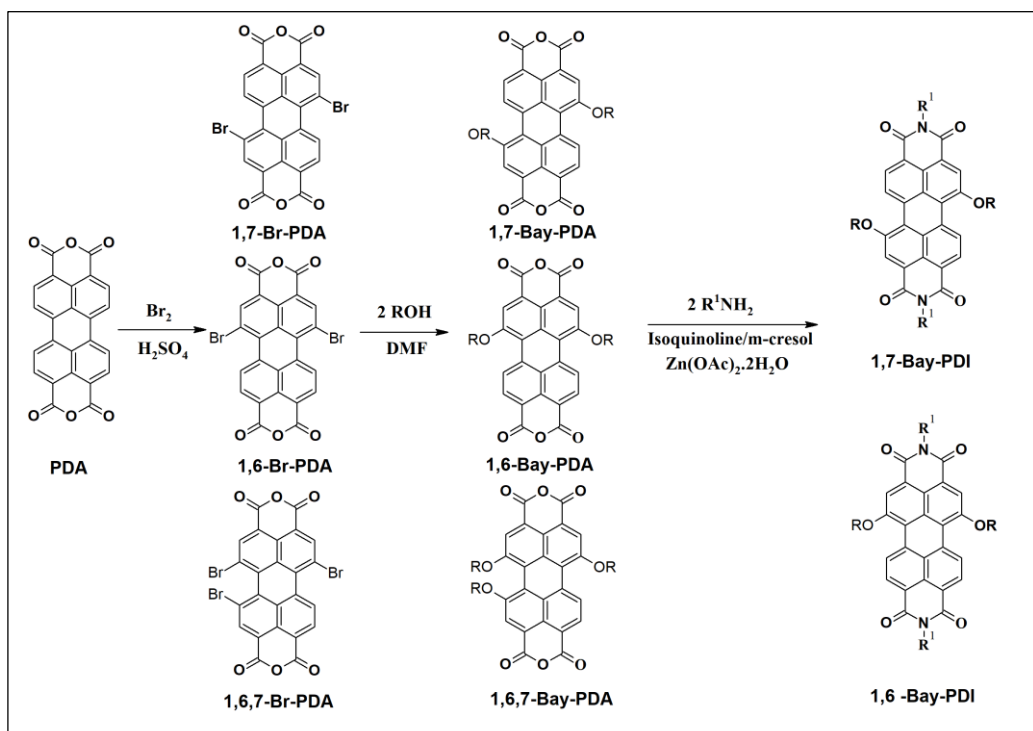
Thermal properties of the synthesized compounds were identified by thermogravimetric analysis, abbreviated as (TGA), and differential scanning calorimetry, abbreviated as (DSC), using Perkin-Elmer/Pyris 1 under either nitrogen or oxygen atmosphere at specific heating rate (10°C) and samples weight around 10 mg. Solution and solid state Electrochemical analysis were measured with Gamry machine workstation equipped with reference 600 computer monitored Potentiostat/Galvanostat/ZRA system under argon atmosphere.

Cyclic voltammetry measurements were conducted in TBAPF₆ solution in acetonitrile with concentration of 0.1M, supporting electrode, at 100 mVs⁻¹ scan rate at room temperature, A glassy carbon was utilized as a working electrode after polishing with 0.05 μm Buehler alumina, platinum wire, and Ag/Ag⁺ couple were applied as counter electrode, and reference electrode, respectively. Ferrocene - Ferrocenium couple was applied as internal reference for the determination of E_{red onset} values.

Current–voltage characteristics (J–V curves) of the DSSC structures [FTO/nc-TiO₂/perylene dye/PDI/I⁻/I₃⁻/PT/FTO] were measured by Keithley 2400-source meter in dark and under illumination using halogen lamp to evaluate their photosensitivity.

3.3 Synthesis of (1,7)-Bay-Substituted Perylene Diimides

The synthetic route of 1, 7-disubstituted perylene diimides is outlined in scheme 3.1. The synthesis of all the reported compounds has been inaugurated with PDA, and final compounds were prepared by three steps include bromination, bay substitution and imidization in overall yield between 70% and 90%.



Scheme 3.1: The synthetic route of 1,7-disubstituted perylene diimides

In the first step, a regioisomeric mixture of (1,7) 1,6-dibrominated perylene dianhydride with a very small amount of 1,6,7-tribrominated perylene dianhydride were prepared from PDA with bromine in sulfuric acid following a known procedure. These compounds (1,7- 1,6- and 1,6,7-Br-PDA) are basically insoluble in various organic solvents therefore the separation of the (1,7) 1,6-dibrominated perylene dianhydride mixture has been performed at the later step for the corresponding bay substituted PDAs.

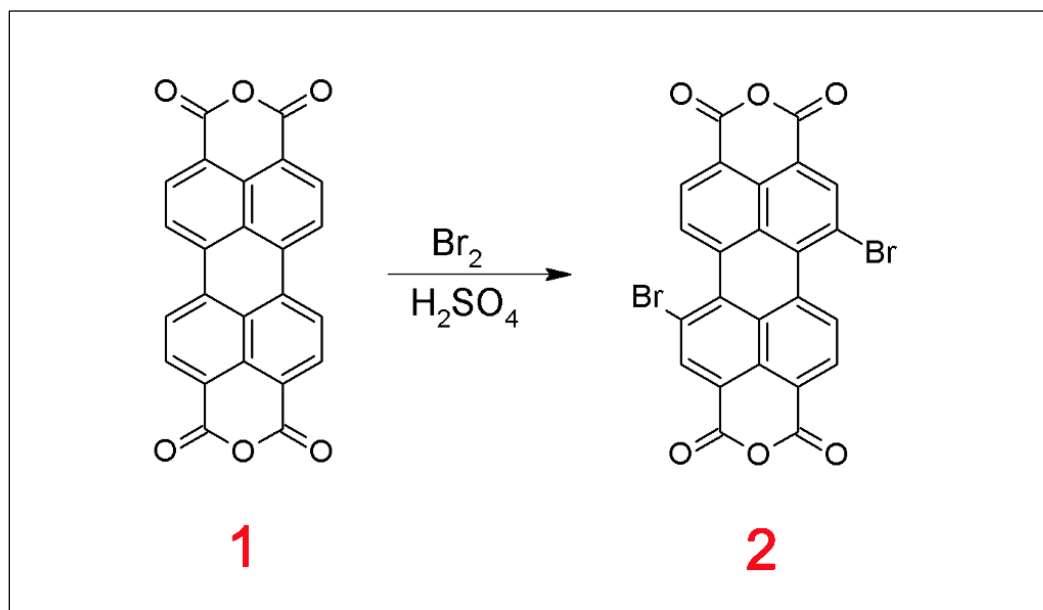
Bromine atoms in the second step were substituted by different substituents to synthesize bay- substituted perylene dianhydride the resulting products were more soluble and 1,6,7-PDA regioisomer was separated. Finally, N, N'-Imidization of 1,7-bay substituted perylene dianhydride with various amines in isoquinoline/m-

cresol at reflux yielded 1, 7- disubstituted as a major product compared to 1, 6- disubstituted PDI.

3.3.1 Synthesis 1,7-Dibromoperylene-3, 4, 9, 10-tetracarboxylic dianhydride (2)

According to procedure reported in [4], PDA (1) (2g, 5.10 mmol) was dissolved in 30 ml of (95-97%) H₂SO₄ and stirred at ambient temperature for about 6 h, and then temperature was increased to 60°C for about 24h. Then (0.06g, 0.236 mmol) of I₂, iodine, was added as a catalyst into the reaction mixture at ambient temperature and the mixture was stirred for about 2 h in same condition and 5 h at 55 °C. (0.8ml, 15,61mmol) of Br₂,bromine, was added drop wise within 1 h to reaction mixture with continuous stirring at ambient temperature, then temperature was increased to 85°C for 24 h and 100°C for 2 h .the extra bromine was evaporated by passing argon gas. To precipitate the compound 20ml of water was added slowly to the reaction mixture and the compound was collected via vacuum filtration.

Finally the collected compound was washed with water by using soxhlet apparatus to remove the excess of sulfuric acid for about 24 h then the crude product was dried at 120°C in vacuum oven.

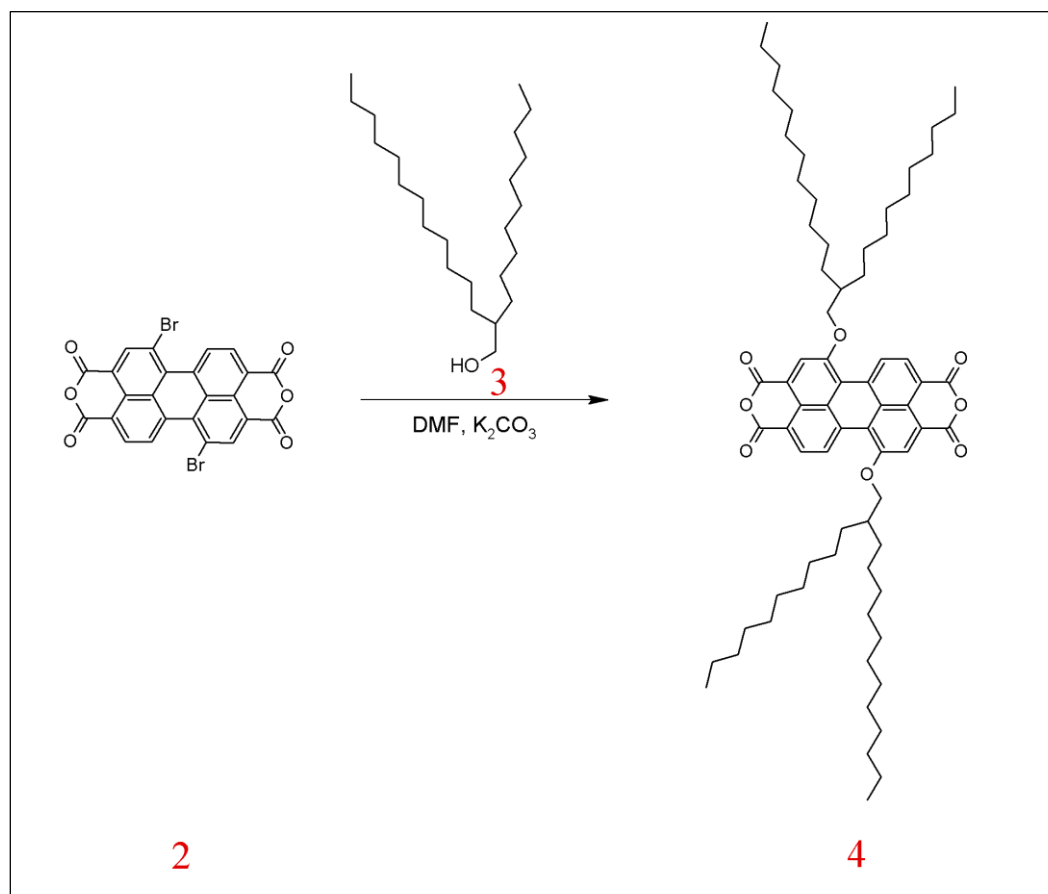


Scheme 3.2: Synthesis of compound 2

FTIR (KBr, cm^{-1}): ν : 3045 (aromatic C-H stretch), 1771, 1725 (anhydride C=O stretch), 1592 (aromatic C=C stretch), 1038 (anhydride C-O-C stretch), 693 (C-Br stretch).

3.3.2 Synthesis of 1, 7-Di (2-decyltetradecanoyl) perylene-3, 4, 9, 10- tetra carboxylic bisanhydride (4)

2 (1g, 1.817 mmol), 2-decyl-1-tertdecanol, 3 (1.88 g, 5.301 mmol), and K_2CO_3 (0.622g, 4.501 mmol) have been dissolved in dried DMF (200 ml). The solution was refluxed with continuous stirring under argon atmosphere for about 12 h. Then the reaction mixture was added to (100ml, 1:1) cold acetic acid: cold water solution and was left overnight for cooling down to $-8\text{ }^\circ\text{C}$. The formed precipitate was then filtered off with vacuum filtration. The collected product was purified with water by soxlet apparatus for 24h and the crude product was dried at $120\text{ }^\circ\text{C}$ using vacuum oven.



Scheme 3.3: synthesis of compound 4

Yield: 69.7% (1.39g); **color:** dark purple powder.

FTIR (KBr, cm⁻¹): ν : 3065 (aromatic C-H stretch), 2920, 2850 (aliphatic C-H stretch), 1763, 1731(anhydride C=O stretch), 1590(aromatic C=C stretch), 1011 (ether C-O-C stretch).

¹H NMR (400 MHz, CDCl₃:CF₃COOD (3:1)): δ H (ppm) = 8.44–8.42 (d, J = 8.0 Hz, 2Ar-H), 8.36–8.34 (d, J = 8.0 Hz, 2Ar-H), 7.5 (s, 2Ar-H), 4.21 (d, J = 7.8 Hz, 2CH₂), 1.87 (m, 2CH), 1.63 (m, 4 CH₂), 1.32–1.15 (m, 36CH₂), 0.86 (m, 4CH₃).

¹³C NMR (100.6 MHz, CDCl₃:CF₃COOD (3:1)): δ C (ppm) = 162.14, 160.92, 138.59, 131.75, 125.28, 123.07, 122.43, 110.22, 74.59, 42.78, 41.43, 41.30, 37.36, 34.04, 30.33, 29.33, 27.13, 22.71, 16.06.

UV-Vis (DMF, λ_{\max} nm): 421, 484, 518.

UV-Vis solid state (λ_{max} nm): 472,498,541.

Fluorescence (DMF, λ_{max} nm): 534, 570. $\Phi_{\text{f}} = 30\%$

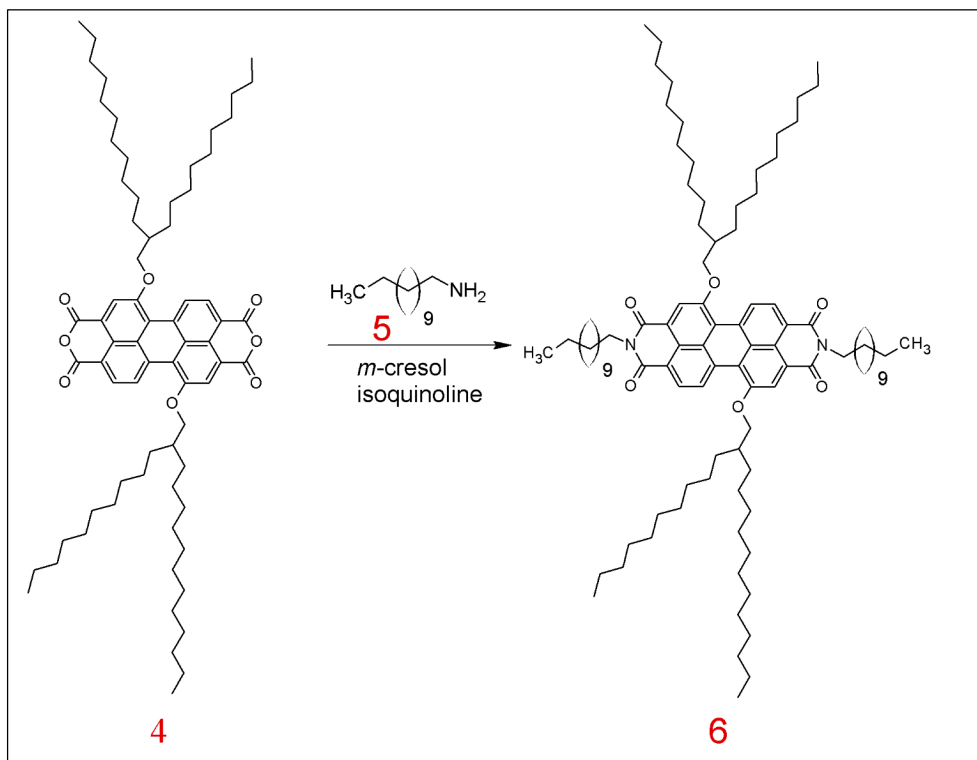
Anal. Calcd for ($\text{C}_{72}\text{H}_{104}\text{O}_8$) (M_w , 1097.59): C, 78.69%; H, 9.55%.

Found: C, 78.62%; H, 9.46%.

3.3.3 Synthesis of N, N'-bisdodecyl-1, 7-di (2-decyltetradecanoyl) perylene- 3, 4, 9, 1-tetracarboxylic bisimide (6)

4 (1 g, 0.911 mmol), dodecyl amine, 5 (0.52g, 2.805 mmol) as well as Zn (OAc)₂·2H₂O (0.2 g, 1.09 mmol) were dissolved and heated under argon atmosphere in a freshly dried solvent mixture of m-cresol (50ml) and isoquinoline (8ml) at 120 °C for around 4 h, 160 °C for 4 h and then the temperature was increased to 200 °C for 2 h to complete imidization. The reaction mixture was then cooled down to 25°C and added to cold methanol (100 ml).

The precipitated compound was filtered off using vacuum filtration, and then washed with methanol, CH₃OH, in Soxhlet apparatus for 24 h to eliminate the unreacted starting materials and high boiling solvents (m-cresol and isoquinoline). The crude product the dried at 120°C using vacuum oven.



Scheme 3.4: Synthesis of compound 6

Yield: 91.95% (1.2 g); **color:** Black powder

FTIR (KBr, cm^{-1}): ν : 3065 (aromatic C-H stretch), 2920, 2850 (aliphatic C-H stretch), 1693, 1656(imide C=O stretch), 1587(aromatic C=C stretch), 1339 (C-N stretch), 1237(ether C-O-C stretch).

^1H NMR (400 MHz, $\text{CDCl}_3:\text{CF}_3\text{COOD}$ (3:1)): δH (ppm)=8.65–8.64 (d, J =7.6 Hz, 2Ar-H), 8.57–8.56 (d, J =7.6 Hz, 2Ar-H), 7.35 (s, 2Ar-H), 4.18 (d, J =7.8 Hz, 2 CH_2), 3.66 (t, J =7.2 Hz, 2 CH_2), 2.35–2.31 (m, 2CH), 1.63 (m, 6 CH_2), 1.42–1.06 (m, 56 CH_2), 0.88–0.83 (m, 6 CH_3).

^{13}C NMR (100.6 MHz, $\text{CDCl}_3:\text{CF}_3\text{COOD}$ (3:1)): Δc (ppm) = 162.14, 160.92, 138.59, 131.75, 125.28, 123.07, 122.43, 110.22, 74.59, 66.93, 42.78, 41.43, 41.30, 37.36, 34.04, 30.33, 29.33, 27.13, 22.71, 16.06.

UV-Vis (DMF, λ_{max} nm): 427, 458, 487, 522.

UV-Vis solid state (λ_{max} nm): 550.

Fluorescence (DMF, λ_{max} nm): 536, 575. $\Phi_{\text{f}} = 14\%$

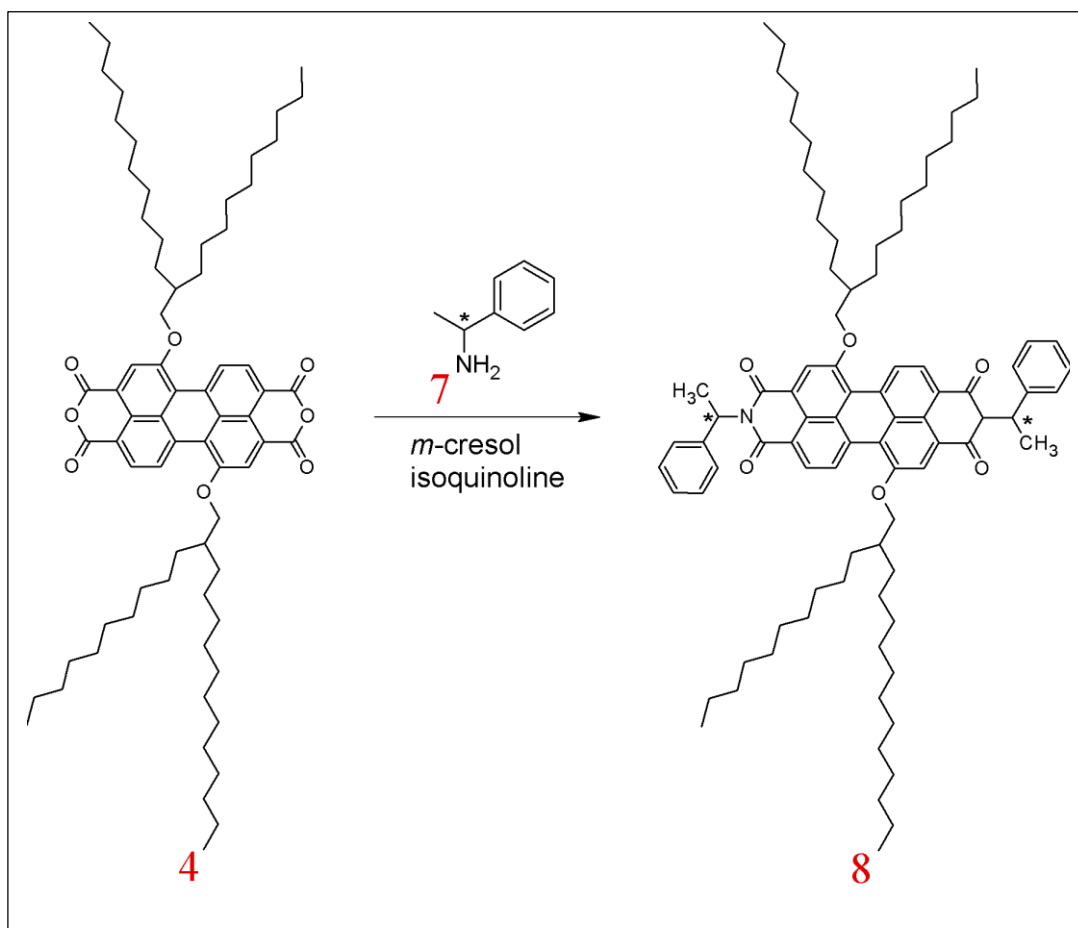
Anal. Calcd for (C₉₅H₁₅₄N₂O₆) (M_w, 1432.26): C, 80%; H, 10.84%; N, 1.96%.

Found: C, 79.8%; H, 11.05%; N, 2.09 %.

3.3.4 Synthesis of N, N'-bis((S)-(-)-1-phenylethyl)-1,7-di(2decyltetradecanoyl) Perylene -3,4,9,10-tetracarboxylic bisimide (8)

4 (1 g, 0.911 mmol), 1-phenylethylamine, 7 (0.36 ml (0.34g) , 2.805 mmol) as well as Zn(OAc)₂·2H₂O (0.2 g, 1.09 mmol) were dissolved and heated under argon atmosphere in a freshly dried solvent mixture of m-cresol ,(50ml) , and isoquinoline,(8 ml), at 120 °C for around 4 h, 160 °C for 4 h and then the temperature was increased to 200°C for 2 h to complete imidization. The reaction mixture was cooled down to 25°C and added to cold methanol, MeOH, (100 ml).

The precipitated compound was filtered off using vacuum filtration, then treated with MeOH in a Soxhlet apparatus for 24 h to eliminate the unreacted starting materials and high boiling solvents (m-cresol and isoquinoline) followed by acetone soxhlet for further purification and dried under vacuum.



Scheme 3.5: Synthesis of compound 8

Yield: 88% (1.048 g); **color:** Black powder

FTIR (KBr, cm^{-1}): ν : 3060 (aromatic C-H stretch), 2920, 2850 (aliphatic C-H stretch), 1694, 1654 (imide C=O stretch), 1585 (aromatic C=C stretch), 1325 (C-N stretch), 1243 (ether C-O-C stretch).

^1H NMR (400 MHz, $\text{CDCl}_3:\text{CF}_3\text{COOD}$ (3:1)): δH (ppm) = 8.44–8.42 (d, $J=8.0$ Hz, 2Ar-H), 8.36–8.34 (d, $J=8.0$ Hz, 2Ar-H), 8.08 (s, 2Ar-H), 7.42–7.40 (d, $J=8.0$ Hz, 4Ar-H), 7.35 (t, $J=7.1$ Hz, 6Ar-H), 6.60 (q, 2CH), 4.32 (d, $J=7.8$ Hz, 2 CH_2), 2.22–2.19 (d, $J=8.0$ Hz, 2 CH_3), 2.02 (m, 2CH), 1.77–1.27 (m, 40 CH_2), 0.86 (m, 4 CH_3).

¹³C NMR (100.6 MHz, CDCl₃:CF₃COOD (3:1)): δ C (ppm) = 165.43, 156.68, 140.43, 139.49, 131.93, 131.24, 130.33, 128.33, 127.47, 126.73, 124.53, 109.90, 73.74, 54.45, 51.90, 44.84, 43.20, 42.52, 37.50, 32.34, 29.47, 27.20, 22.45, 19.89, 15.42.

UV-Vis (DMF, λ_{\max} nm): 430, 483, 521.

UV-Vis solid state (λ_{\max} nm): 564.

Fluorescence (DMF, λ_{\max} nm): 536, 576, 636. $\Phi_f = 10\%$

Anal. Calcd for (C₈₈H₁₂₂N₂O₆) (M_w, 1303.92): C, 81.06%; H, 9.43%; N, 2.15%.

Found: C, 80.95%; H, 9.37%; N, 2.10 %.

3.4 DSSC Device Fabrication

3.4.1 Transparent Conducting Oxide Substrates (TCO)

Selection of appropriate TCOs is important for fabricating DSSC devices since they work as current collectors in the devices. TCO glass substrates should exhibit high electrical conductivity, low visible light absorption and low resistivity. However decreasing resistivity is correlated with decreasing transmission of given material.

TCOs should show high stability upon heating, typically TCOs remain stable to the temperatures slightly above their optimized deposition temperature. Some sorts of TCO such as indium doped tin oxide, abbreviated as ITO, show an increase in resistivity by 71%-162% after heating to 450-500 °C for 45-60 min. also, ITOs show significant conductivity losses when heating over ~ 200°C, losing conductivity can be related to the dropping of the oxygen vacancies which work like electron suppliers.

By comparison, SnO₂ films doped with fluorine (FTO) are generally very stable and more applicable for fabrication of DSSC devices. In this work, FTO glasses were used,

initially, the FTO glasses show resistivity of $\sim 15\text{-}20 \text{ } \Omega/\text{sq}$ using multimeter measurement.

Previous to the TiO_2 layers deposition, FTO glasses were washed by subsequent sonification in acetone, ethanol and distilled water 15 minutes in each solvent, if necessary cleaned FTO glasses were kept in dry ethanol (EtOH). Air spray was used to dry the glasses before applying the TiO_2 layers.

3.4.2 Preparation of TiO_2 Compact Layer

A TiO_2 compact layer was prepared using procedure reported by [63], 3 ml of titanium isopropoxide and 9 ml of absolute ethanol were mixed in a beaker, at the same time a 2nd solution of 2 ml acetyl acetone and 6 ml ethanol were mixed, then in an ice bath the previous solutions were stirred for 24h and diluted with ethanol in 1:1 ratio.

Then TiO_2 compact layer was coated on the conducting FTO glass using spin coating technique starting from 4000 rpm for 40 sec to 3000 rpm, 2000 rpm and 1000 rpm 10 sec for each. Then the prepared film was sintered at 450°C for 30 min.

3.4.3 Preparation of Nanocrystalline TiO_2 Layer

A mesoporous TiO_2 layer which is thicker than the compact layer to adsorb the sensitizer on the surface was prepared using technique reported [64] and employed commercial TiO_2 (P25, Degussa), TiO_2 nanoparticles of 6g was blended in a porcelain mortar with 2ml water containing 0.2 ml acetylacetone to avoid reaggregation of the particles, grinding process was continued with slow addition of water (8ml) and Triton X-100 (0.1ml) to facilitate the diffusion of the colloids until forming thick paste without any clots.

The mesoporous layer was coated as a 2nd layer on the conducting FTO glass substrate which was coated previously with the compact layer and spin coated at 4000 rpm , 3000 rpm, 2000 rpm and 1000 rpm for 40 sec,5sec,5sec and 3sec respectively. Then the film was sintered at 450-550 °C for 45 min.

3.4.4 Sensitization

Perylene dye solutions were prepared in freshly dried organic solvents (CHL, DMF and NMP) with a concentration of 0.3 - 0.5 mM figure 3.1 shows all the perylene dyes used for fabrication of the DSSC devices in this project.

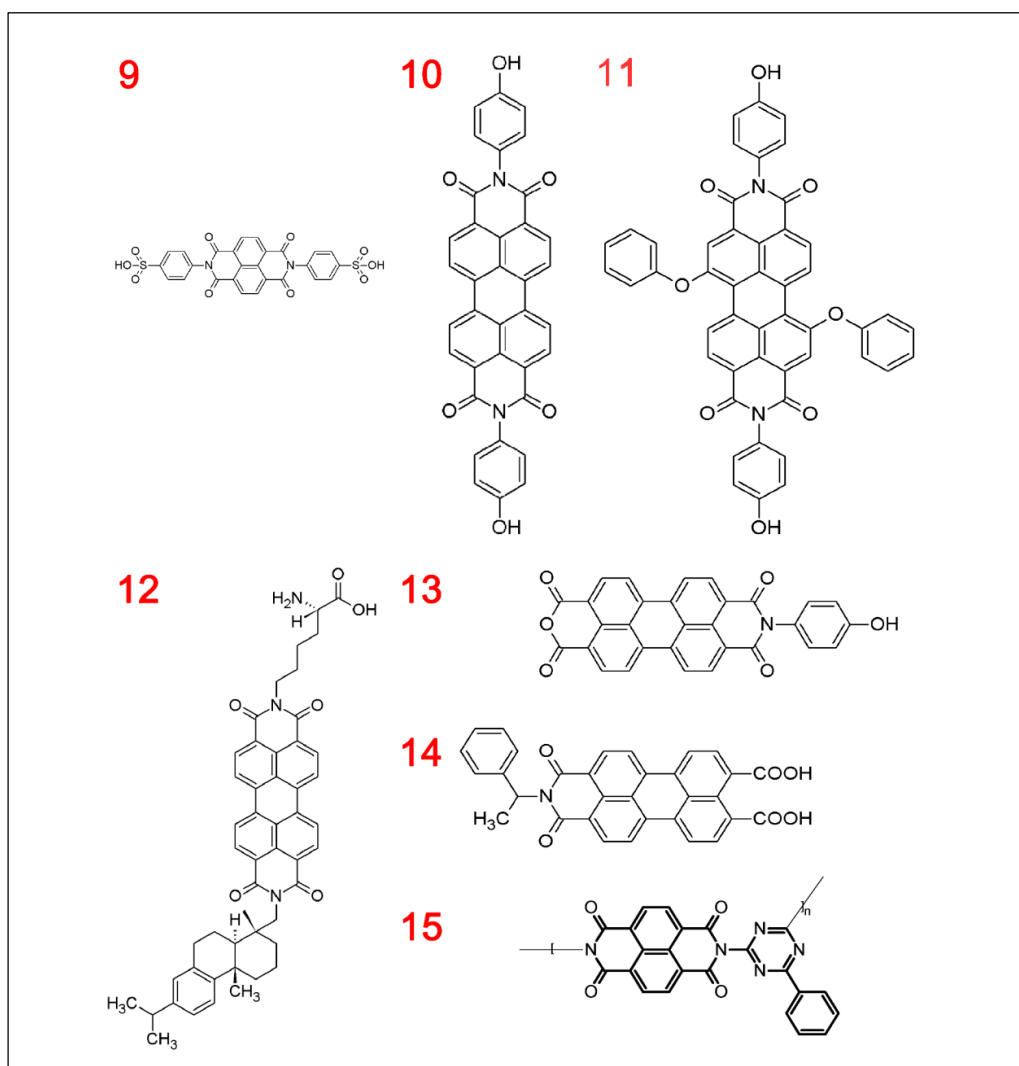


Figure 3.6: Dye structures used for fabrication of DSSCs

The TiO₂ coated electrode was immersed into dye solutions and kept for 24 h, the dye sensitization was done immediately after the sintering process at 450-550 °C and cooling to 70-100 °C to prevent the rehydration of TiO₂ electrode which lowers the electron injection efficiency of the sensitizer. After completion of sensitization, the electrode was removed from the dye solution and washed by dried acetonitrile to remove the excess of dye solution.

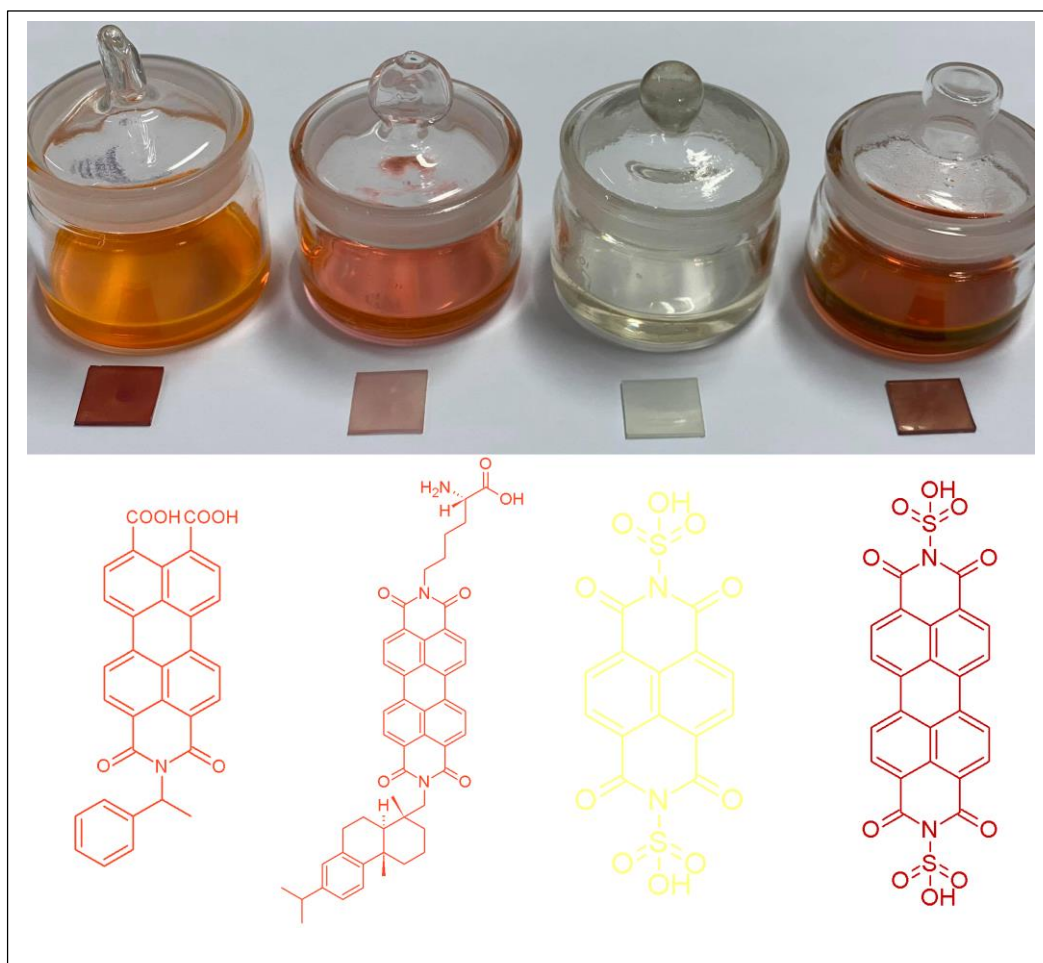


Figure 3.2: The dyes adsorbed on the TiO₂ layers

3.4.5 Deposition of the Counter Electrode

After cleaning the FTO glass substrate as mentioned in section 3.3.1, the FTO glass substrate was pretreated with 5% NaOH solution and rinsed with water prior to the deposition of the platinum layer. Platinization of counter electrode was accomplished by spin coating of the FTO glass substrates with hydrogen hexachloropalladate (IV) solution (0.5%) in freshly dried isopropanol and annealed at 450°C for 30 min after evaporating the solution for few minutes at room temperature as shown in figure 3.3.

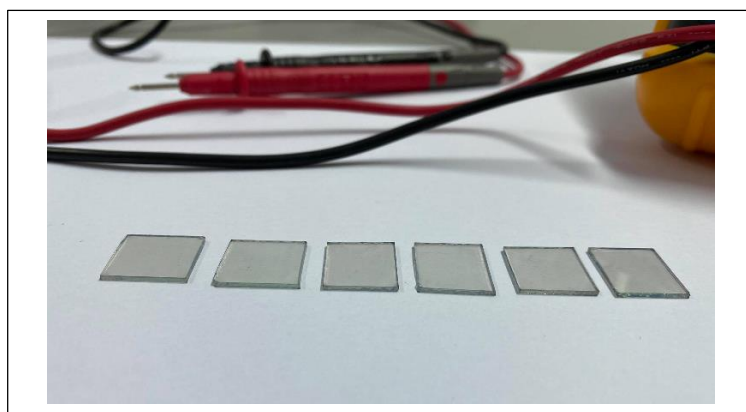


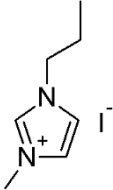
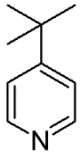
Figure 3.3: Pt coated counter electrode

The catalytic activity of platinum decreases by exposing to the air at room temperature therefore the platinized counter electrode should be processed within few hours after sintering at 450 °C.

3.4.6 Preparation of the Redox Mediator

Redox electrolyte was prepared by dissolving 1-Methyl-3-propyl-imidazolium iodide (0.6 M), lithium iodide (0.07 M) and iodine (0.05 M) in dried acetonitrile beside 0.05 M t-butyl pyridine was used as an additive. Table 3.1 shows the composition of the liquid electrolyte for DSSCs.

Table 3.1: Materials used for preparing the liquid electrolyte

| Compound | Structure | MWt /g.mol ⁻¹ | Density g.cm ⁻³ | Mass mg | Concentration mol.L ⁻¹ | Volume ml |
|----------------|---|-----------------------------|-------------------------------|------------|--------------------------------------|--------------|
| PMII |  | 252.1 | 1.54 | 25.3 | 0.6 | 0.164 |
| Lithium iodide | LiI | 133.85 | 4.08 | 9.37 | 0.07 | 0.0023 |
| Iodine | I ₂ | 126.9 | 4.93 | 6.35 | 0.05 | 0.0013 |
| TBP |  | 135.2 | 0.923 | 6.83 | 0.05 | 0.0074 |
| Acetonitrile | CH ₃ CN | 41.05 | 0.786 | 0.786 | 0.02 | 1 |

3.4.7 Sealing of the Device

The DSSCs were assembled in sandwich geometry by replacing the working electrode on the top of the counter electrode, the two electrodes were held together by using binders then few drops of the freshly prepared liquid electrolyte was inserted to the gap between the working electrode and counter electrode immediately to prevent the rehydration of the electrodes, the excess of electrolyte was carefully wiped off using paper towel.

The fabricated cell (open cell) was lasting until the evaporation of whole electrolyte and the performance of the cell was decreasing over the time however it was giving chance for plenty of measurements.

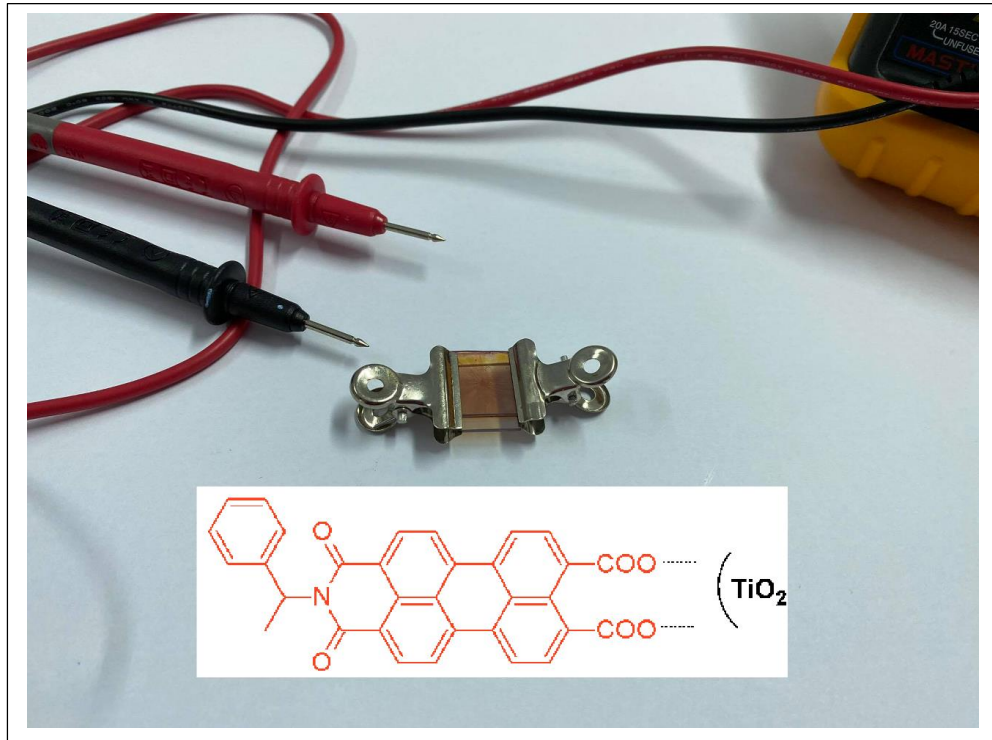


Figure 3.4: Fabricated DSSC based on dye 14

3.5 DSSC Device Characterization

3.5.1 Dye Solar Cells Parameters

Determination of current-voltage characteristic under dark and light radiation of different intensities represent the standard solar cell characterization techniques.

The current-voltage characteristics of solar cells were identified based on Schottky thermionic emission formula [65].

$$I(v) = I_{ph} - I_{0,exp} \left(\frac{q \cdot (v + I \cdot R_s)}{n \cdot K \cdot T} - 1 \right) - \frac{v + I \cdot R_s}{R_p} \quad (11)$$

Where:

| | |
|----------|--------------------------|
| R_s | Series resistance |
| R_{sh} | Shunt resistance |
| n | Ideality parameter |
| I_0 | Diode saturation current |
| I_p | Photocurrent. |

In a one-diode system, the schottky equation models the dark current but provides only simplified characterization of the present system, however it provides reasonable fit for most solar devices and is helpful for the general study of the I-V curves.

I-V data characteristics were obtained v keithley 2400-source meter in dark and under illumination using halogen lamp and labview software for acquiring the necessary data.

3.5.1.1 Short-Circuit Current Density (I_{sc})

The highest current that can be obtained from device at the condition where the cell voltage (V) is equal to zero. I_{sc} is directly proportional to the light intensity.

$$I_{sc} = I_{max} = I(V = 0) \quad (12)$$

3.5.1.2 Open-Circuit Potential (V_{oc})

The maximum voltage of a solar cell device measured when the current flow through the cell is zero at known light intensity. Open-circuit potential increases linearly with the light intensity.

$$V_{sc} = V_{max} = V(I = 0) \quad (13)$$

3.5.1.3 Power maximum (P_{max})

The generated power of a solar devices was calculated using the following equation:

$$P=V \times I \quad (14)$$

The power maximum can be obtained from the power curve by plotting the calculated power versus the applied potential.

3.5.1.4 The Fill Factor (FF)

The fill factor is one of the important parameters to specify the quality, ideality and overall capacities of the solar cell devices. The FF is the ratio of the maximum generated current and voltage (P_{max}) to the values of short-circuit current and open-circuit voltage as shown in the following equation[30]:

$$\frac{I_{max} \cdot V_{max}}{I_{sc} \cdot V_{oc}} \quad (15)$$

The ideal solar devices show power maximum exactly at the I_{sc} and E_{oc} and the FF is equal to 1. However, the non-ideal cases caused by parasitic effects such as series and shunt resistances. The fill factor for DSSC devices range typically between 0.6-0.8 based on whole device and usually it is increasing with decreasing the light intensity.

3.5.1.5 Power Conversion Efficiency (PCE)

The PCE reveals the performance of the solar devices and it can be defined as the ratio of maximum generated power to electrical incident power from light source (should be know).

$$\eta = \frac{V_{OC} I_{sc} FF}{P_{in}} * 100\% \quad (16)$$

The power conversion efficiency is a function of open-circuit voltage, short-circuit current as well as the fill factor, accordingly the optimization of those three characteristics improves the whole solar cell performance and efficiency.

Chapter 4

DATA AND CALCULATIONS

4.1 Calculations of Optical Parameters

4.1.1 Molar Absorption Coefficients

The maximum absorption coefficients of the synthesized compounds were calculated according to Beer Lambert's law which states the linear relationship between the absorbance and concentration of absorbed species using the following equation:

$$\epsilon_{\max} = A / Cl \quad (17)$$

| | | |
|-------------------|------------------------------|--|
| ϵ_{\max} | Molar absorption coefficient | $L \cdot \text{mol}^{-1} \cdot \text{cm}^{-1}$ |
| A | Absorbance | - |
| C | Concentration | mol.L^{-1} |
| L | Cell length | cm. |

Calculation of ϵ_{\max} for 6:

To estimate ϵ_{\max} , at least five various concentration of the synthesized compounds were prepared in a range between ($1 \times 10^{-5} \text{M}$ - $1 \times 10^{-6} \text{M}$), their maximum absorbance regarding to their λ_{\max} were measured, then line graph was obtained by plotting the absorbance versus concentrations and the slop was calculated which represent the maximum extinction coefficient.

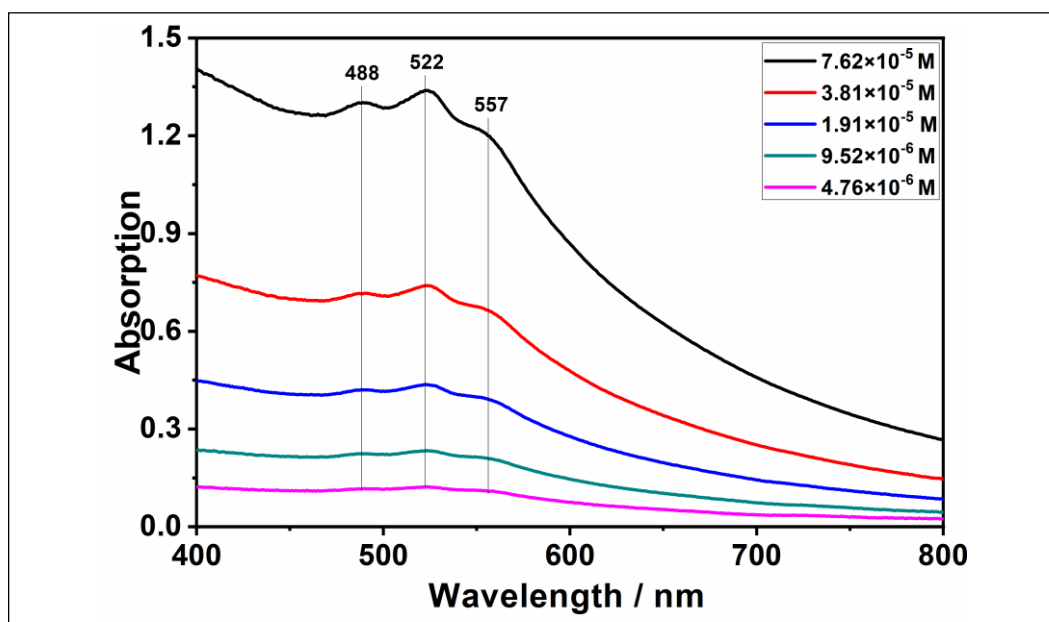


Figure 4.1: Concentration dependent spectra of 6 in chloroform

Table 4.1: Concentration, maximum wavelength and absorbance of 6 in chloroform

| Concentration | λ_{\max} | Absorbance |
|------------------------|------------------|------------|
| 7.762×10^{-5} | 524 | 1.42 |
| 3.81×10^{-5} | 524 | 0.71 |
| 1.91×10^{-5} | 524 | 0.38 |
| 9.52×10^{-6} | 524 | 0.19 |
| 4.76×10^{-6} | 524 | 0.12 |

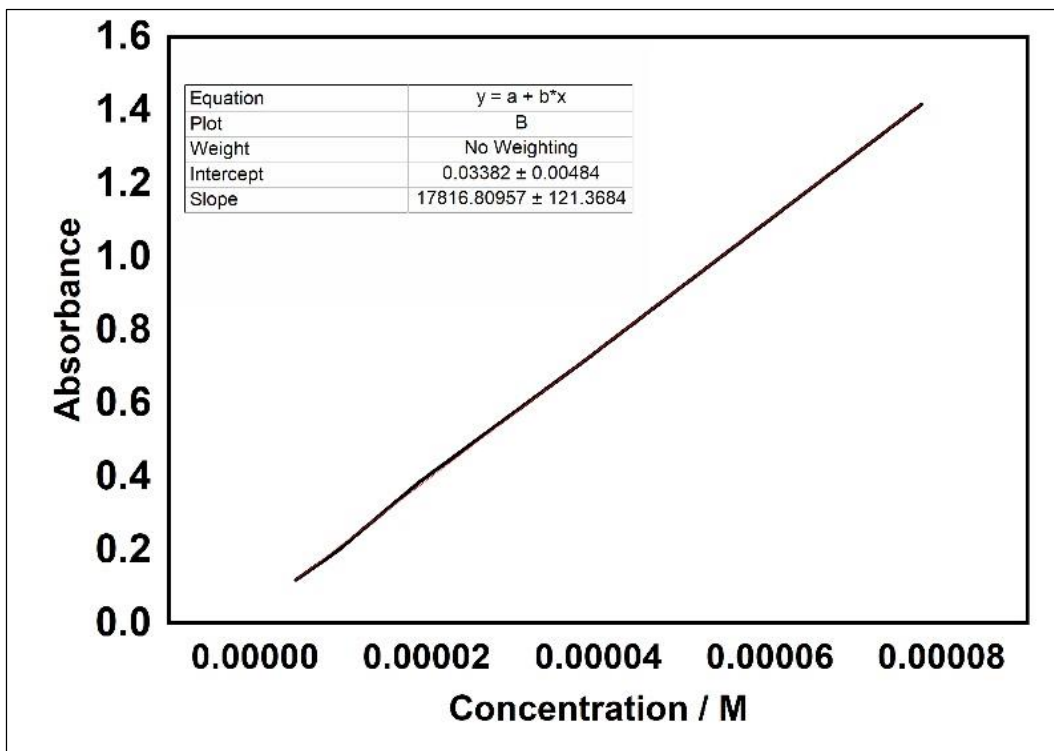


Figure 4.2: Absorbance vs. Concentration of 6 in chloroform

As shown in figure 4.2 the slope, ϵ_{\max} , is $17816.8 \text{ L} \cdot \text{mol}^{-1} \cdot \text{cm}^{-1}$ for 6 in chloroform, in different solvents, ϵ_{\max} for the synthesized perylene diimides were calculated using the same way and the obtained results were shown in the following tables.

Table 4.2: Molar absorption coefficients of **4** in various solvents

| Solvent | 4 | |
|----------------|------------------|-------------------|
| | λ_{\max} | ϵ_{\max} |
| CHL | 514 | 5000 |
| TCE | 522 | 5500 |
| TFAc | 531 | 12500 |
| NMP | 518 | 14000 |
| DMF | 518 | 12500 |
| DMSO | 523 | 16500 |

Table 4.3: Molar absorption coefficients of **6** in various solvents

| Solvent | 6 | |
|----------------|------------------|-------------------|
| | λ_{\max} | ϵ_{\max} |
| CHL | 524 | 17817 |
| TCE | 528 | 18000 |
| TFAc | 534 | 14500 |
| NMP | 523 | 13600 |
| DMF | 522 | 11600 |

Table 4.4: Molar absorption coefficients of 8 in various solvents

| Solvent | 8 | |
|---------|------------------|-------------------|
| | λ_{\max} | ϵ_{\max} |
| CHL | 526 | 25500 |
| TCE | 528 | 20000 |
| TFAc | 535 | 36000 |
| NMP | 526 | 13000 |
| DMF | 521 | 22000 |
| DMSO | 526 | 24000 |

4.1.2 Fluorescence Quantum Yields

Fluorescence quantum yield (Φ_f) is an important photo physical parameter of the investigated chromophores/fluorophores. Φ_f could define as the ratio of the absorbed /emitted photons through the fluorescence deactivation process.

Fluorescence quantum yield can be determined by either the comparative technique reported in [66] which is more accurate, reliable but time consuming, or by the single point method which based on using a standard sample (reference) with known Φ_f value as well as solutions of the reference and the sample with same absorbance at same excitation wavelength (λ_{exc}) this method is more practical and faster compared to the first method , the Φ_f value of the sample is calculated via the ratio of integrated fluorescence intensities of the reference and the sample under same condition according to the following equation:

$$\Phi_f = A_R/A_S \times (S_S/S_R) \times (n_S/n_R)^2 \times \Phi_R \quad (18)$$

| | |
|----------|--|
| Φ_f | Fluorescence quantum yield of sample |
| Φ_R | Fluorescence quantum yield of reference |
| A_R | Absorbance of the reference at λ_{exc} |
| A_S | Absorbance of the sample at λ_{exc} |
| n_s | Refractive index of sample |
| n_R | Refractive index of reference |
| S_S | Integrated emission area of the sample |
| S_R | Integrated emission area of the reference. |

Reference used to calculate the Φ_f values for the synthesized compounds was N, N'-bis(dodecyl)-3,4,9,10-perylenebis(dicarboximide) with $\Phi_f=1$ at $\lambda_{exc}=485\text{nm}$.

Φ_f calculation of 4 in CHL at $\lambda_{exc}=485\text{nm}$:

| | |
|----------|--|
| Φ_R | 1 |
| A_R | 0.1003 |
| A_S | 0.1003 |
| n_s | 1.445 |
| n_R | 1.445 |
| S_S | 197.076 counts. (cm.sec) ⁻¹ |
| S_R | 851.81 counts. (cm.sec) ⁻¹ |

$$\Phi_f = 0.1003/0.1003 \times \left(197.076/851.81\right) \times \left(1.445/1.445\right)^2 \times 1 = 0.23$$

The Φ_f values of the synthesized perylene diimides were calculated using the same way in various solvents and the data obtained were listed in the following table.

Table 4.5: Fluorescence Quantum Yields of 4, 6 and 8 in different solvents at $\lambda_{exc}=485\text{nm}$.

| Solvent | Fluorescence Quantum Yields (Φ_f) | | |
|---------|--|------|------|
| | 4 | 6 | 8 |
| CHL | 0.23 | 0.12 | 0.18 |
| TCE | 0.30 | 0.12 | 0.14 |
| TFAc | 0.09 | 0.10 | 0.10 |
| NMP | 0.06 | 0.08 | 0.10 |
| DMF | 0.08 | 0.14 | 0.10 |
| DMSO | 0.05 | - | 0.10 |

4.1.3 Half-Width of Selected Absorption $\Delta\bar{\nu}_{1/2}$

A general definition of half width of selected absorption is either the full width at half maximum or half the optical band width value (as frequency). The half width of the synthesized perylene diimides have been calculated using to the following equation:

$$\Delta\bar{\nu}_{\frac{1}{2}} = \bar{\nu}_I - \bar{\nu}_{II} \quad (19)$$

$\bar{\nu}_I$ & $\bar{\nu}_{II}$ which are obtained from the absorption spectra of the investigated compound represent the frequencies in cm^{-1} and $\Delta\bar{\nu}_{\frac{1}{2}}$ represent the half width of selected absorption in cm^{-1} .

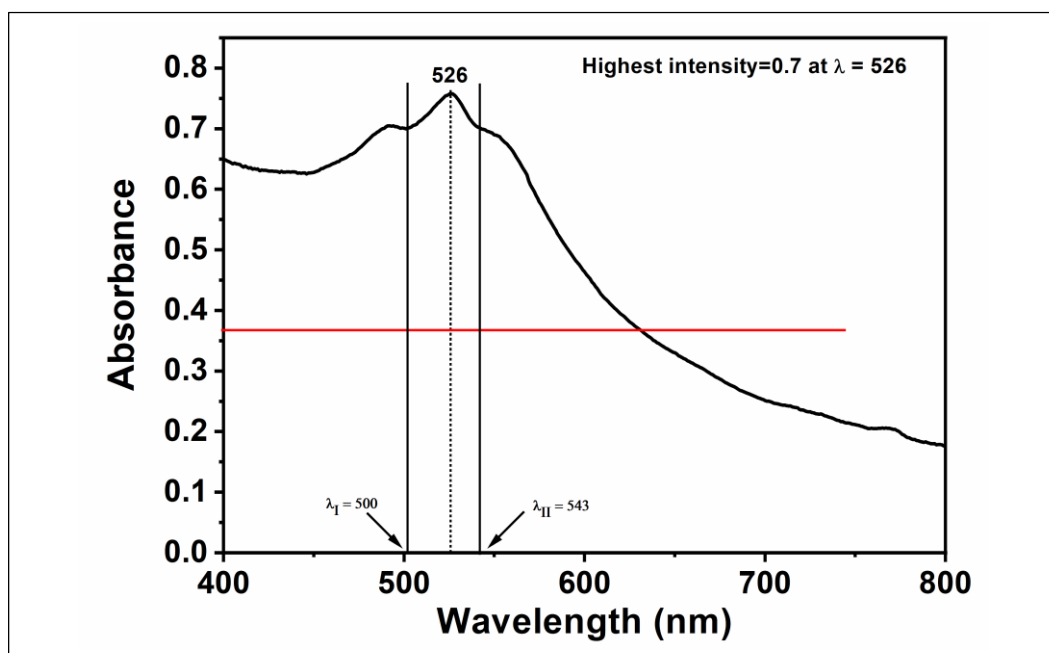


Figure 4.3: Half width estimation of 8 in chloroform

From figure 4.3:

$$\lambda_I = 500 \text{ nm}$$

$$\lambda_I = 500 \text{ nm} \times \frac{1\text{m}}{10^9\text{nm}} \times \frac{100\text{ cm}}{1\text{m}} = 0.00005 \text{ cm}$$

$$\bar{\nu}_I = \frac{1}{0.00005 \text{ cm}} = 20000 \text{ cm}^{-1}$$

$$\lambda_{II} = 543 \text{ nm}$$

$$\lambda_{II} = 543 \text{ nm} \times \frac{1m}{10^9nm} \times \frac{100 \text{ cm}}{1m} = 0.0000543 \text{ cm}$$

$$\bar{\nu}_{II} = \frac{1}{0.0000543 \text{ cm}} = 18416.21 \text{ cm}^{-1}$$

$$\Delta\bar{\nu}_{\frac{1}{2}} = 20000 - 18416.21 = 1583.79 \text{ cm}^{-1}$$

Table 4.6: Half width of 4, 6 and 8 in various solvents:

| Solvent | Half-width $\Delta\bar{\nu}_{1/2}$ (cm ⁻¹) | | |
|---------|--|--------|--------|
| | 4 | 6 | 8 |
| CHL | 1540.6 | 1327.8 | 1583.8 |
| TCE | 1464.0 | 1464.5 | 1601.9 |
| TFAc | 5356.7 | 1628.3 | 1530.4 |
| NMP | 954.77 | 1273.7 | 1481.3 |
| DMF | 1071.3 | 1244.3 | 1442.3 |
| DMSO | 1470.1 | - | 1614.0 |

4.1.4 Theoretical Radiative Life Times (t_0)

Theoretical radiative life time represents the duration (life-time) of the excited molecule without radiation less deactivation to the ground state. t_0 of the synthesized perylene diimides was calculated by using the following equation:

$$t_0 = \frac{3.5 \times 10^8}{\bar{\nu}^2 \max \varepsilon_{max} \Delta\bar{\nu}_{1/2}} \quad (20)$$

t_0 Theoretical radiative life time (ns)

$\bar{\nu}^2 \max$ Mean frequency of λ_{max} (cm⁻¹)

ε_{max} Maximum Extinction Coefficients at λ_{max}

$\Delta\bar{\nu}_{1/2}$ Half width (cm⁻¹).

Theoretical radiative life time of 5 /chloroform:

$$t_0 = \frac{3.5 \times 10^8}{(19011.41)^2 \times 25384.97 \times 1583.97} = 2.408 \times 10^{-8} s$$

$$t_0 = 2.408 \times 10^{-8} s \times \frac{10^9 ns}{1s} = 24.08 ns$$

Theoretical radiative life time of the synthesized perylene diimides were calculated using the same way in various solvents and the results were listed in the following tables:

Table 4.7: Theoretical radiative life time (ns) of 4

| Solvent | 4 | | | | |
|---------|-----------------|------------------|---------------------|-------------------------|-------|
| | λ_{max} | ϵ_{max} | $\bar{\nu}^2_{max}$ | $\Delta\bar{\nu}_{1/2}$ | t_0 |
| CHL | 514 | 4496.75 | 3.78×10^8 | 1540.6 | 130.0 |
| TCE | 522 | 5144.79 | 3.66×10^8 | 1464.0 | 125.0 |
| TFAc | 531 | 12346.68 | 3.54×10^8 | 5356.68 | 15.0 |
| NMP | 518 | 13676.00 | 3.72×10^8 | 954.77 | 73.0 |
| DMF | 518 | 12192.00 | 3.72×10^8 | 1071.26 | 71.0 |
| DMSO | 523 | 16316.96 | 3.65×10^8 | 1470.13 | 40.0 |

Table 4.8: Theoretical radiative life time (ns) of 6

| Solvent | 6 | | | | |
|---------|------------------|-------------------|--------------------|-------------------------|-------|
| | λ_{\max} | ϵ_{\max} | $\bar{\nu}^2 \max$ | $\Delta\bar{\nu}_{1/2}$ | t_0 |
| CHL | 524 | 17817 | 3.64×10^8 | 1327.84 | 45.0 |
| TCE | 528 | 18000 | 3.58×10^8 | 1464.51 | 40.0 |
| TFAc | 534 | 14500 | 3.50×10^8 | 1628.34 | 45.0 |
| NMP | 523 | 13600 | 3.65×10^8 | 1273.68 | 55.0 |
| DMF | 522 | 11600 | 3.67×10^8 | 1244.32 | 66.0 |

Table 4.9: Theoretical radiative life time (ns) of 8

| Solvent | 8 | | | | |
|---------|------------------|-------------------|--------------------|-------------------------|-------|
| | λ_{\max} | ϵ_{\max} | $\bar{\nu}^2 \max$ | $\Delta\bar{\nu}_{1/2}$ | t_0 |
| CHL | 526 | 25500 | 3.61×10^8 | 1583.8 | 24.0 |
| TCE | 528 | 20000 | 3.58×10^8 | 1601.9 | 31.0 |
| TFAc | 535 | 36000 | 3.49×10^8 | 1530.4 | 18.0 |
| NMP | 526 | 13000 | 3.61×10^8 | 1481.3 | 51.0 |
| DMF | 521 | 22000 | 3.68×10^8 | 1442.3 | 32.0 |
| DMSO | 526 | 24000 | 3.61×10^8 | 1614.0 | 27.0 |

4.1.5 Theoretical Fluorescence Life-Time (t_f)

The average theoretical time that the molecule stays in excited state before the radiative deactivation (fluorescence) is called theoretical fluorescence life time (t_f) and it was calculated with the following equation:

$$t_f = t_0 \times \Phi_f \quad (21)$$

t_f Theoretical Fluorescence life-time (ns)

t_0 Theoretical radiative life time (ns)

Φ_f Fluorescence quantum yield.

Theoretical fluorescence life-time of 8 in chloroform

$$t_f = 24 \times 0.18 = 4.4 \text{ ns}$$

Theoretical fluorescence life time of the synthesized perylene diimides were calculated in the same way and the results were listed in the following table.

Table 4.10: Theoretical Fluorescence life-time of 4, 6 and 8 in various solvents:

| Solvent | Theoretical Fluorescence life-time (t_f) (ns) | | |
|---------|--|-----|-----|
| | 4 | 6 | 8 |
| CHL | 31.0 | 5.2 | 4.4 |
| TCE | 40.0 | 4.6 | 4.4 |
| TFAc | 1.5 | 4.4 | 1.1 |
| NMP | 4.0 | 4.4 | 3.1 |
| DMF | 6.0 | 9.5 | 3.2 |
| DMSO | 2.0 | - | 1.0 |

4.1.6 Theoretical Fluorescence Rate Constant (K_f)

Theoretical fluorescence rate constant refers to the rate of fluorescence radiation of a molecule and it is obtained from the following equation.

$$K_f = \frac{1}{t_0} \quad (22)$$

K_f Theoretical Fluorescence rate constant in s^{-1}

t_0 Theoretical radiative life-time in s.

Theoretical fluorescence rate constant of 8 in chloroform:

$$K_f = \frac{1}{2.4 \times 10^{-8} s} = 0.50 \times 10^8 s^{-1}$$

Theoretical fluorescence rate constant of the synthesized perylene diimides were calculated in the same way and the results were listed in the following table:

Table 4.11: Theoretical Fluorescence rate constant of 4, 6 and 8 in various solvents

| Solvent | Theoretical Fluorescence rate constant (K_f) $\times 10^8$ (s^{-1}) | | |
|---------|--|------|------|
| | 4 | 6 | 8 |
| CHL | 0.08 | 0.25 | 0.50 |
| TCE | 0.08 | 0.30 | 0.40 |
| TFAc | 0.70 | 0.25 | 0.60 |
| NMP | 0.14 | 0.20 | 0.20 |
| DMF | 0.14 | 0.20 | 0.30 |
| DMSO | 2.52 | - | 0.40 |

4.1.7 Radiationless Deactivation Rate Constant (K_d)

The rate constant (K_d) of the synthesized perylene diimides was calculated according to the equation below

$$K_d = \left(\frac{K_f}{\Phi_f} \right) - K_f \quad (23)$$

K_d Radiationless deactivation rate constant (s^{-1})

K_f Fluorescence rate constant (s^{-1})

Φ_f Fluorescence quantum yield.

Radiationless deactivation rate constant of 8 in chloroform

$$K_d = \left(\frac{0.5 \times 10^8}{0.18} \right) - 0.5 \times 10^8 = 2.0 \times 10^8 s^{-1}$$

Table 4.12: Radiationless Deactivation Rate Constant of 4, 6 and 8 in various solvents

| Solvent | Radiationless Deactivation Rate Constant (K_d) $\times 10^8$ (S^{-1}) | | |
|---------|--|------|------|
| | 4 | 6 | 8 |
| CHL | 0.32 | 0.20 | 2.0 |
| TCE | 0.21 | 0.20 | 2.0 |
| TFAc | 7.0 | 2.00 | 9.0 |
| NMP | 3.0 | 2.00 | 4.0 |
| DMF | 2.0 | 0.90 | 3.0 |
| DMSO | 5.0 | - | 10.0 |

4.1.8 Oscillator Strength (f)

The electronic transition strength is represented by the oscillator strength which is a dimensionless parameter, f of the synthesized perylene diimides was calculated via the following equation:

$$f = 4.32 \times 10^{-9} \times \Delta\bar{\nu}_{1/2} \times \varepsilon_{max} \quad (24)$$

F Oscillator strength

$\Delta\bar{\nu}_{1/2}$ Half width of selected absorption in cm^{-1}

ε_{max} Maximum Extinction Coefficients in $\text{L.mol}^{-1}.\text{cm}^{-1}$.

Oscillator strength of PDI-PEA/ chloroform

$$f = 4.32 \times 10^{-9} \times 1583.8 \times 25500 = 0.20$$

Table 4.13: Oscillator strength of 4, 6 and 8 in various solvents

| Solvent | Oscillator Strength (f) | | |
|---------|-----------------------------|-------------|---------|
| | PDA-Decanol | PDI-Dodecyl | PDI-PEA |
| CHL | 0.05 | 0.10 | 0.20 |
| TCE | 0.06 | 0.10 | 0.15 |
| TFAc | 0.30 | 0.10 | 0.25 |
| NMP | 0.10 | 0.08 | 0.10 |
| DMF | 0.10 | 0.06 | 0.14 |
| DMSO | 0.10 | - | 0.17 |

4.1.9 Singlet Energies (E_s)

The minimum amount of energy required to excite a chromophore/fluorophore from the singlet ground state (s_0) to the first level of excited state (s_1) is the singlet energies E_s and it was calculated via the following equation.

$$E_s = \frac{2.86 \times 10^5}{\lambda_{max}} \quad (25)$$

E_s Singlet energy in $Kcal.mol^{-1}$

λ_{max} Maximum absorption wavelength in \AA .

Singlet energies of PDI-PEA in chloroform:

$$\lambda_{max} = 526 \text{ nm} \times \frac{10\text{\AA}}{1\text{nm}} = 5260$$

$$E_s = \frac{2.86 \times 10^5}{5260} = 54.4 \text{ Kcal.mol}^{-1}$$

Singlet energies of 8 in chloroform

$$\lambda_{max} = 526 \text{ nm} \times \frac{10\text{\AA}}{1\text{nm}} = 5260$$

$$E_s = \frac{2.86 \times 10^5}{5260} = 54.4 \text{ Kcal.mol}^{-1}$$

Table 4.14: Singlet energies of 4, 6 and 8 in various solvents

| Solvent | Singlet energies (Es) Kcal.mol ⁻¹ | | |
|---------|---|------|------|
| | 4 | 6 | 8 |
| CHL | 55.6 | 54.6 | 54.4 |
| TCE | 55.0 | 54.3 | 54.2 |
| TFAc | 54.3 | 53.7 | 53.6 |
| NMP | 54.9 | 54.9 | 55.0 |
| DMF | 55.6 | 54.9 | 55.0 |
| DMSO | 54.8 | - | 54.0 |

Table 4.15: Photophysical properties of compounds 4, 6 and 8 in various organic solvents

| Solvent | λ_{\max} | ϵ_{\max} | f | Φ_f | τ_0 | τ_f | k_f | kd | Es |
|-------------------|------------------|-------------------|-------|----------|----------|----------|-------------------|-------------------|------|
| 4 | | | | | | | | | |
| CHCl ₃ | 514 | 5000 | 0.050 | 0.20 | 130.0 | 31.0 | 8×10^6 | 3.2×10^7 | 55.6 |
| TCE | 522 | 5500 | 0.060 | 0.30 | 125.0 | 40.0 | 8×10^6 | 2.1×10^7 | 55.0 |
| TFAc | 531 | 12500 | 0.30 | 0.09 | 15.0 | 1.5 | 7×10^7 | 7.0×10^8 | 54.3 |
| NMP | 518 | 14000 | 0.10 | 0.05 | 73.0 | 4.0 | 1.4×10^7 | 3.0×10^8 | 54.9 |
| DMF | 518 | 12500 | 0.10 | 0.08 | 71.0 | 6.0 | 1.4×10^7 | 2.0×10^8 | 55.6 |
| DMSO | 523 | 16500 | 0.10 | 0.05 | 40.0 | 2.0 | 2.5×10^7 | 5.0×10^8 | 54.8 |
| 6 | | | | | | | | | |
| CHCl ₃ | 524 | 17817 | 0.10 | 0.12 | 45.0 | 5.2 | 2.3×10^7 | 2.0×10^8 | 54.6 |
| TCE | 528 | 18000 | 0.10 | 0.12 | 40.0 | 4.6 | 3.0×10^7 | 2.0×10^8 | 54.3 |
| TFAc | 534 | 14500 | 0.10 | 0.10 | 45.0 | 4.4 | 2.5×10^7 | 2.0×10^8 | 53.7 |
| NMP | 523 | 13600 | 0.08 | 0.08 | 55.0 | 4.4 | 2.0×10^7 | 2.0×10^8 | 54.9 |
| DMF | 522 | 11600 | 0.06 | 0.14 | 66.0 | 9.5 | 2.0×10^7 | 0.9×10^8 | 54.9 |
| 8 | | | | | | | | | |
| CHCl ₃ | 526 | 25500 | 0.20 | 0.18 | 24.0 | 4.4 | 5.0×10^7 | 2.0×10^8 | 54.4 |
| TCE | 528 | 20000 | 0.15 | 0.14 | 31.0 | 4.4 | 4.0×10^7 | 2.0×10^8 | 54.2 |
| TFAc | 535 | 36000 | 0.25 | 0.10 | 18.0 | 1.1 | 6.0×10^7 | 9.0×10^8 | 53.6 |
| NMP | 526 | 13000 | 0.10 | 0.10 | 51.0 | 3.1 | 2.0×10^7 | 4.0×10^8 | 55.0 |
| DMF | 521 | 22000 | 0.14 | 0.10 | 32.0 | 3.2 | 3.0×10^7 | 3.0×10^8 | 55.0 |
| DMSO | 526 | 24000 | 0.17 | 0.10 | 27.0 | 1.0 | 4.0×10^7 | 10×10^8 | 54.0 |

4.2 Electrochemistry of the Synthesized Compounds

The electrochemical characterization of the synthesized compounds 4, 6 and 8 were investigated by cyclic voltammetry technique (CV) in acetonitrile containing 0.1 M TBAP6 as a supporting electrode at 100 mVs^{-1} scan rate.

Redox potentials/ Half-wave potentials, HOMO/LUMO energy levels and the optical band gap energies were calculated from cyclic voltammetry.

4.2.1 Redox Potential / Half-Wave Potential ($E_{1/2}$)

Anodic peak potential (E_{pa}), cathodic peak potential (E_{pc}), the anodic peak current (i_{pa}), and the cathodic peak current (i_{pc}) represent the parameters of great interest for a reversible cyclic voltammogram as displayed in Figure 4.4.

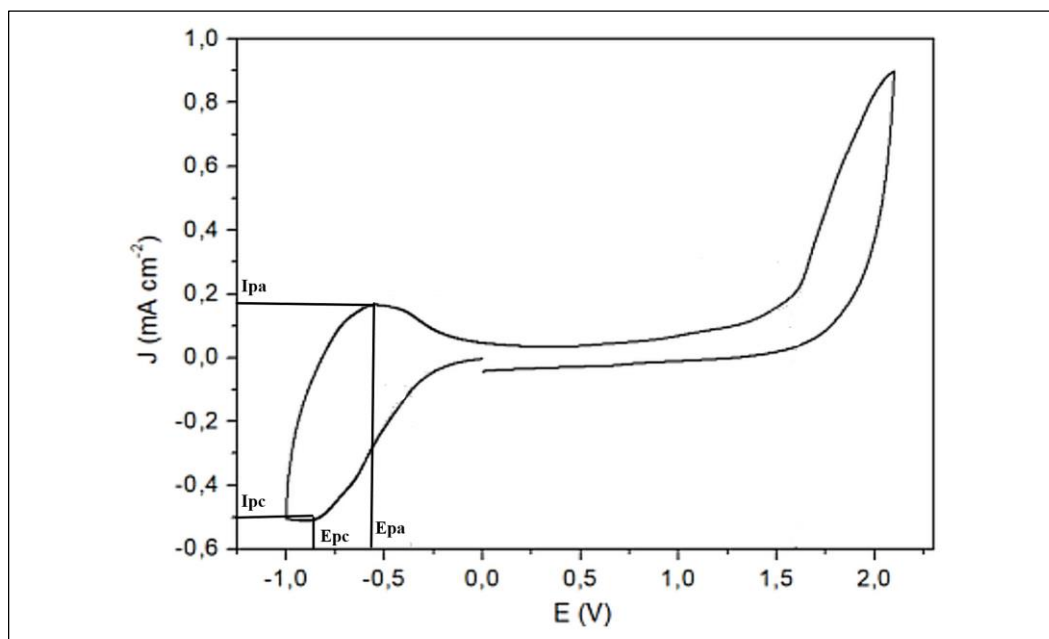


Figure 4.4: Cyclic voltammogram for compound 8 in acetonitrile at 100 mVs^{-1} scan rate showing parameters E_{pc} , E_{pa} , I_{pc} and I_{pa}

Redox potential or half-wave potential is related to the standard potential for the half reaction and is often used for qualitative analysis of the species. The redox potential ($E_{1/2}$) of the reversible redox couple can be calculated according to the following equation:

$$E_{1/2} = \frac{E_{pc} + E_{pa}}{2} \quad (26)$$

$E_{1/2}$: Half wave potential in (V)

E_{pc} : Potential of cathodic peak in (V)

E_{pa} : Potential of anodic peak in (V).

Redox potential of compound 8:

The cyclic voltammogram of compound 8 in acetonitrile as shown in figure 4.4 illustrated one reversible reduction peak where E_{pc} and E_{pa} are -0.820 and - 0.530 respectively, the redox potential were calculated according to the reference electrode (Ag/AgCl) following equation (26):

$$E_{red1/2} \text{ vs } Ag/AgCl = \frac{-0.820 - 0.530}{2} = -0.675 \text{ V}$$

The peak separation (ΔE) for a reversible, 'Nernstian', redox couple provides information about the number of electrons (n transferred per mole and it can be evaluated by using the following equation:

$$\Delta E = E_{pa} - E_{pc} = \frac{0.059}{n} \text{ V} \quad (27)$$

Peak separation of compound 8 is calculated using equation (27)

$$\Delta E = -0.530 + 0.820 = 0.29 \text{ V} = 290 \text{ mV}$$

The oxidation potential (E_{ox}) of the internal reference Ferrocene was calculated 0.410 V, the redox potential of the species can be evaluated according to the Ferrocene (Fc) as shown in the following equation.

$$E_{red1/2} vs Fc = E_{red1/2} vs Ag/AgCl - E_{ox} vs Ag/AgCl \quad (28)$$

The redox potential of compound 8 vs ferrocene were calculated according to equation (28).

$$E_{red1/2} vs Fc = -0.675 - 0.410 = 1.085 V$$

The redox potential of the synthesized compound 4, 6 and 8 were calculated in the same way and the data were listed in table 4.16.

4.2.2 LUMO/HOMO Energy Levels

For organic semiconductors, the energy needed to extract an electron from a molecule through oxidation process is represented by HOMO, and LUMO represents the energy required to inject an electron into molecule thus implying reduction process. These processes can be determined via cyclic voltammetry technique by measuring the redox potentials E_{red} and E_{ox} .

LUMO and HOMO energy levels can be calculated according to the following equation:

$$E_{HOMO/LUMO} = [(E_{ox/red} \text{ (onset)} - E_{1/2} \text{ (ferrocene)}) + 4.8] \text{ eV} \quad (29)$$

LUMO and HOMO energy levels of compound 8 were calculated based on the absolute energy of Fc/Fc⁺ ($E_{1/2} \text{ (ferrocene)} = 0.410$) using equation 28 and the E_{red} and E_{ox} onset were -0.370 and 1.58 respectively as shown in figure 4.5.

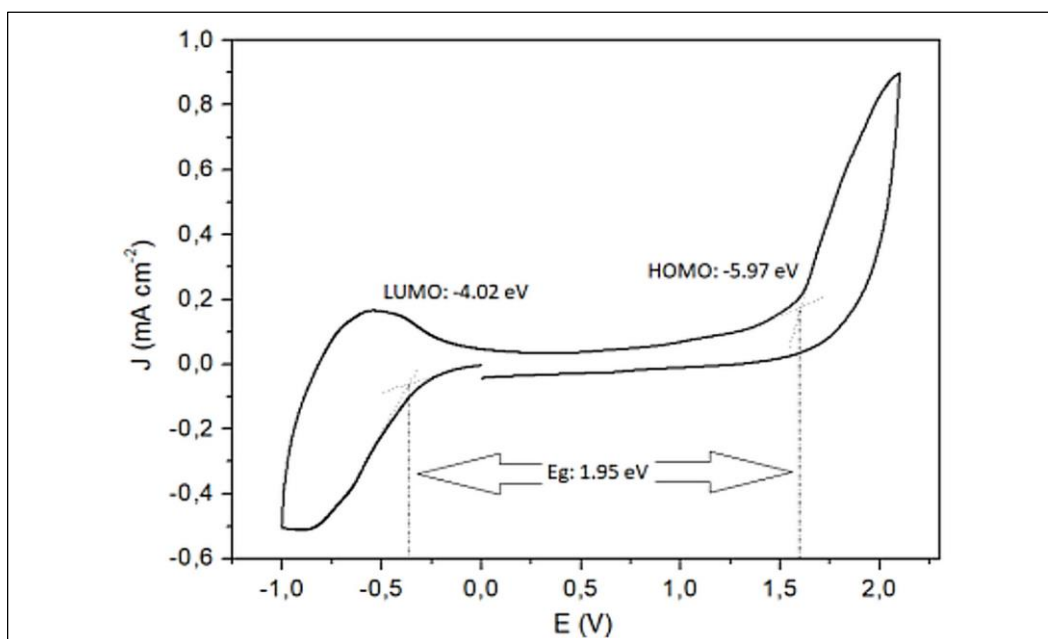


Figure 4.5: Cyclic voltammogram for compound 8 in acetonitrile at 100 mVs^{-1} scan rate showing parameters $E_{\text{ox/redonset}}$ and HOMO/LUMO energies

LUMO energy level of compound 8

$$E_{\text{LUMO}} = [(E_{\text{red,onset}} - E_{1/2}(\text{ferrocene})) + 4.8] \text{ eV}$$

$$E_{\text{LUMO}} = [(-0.370 - 0.410) + 4.8] \text{ eV} = -4.02 \text{ eV}.$$

HOMO energy level of compound 8

$$E_{\text{HOMO}} = [(E_{\text{ox,onset}} - E_{1/2}(\text{ferrocene})) + 4.8] \text{ eV}$$

$$E_{\text{HOMO}} = [(1.580 - 0.410) + 4.8] \text{ eV} = -5.97 \text{ eV}.$$

The HOMO/LUMO energy levels of the synthesized compounds were calculated using the same way and the data were listed in table 4.16.

4.2.3 The Optical Band Gap Energy

In organic molecules, the energy levels of the electronic states correspond to the energy carried by UV-visible radiation. At resonance, the molecules can absorb sufficient energy to excite an electron from the low-energy molecular orbital (ground state) to higher energy molecular orbital (excited state). These transitions can be measured

using a UV-Vis spectrophotometer. The optical band gap energy ($E_{g_{opt}}$) corresponds to the energy of the long wavelength edge of the absorption band. The longest absorption wavelength λ_{onset} is used to calculate the optical gap energy, $E_{g_{opt}}$, according to the following equation.

$$E_{g_{opt}} = \frac{1240 \text{ eV}}{\lambda} \quad (30)$$

$E_{g_{opt}}$: Optical band gap energy

λ : Cut-off wavelength of the absorption band (λ_{onset}) in nm.

The absorption spectra of compound 8 and the λ_{onset} were shown in figure 4.6, and the optical band gap energy were calculated using equation 30.

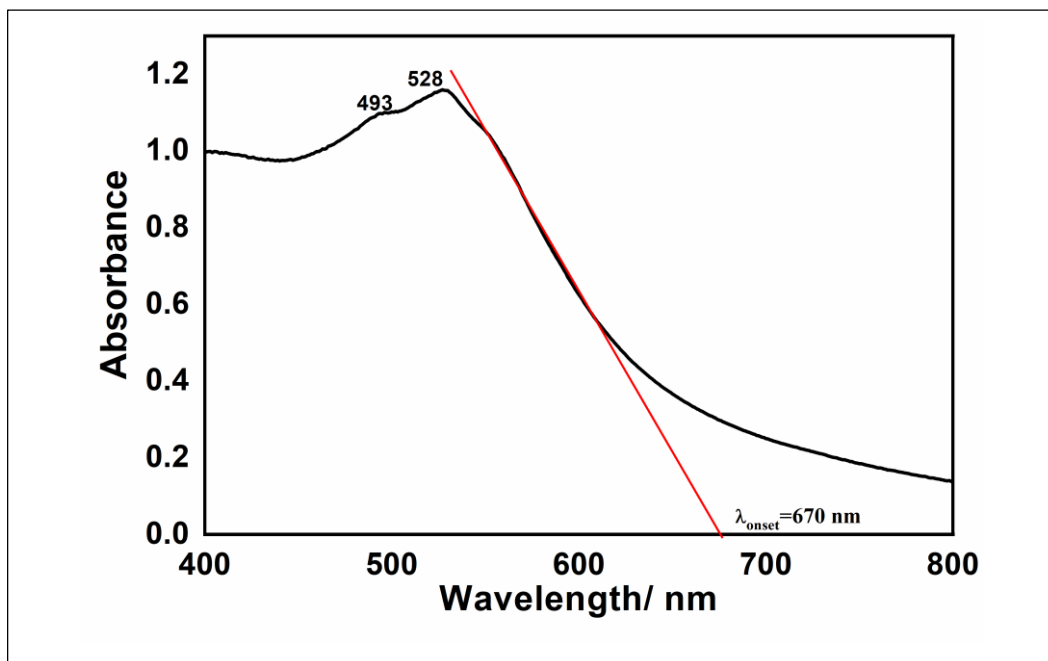


Figure 4.6: Absorption spectrum of compound 8 in TCE

$$E_{g_{\text{opt}}} = \frac{1240 \text{ eV}}{670 \text{ nm}} = 1.85 \text{ eV}$$

The optical band gap energies of the synthesized compounds were calculated in the same way and the data were listed in table 4.16.

Table 4.16: Cyclic voltammetry data, electrochemical and optical band gap energy, HOMO/LUMO energies of compounds 4, 6 and 8

| Compound | E_{pc} (V) | E_{pa} (V) | ΔE_p (mV) | $E_{red,onset}$ (V) | $E_{1/2}$ vs Ag/AgCl (V) | E_{Fc} vs Ag/AgCl (V) | $E_{1/2}$ vs Fc (V) | E_{ox} vs Ag/AgCl (V) | $E_{g_{cv}}$ (eV) | $E_{g_{opt}}$ (eV) | HOMO (eV) | LUMO (eV) |
|----------|-----------------|-----------------|----------------------|------------------------|--------------------------------|-------------------------------|---------------------------|-------------------------------|----------------------|-----------------------|--------------|--------------|
| 4 | -0.74 | -0.61 | 130 | -0.37 | -0.675 | 0.41 | -1.09 | 1.93 | 1.88 | 1.77 | -5.94 | -4.02 |
| 6 | -0.54 | -0.48 | 60 | -0.37 | -0.510 | 0.41 | -0.92 | 1.78 | 1.89 | 1.90 | -5.52 | -4.02 |
| 8 | -0.82 | -0.53 | 290 | -0.37 | -0.675 | 0.41 | -1.09 | 1.91 | 1.95 | 1.90 | -5.54 | -4.02 |

4.3 Dye sensitized Solar Cell Characterization

4.3.1 Short Circuit Current (I_{sc})

Short circuit represents the highest current that can be obtained from the solar device at zero cell voltage. I_{sc} is directly proportional to the light intensity. And it can be determined from the I-V curve figure 4.7.

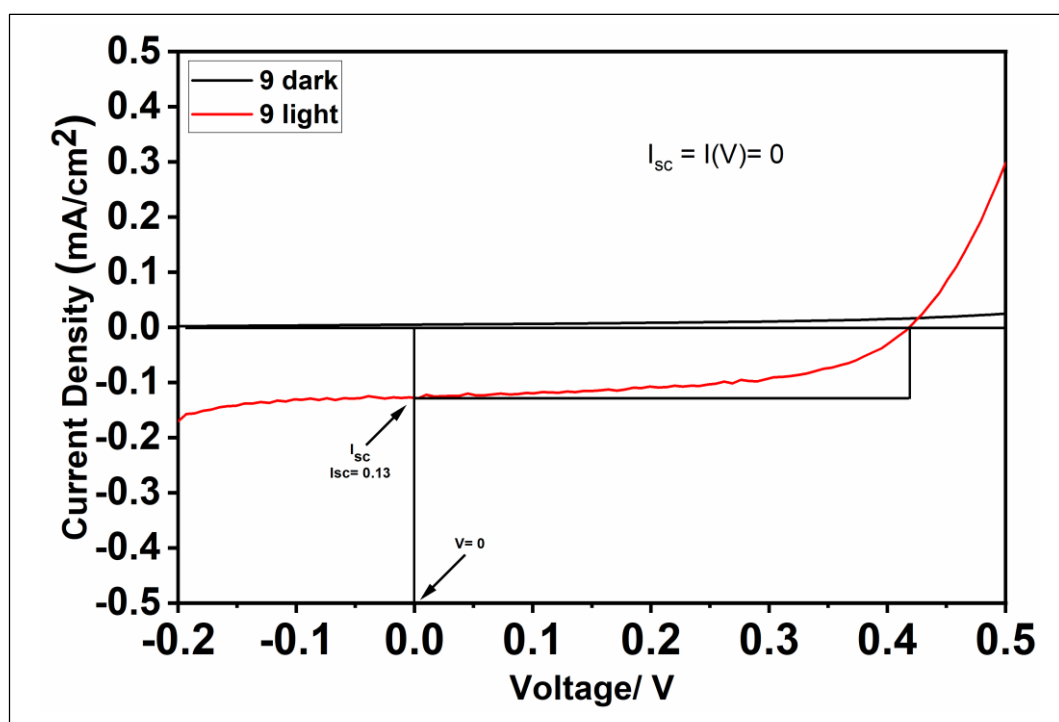


Figure 4.7: Graphic illustration of I_{sc} on I-V curve of dye 9 in dark and under light illumination at $100\text{mW}/\text{cm}^2$

DSSCs were fabricated based on various perylene dyes, their short circuit current were determined using same method showed above and the obtained data were listed in the following table.

Table 4.17: Short circuit current I_{sc} of DSSC using various compounds

| Compound | 4 | 9 | 10 | 11 | 12 | 13 | 14 | 15 |
|---------------------------------|------|-------|-------|-------|-------|-------|-------|-------|
| I_{sc} (mA.cm ⁻²) | 0.06 | 0.130 | 0.138 | 0.110 | 0.072 | 0.042 | 0.058 | 0.044 |

4.3.2 Open Circuit Voltage (V_{oc})

Open circuit voltage point out the highest voltage that can be obtained from the solar cell devise under light illumination and where the current flow is equal to zero, open circuit voltage is also directly proportional to the light intensity. V_{oc} can be determined from the I-V curve figure 4.8.

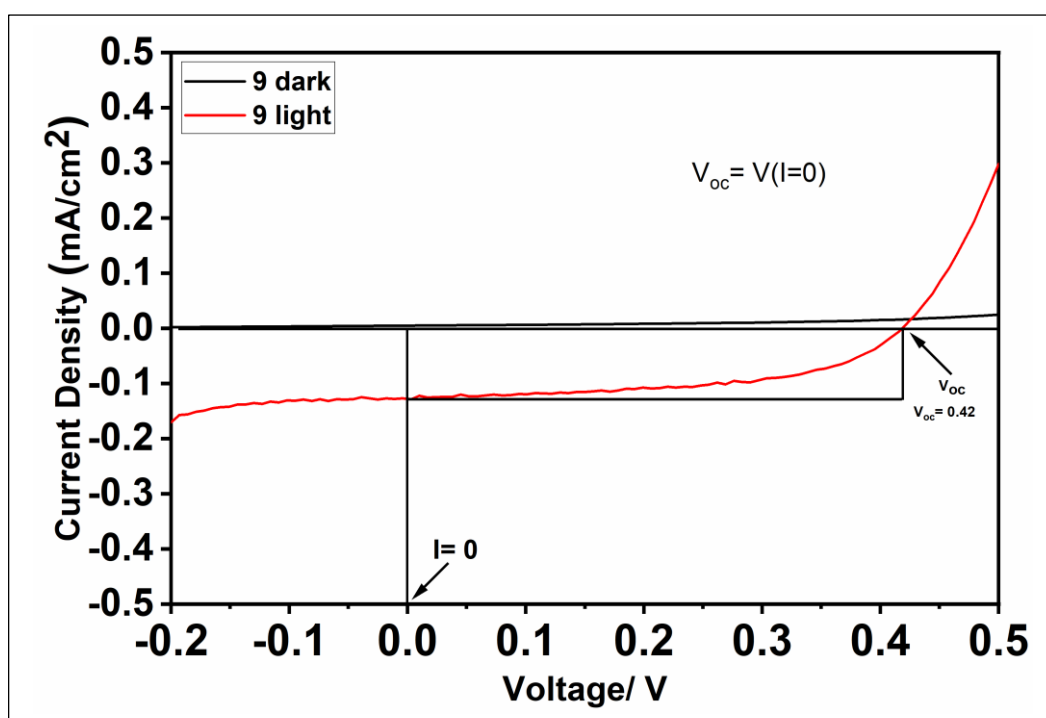


Figure 4.8: Graphic illustration of V_{oc} on I-V curve of dye 9 in dark and under light illumination at 100mW/cm²

DSSCs were fabricated based on various perylene dyes, their open circuit voltage were determined using same method showed above and the obtained data were listed in the following table.

Table 4.18: Open circuit voltage V_{oc} of DSSC using various compounds

| Compound | 4 | 9 | 10 | 11 | 12 | 13 | 14 | 15 |
|--------------|------|------|------|------|------|------|------|------|
| V_{oc} (V) | 0.23 | 0.42 | 0.30 | 0.28 | 0.37 | 0.50 | 0.24 | 0.25 |

4.3.3 Power Maximum (P_{max})

The generated solar cell power can be calculated using the following equation

$$P = V \times I \quad (31)$$

The power maximum (P_{max}) can be obtained by plotting the resulting power from the equation above versus the applied voltage.

The maximum power can be also represented visually by figuring out the largest rectangle area which fit within the I-V curve. V_{max} and I_{max} are the voltage and current obtained from the I-V curve of Dye 1 at the power maximum figure 4.9.

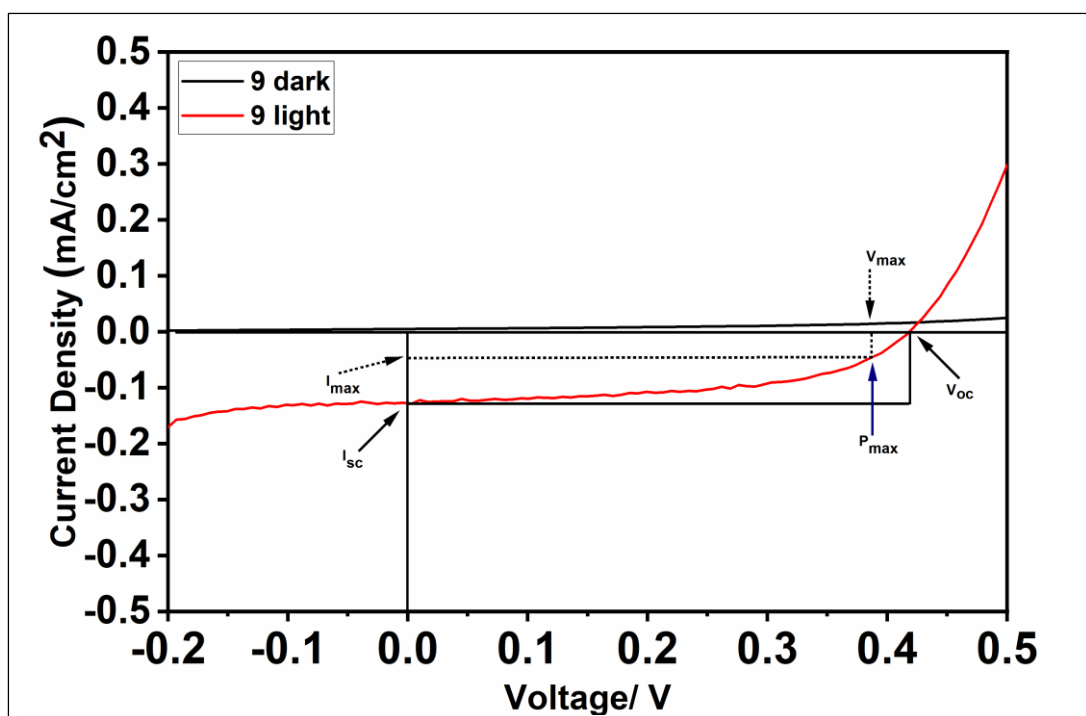


Figure 4.9: I-V curve with the photovoltaic parameters of dye 9 in dark and under light illumination at $100\text{mW}/\text{cm}^2$

DSSCs were fabricated using various perylene dyes and their I_{max} , V_{max} and P_{max} were determined and the data obtained were listed in the following table.

Table 4.19: V_{max} , I_{max} and P_{max} of DSSC using various compounds

| Compound | V_{max} (V) | I_{max} (mA/cm^2) | P_{max} (mW) |
|----------|----------------------|--|-----------------------|
| 4 | 0.150 | 0.031 | 0.005 |
| 9 | 0.390 | 0.047 | 0.018 |
| 10 | 0.255 | 0.051 | 0.013 |
| 11 | 0.240 | 0.041 | 0.010 |
| 12 | 0.340 | 0.025 | 0.009 |
| 13 | 0.420 | 0.011 | 0.0046 |
| 14 | 0.211 | 0.020 | 0.0042 |
| 15 | 0.210 | 0.013 | 0.0027 |

4.3.4 Fill Factor (FF)

Fill factor is an important parameters to examine the quality and capability of the fabricated solar cell, and it is defined as the ratio of the generated power maximum (P_{max}) to the theoretical power of the cell. The fill factor can be calculated using the following equation

$$FF = \frac{P_{max}}{P_{theoretical}} = \frac{V_{max} \times I_{max}}{V_{oc} \times I_{sc}} \quad (32)$$

The ideal solar cell is achieved when FF is equal to 1, i.e., I_{max} and V_{max} are exactly at the V_{oc} and I_{sc} .

The fill factor of DSSC using compound 9:

$$\frac{0.39 \times 0.047}{0.42 \times 0.13} = 0.34$$

The fill factor of DSSC using various compounds was calculated using the same equation and the obtained data were listed in the following table.

Table 4.20 V_{max} , I_{max} , V_{oc} , I_{sc} and FF of DSSC using various compounds

| Dye | V_{oc} (V) | V_{max} (V) | I_{sc} (mA cm ⁻²) | I_{max} (mA cm ⁻²) | FF |
|-----|--------------|---------------|---------------------------------|----------------------------------|------|
| 4 | 0.23 | 0.15 | 0.06 | 0.031 | 0.34 |
| 9 | 0.42 | 0.39 | 0.13 | 0.047 | 0.37 |
| 10 | 0.3 | 0.255 | 0.138 | 0.051 | 0.31 |
| 11 | 0.28 | 0.24 | 0.11 | 0.041 | 0.33 |
| 12 | 0.37 | 0.34 | 0.072 | 0.025 | 0.32 |
| 13 | 0.5 | 0.42 | 0.042 | 0.011 | 0.22 |
| 14 | 0.234 | 0.211 | 0.058 | 0.02 | 0.31 |
| 15 | 0.25 | 0.21 | 0.044 | 0.013 | 0.25 |

4.3.5 Efficiency (η)

Efficiency represent the ratio of the generated maximum power (P_{\max}) / the input power P_{in} from the light source. The efficiency was calculated using the following equation.

$$\eta\% = \frac{V_{oc} I_{sc} FF}{P_{in}} \times 100 \quad (33)$$

The efficiency of DSSC using dye 9:

$$\eta\% = \frac{0.42 \cdot 0.13 \cdot 0.34}{100} \times 100 = 0.02$$

The efficiency of DSSC using various compounds was calculated using the same equation and the collected data were listed in the following table.

Table 4.21 Photovoltaic parameters for dyes. Solar simulation, at 100 mW/cm²

| Dye | V_{oc} (V) | V_{\max} (V) | I_{sc} (mA cm ⁻²) | I_{\max} (mA cm ⁻²) | ff | PCE% *10 ⁻² |
|-----|--------------|----------------|------------------------------------|--------------------------------------|------|---------------------------|
| 4 | 0.23 | 0.15 | 0.06 | 0.031 | 0.34 | 0.4 |
| 9 | 0.42 | 0.39 | 0.13 | 0.047 | 0.37 | 2 |
| 10 | 0.3 | 0.255 | 0.138 | 0.051 | 0.31 | 1.3 |
| 11 | 0.28 | 0.24 | 0.11 | 0.041 | 0.33 | 1 |
| 12 | 0.37 | 0.34 | 0.072 | 0.025 | 0.32 | 0.9 |
| 13 | 0.5 | 0.42 | 0.042 | 0.011 | 0.22 | 0.5 |
| 14 | 0.234 | 0.211 | 0.058 | 0.02 | 0.31 | 0.4 |
| 15 | 0.25 | 0.21 | 0.044 | 0.013 | 0.25 | 0.3 |

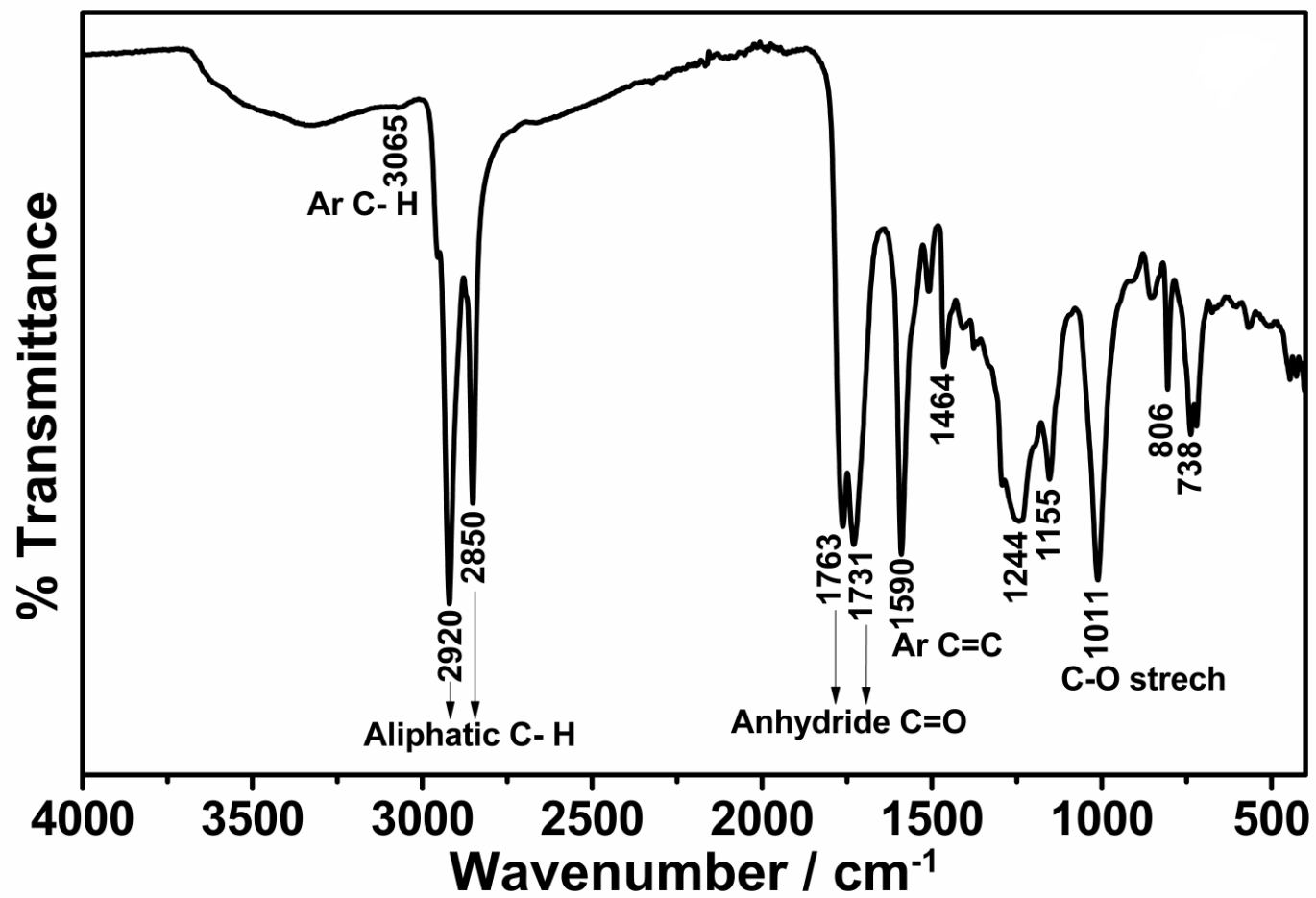


Figure 4.10: FT-IR spectrum of 4

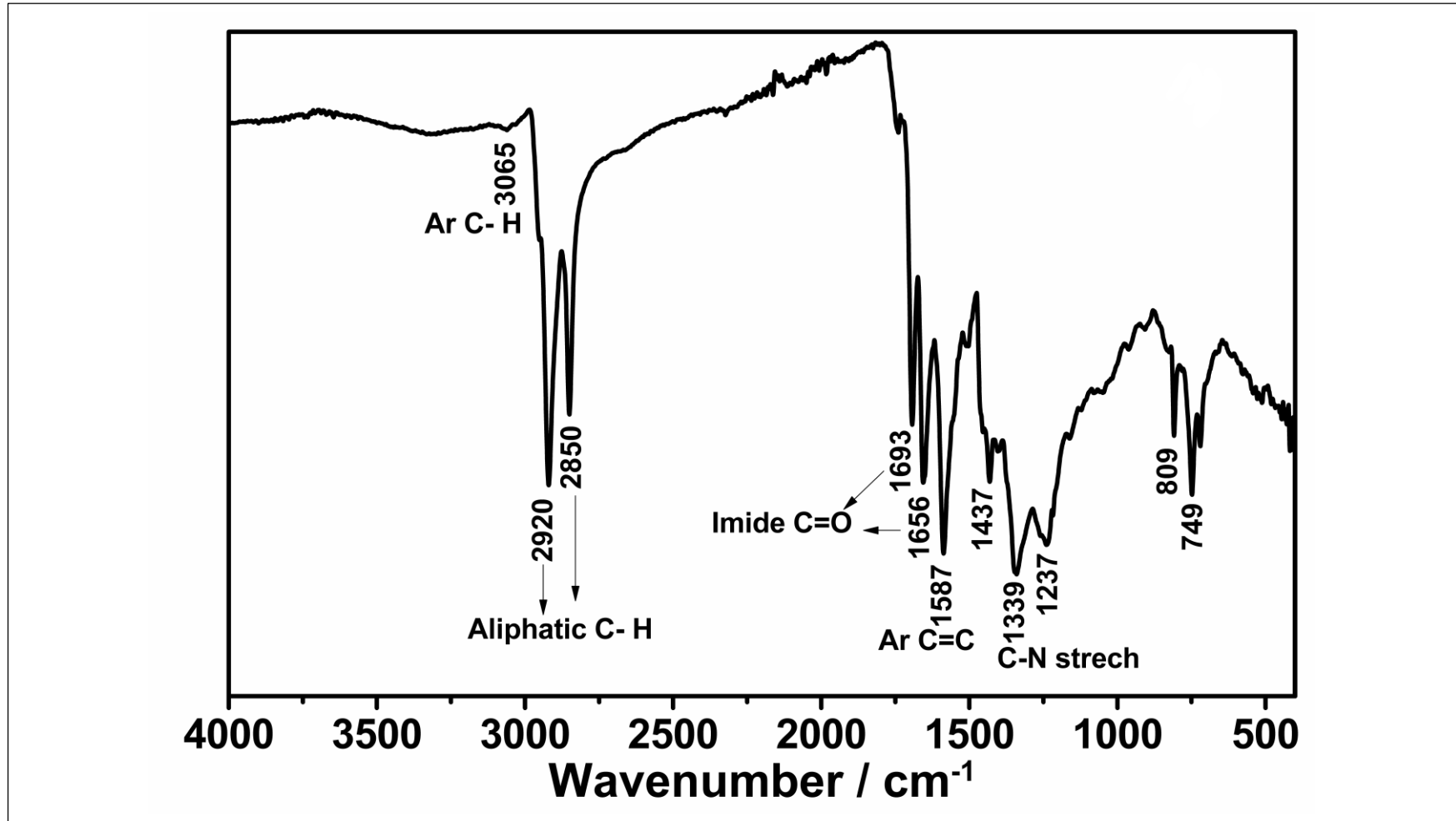


Figure 4.11: FT-IR spectrum of 6

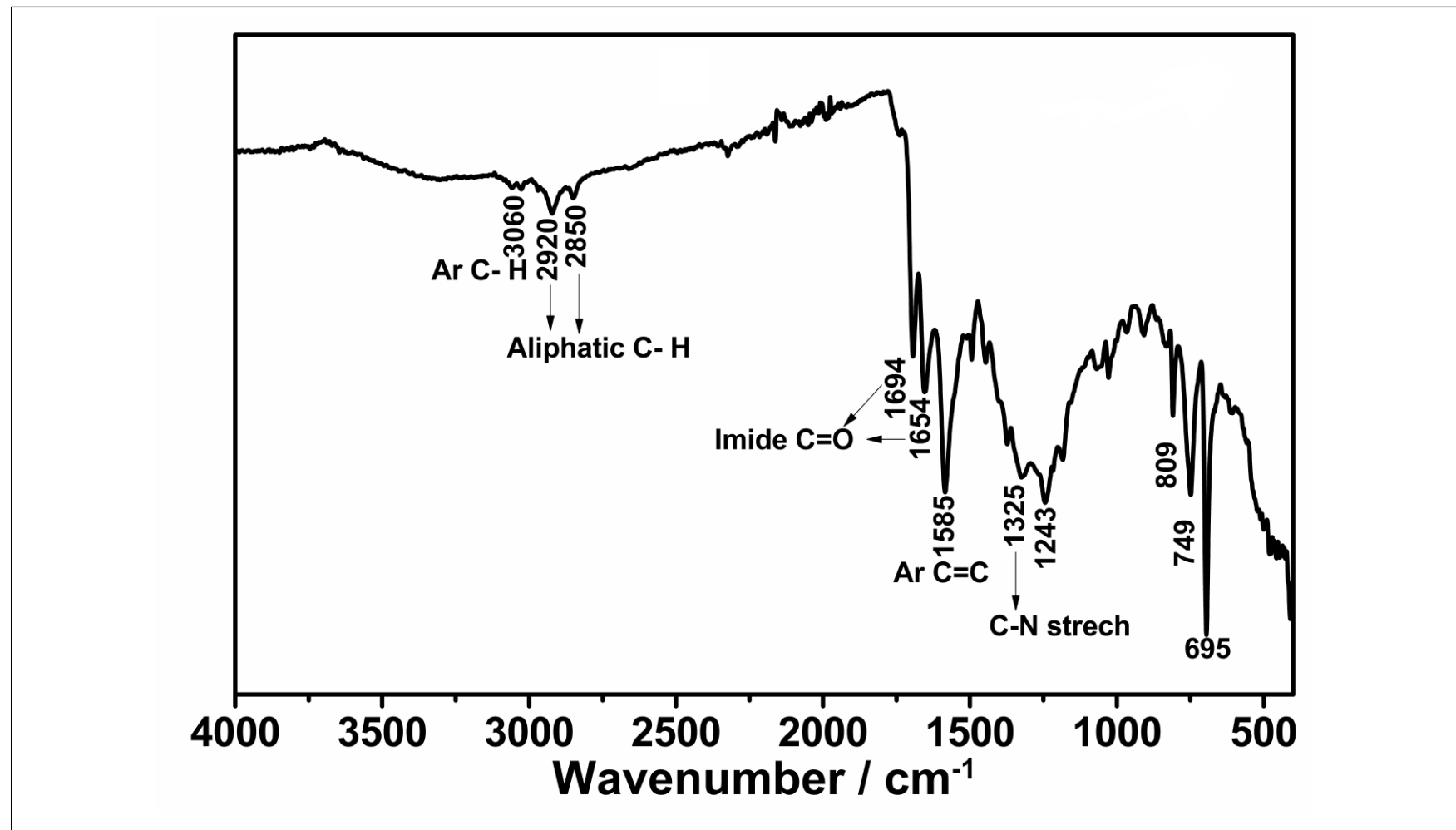


Figure 4.12: FT-IR spectrum of 8

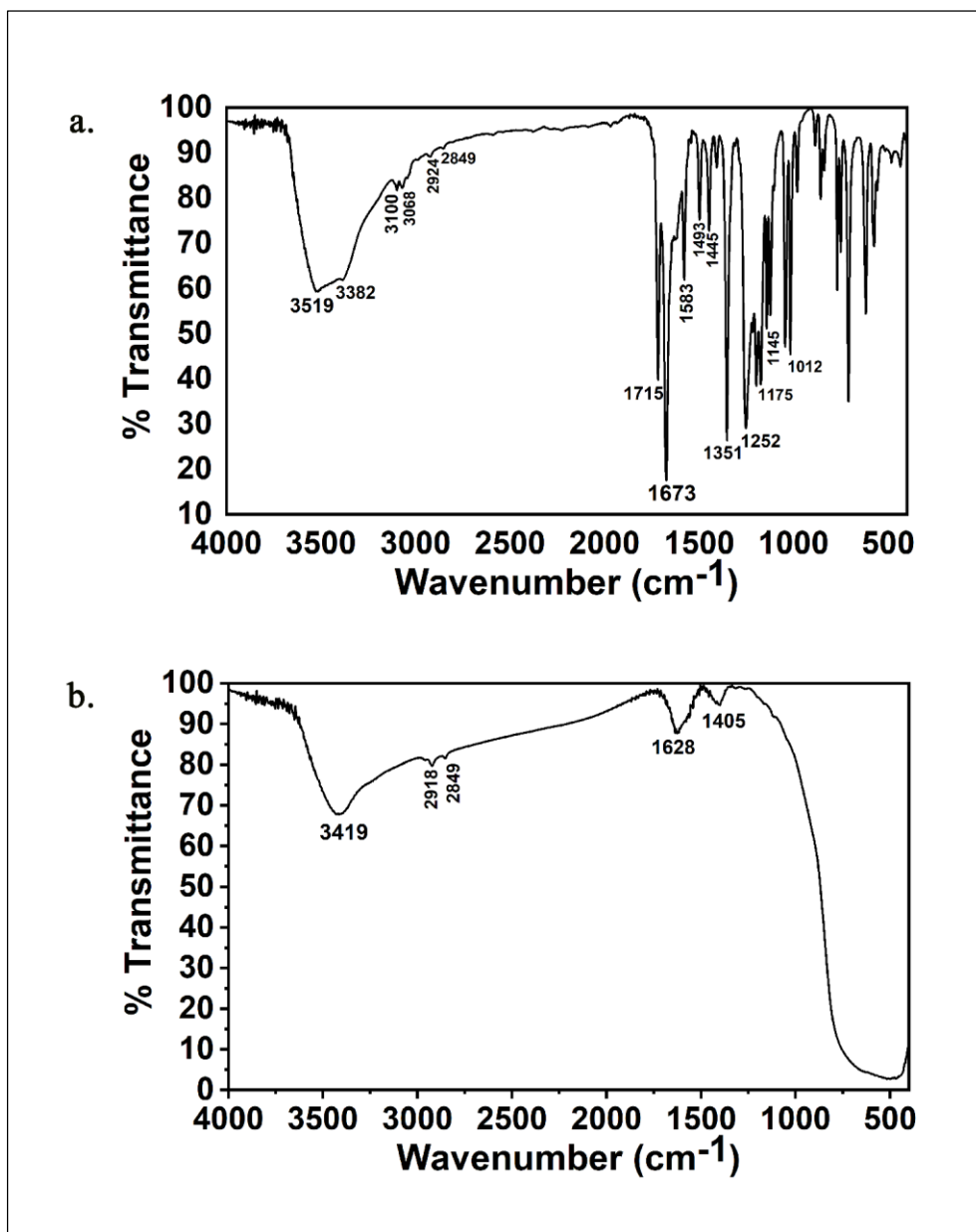


Figure 4.13: FT-IR spectra of a. dye 9 and b. dye 9 adsorbed on TiO₂

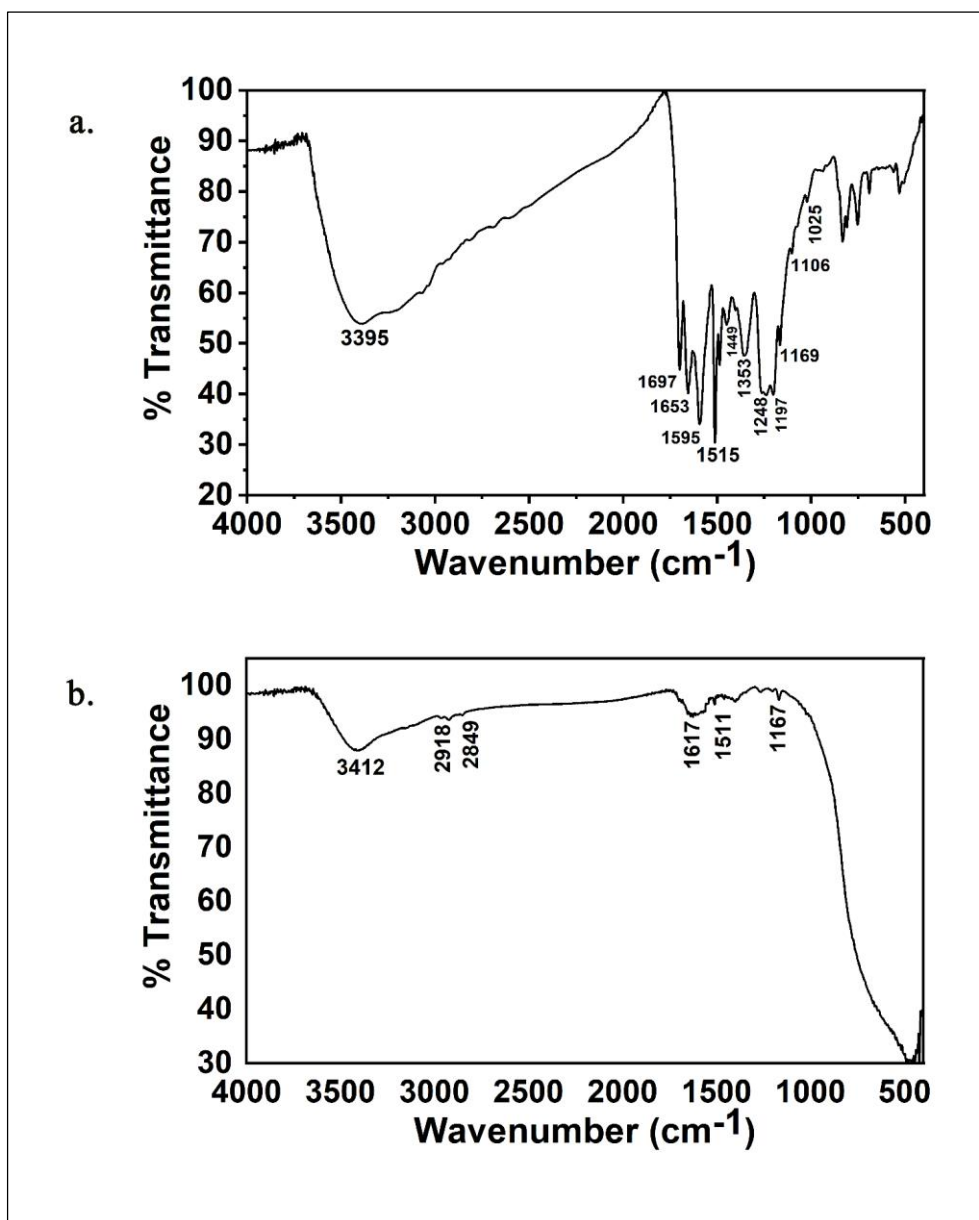


Figure 4.14: FT-IR spectra of a. dye 10 and b. dye 10 adsorbed on TiO₂

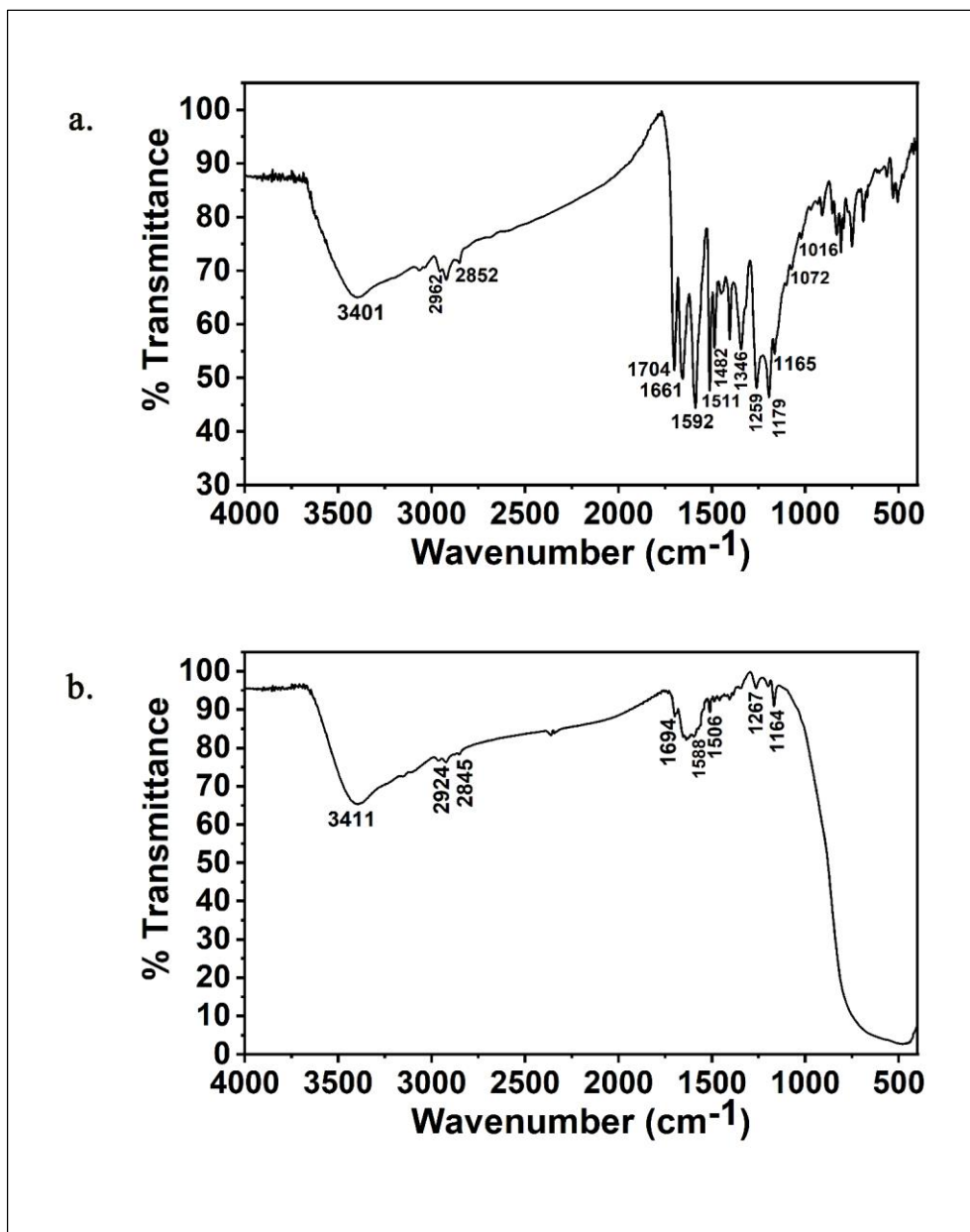


Figure 4.15: FT-IR spectra of a. dye 11 and b. dye 11 adsorbed on TiO_2

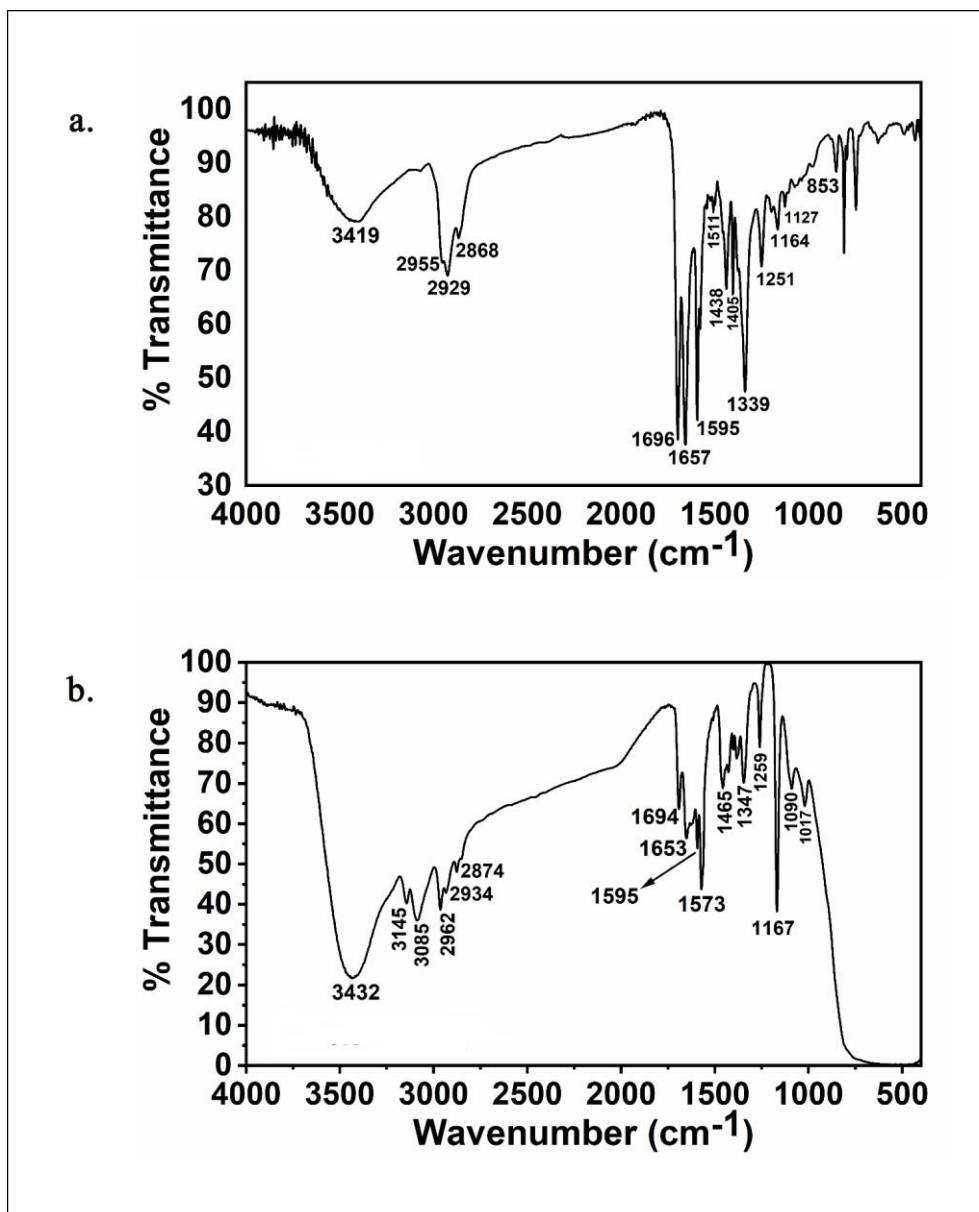


Figure 4.16: FT-IR spectra of a. dye 12 and b. dye 12 adsorbed on TiO_2

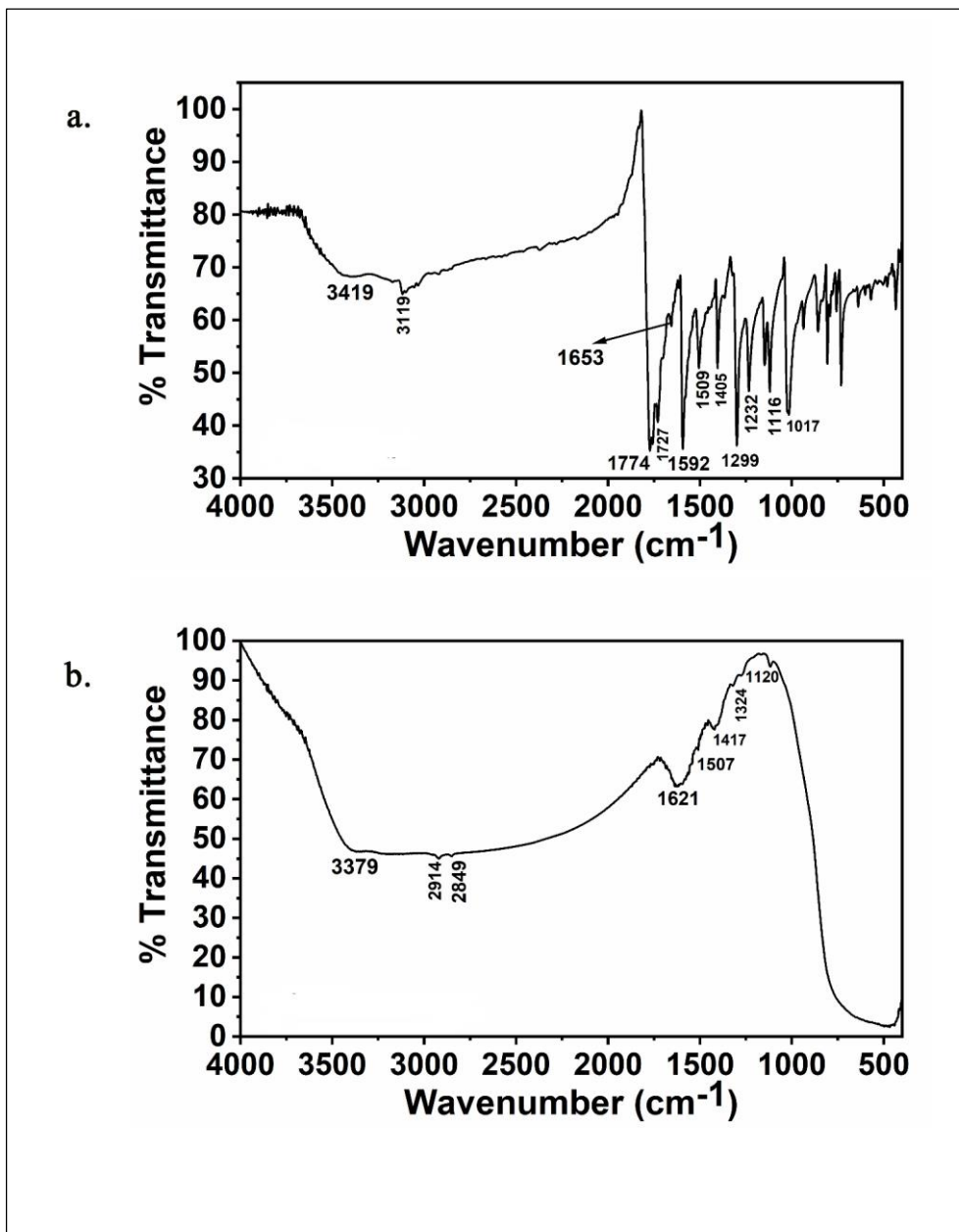


Figure 4.17: FT-IR spectra of a. dye 13 and b. dye 13 adsorbed on TiO_2

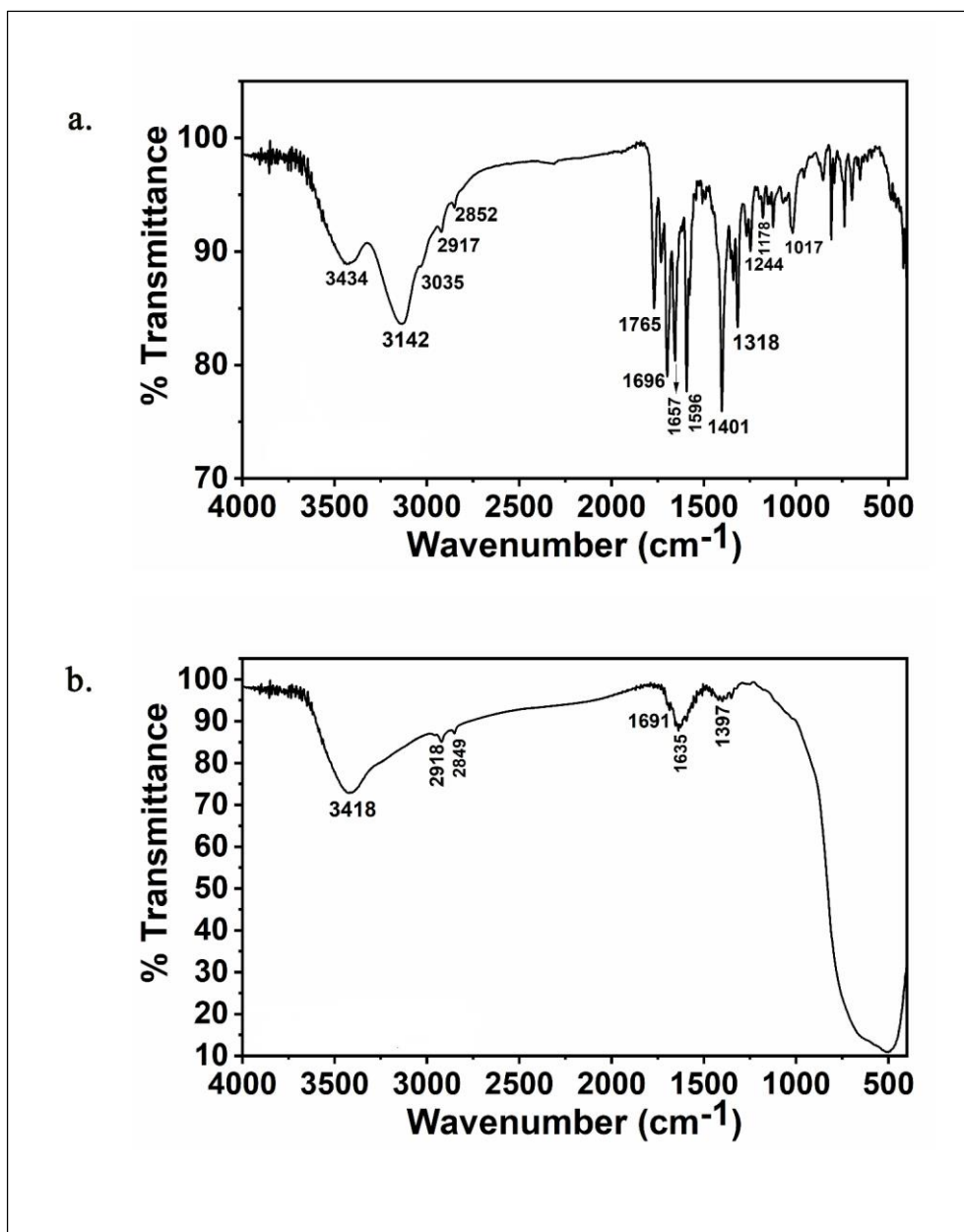


Figure 4.18: FT-IR spectra of a. dye 14 and b. dye 14 adsorbed on TiO_2

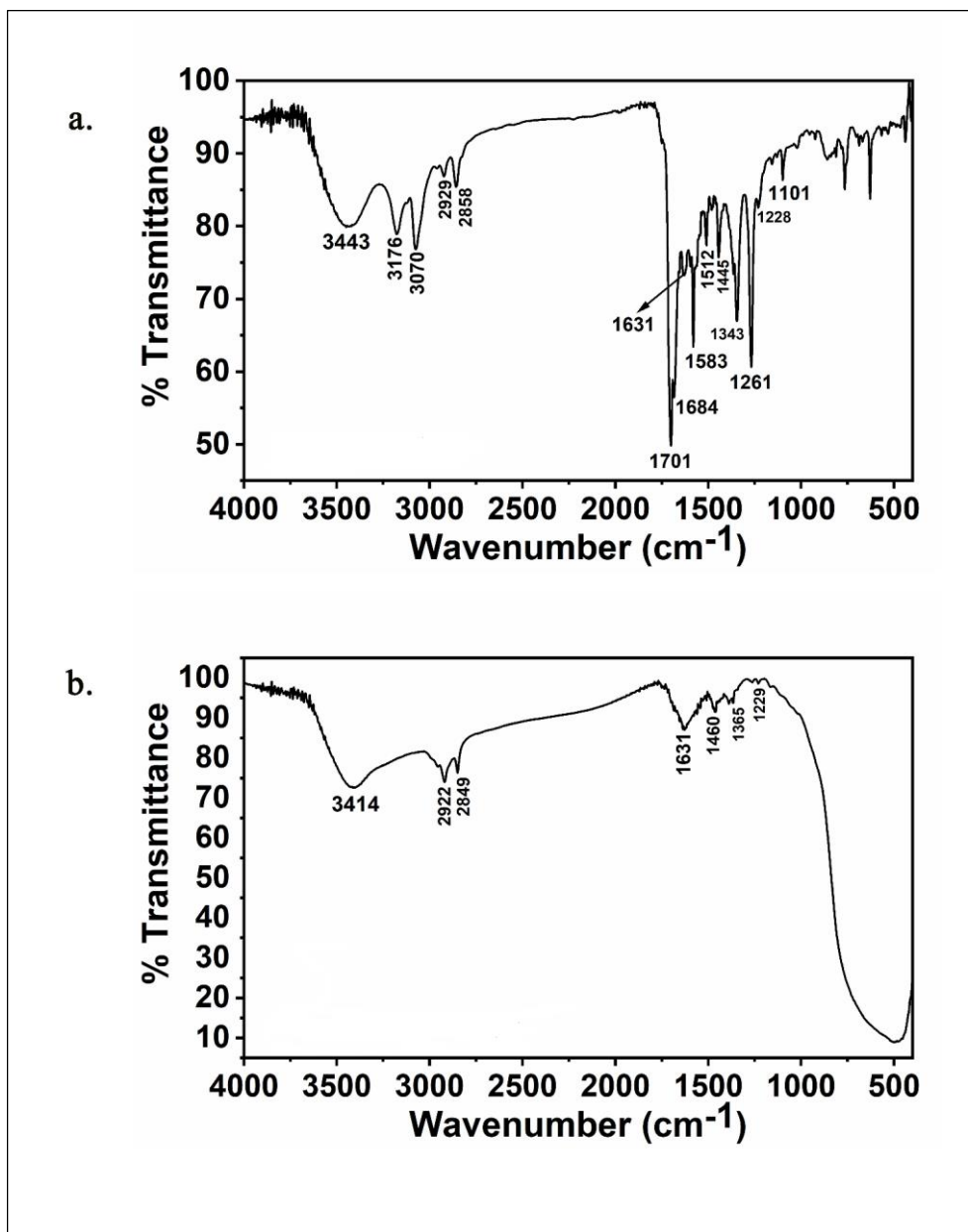


Figure 4.19: FT-IR spectra of a. dye 15 and b. dye 15 adsorbed on TiO

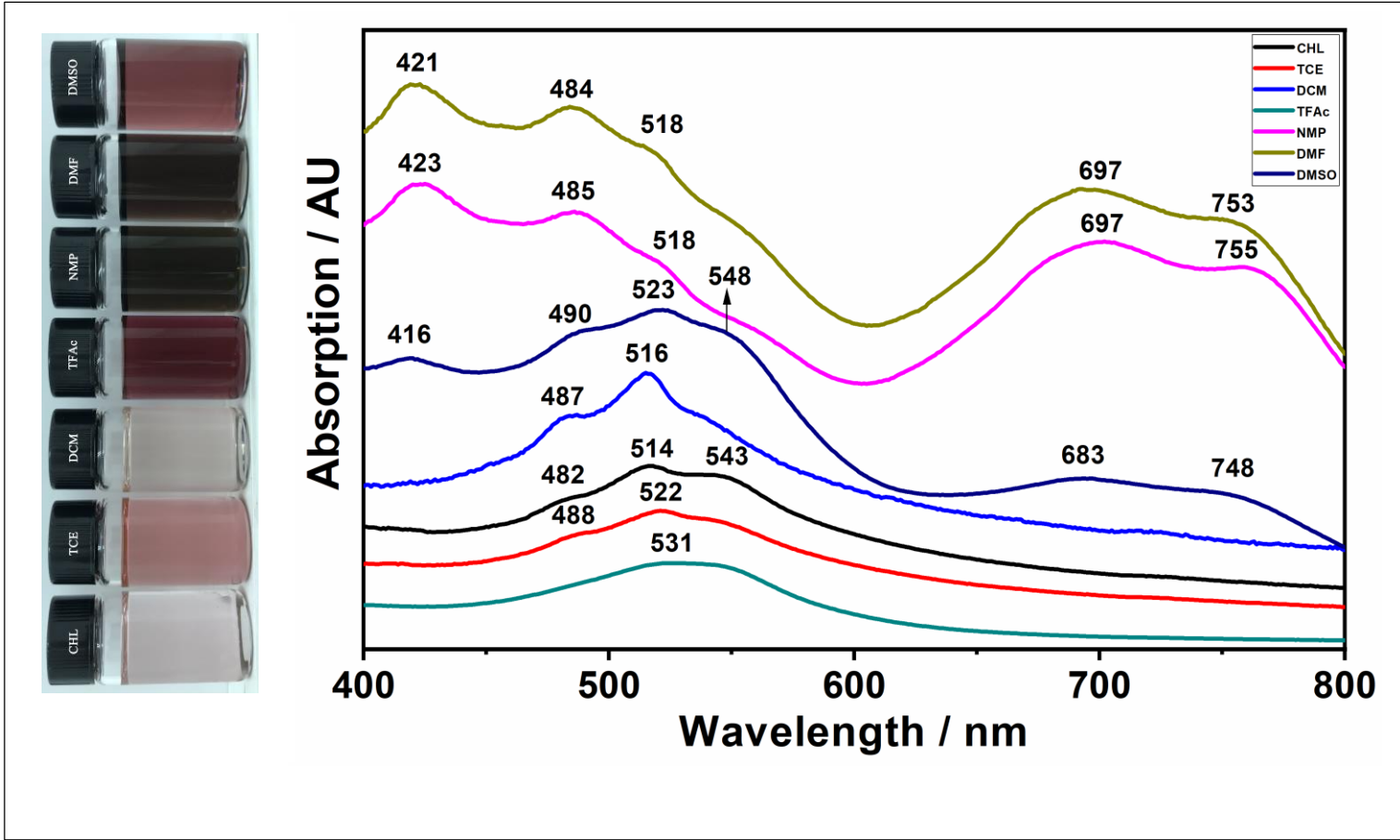


Figure 4.20: UV/Vis spectra of 4 in various solvents at (1×10^{-5} M)

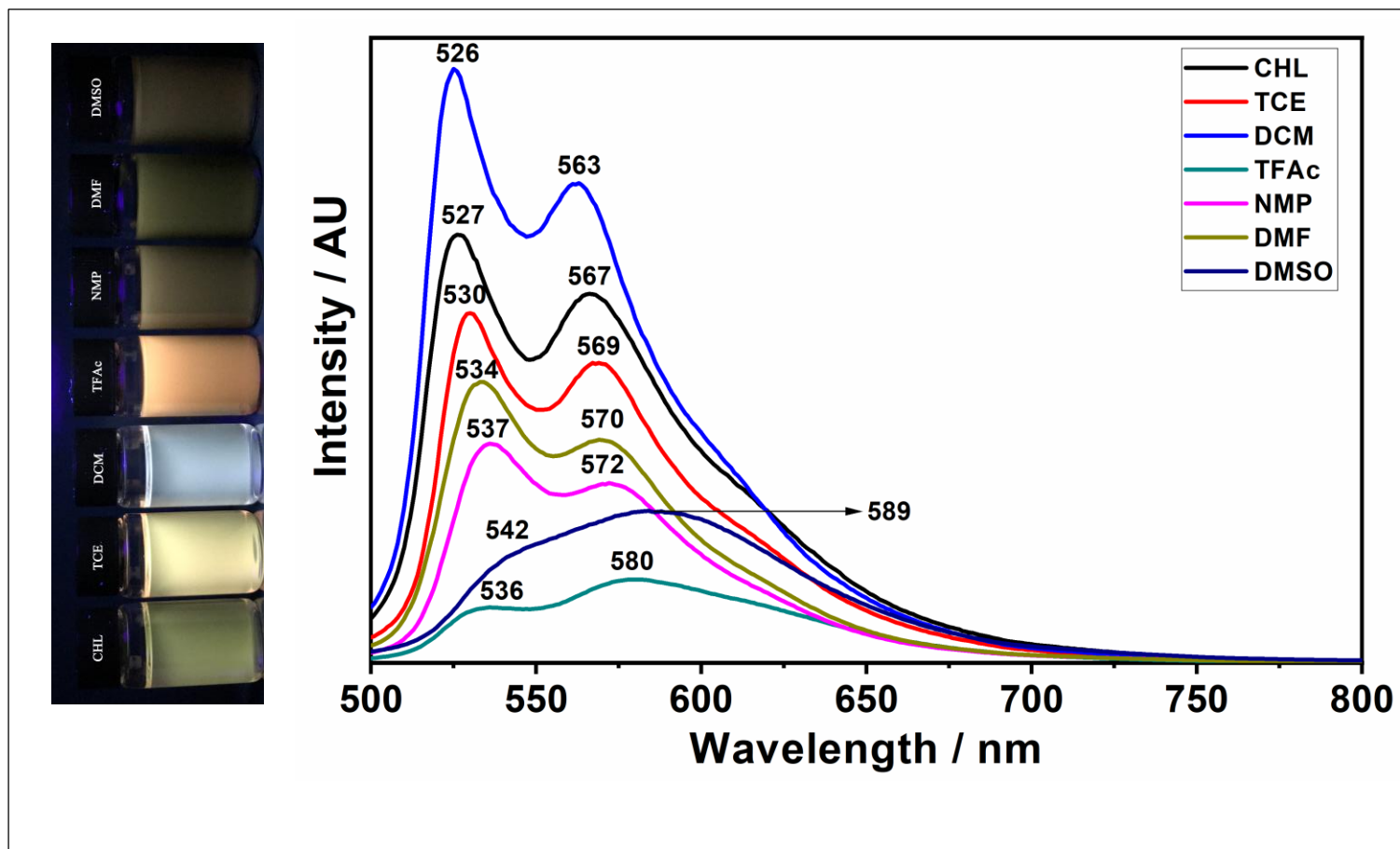


Figure 4.21: Emission spectra of 4 in various solvents at $\lambda_{exc.} = 485\text{nm}$

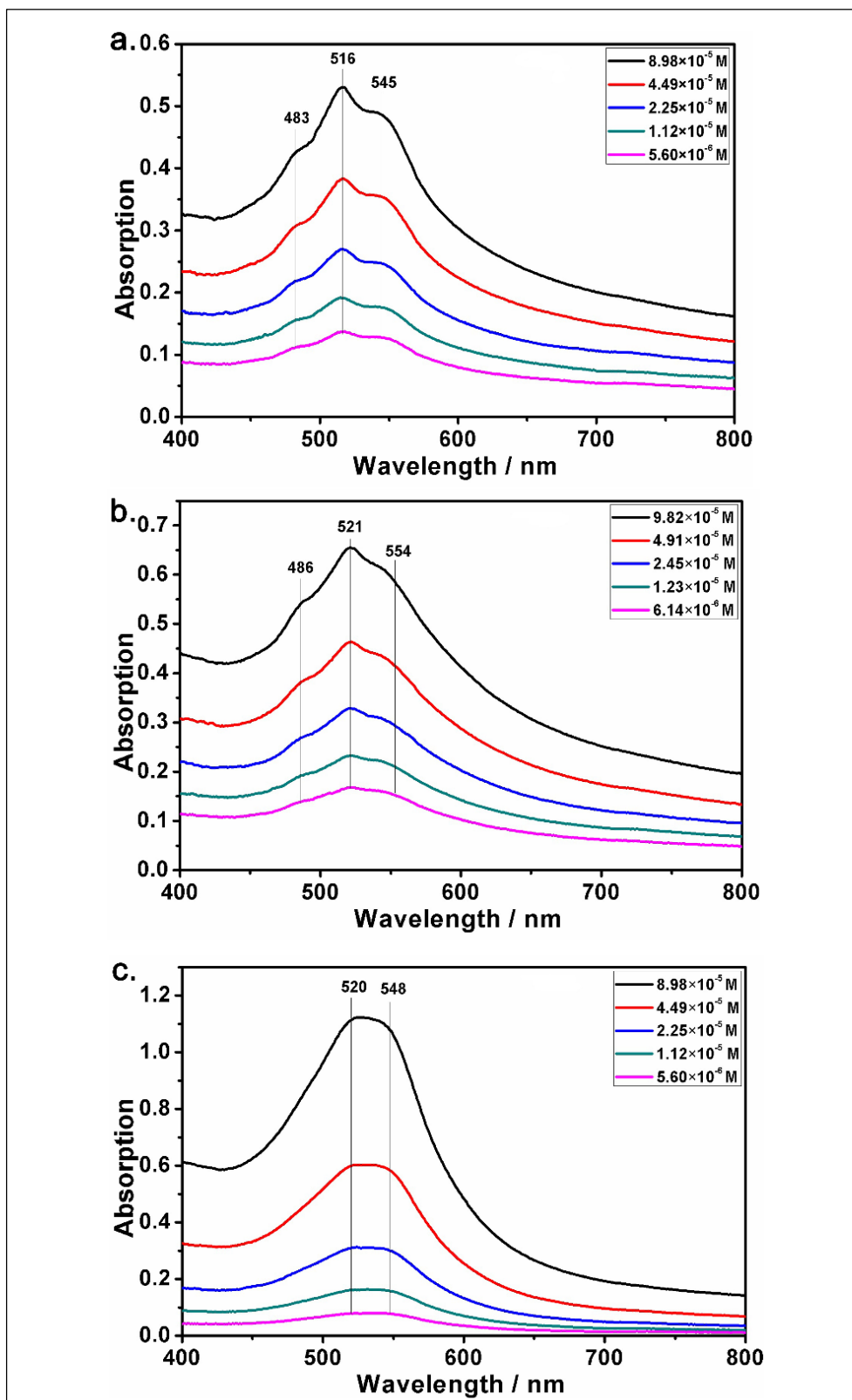


Figure 4.22: Concentration dependent spectra \ UV/Vis of 4 the solvents of (a), (b) and (c) are: CHL, TCE and TFAc respectively

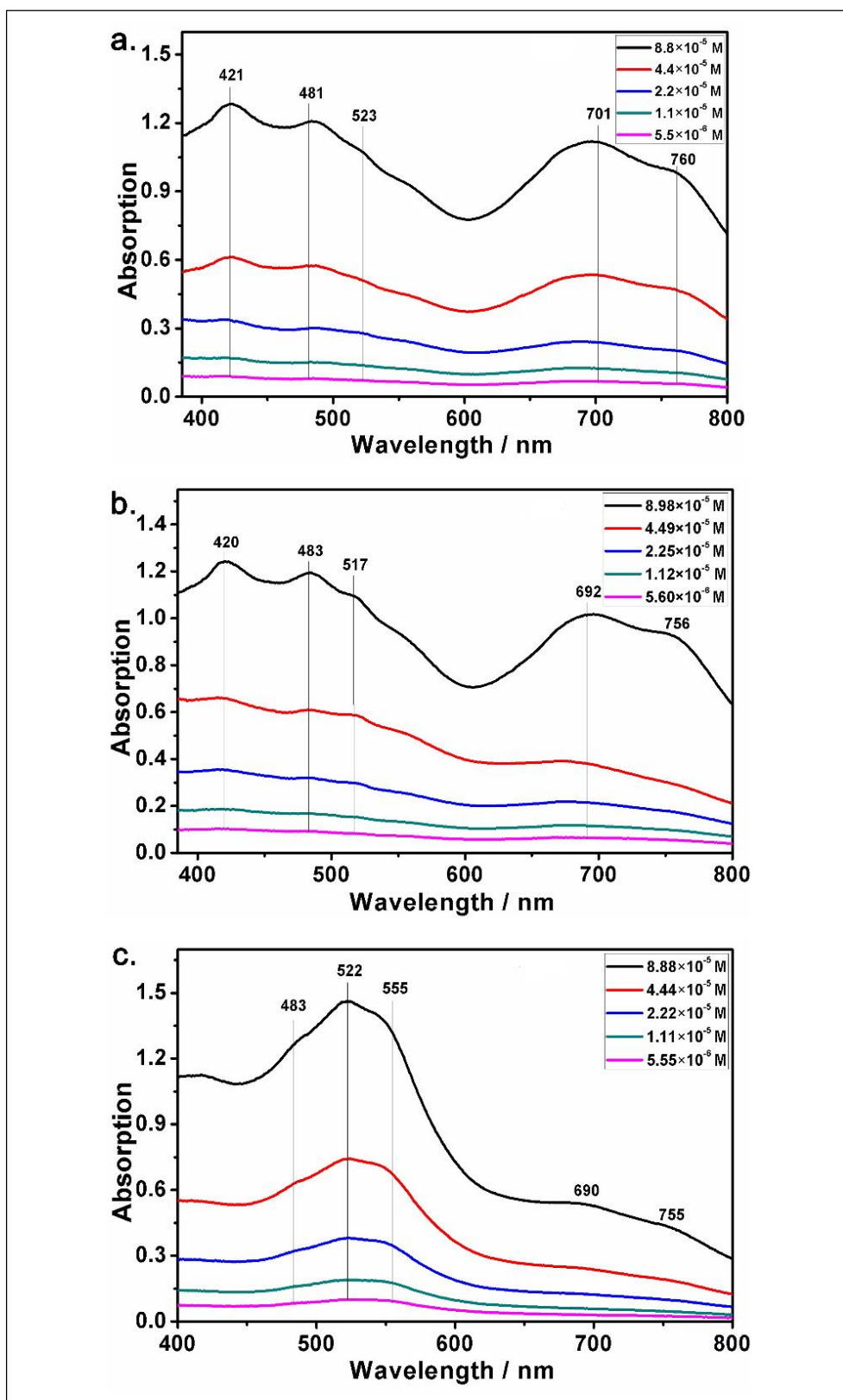


Figure 4.23: Concentration dependent spectra \ UV/Vis of 4 the solvents of (a), (b) and (c) are: NMP, DMF and DMSO respectively

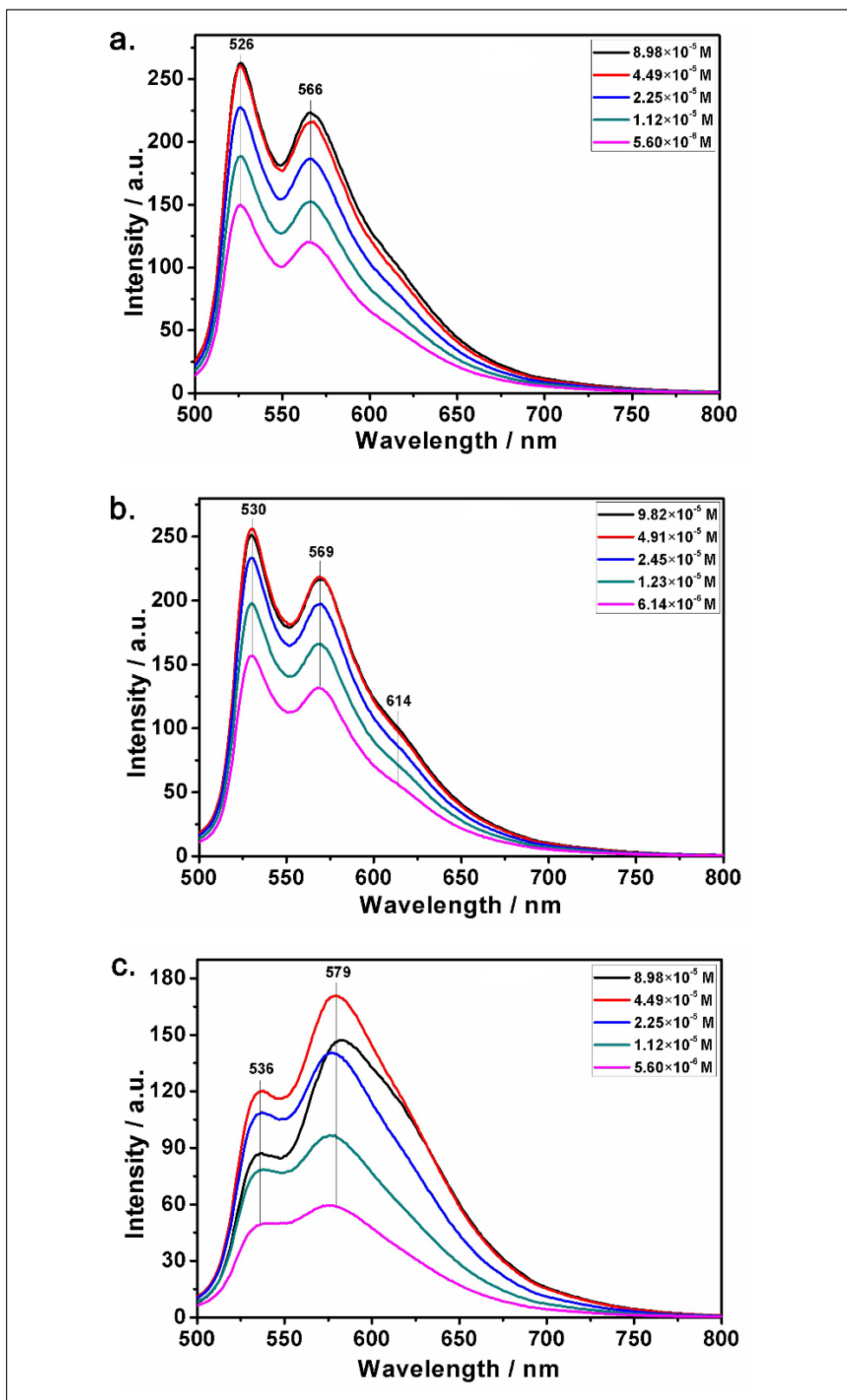


Figure 4.24: Concentration dependent spectra \ emission of 4 the solvents of (a), (b) and (c) are: CHL, TCE and TFAc respectively at $\lambda_{exc.} = 485\text{nm}$

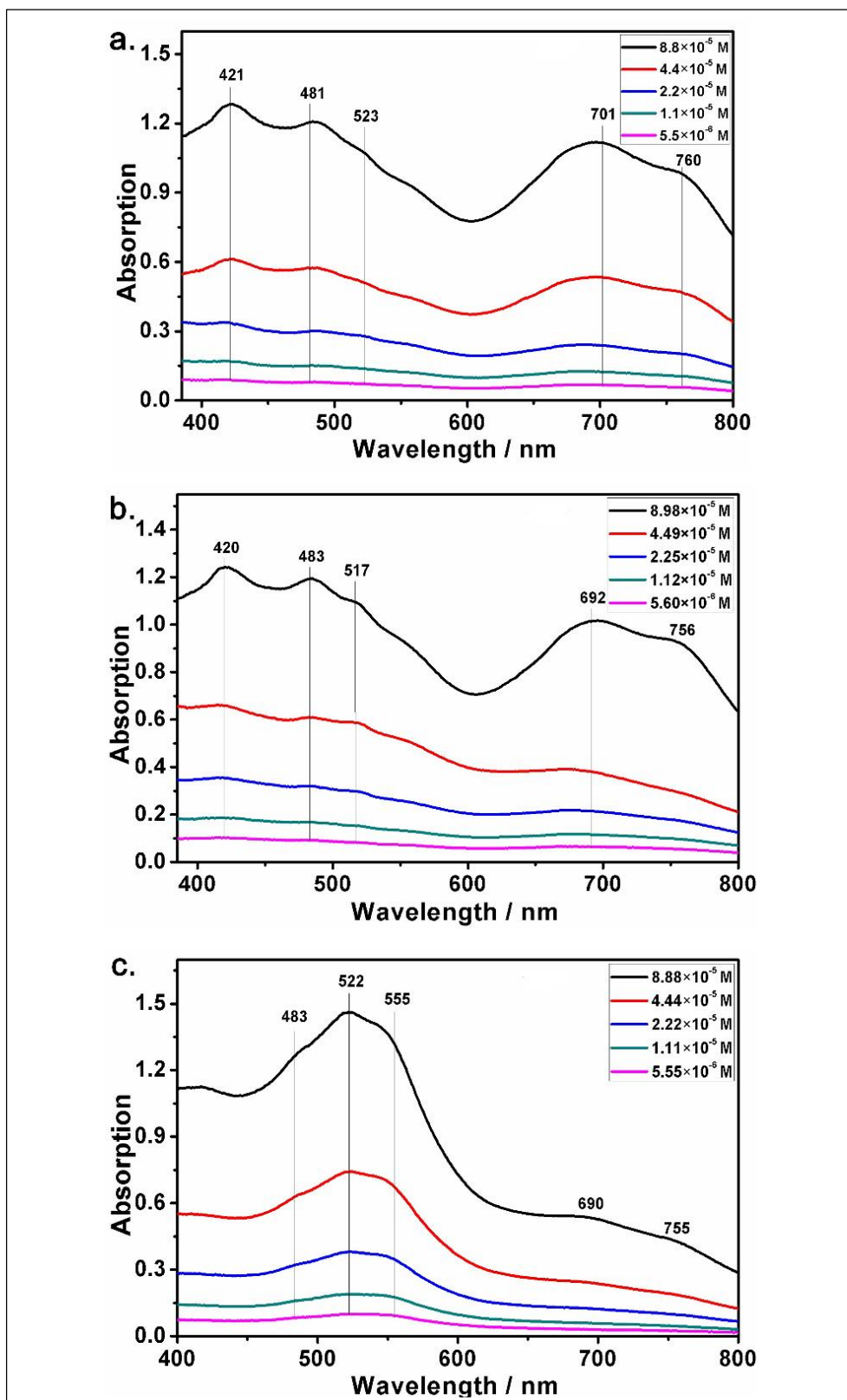


Figure 4.25: Concentration dependent spectra \ emission of 4 the solvents of (a), (b) and (c) are: NMP, DMF and DMSO respectively at $\lambda_{exc.} = 485$ nm

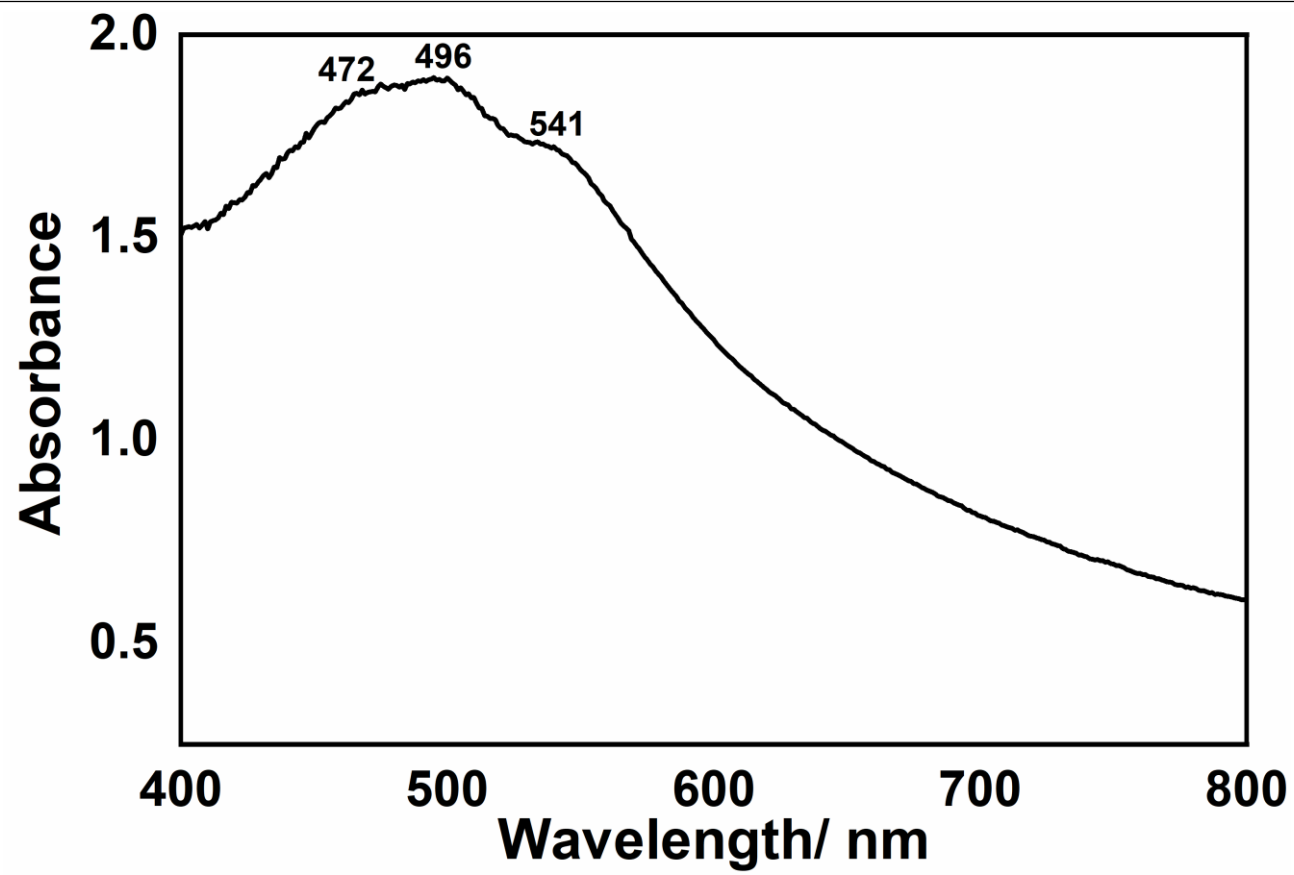


Figure 4.26: UV/ Vis in solid state spectrum of 4

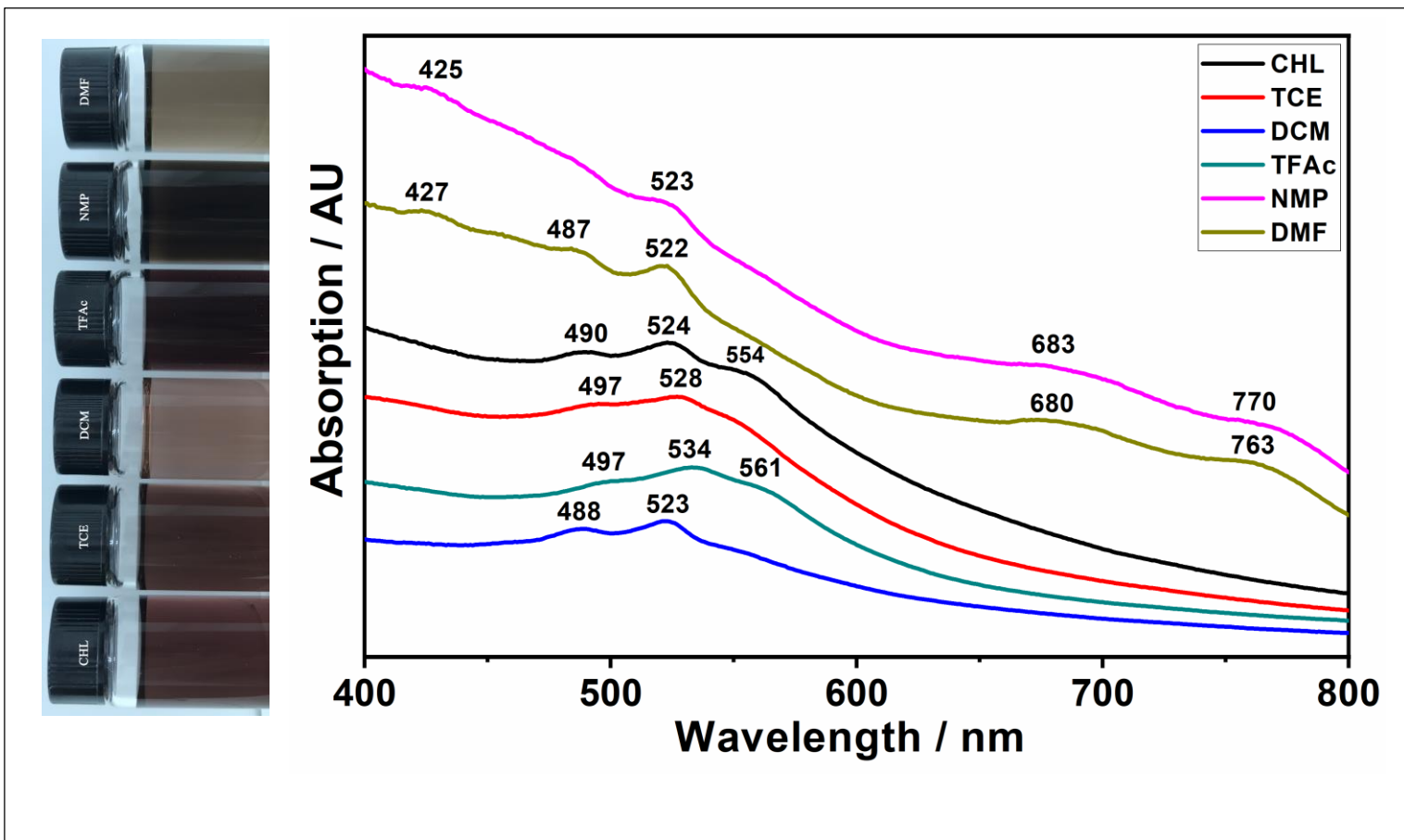


Figure 4.27: UV/Vis spectra of 6 in various solvents at (1×10^{-5} M)

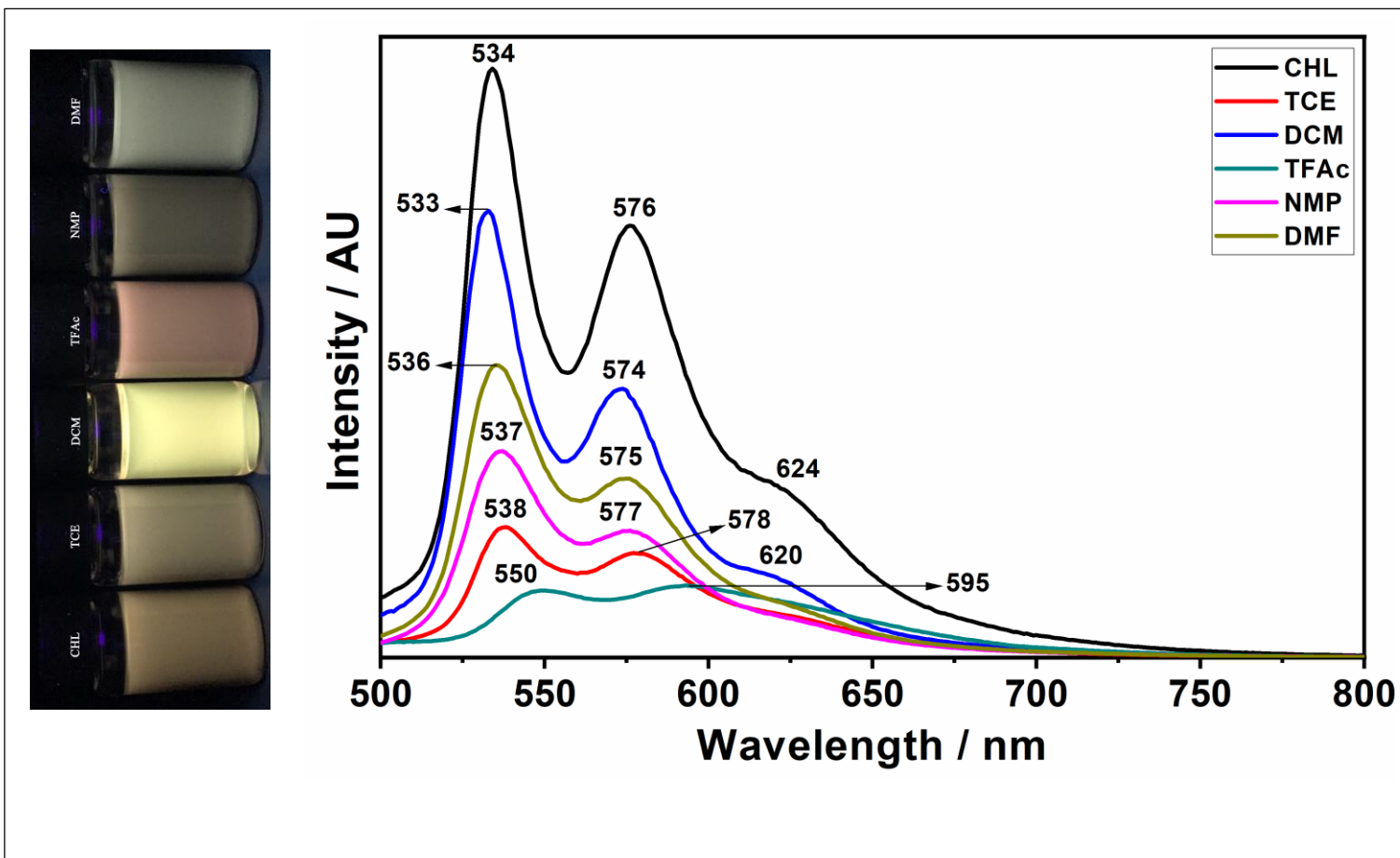


Figure 4.28: Emission spectra of 6 in various solvents at $\lambda_{exc.} = 485\text{nm}$

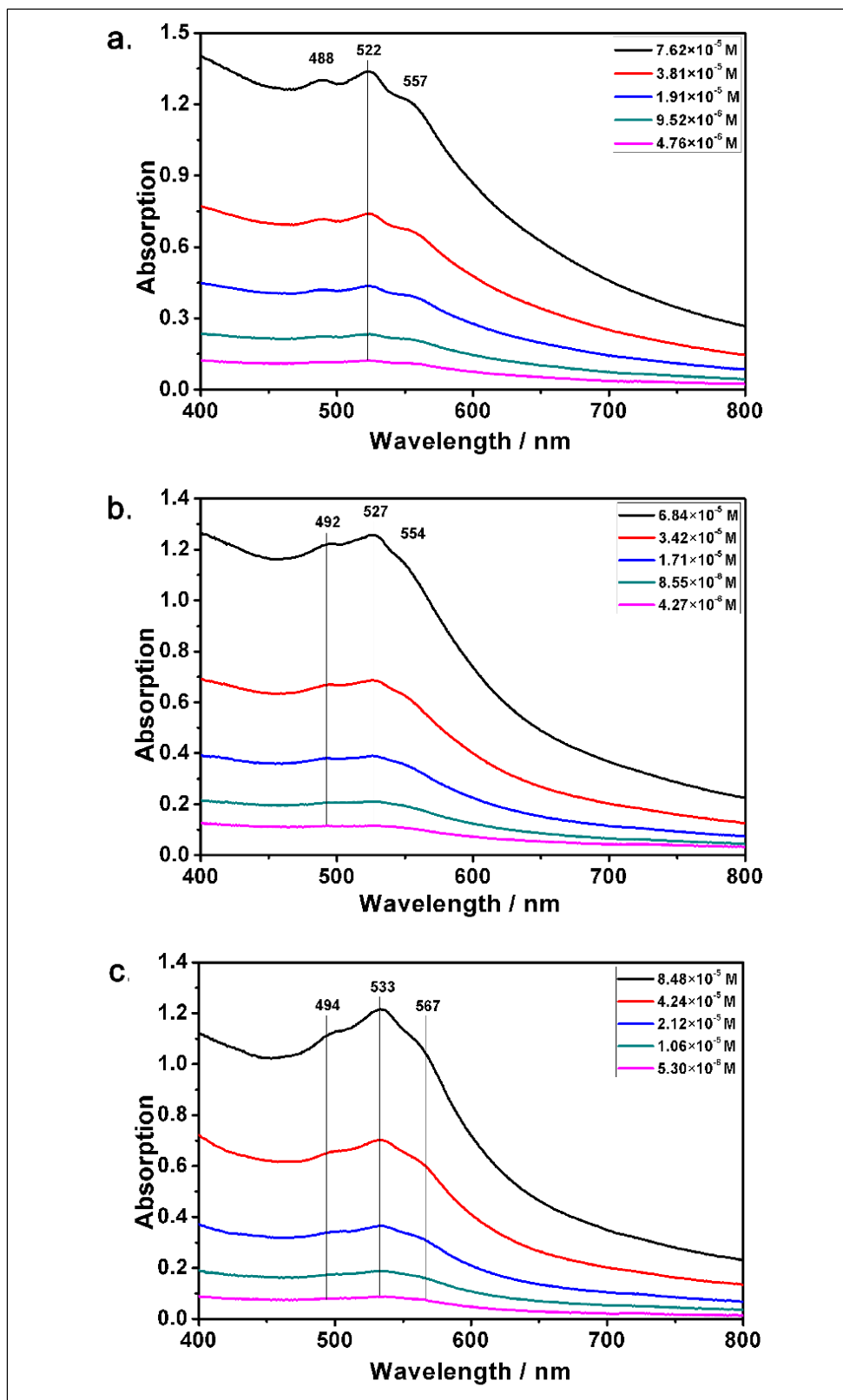


Figure 4.29: Concentration dependent spectra \ UV/Vis of 6 the solvents of (a), (b) and (c) are: CHL, TCE and TFAc respectively

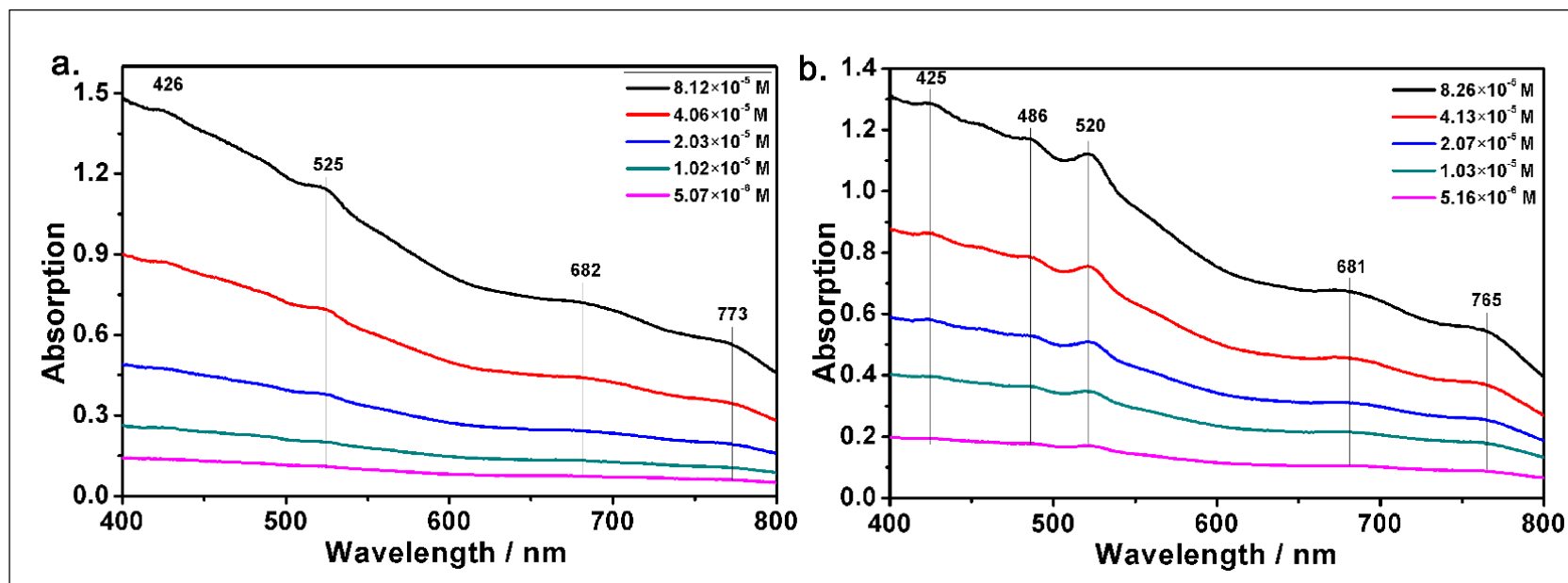


Figure 4.30: Concentration dependent UV\Vis spectra of 6, the solvents of (a) and (b) are: NMP and DMF respectively

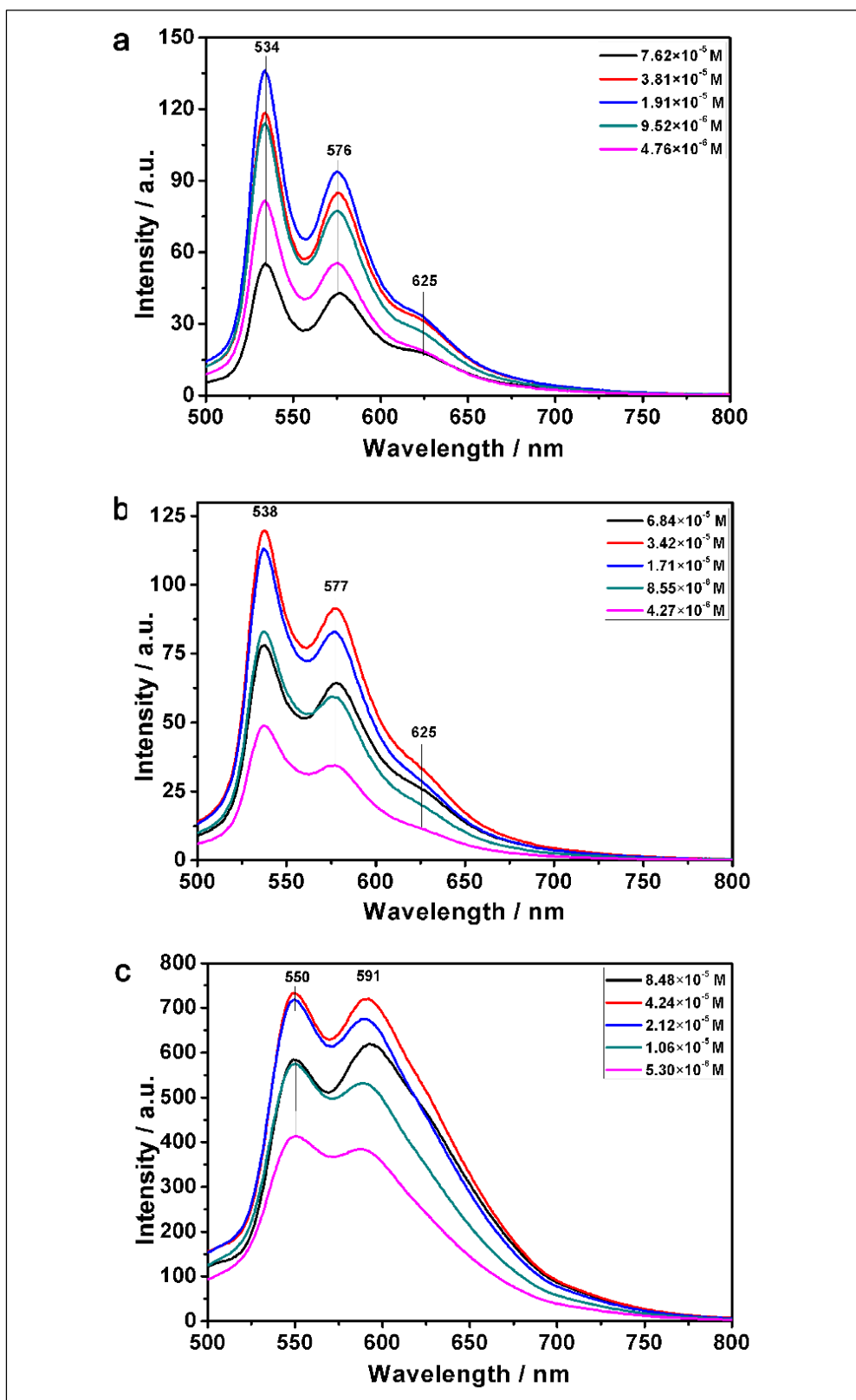


Figure 4.31: Concentration dependent spectra/ emission of 6 the solvents (a), (b) and (c) are: CHL, TCE and TFAc respectively at $\lambda_{exc.} = 485\text{nm}$

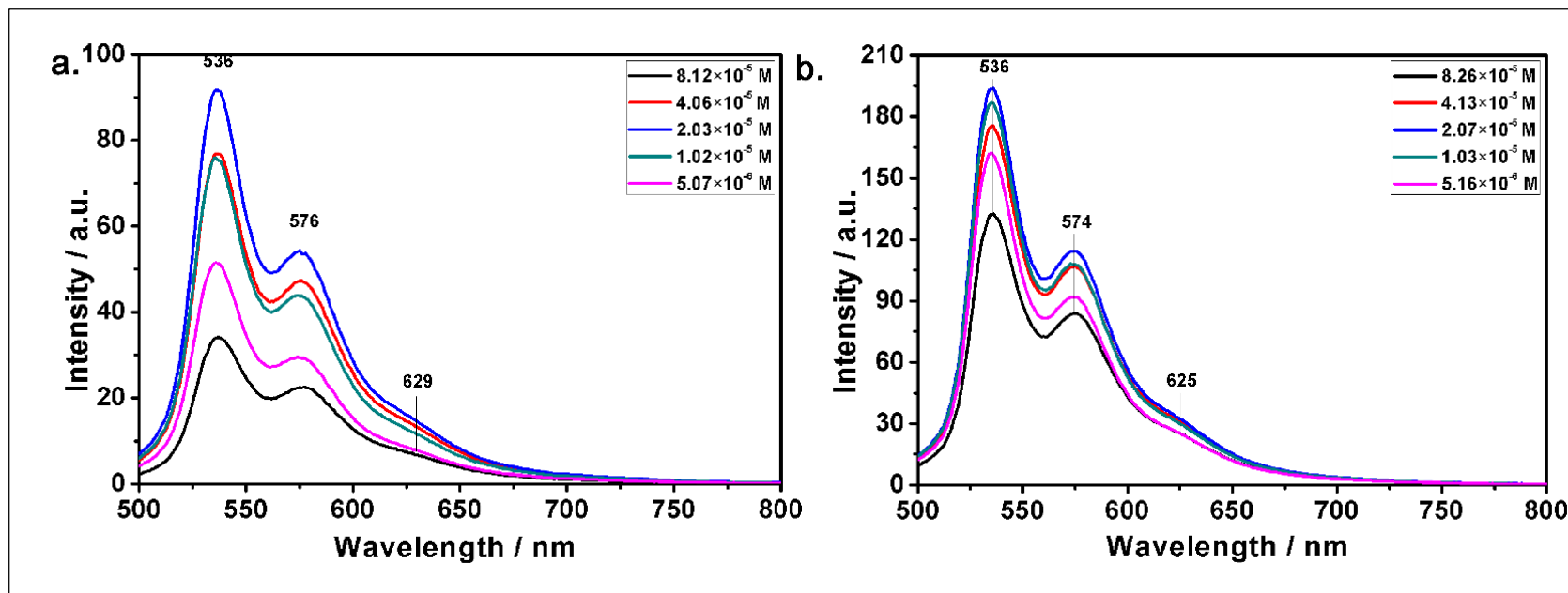


Figure 4.32: Concentration dependent spectra /emission of 6 the solvents of (a) and (b) are: NMP and DMF respectively at $\lambda_{exc.} = 485\text{nm}$

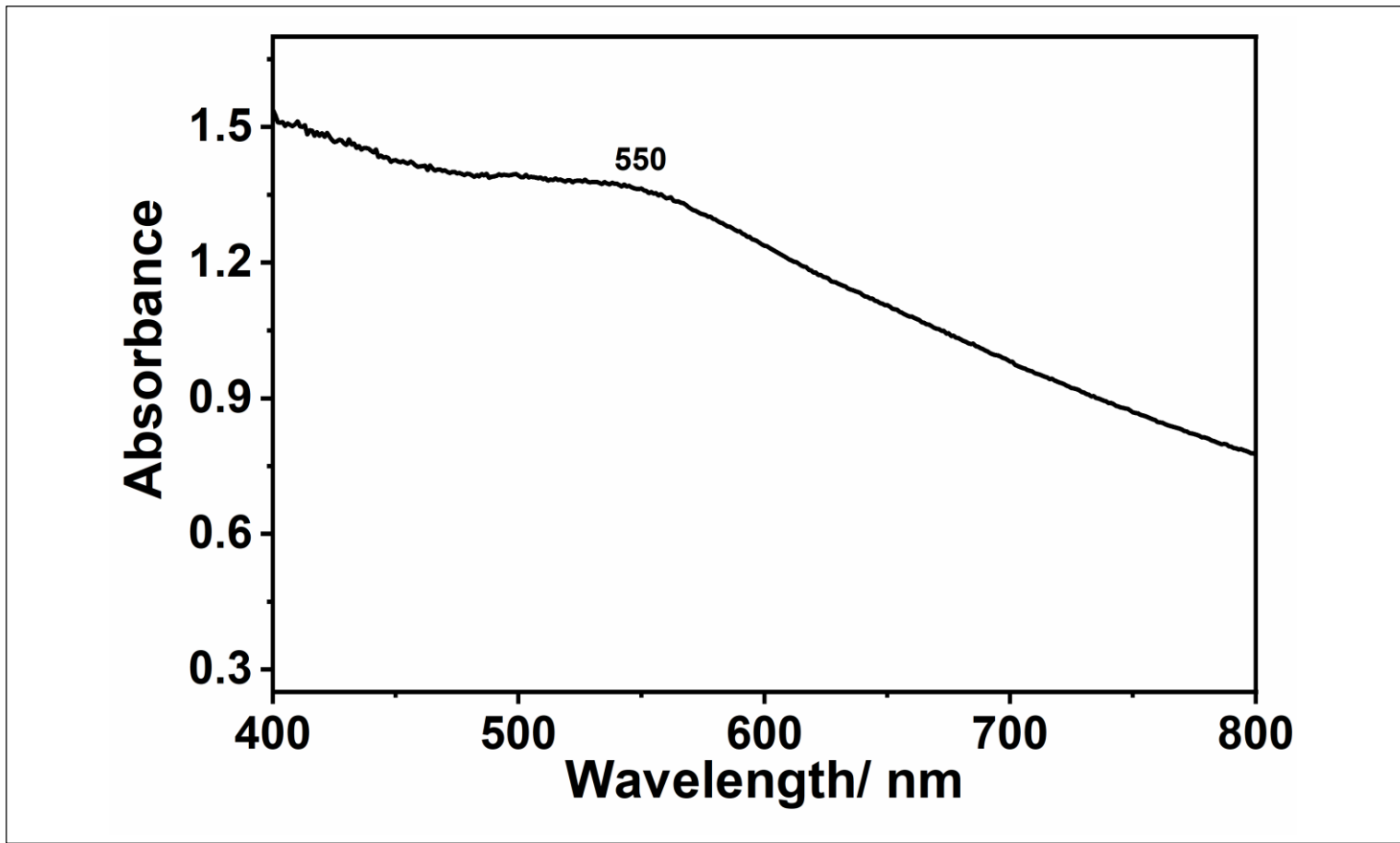


Figure 4.33: Solid state UV/ Vis spectrum of 6

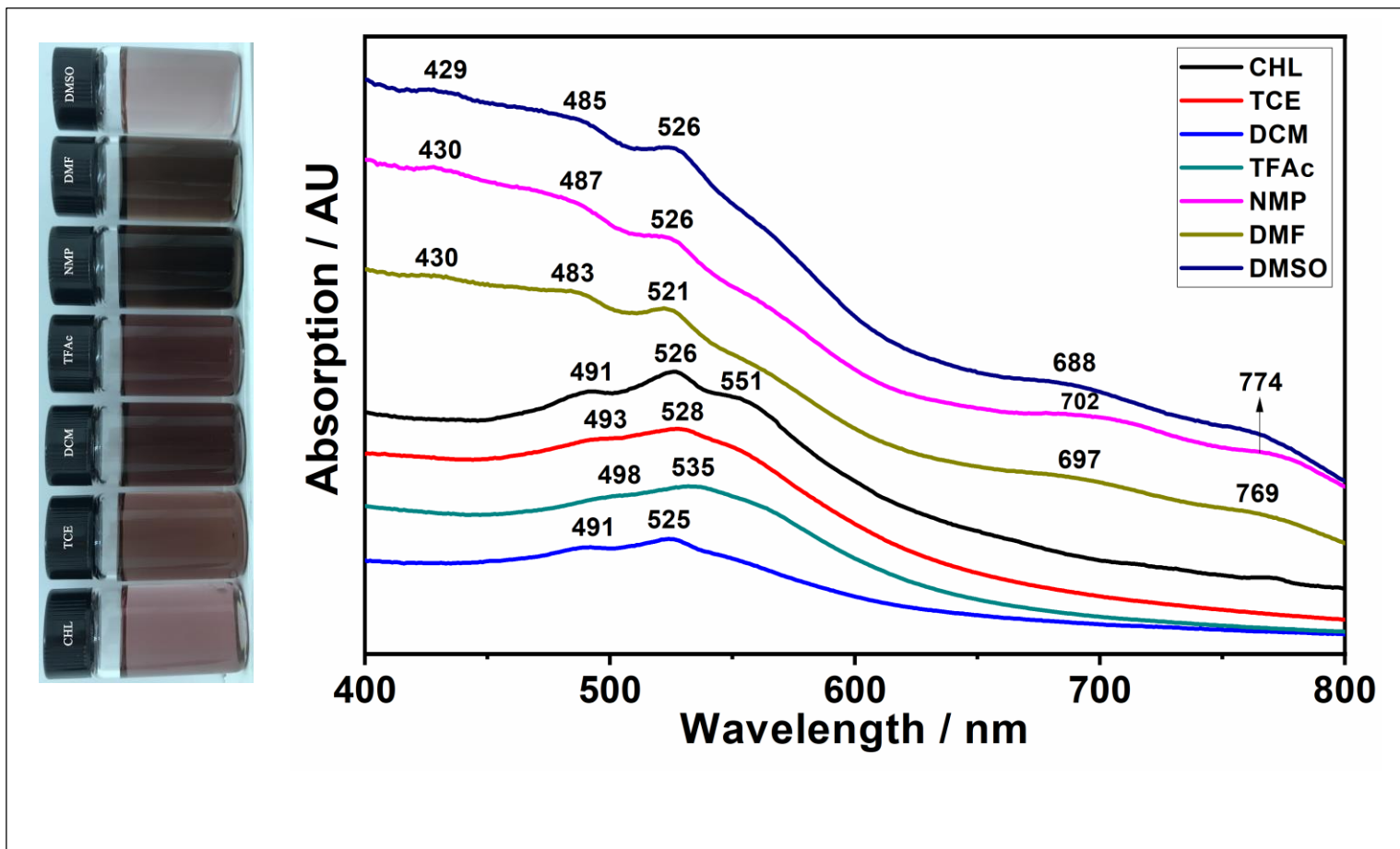


Figure 4.34: UV/Vis absorption spectra of 8 in various solvents at (1×10^{-5} M)

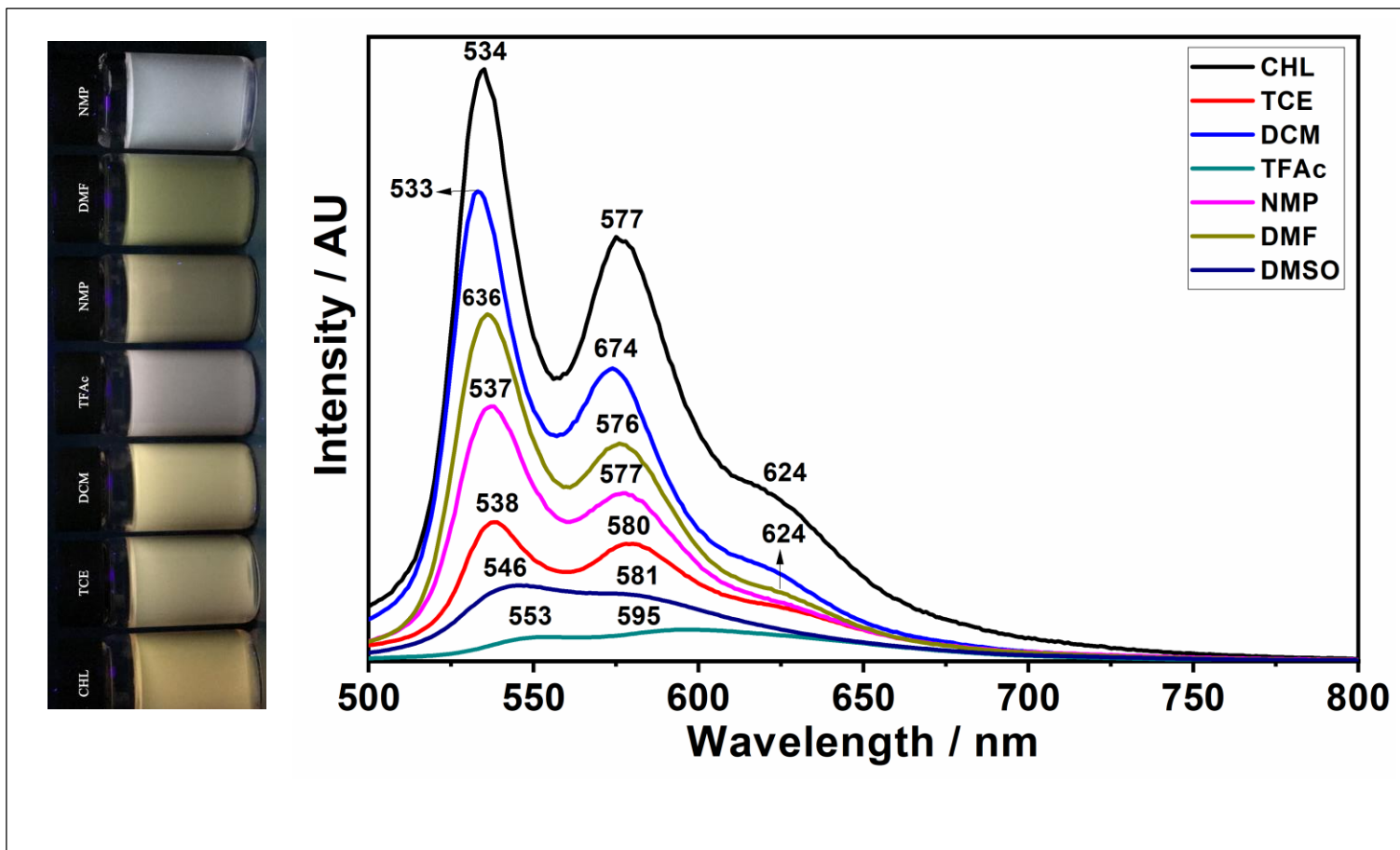


Figure 4.35: Emission spectra of 8 in various solvents at $\lambda_{exc} = 485\text{nm}$

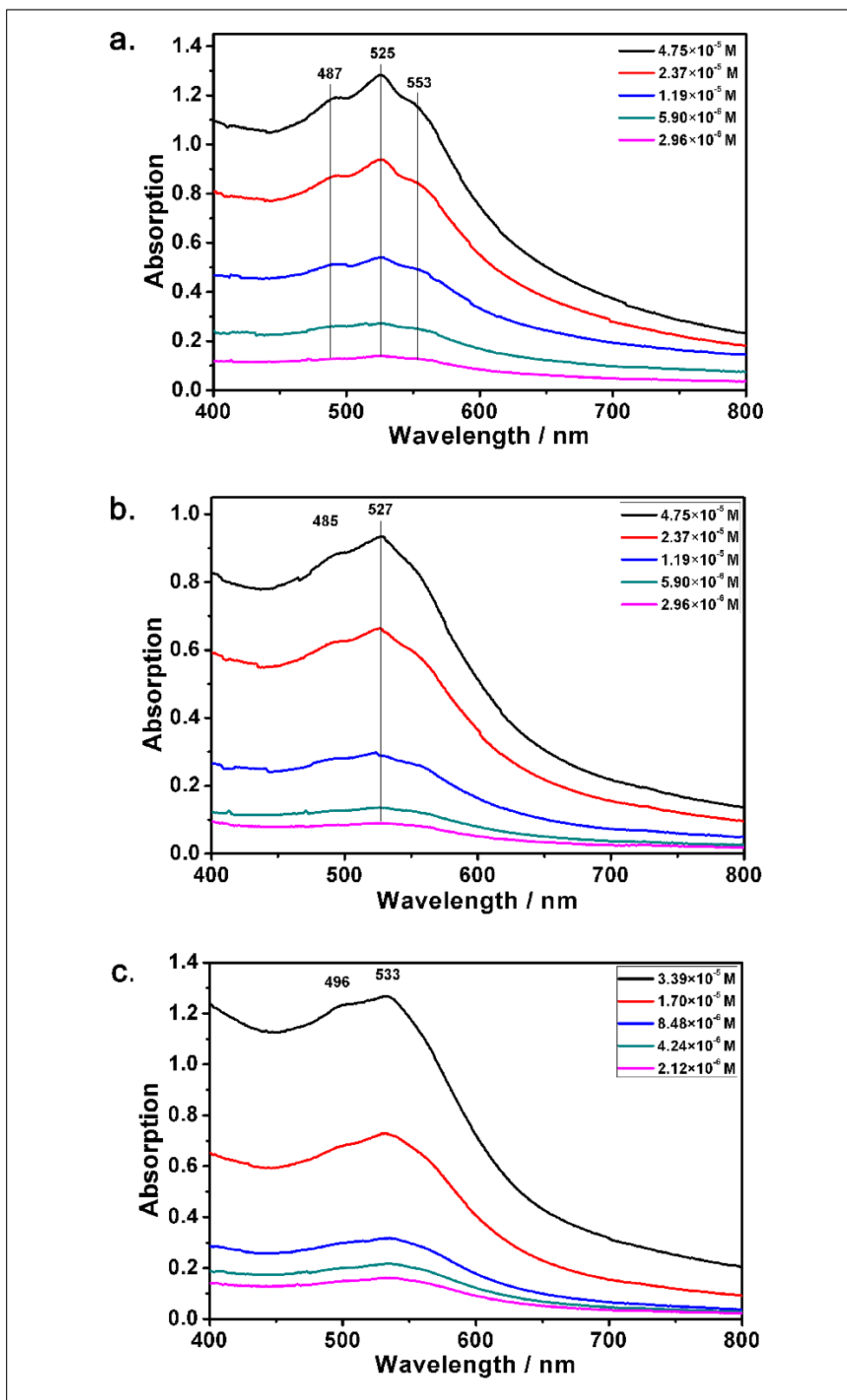


Figure 4.36: Concentration dependent UV\Vis spectra of 8. The solvents of (a), (b) and (c) are: CHL, TCE and TFAc respectively

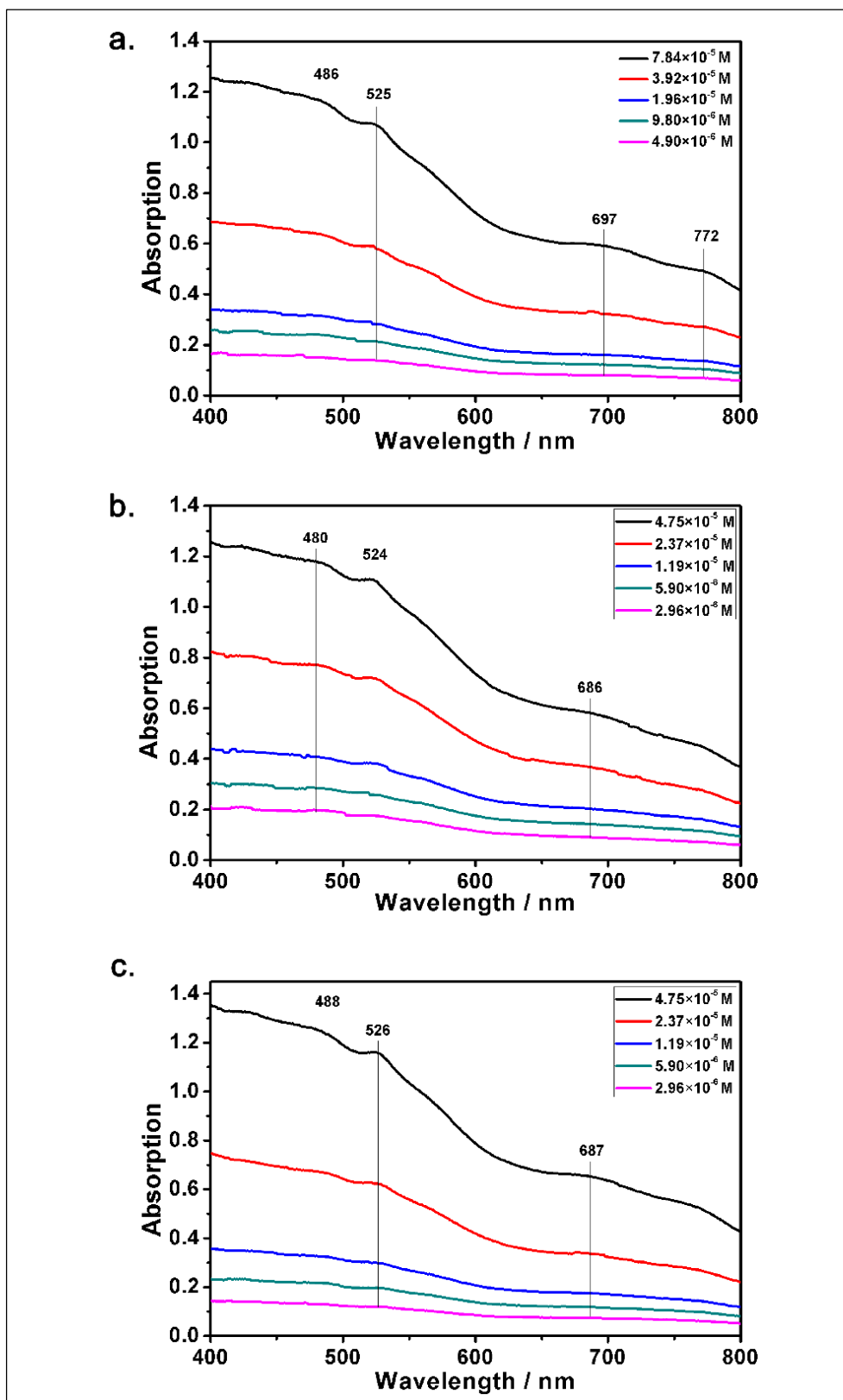


Figure 4.37: Concentration dependent UV\Vis spectra of 8. The solvents of (a), (b) and (c) are: NMP, DMF and DMSO respectively

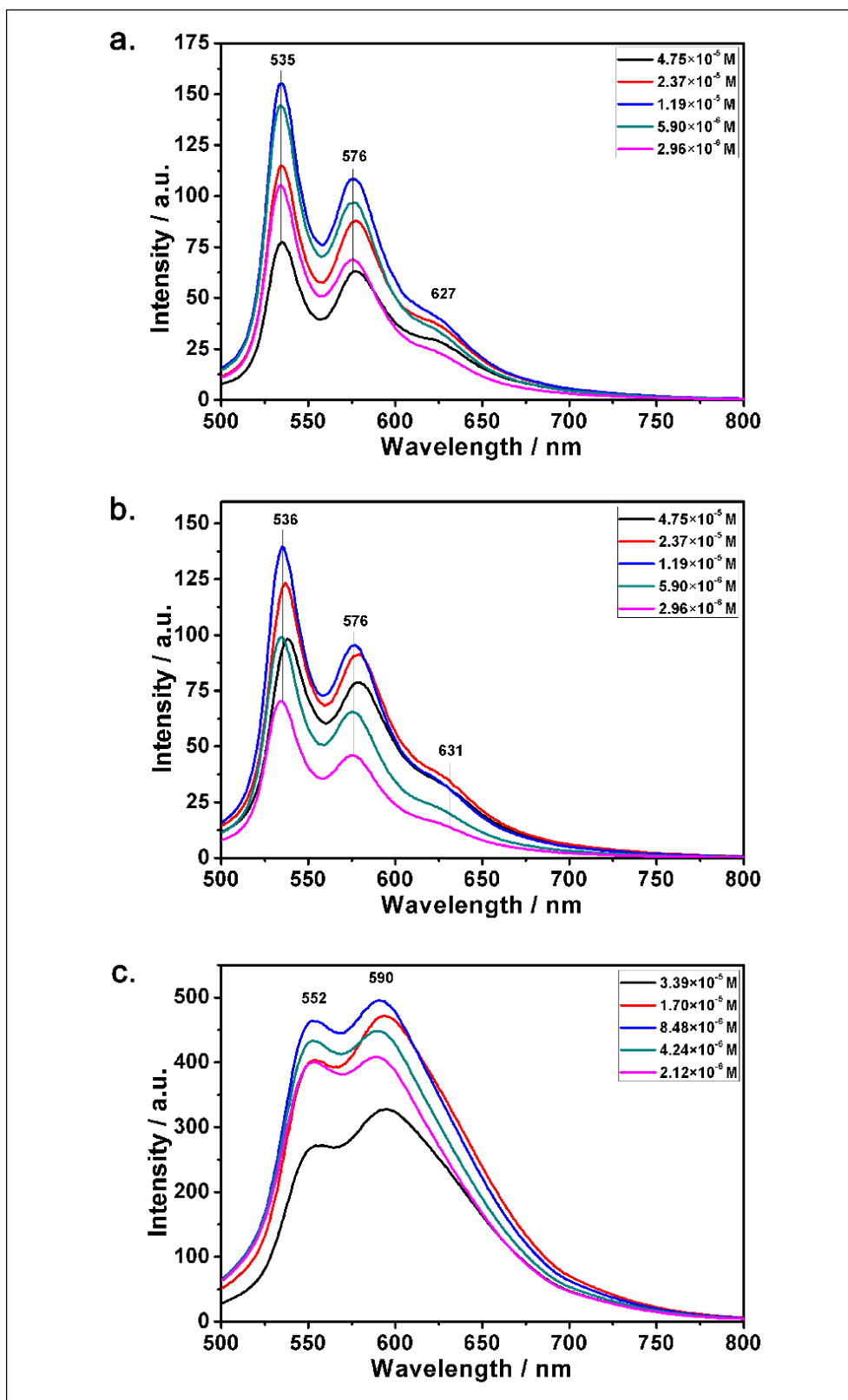


Figure 4.38: Concentration dependent spectra/ emission of 8, the solvents of (a), (b) and (c) are: CHL, TCE and TFAc respectively at $\lambda_{exc.} = 485\text{nm}$

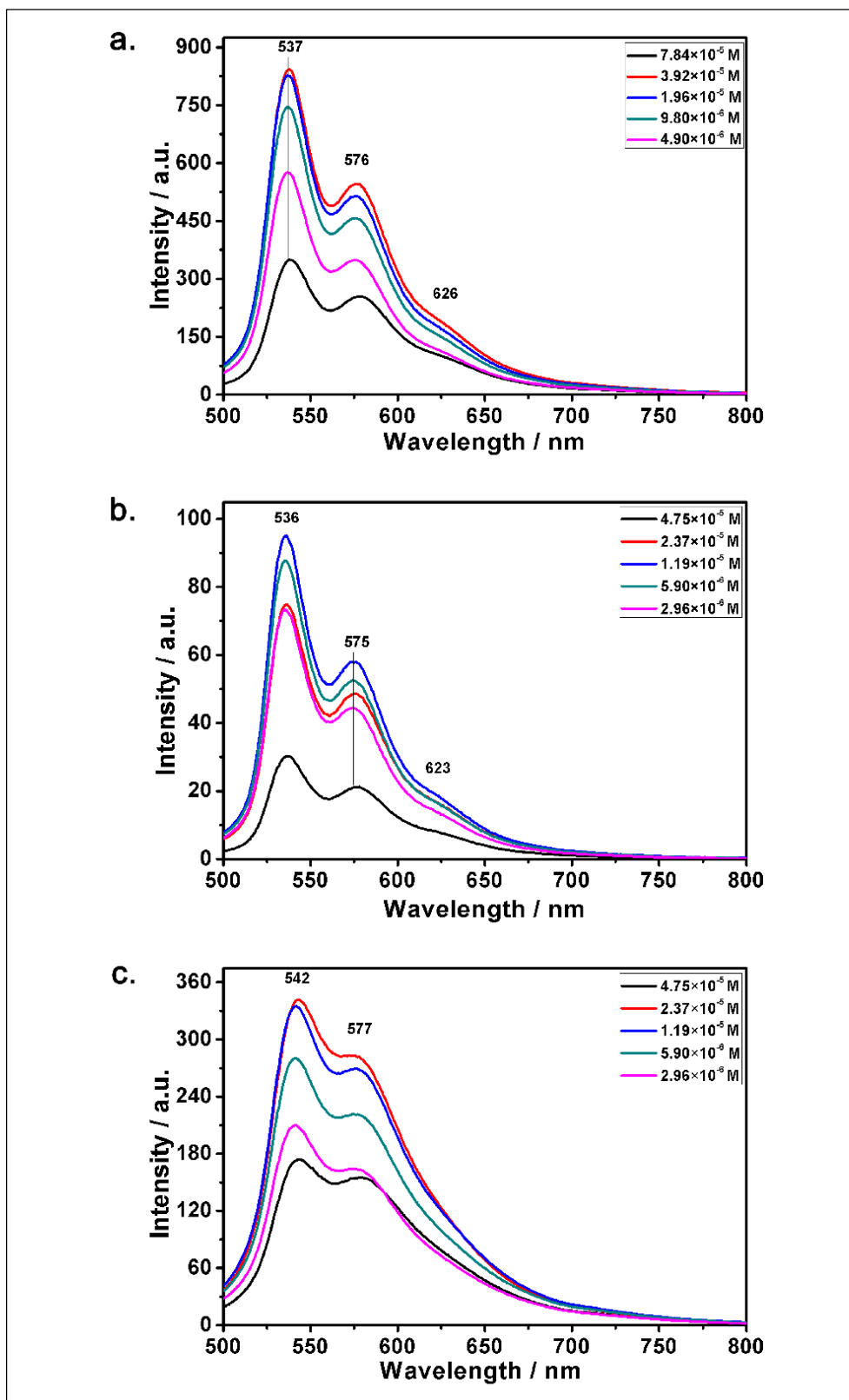


Figure 4.39: Concentration dependent emission spectra of 8, the solvents of (a), (b) and (c) are: NMP, DMF and DMSO respectively at $\lambda_{exc.} = 485$ nm

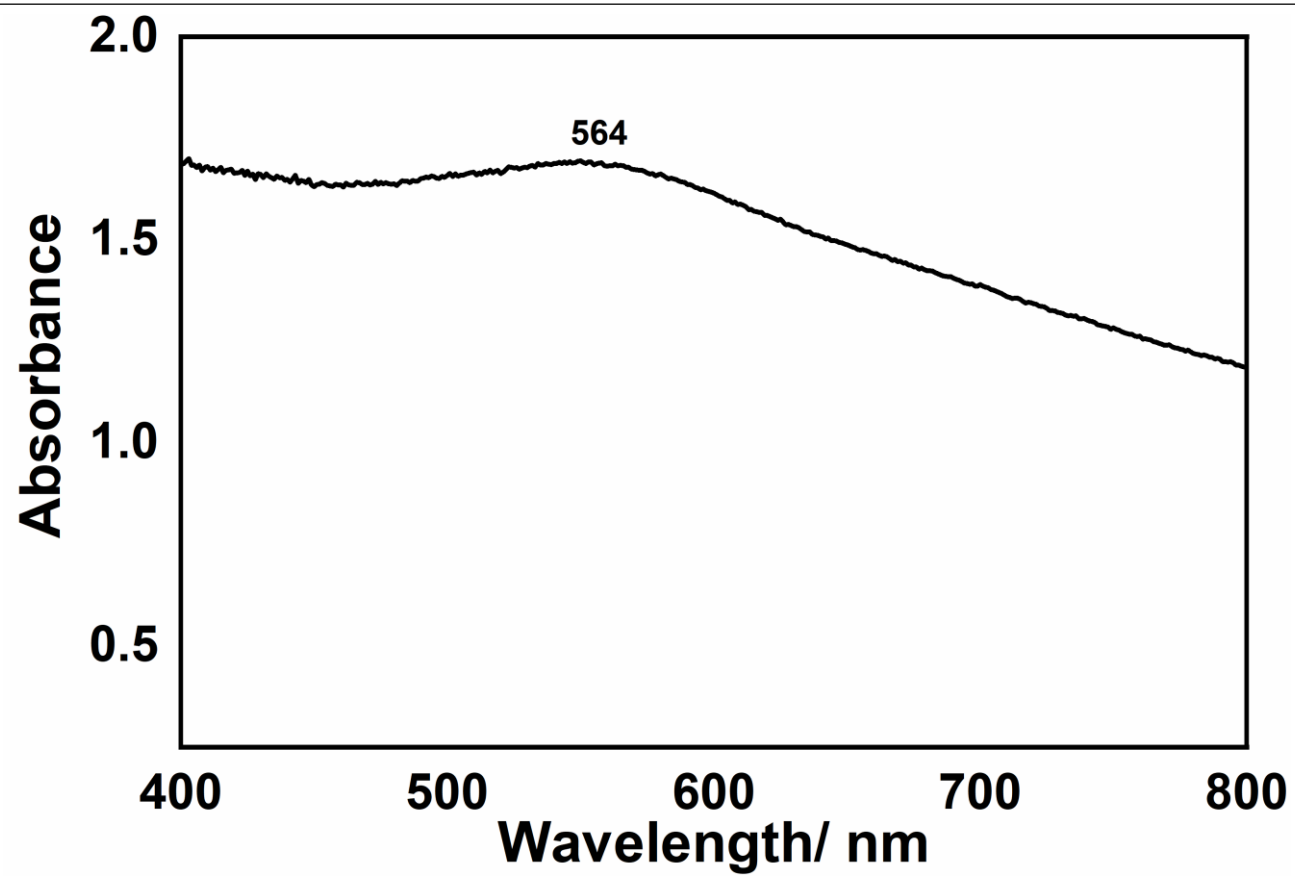


Figure 4.40: UV/ Vis spectrum of 8 in solid state

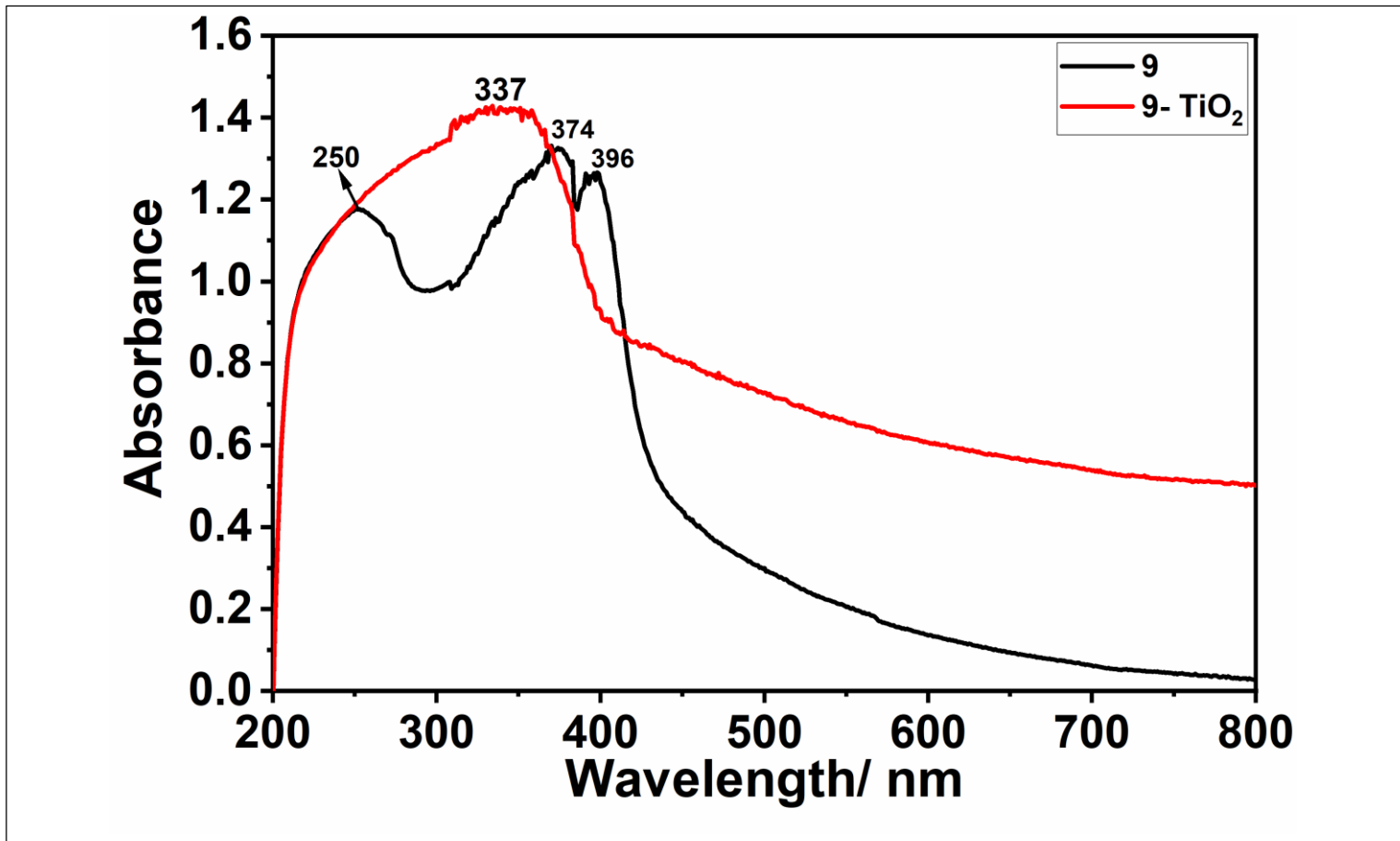


Figure 4.41: UV/ Vis spectrum of 9 in solid state and 9 adsorbed on TiO₂

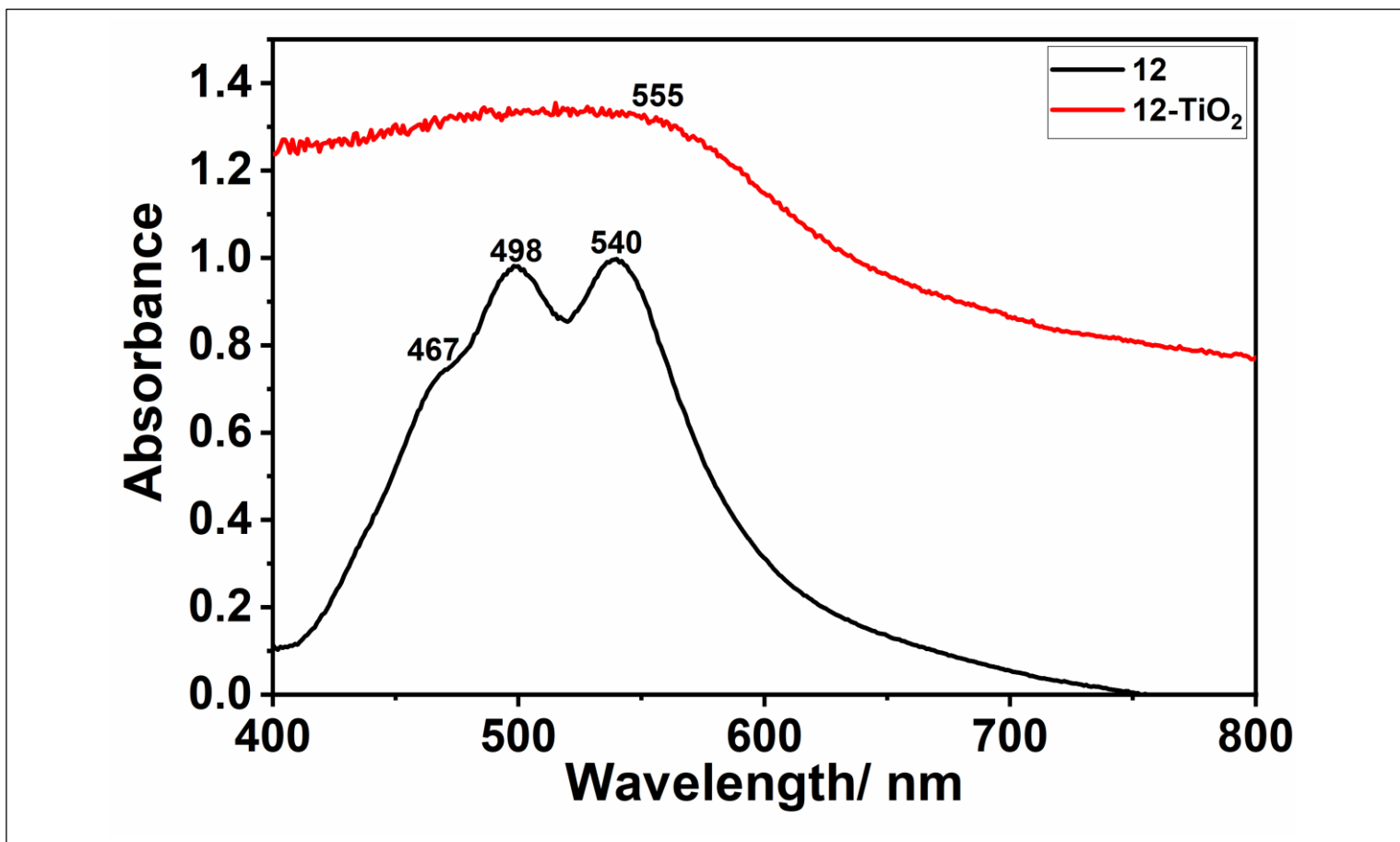


Figure 4.42: UV/ Vis spectrum of 12 in solid state and 12 adsorbed on TiO₂

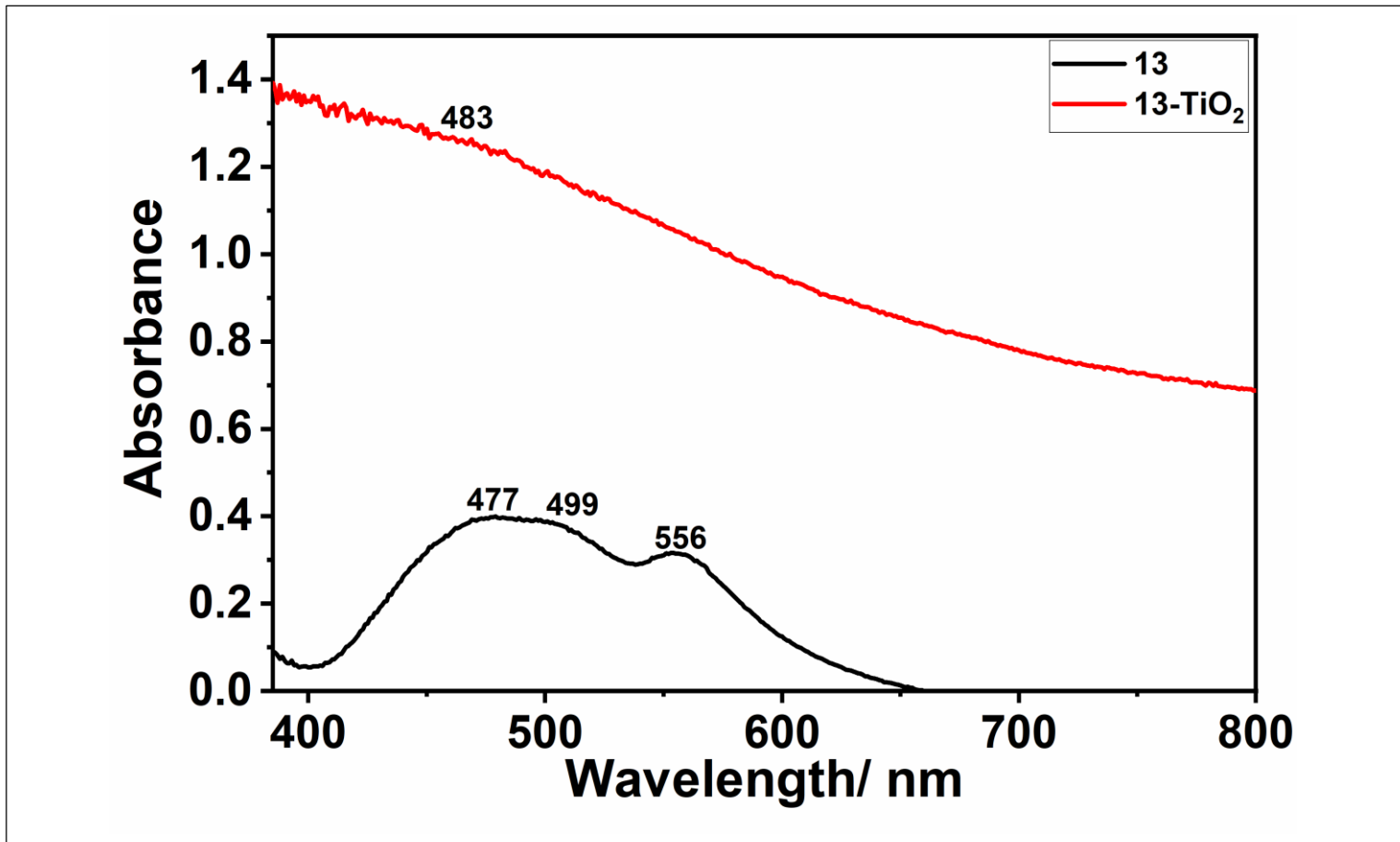


Figure 4.43: UV/ Vis spectrum of 13 in solid state and 13 adsorbed on TiO₂

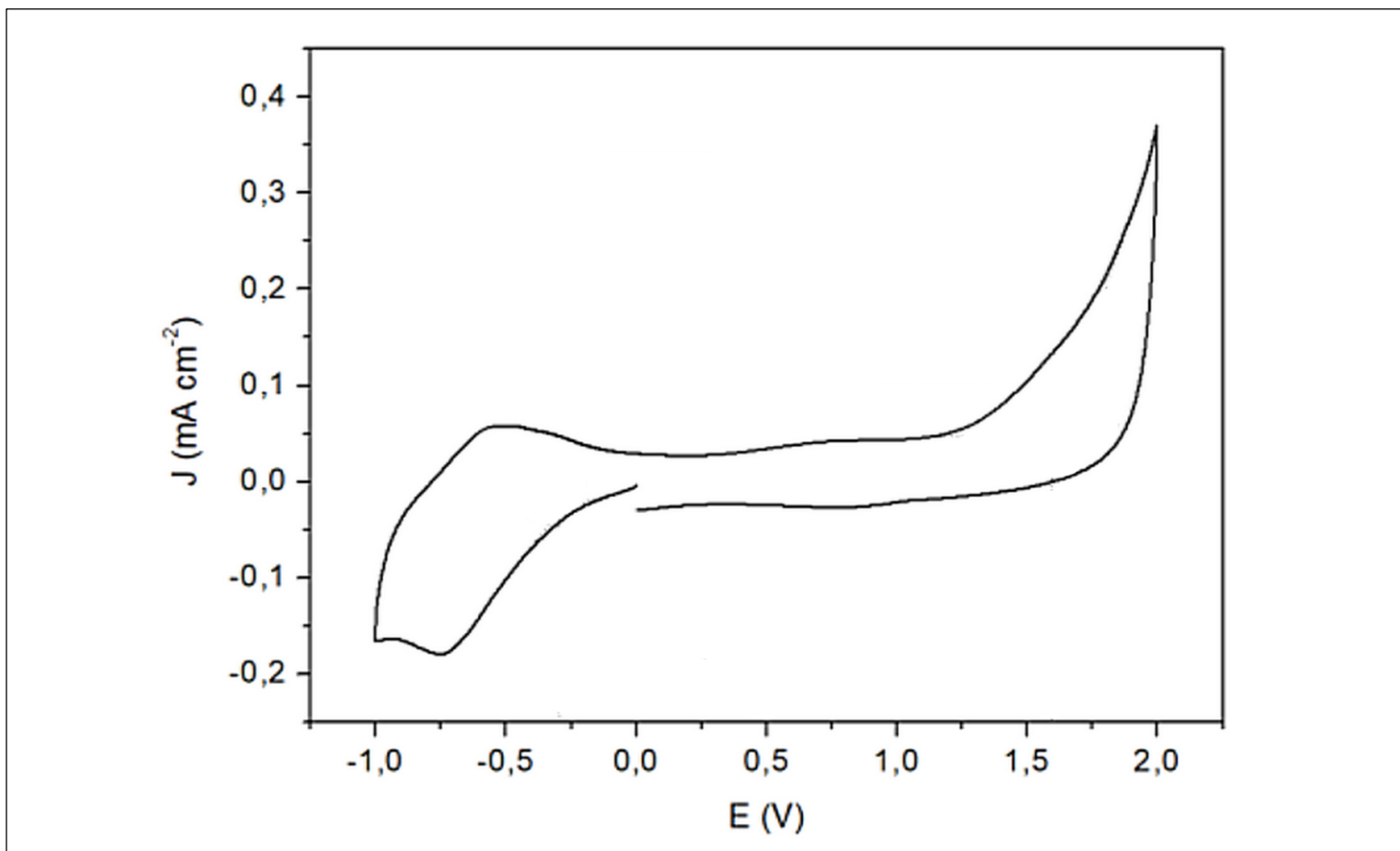


Figure 4.44: Cyclic voltammogram of 4 in acetonitrile solution at 100 mVs⁻¹, supporting electrolyte 0.1 M TBAPF₆

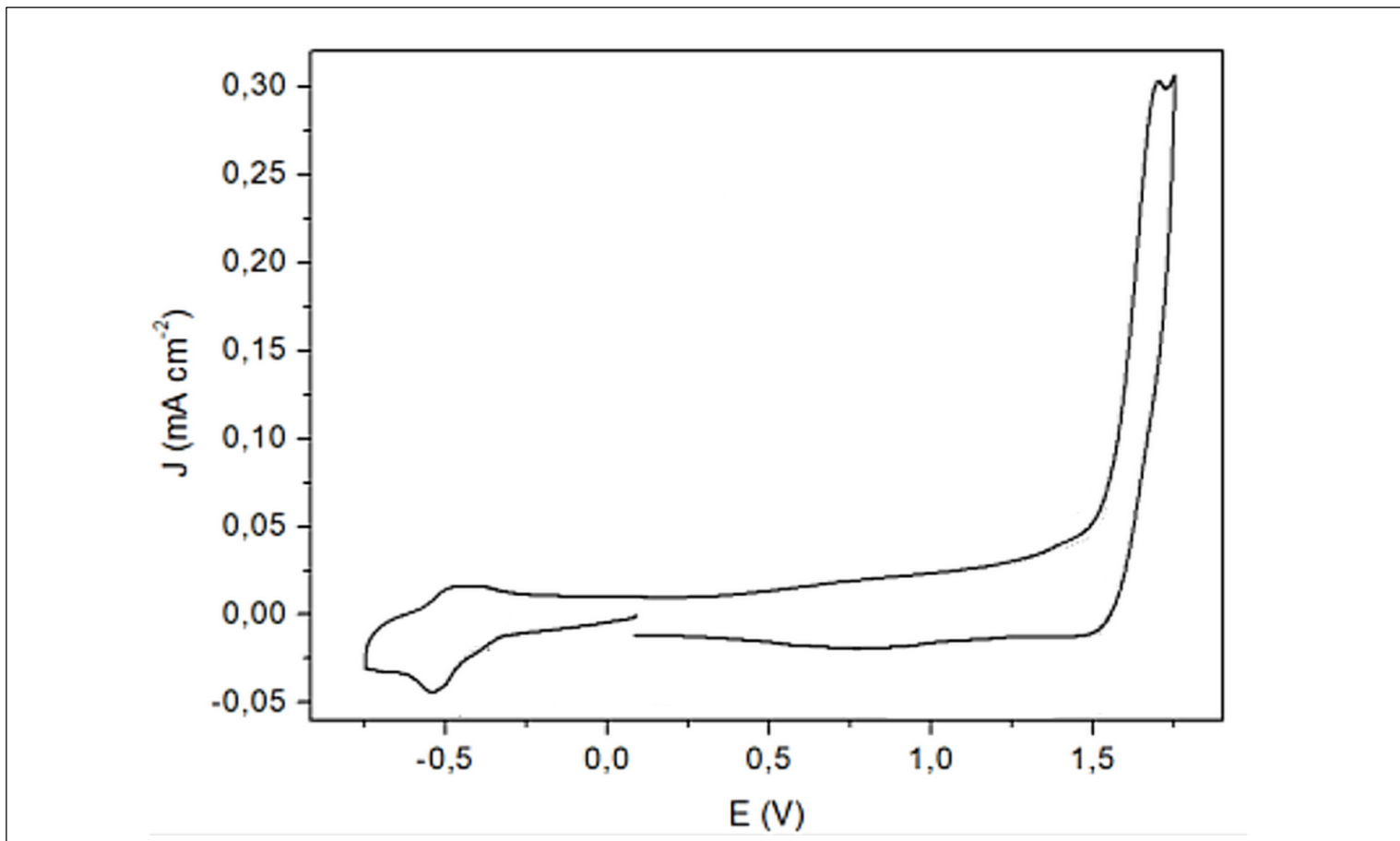


Figure 4.45: Cyclic voltammogram of 6 in acetonitrile solution at 100 mVs^{-1} , supporting electrolyte 0.1 M TBAPF_6

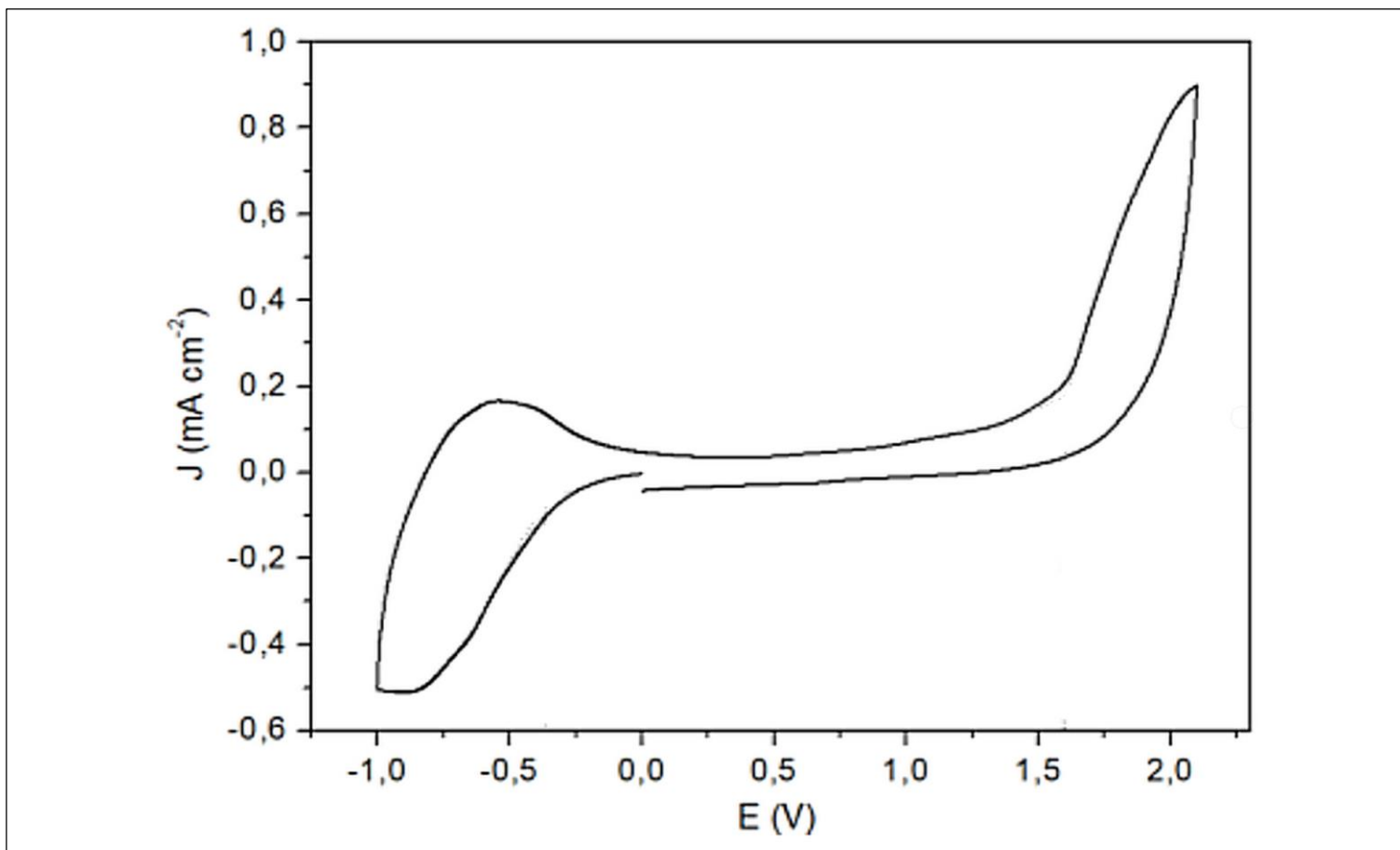


Figure 4.46: Cyclic voltammogram of 8 in acetonitrile solution at 100 mVs^{-1} , supporting electrolyte 0.1 M TBAPF_6

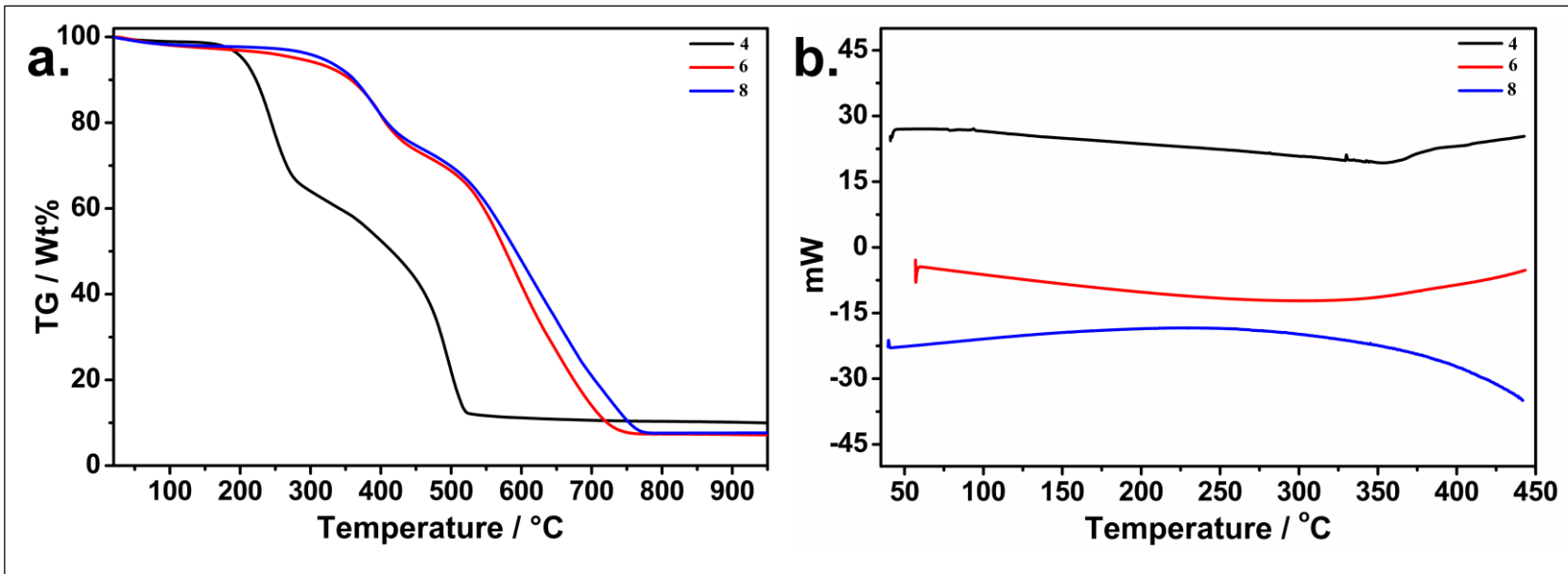


Figure 4.47: TGA curves a. and DSC thermograms b. of 4, 6 and 8 at $10^{\circ}\text{C min}^{-1}$ heating rate

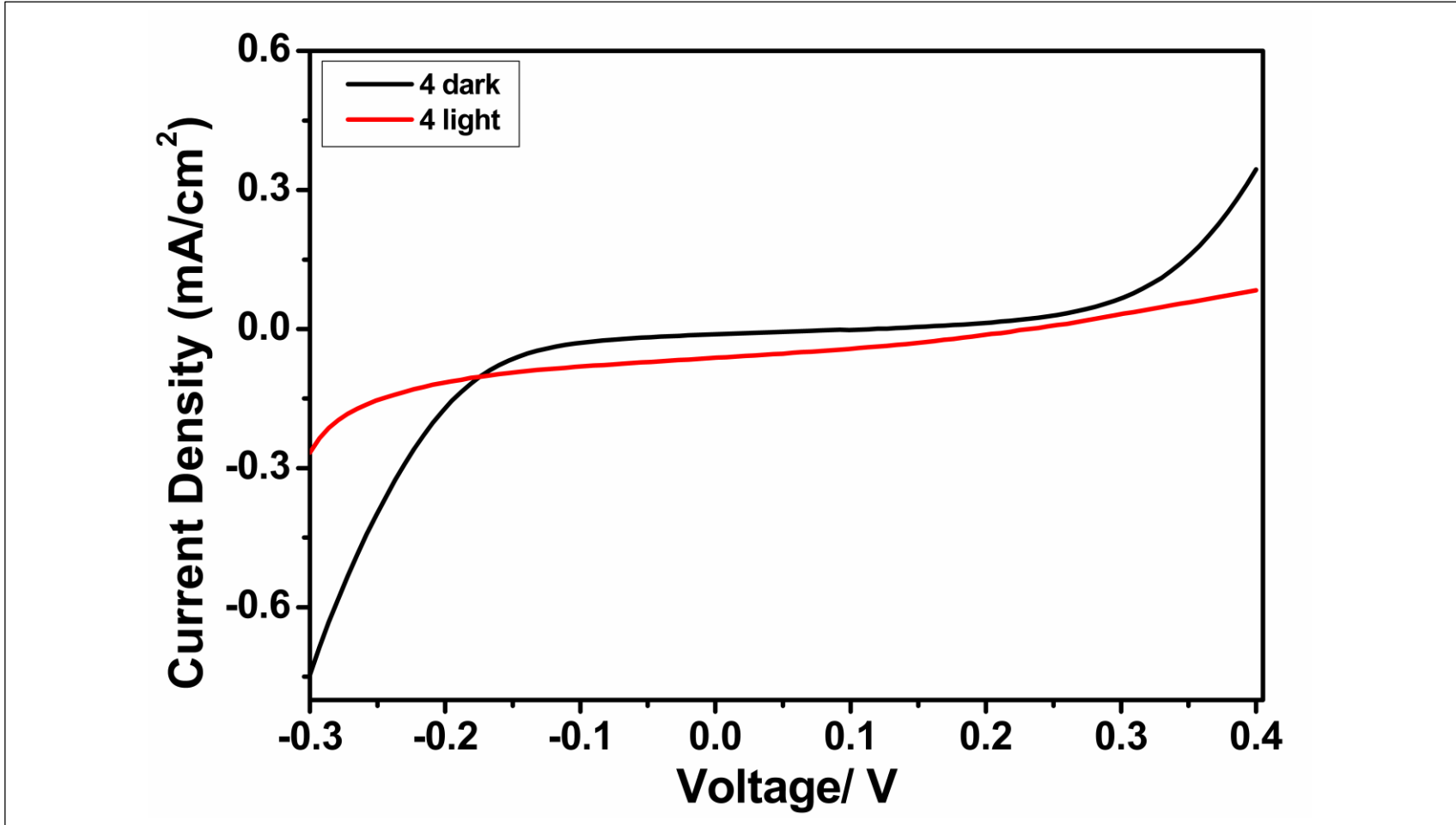


Figure 4.48: I-V characteristics of 4 in the dark and under 100mW/cm² illumination

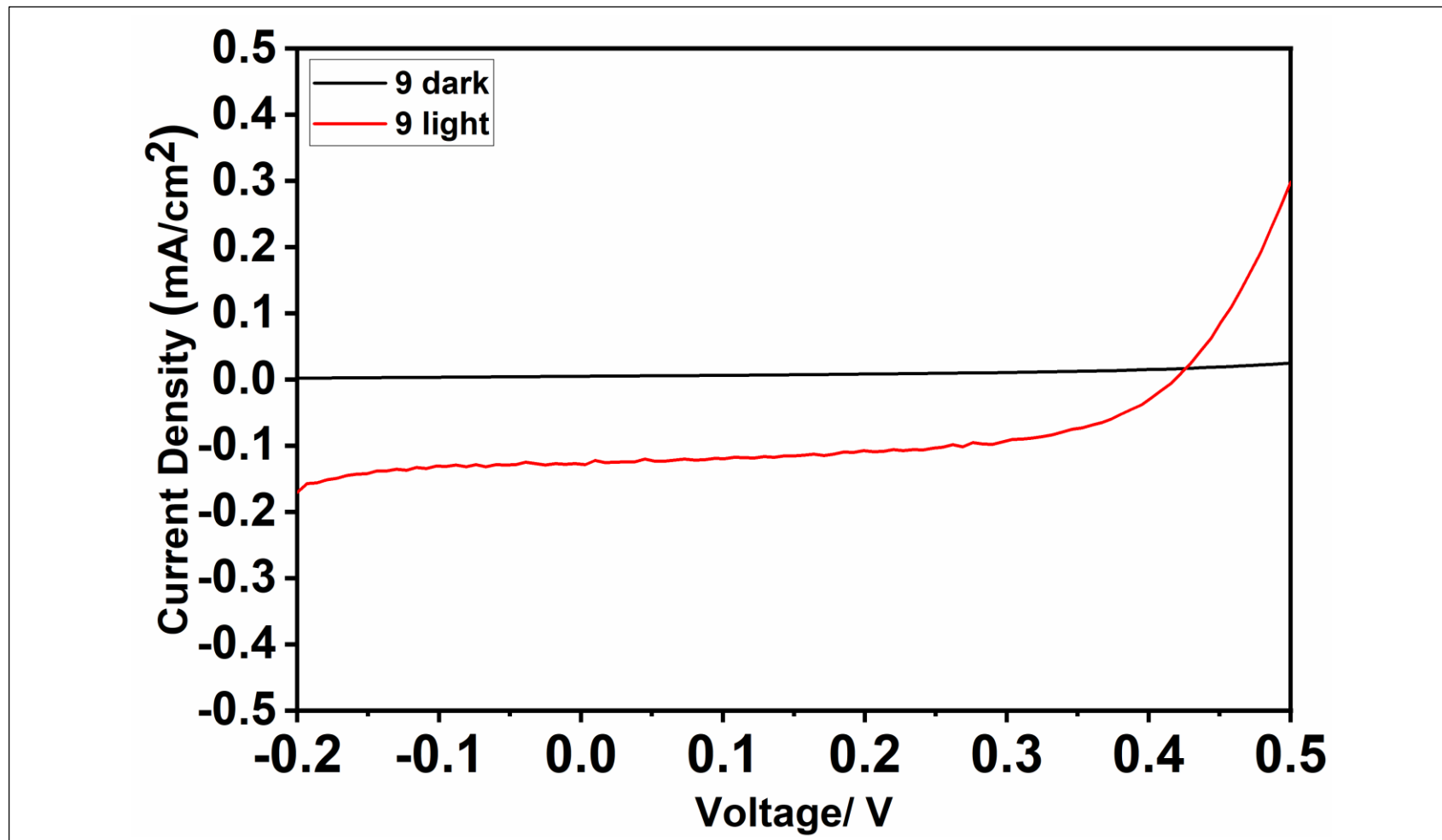


Figure 4.49: I-V characteristics of 9 in the dark and under 100mW/cm² illumination

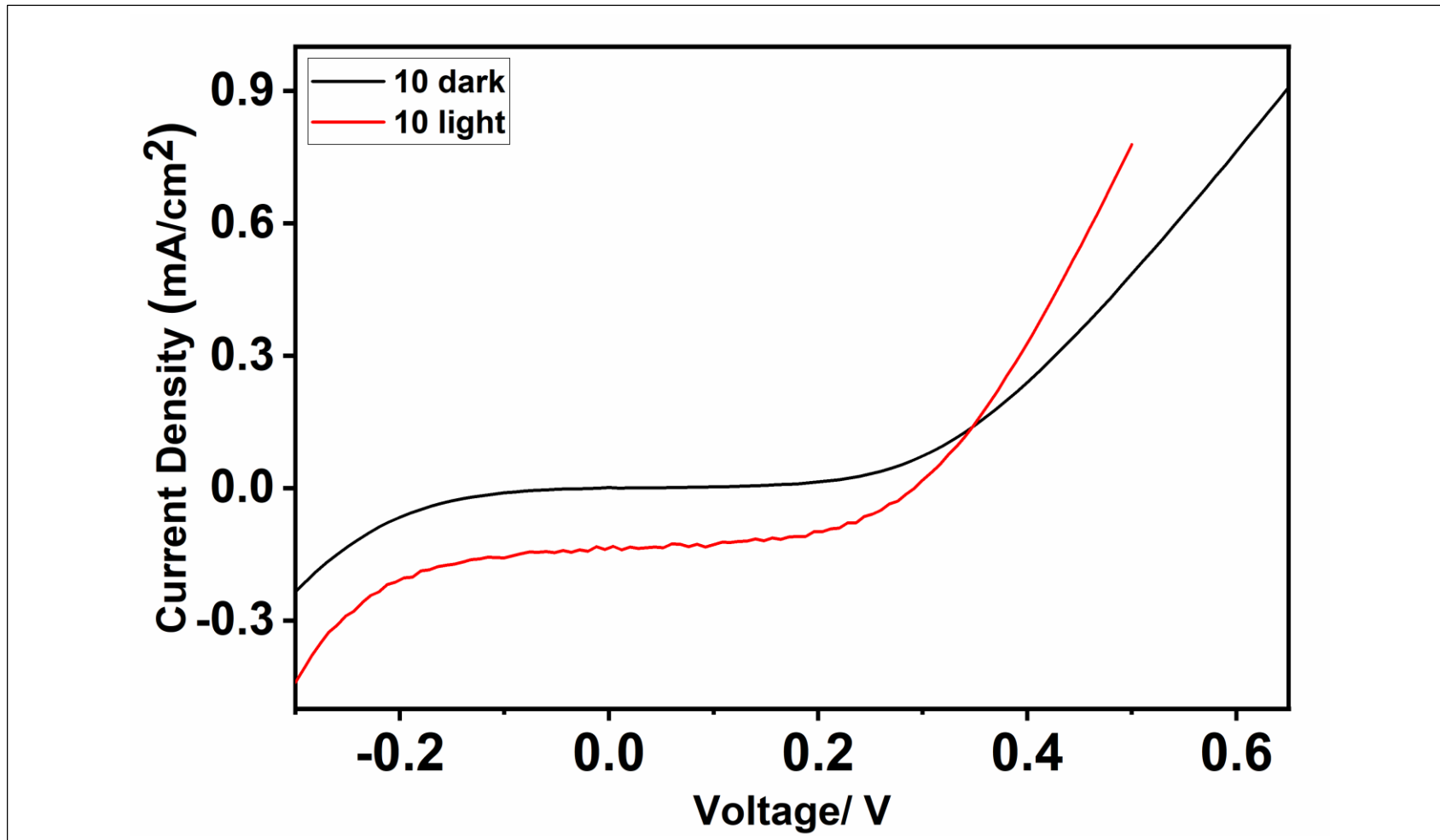


Figure 4.50: I-V characteristics of 10 in the dark and under 100mW/cm² illumination

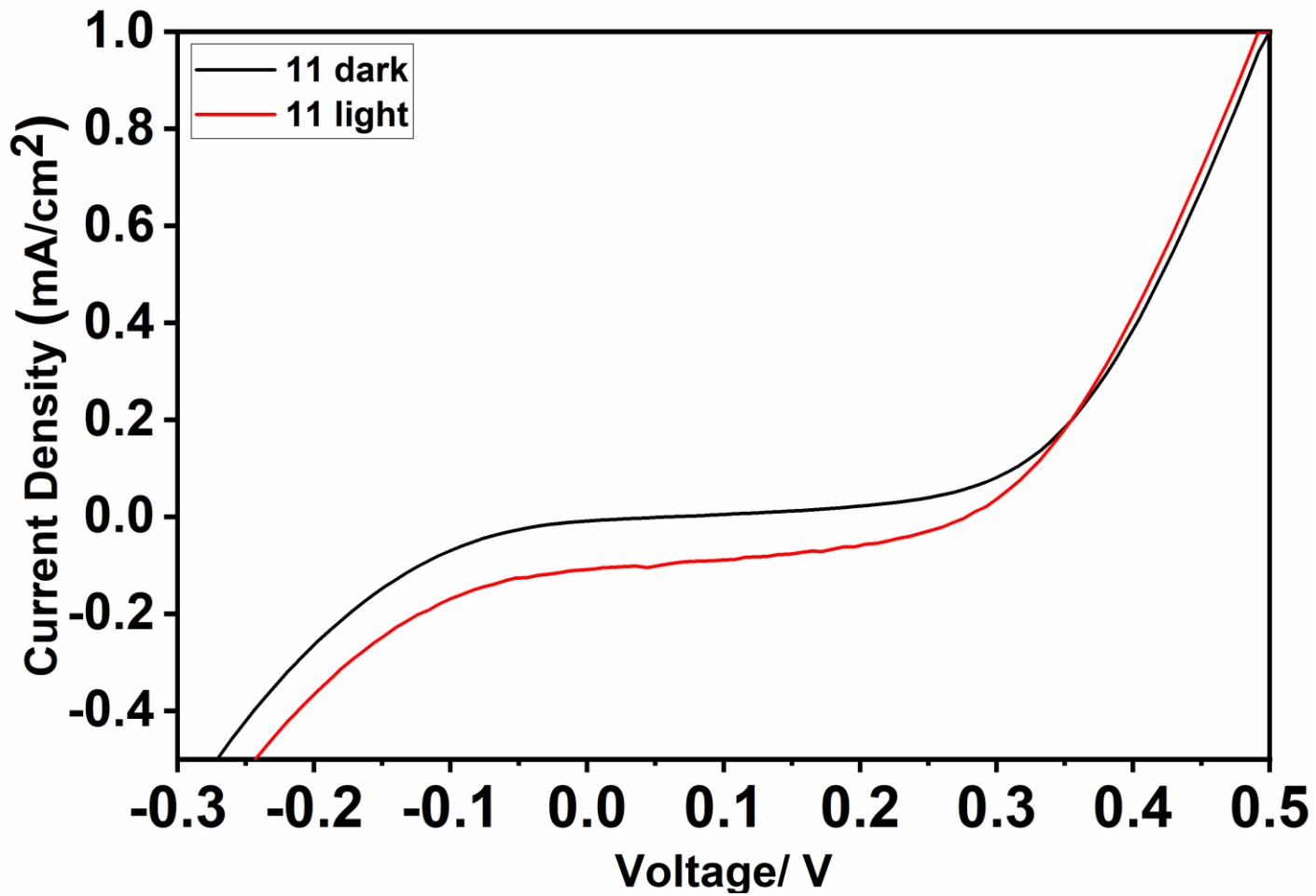


Figure 4.51: I-V characteristics of 11 in the dark and under 100mW/cm² illumination

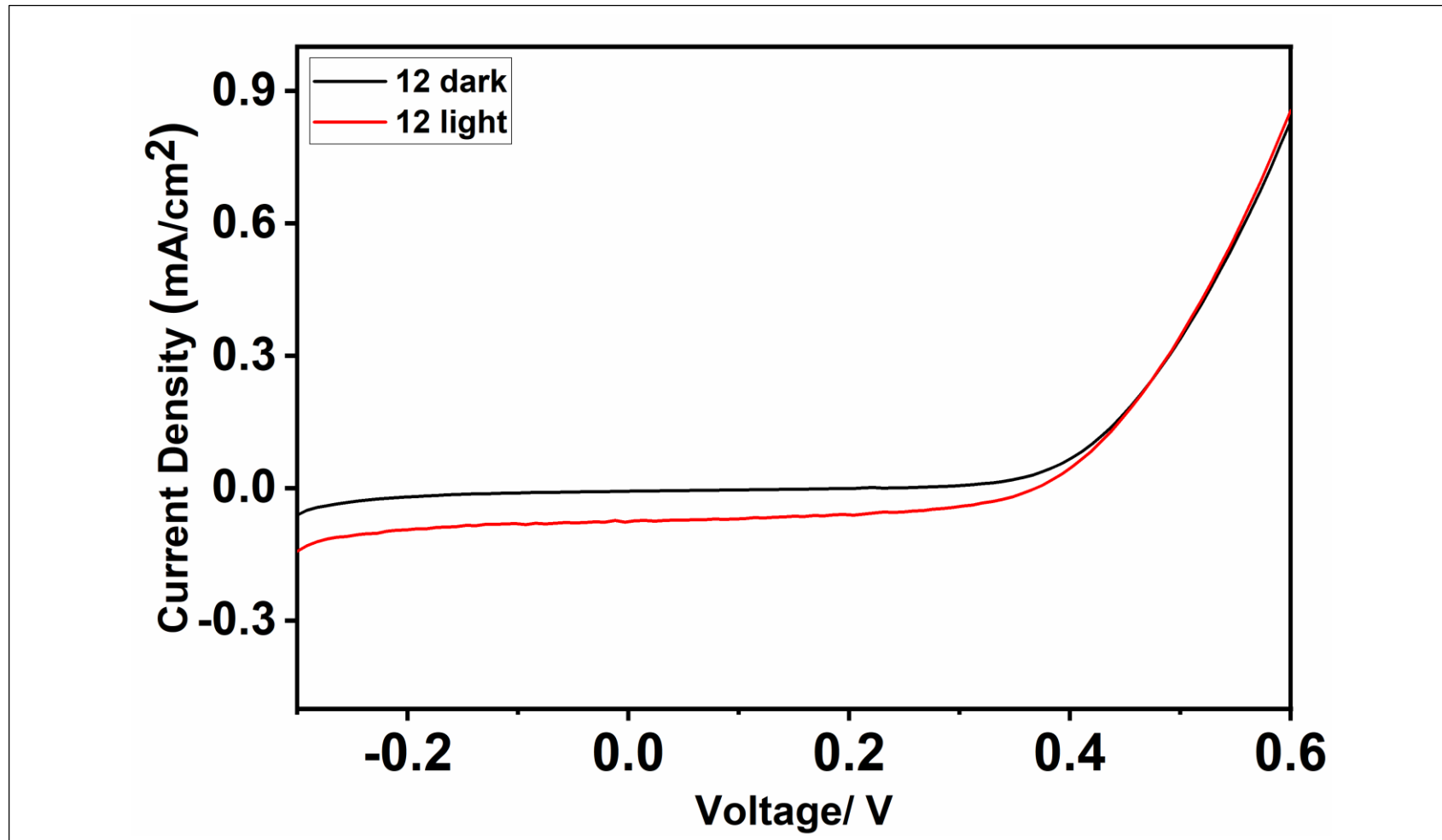


Figure 4.52: I-V characteristics of 12 in the dark and under 100mW/cm² illumination

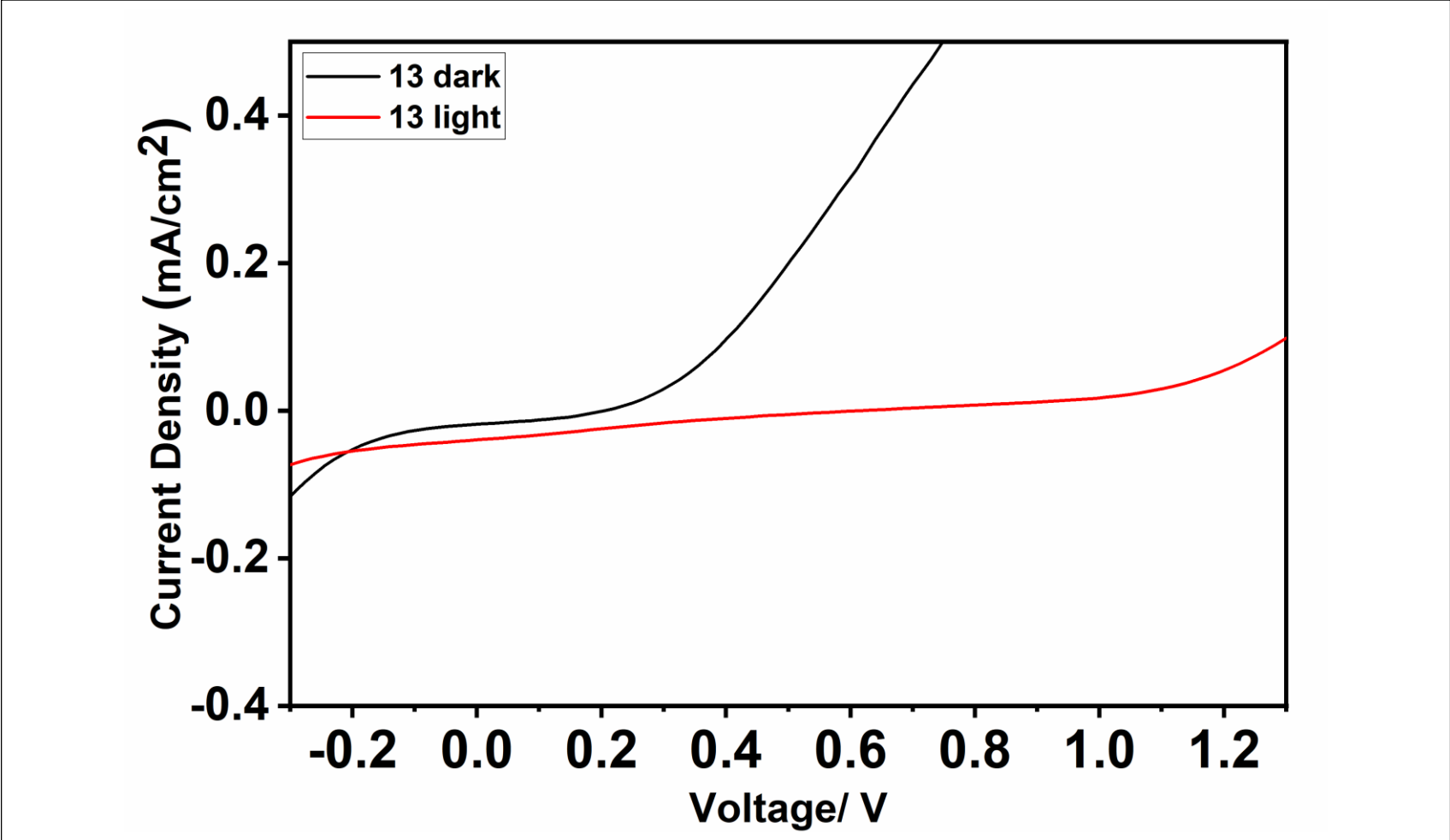


Figure 4.53: I-V characteristics of 13 in the dark and under 100mW/cm² illumination

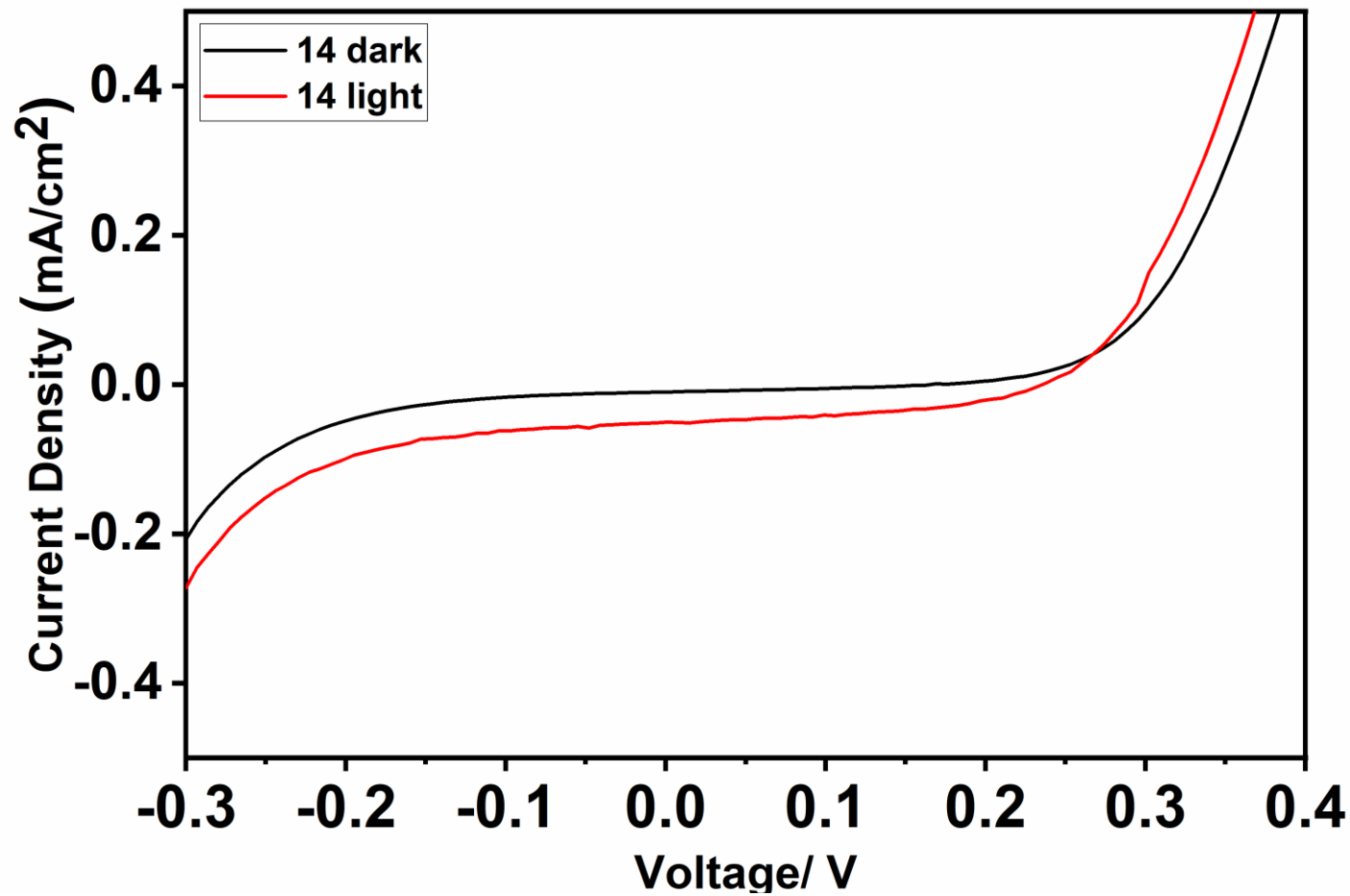


Figure 4.54: I-V characteristics of 14 in the dark and under 100mW/cm² illumination

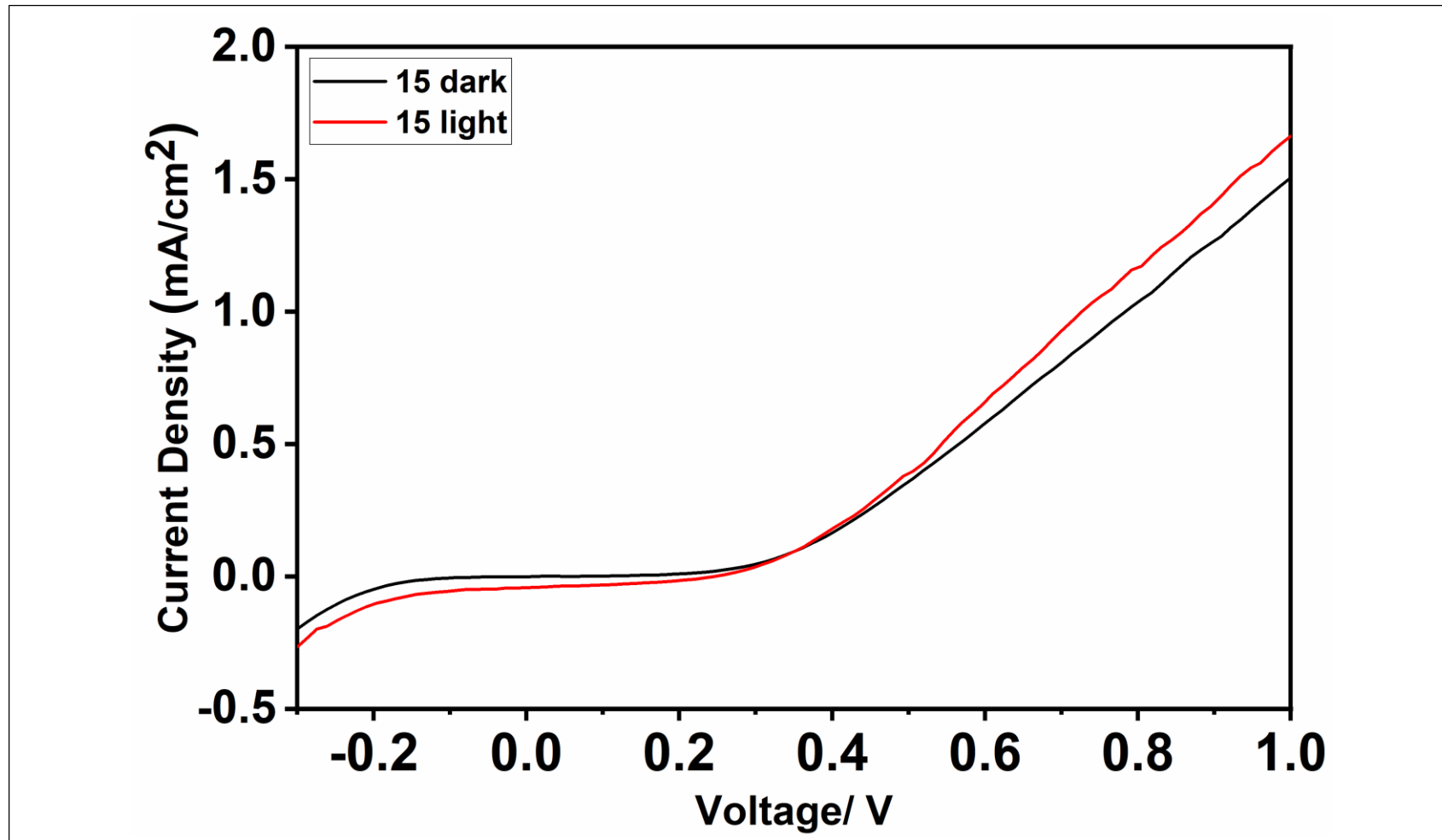


Figure 4.55: I-V characteristics of 15 in the dark and under 100mW/cm² illumination

Chapter 5

RESULT AND DISCUSSION

5.1 Synthesis of (4) and IR Spectra Analysis

Synthesis of 1,7(6)-di(2-decyl-1-tetradecanoyl)perylene-3,4,9,10-tetracarboxylic acid bisanhydride (4) was successfully synthesized according to the procedure reported in section 3.3.2. Compound 4 was purified by recrystallization technique using DMF-MeOH mixture and the crude product was dark purple color with a percent yield of 69.7%.

The structural analysis of compound 4 has been done by FTIR spectrophotometer using KBr pellet figure 4.10, the main characteristic peaks were 3065 cm^{-1} (aromatic C-H stretch), 2920 and 2850 cm^{-1} (aliphatic C-H stretch), 1763 and 1731 cm^{-1} (anhydride C=O stretch), 1590 cm^{-1} (aromatic C=C stretch), 1011 cm^{-1} (ether C-O-C stretch) and 806 and 738 cm^{-1} (aromatic C-H bending).

5.2 Synthesis of (6) and IR Spectra Analysis

Synthesis of N,N'-bis-(dodecyl)-1,7(6)- di(2-decyl-1-tetradecanoyl) perylene-3,4,9,10-tetracarboxy bisimide (6) was successfully synthesized according to the procedure reported in section 3.3.3. Compound 6 was purified by recrystallization technique using hot TCE and the crude product was black color with a high percent yield of 91.95%.

The structural analysis of compound 4 has been done by FTIR spectrophotometer using KBr pellet figure 4.11, the main characteristic peaks were 3065 cm^{-1} (aromatic C-H stretch), 2920 and 2850 cm^{-1} (aliphatic C-H stretch), 1693 and 1656 cm^{-1} (imide C=O stretch), 1587 cm^{-1} (aromatic C=C stretch), 1339 cm^{-1} (C-N stretch), 1237 cm^{-1} (ether C-O-C stretch) and 809 and 749 cm^{-1} (aromatic C-H bending).

Comparing the FTIR spectra of compound 4 figure 4.10 and compound 6 figure 4.11 shows that peaks of anhydride carbonyl at 1763 and 1731 cm^{-1} for compound 4 were replaced with imide carbonyl peaks at 1693 and 1656 cm^{-1} for compound 6, with the appearance of C-N stretch at 1339 cm^{-1} confirmed the synthesis of compound 6.

5.3 Synthesis of (8) and IR Spectra Analysis

N,N'-bis-((S)-(-)-1-phenylethyl)-1,7(6)-di(2-decyl-1-tetradecanoyl)perylene-3,4,9,10-tetracarboxy bisimide (8) was successfully synthesized according to the procedure reported in section 3.3.4. Compound 8 was purified by recrystallization technique using hot NMP and the crude product was black color with a high percent yield of 88%.

The structural analysis of compound 8 has been done by FTIR spectrophotometer using KBr pellet figure 4.12, the main characteristic peaks were 3060 cm^{-1} (aromatic C-H stretch), 2920 and 2850 cm^{-1} (aliphatic C-H stretch), 1694 and 1654 cm^{-1} (imide C=O stretch), 1585 cm^{-1} (aromatic C=C stretch), 1325 cm^{-1} (C-N stretch), 1243 cm^{-1} (ether C-O-C stretch) and 809 and 749 cm^{-1} (aromatic C-H bending).

Comparing the FTIR spectra of compound 4 figure 4.10 and compound 8 figure 4.12 shows that peaks of anhydride carbonyl at 1763 and 1731 cm^{-1} for compound 3 were

replaced with imide carbonyl peaks at 1694 and 1654 cm^{-1} for compound 8, with the appearance of C-N stretch at 1325 cm^{-1} confirmed the synthesis of compound 8.

5.4 NMR Spectra Analysis

The synthesized compounds were also characterized by ^1H NMR and ^{13}C NMR and all the data with the assigned structures were presented below.

^1H NMR and ^{13}C NMR analysis of compound 4:

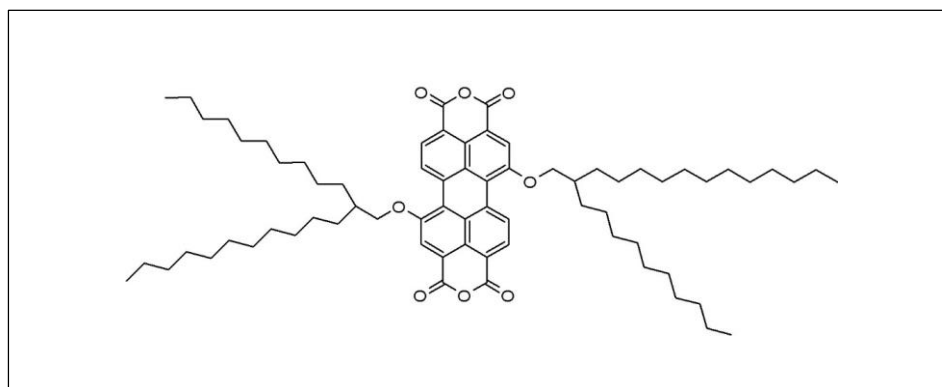


Figure 5.1: Structure of compound 4

^1H NMR (400 MHz, $\text{CDCl}_3:\text{CF}_3\text{COOD}$ (3:1)): δH (ppm) = 8.44–8.42 (d, J = 8.0 Hz, 2Ar-H), 8.36–8.34 (d, J = 8.0 Hz, 2Ar-H), 7.5 (s, 2Ar-H), 4.21 (d, J = 7.8 Hz, 2CH₂), 1.87 (m, 2CH), 1.63 (m, 4 CH₂), 1.32–1.15 (m, 36CH₂), 0.86 (m, 4CH₃).

^{13}C NMR (100.6 MHz, $\text{CDCl}_3:\text{CF}_3\text{COOD}$ (3:1)): δC (ppm) = 162.14, 160.92, 138.59, 131.75, 125.28, 123.07, 122.43, 110.22, 74.59, 42.78, 41.43, 41.30, 37.36, 34.04, 30.33, 29.33, 27.13, 22.71, 16.06.

^1H NMR and ^{13}C NMR analysis of compound 6:

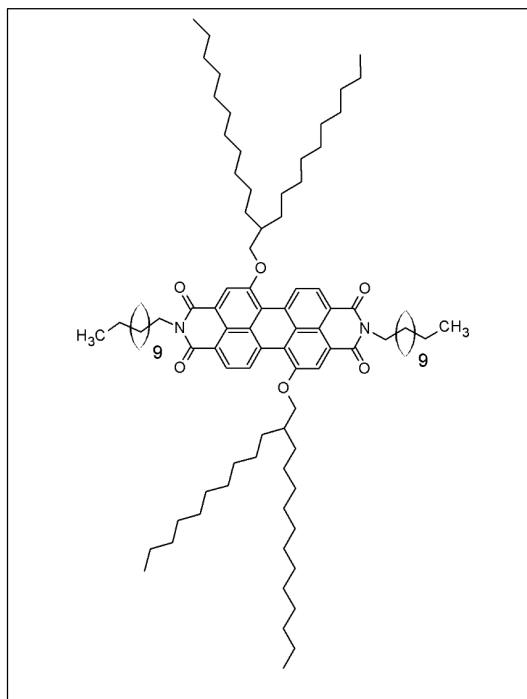


Figure 5.2: Structure of compound 6

^1H NMR (400 MHz, $\text{CDCl}_3:\text{CF}_3\text{COOD}$ (3:1)): δH (ppm)=8.65–8.64 (d, J =7.6 Hz, 2Ar-H), 8.57–8.56 (d, J =7.6 Hz, 2Ar-H), 7.35 (s, 2Ar-H), 4.18 (d, J =7.8 Hz, 2 CH_2), 3.66 (t, J =7.2 Hz, 2 CH_2), 2.35–2.31 (m, 2CH), 1.63 (m, 6 CH_2), 1.42–1.06 (m, 56 CH_2), 0.88–0.83 (m, 6CH₃).

^{13}C NMR (100.6 MHz, $\text{CDCl}_3:\text{CF}_3\text{COOD}$ (3:1)): Δc (ppm) = 162.14, 160.92, 138.59, 131.75, 125.28, 123.07, 122.43, 110.22, 74.59, 66.93, 42.78, 41.43, 41.30, 37.36, 34.04, 30.33, 29.33, 27.13, 22.71, 16.06.

^1H NMR and ^{13}C NMR analysis of compound 8:

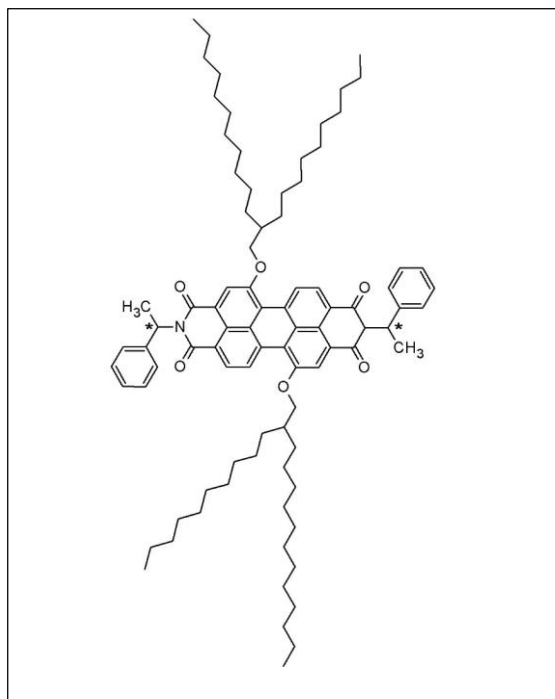


Figure 5.3: structure of compound 8

^1H NMR (400 MHz, $\text{CDCl}_3:\text{CF}_3\text{COOD}$ (3:1)): δH (ppm) = 8.44–8.42 (d, $J=8.0$ Hz, 2Ar–H), 8.36–8.34 (d, $J=8.0$ Hz, 2Ar–H), 8.08 (s, 2Ar–H), 7.42–7.40 (d, $J=8.0$ Hz, 4Ar–H), 7.35 (t, $J=7.1$ Hz, 6Ar–H), 6.60 (q, 2CH), 4.32 (d, $J=7.8$ Hz, 2CH₂), 2.22–2.19 (d, $J=8.0$ Hz, 2CH₃), 2.02 (m, 2CH), 1.77–1.27 (m, 40CH₂), 0.86 (m, 4CH₃).

^{13}C NMR (100.6 MHz, $\text{CDCl}_3:\text{CF}_3\text{COOD}$ (3:1)): δC (ppm) = 165.43, 156.68, 140.43, 139.49, 131.93, 131.24, 130.33, 128.33, 127.47, 126.73, 124.53, 109.90, 73.74, 54.45, 51.90, 44.84, 43.20, 42.52, 37.50, 32.34, 29.47, 27.20, 22.45, 19.89, 15.42.

5.5 Solubility of 1, 7-Bay-substituted PDIs

The solubility of compounds 4, 6 and 8 was shown in table 5.1. The synthesized compounds showed good solubility in different organic solvents because of the N-substitution in imide position which is mainly enhance the solubility of perylene compounds by disturbing the π - π molecular interactions of perylene aromatic cores. It is also important to mention that the bay-substitution with 2-decyl-1-tetradecnoyl group at 1, 7 position of perylene core improved the solubility of the compounds due to the twisting in perylene core.

Table 5.1: Solubility (solubility/color) of **4**, **6** and **8** in different organic solvents. Measured at a concentration of 1 mg ml⁻¹ in solvents at 25 °C.

| Solvent | solubility/color | | |
|-------------------|------------------|----------------|----------------|
| | 4 | 6 | 8 |
| CHCl ₃ | ± pink | ± red brown | ± violet |
| TCE | ± pink | + dark cherry | + light cherry |
| DCM | ± grey | ± light violet | ± cherry |
| TFAc | + cherry | + dark cherry | + cherry |
| NMP | + dark green | + red brown | + maroon |
| DMF | + dark grey | ± brown | + brown |
| DMSO | + purple | – | + light violet |
| m-Cresol | + cherry | ± dark cherry | ± dark cherry |

(+): soluble at room temperature.

(±): partially soluble on heating at 35 °C in sonicator.

5.6 UV/Vis Spectra Analysis

The UV/Vis spectra of compounds 4, 6 and 8 in various solvents of different polarities were shown in figures 4.20- 4.40.

Modifying the photo electronic properties of perylene dianhydrides and diimides can be achieved via bay substitution of the electron deficient aromatic perylene core. As shown in figures 4.20, 4.27 and 4.34 there is a dramatic change in the absorption spectra of the synthesized compounds taken in various solvents including the loss of the fine vibronic structure, broadening the peaks as well as decreasing the molar absorption coefficients (ϵ_{\max}) table 4.15 which indicates the molecular aggregation tables 5.2, 5.3 and 5.4 due to the PDI molecular scaffolds allowing π - π intermolecular interactions. This dramatic change is probably because of the distortion of the PDI core by the swallow-tail substituent.

The lowest 0-0/0-1 absorbance band ratios and longest wavelength absorption band for compounds 4, 6 and 8 were observed in polar aprotic solvents NMP, DMF and DMSO which indicate the solvent dependent aggregation behavior. Polar solvents strongly stabilize the excited states, lower its energy and red shift the maximum absorption wavelength which indicate the solvatochromic effect for all compounds in polar solvents.

Aggregation of bay substituted PDIs refers to self-organization of the molecules through intermolecular and intramolecular interactions in solution or interface of solid-liquid and it can be characterized by broadened absorbance bands and a decreased ratio of the 0-0/0-1 absorbance bands (≤ 1.5).

Aggregation and bathochromic shift as seen from the absorbance spectra and the ratio of the absorbance intensities the synthesized compounds 4, 6 and 8 indicate the existence of the head-to-tail interaction which is called j-aggregation.

It is important to mention that the absorption spectra of compounds 4, 6 and 8 in solution and upon microfiltration via 0.25 μ m SPR micro filter were found to be almost the same as shown in figure 5.4 in terms of wavelength range and peak shapes and positions which indicate that the size of aggregates is less than 0.25 μ m.

Table 5.2: Ratio of absorption intensities of **4** in various solvents

| Solvent | Absorption Intensities of the Peaks | | |
|-------------------|-------------------------------------|-----------------------|---|
| | $A^{(0\rightarrow1)}$ | $A^{(0\rightarrow0)}$ | $A^{(0\rightarrow0)}/A^{(0\rightarrow1)}$ |
| CHCl ₃ | 0.3 | 0.36 | 1.2 |
| TCE | 0.29 | 0.343 | 1.182759 |
| DCM | 0.1228 | 0.145 | 1.180782 |
| NMP | 1.12 | 0.99 | 0.883929 |
| DMF | 0.752 | 0.696 | 0.925532 |
| DMSO | 1.215 | 1.285 | 1.057613 |

Table 5.3: Ratio of absorption intensities of **6** in various solvents

| Solvent | Absorption Intensities of the Peaks | | |
|-------------------|-------------------------------------|-----------------------|---|
| | $A^{(0\rightarrow1)}$ | $A^{(0\rightarrow0)}$ | $A^{(0\rightarrow0)}/A^{(0\rightarrow1)}$ |
| CHCl ₃ | 0.71 | 0.76 | 1.070423 |
| TCE | 1.236 | 1.29 | 1.043689 |
| DCM | 0.382 | 0.3986 | 1.043455 |
| TFAc | 0.9129 | 0.989 | 1.083361 |
| NMP | 1.1245 | 1.032 | 0.917741 |
| DMF | 1.225 | 1.158 | 0.945306 |
| DMSO | 1.071 | 1.012 | 0.944911 |

Table 5.4: Ratio of absorption intensities of **8** in various solvents

| Solvent | Absorption Intensities of the Peaks | | |
|-------------------|-------------------------------------|-----------------------|---|
| | $A^{(0\rightarrow1)}$ | $A^{(0\rightarrow0)}$ | $A^{(0\rightarrow0)}/A^{(0\rightarrow1)}$ |
| CHCl ₃ | 0.921 | 0.931 | 1.010858 |
| TCE | 0.878 | 0.906 | 1.031891 |
| DCM | 0.58 | 0.61 | 1.051724 |
| TFAc | 0.9425 | 1.017 | 1.079045 |
| NMP | 0.906 | 0.727 | 0.802428 |
| DMF | 0.6865 | 0.66 | 0.961398 |

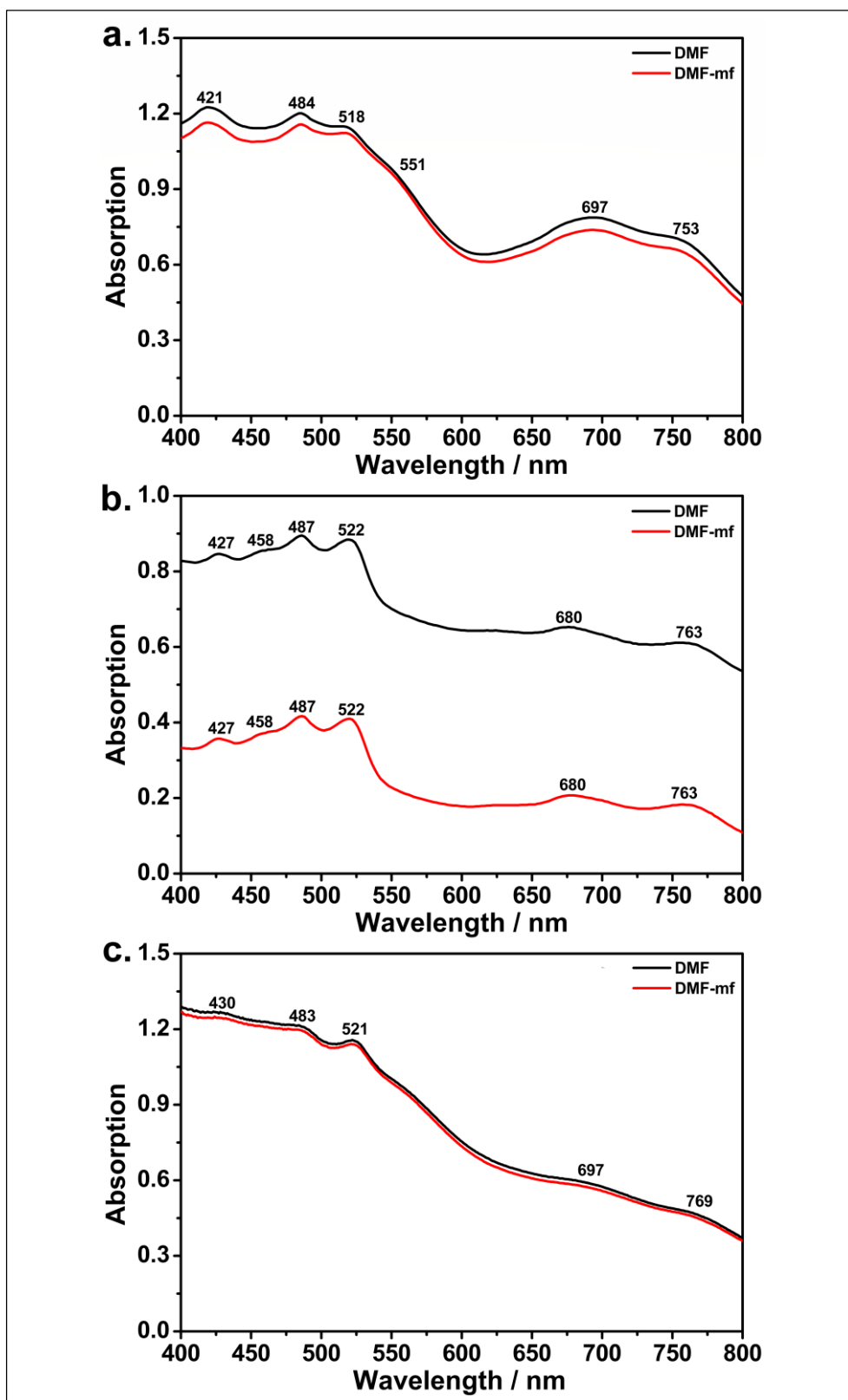


Figure 5.4: UV-Vis spectra of compounds a.4, b.6 and c.8 in DMF and upon microfiltration

5.7 Emission Spectra Analysis

The emission spectra of compounds 4, 6 and 8 in various solvents of different polarities were taken at $\lambda_{exc.} = 485\text{nm}$ and shown in figures 4.20- 4.40.

The emission spectra of compound 4 figure 4.21 showed three characteristic emission peaks with an excimer like emission and red shift in TFAc and DMSO due to the formation of ground state complexes with limited π - π stacking interaction.

The emission spectra of compounds 6 and 8 figures 4.28 and 4.35 showed three characteristic emission peaks without any excimer emission except in TFAc where they showed broad excimer like emission and red shift due to the formation of ground state complexes with limited π - π stacking interaction.

The fluorescence quantum yields of compounds 4, 6 and 8 were calculated in various solvents using *N,N'*-bis-dodecyl-3,4,9,10-perylenebis(dicarboximide) in CHL as reference and the data were listed in table 4.15 , the Φ_f values for the synthesized compounds were relatively low because of the broad absorption through the UV/Vis regions , j-aggregation as well as quenched fluorescent emission of bay substituted diimides and dianhydrides which lead to the photoinduced electron transfer or other non-radiative decay processes. The lowest fluorescence quantum yield values all perylene dyes were observed in DMSO due to the efficient fluorescence quenching of the sulfur in dimethyl sulfoxide (DMSO) as mentioned in the literatures.

Compounds 4, 6 and 8 showed large Stokes shift as shown in the following tables, A large Stokes shift may indicate a fast relaxation process and could also be due to intramolecular electron-transfer from the electron donating unit (2-decyl-1-

tetradecanol) at the bay position to the electron accepting unit (perylene diimide core) (donor- π -acceptor structure) .

Table 5.5: Absorption, emission wavelengths and calculated Stoke's shifts ($\Delta\nu$) of 4 in various solvents

| Solvent | $\lambda_{\text{abs}}/\text{nm}$ | $\lambda_{\text{abs, max}}/\text{nm}$ | $\lambda_{\text{em}}/\text{nm}$ | $\lambda_{\text{em, max}}/\text{nm}$ | $\Delta\nu/\text{cm}^{-1}$ |
|-------------------|----------------------------------|---------------------------------------|---------------------------------|--------------------------------------|----------------------------|
| CHCl ₃ | 482,514,543 | 514 | 527,567 | 527 | 769230.7692 |
| TCE | 488,522,546 | 522 | 530,569 | 530 | 1250000 |
| DCM | 487,516,538 | 516 | 526,563 | 526 | 1000000 |
| TFAc | 531 | 531 | 536,580 | 536 | 2000000 |
| NMP | 485,518,558 | 518 | 537,572 | 537 | 526315.7895 |
| DMF | 484,518,551 | 518 | 534,570 | 534 | 625000 |
| DMSO | 490,523,548 | 523 | 542,589 | 542 | 526315.7895 |

Table 5.6: Absorption, emission wavelengths and calculated Stoke's shifts ($\Delta\nu$) of 6 in various solvents

| Solvent | $\lambda_{\text{abs}}/\text{nm}$ | $\lambda_{\text{abs, max}}/\text{nm}$ | $\lambda_{\text{em}}/\text{nm}$ | $\lambda_{\text{em, max}}/\text{nm}$ | $\Delta\nu/\text{cm}^{-1}$ |
|-------------------|----------------------------------|---------------------------------------|---------------------------------|--------------------------------------|----------------------------|
| CHCl ₃ | 490,524,554 | 524 | 534,576,624 | 534 | 10000000 |
| TCE | 497,528 | 528 | 538,578 | 538 | 10000000 |
| DCM | 488,523,554 | 523 | 533,574,620 | 533 | 10000000 |
| TFAc | 497,534,561 | 534 | 550,595 | 550 | 6250000 |
| NMP | 425,523 | 523 | 537,577 | 537 | 7142857.143 |
| DMF | 487,522 | 522 | 536,575 | 536 | 7142857.143 |

Table 5.7: Absorption, emission wavelengths and calculated Stoke's shifts ($\Delta\nu$) of 8 in various solvents

| Solvent | $\lambda_{\text{abs}}/\text{nm}$ | $\lambda_{\text{abs, max}}/\text{nm}$ | $\lambda_{\text{em}}/\text{nm}$ | $\lambda_{\text{em, max}}/\text{nm}$ | $\Delta\nu/\text{cm}^{-1}$ |
|-------------------|----------------------------------|---------------------------------------|---------------------------------|--------------------------------------|----------------------------|
| CHCl ₃ | 491,526,551 | 526 | 534,577,624 | 534 | 1250000 |
| TCE | 493,528 | 528 | 538,580 | 538 | 1000000 |
| DCM | 491,525 | 525 | 533,574,624 | 533 | 1250000 |
| TFAc | 498,535 | 535 | 553,595 | 553 | 555555.5556 |
| NMP | 487,526 | 526 | 537,577,624 | 537 | 909090.9091 |
| DMF | 483,521 | 521 | 536,576,624 | 536 | 666666.6667 |
| DMSO | 485,526 | 526 | 546,581 | 546 | 500000 |

5.8 Solid State UV/Vis and Emission of the Synthesized Compounds

The solid state UV/Vis spectra of compounds 4, 6 and 8 were shown in figures 4.26, 4.33 and 4.40 were quite different as compared to their absorption spectra in solution in view of the spectral shapes and peak positions. This difference is because of the intermolecular interaction in solid state.

Solid state fluorescence of compounds 4, 6 and 8 were examined but no fluorescence was observed confirming the existence of aggregation which cause quenching in solid state through the swallow-tail substituent (2-decyl-1-tetradecanol) at the bay position of perylene dye.

5.9 Electrochemistry of the Synthesized Compounds

The redox potentials, HOMO/LUMO energies and Band gap energies of the synthesized compounds 4,6 and 8 were investigated using cyclic voltammetry technique in acetonitrile containing 0.1 M TBAPF₆ as a supporting electrolyte and the collected data were listed in table 4.16.

As shown in figures 4.44, 4.45 and 4.46 compounds 4, 6 and 8 each have one irreversible oxidation peak and one reversible reduction peak since the two step reduction peaks cannot be clearly separated due to the disturbed planarity of the perylene core by bay substitution.

The redox potential of compounds 4, 6 and 8 were ($E_{1/2\text{red}} = -1.085, -0.92$ and -1.085V vs Fc/Fc^+ respectively) with the peak potential separation ΔE_p of 130, 60 and 290mV for compounds 4, 6 and 8 respectively which confirm the reversibility of the systems.

Notably the redox potential of compound 6 was slightly more positive compared to the other compounds which indicate easier reduction ability and higher reduction rate. As well as its peak potential separation was within the range of 60-70 mV which indicated that the reversibility of the electron transfer process in the system was well maintained compared to compounds 4 and 8.

PDI derivatives with substituents in the bay positions are generally somewhat more readily reduced compared to unsubstituted perylene diimides [61]. This is probably due to the electron donating effect of the substituents as well as the extension of conjugation incorporated in their core bay positions.

The HOMO and LUMO energies were also calculated by CV and shown in Table 4. Using $E_{ox/red}$, onset for the measurements in acetonitrile solution. The HOMO energy values were calculated as ($E_{HOMO} = -5.90, -5.91$ and -5.97 eV for compounds 4, 6 and 8 respectively). And the LUMO energy values were ($E_{LUMO} = -4.02, -4.02$ and -4.02 eV for compounds 4, 6 and 8 respectively).

The electrochemical band gap energies were also estimated using this relationship ($E_{gcv} = E_{LUMO} - E_{HOMO}$), E_{gcv} values for compounds 4, 6 and were (1.88, 1.89 and 1.95 eV respectively).

The introduction of electron donating ,2-decyl-1-tetradecanoyl substituent in bay position of perylene moiety usually causes a HOMO- and LUMO-raising effect, and the HOMO-raising effect is more significant compared to the un substituted PDIs (my article), thus causing a smaller energy gap.

5.10 Thermal Stability of the Synthesized Compounds

Thermal stability of compounds 4, 6 and 8 were investigated by DSC technique under nitrogen atmosphere and TGA technique under oxygen atmosphere with heating rate of $10^{\circ}\text{C min}^{-1}$ as shown in figure 4.47.

All compounds showed no glass transition or melting in DSC within the range of 0-450 $^{\circ}\text{C}$, the DSC results indicate that the compounds 4, 6 and 8 are not mesomorphic due to the π - π intermolecular interactions including molecular aggregation.

The thermo gravimetric analysis data of compounds 4, 6 and 8 reveals stability up to 209, 347 and 336 $^{\circ}\text{C}$ respectively. For compound 6, a weight loss of 34.4% of its initial weight observed between 209 and 285 $^{\circ}\text{C}$, and 90% weight loss at 900 $^{\circ}\text{C}$ and 10% char yield was observed.

Compound 8, a weight loss of 24.4% of its initial weight observed between 347 and 425 $^{\circ}\text{C}$, and 93% of its weight was lost rapidly at around 900 $^{\circ}\text{C}$ and about 7% char yield was observed. And 23% weight loss temperature for compound 8 was between 336 and 415 $^{\circ}\text{C}$ and 92% weight loss temperature of its initial weight was 900 $^{\circ}\text{C}$ and about 8% char yield was observed. The collected data reveals that compounds 6 and 8 show higher thermal stability than compound 4 probably due to the bay substitution of rigid perylene chromophoric structures, the intermolecular forces and rigidity and symmetry of the compound.

5.11 Photovoltaic Performance

The performances of DSSCs based on the 4-15 dyes were measured under AM 1.5 irradiation (100 mW cm^{-2}). Figures 4.48-4.54 show the photocurrent density-voltage curves (I–V) of the DSSCs based on the 9-15 dyes and the corresponding data are listed in Table 4. 21.

The large and swallow tail substituent at the bay area of the perylene core in dye 4 has a good effect on the optical and electrochemical properties as well as the photovoltaic performance with I_{sc} , V_{oc} , FF and efficiency of 0.06, 0.23, 3.0 and 0.04 respectively, however dye 4 showed high tendency of aggregation in solution and solid state which decreased the device performance.

Dye 9 -based device exhibited a higher efficiency (PCE) of 0.02% compared to the other examined dyes with $V_{oc}= 0.42\text{V}$, $I_{sc}= 0.13\text{mA.cm}^{-2}$ and $FF= 0.34$. While the PCE of dye 10-based device was 0.013% with $V_{oc}=0.3\text{V}$, $I_{sc}=0.138 \text{ mA.cm}^{-2}$ and $FF= 0.31$, the PCE of dye 11-based device was 0.01% with $V_{oc}= 0.28\text{V}$, $I_{sc}= 0.11 \text{ mA.cm}^{-2}$ and $FF=0.33$, the PCE of dye 12-based device was 0.009% with $V_{oc}=0.37\text{V}$, $I_{sc}=0.072 \text{ mA.cm}^{-2}$ and $FF=0.32$, the PCE of dye 13-based device was 0.005% with $V_{oc}=0.5\text{V}$, $I_{sc}= 0.042 \text{ mA.cm}^{-2}$ and $FF= 0.22$, the PCE of dye 14-based device was 0.004% with $V_{oc}= 0.234\text{V}$, $I_{sc}= 0.058 \text{ mA.cm}^{-2}$ and $FF= 0.31$ and the PCE of dye 15-dye device was only 0.003% with $V_{oc}=0.25\text{V}$, $I_{sc}=0.044 \text{ mA.cm}^{-2}$ and $FF= 0.25$.

Notably for dyes 10-14 (perylene dyes), relatively low efficiencies were observed properly due to the strong electron withdrawing nature of perylene core leading to inhibit the transfer of photo-generated electrons from the electron donor side to the

acceptor and anchoring side of the molecule, as well as the molecular aggregation which prevents the formation of a homogeneous continuous PDI films.

5.12 FT-IR Spectra of Dyes 9-15

The structural analysis of Dye 9 has been done by FTIR spectrophotometer using KBr pellet, the main characteristic peaks were 3382 cm^{-1} (O-H stretch), 3068 cm^{-1} (aromatic C-H stretch), 1715 and 1673 cm^{-1} (imide C=O stretch), 1583 cm^{-1} (aromatic C=C stretch), 1351 cm^{-1} (S=O stretch) and 809 and 749 cm^{-1} (aromatic C-H bending). The FT-IR spectra of dye 9 adsorbed on TiO_2 showed a broadening of all the singles that are attributed to adsorption on the TiO_2 surface via the sulfonic acid group as well as the disappearing of O-H stretch peak as shown in figure 4.13.

The structural analysis of Dye 10 has been done by FTIR spectrophotometer using KBr pellet, the main characteristic peaks were 3395 cm^{-1} (O-H stretch), 3070 cm^{-1} (aromatic C-H stretch), 1697 and 1653 cm^{-1} (imide C=O stretch), 1595 cm^{-1} (aromatic C=C stretch), 1353 cm^{-1} (C-N stretch) and 809 and 749 cm^{-1} (aromatic C-H bending). The FT-IR spectra of dye 10 adsorbed on TiO_2 showed a broadening of all the peaks that are attributed to adsorption on the TiO_2 surface via the hydroxyl group as well as the disappearing of the O-H stretch peak as shown in figure 4.14.

The structural analysis of Dye 11 has been done by FTIR spectrophotometer using KBr pellet, the main characteristic peaks were 3401 cm^{-1} (O-H stretch), 3070 cm^{-1} (aromatic C-H stretch), 1704 and 1661 cm^{-1} (imide C=O stretch), 1592 cm^{-1} (aromatic C=C stretch), 1346 cm^{-1} (C-N stretch) 1199 (C-O-C ether), 1179 (C-O-C stretch) and 809 and 749 cm^{-1} (aromatic C-H bending). The FT-IR spectra of dye 11 adsorbed on TiO_2 was also done as shown in figure 4.15.

The structural analysis of Dye 12 has been done by FTIR spectrophotometer using KBr pellet, the main characteristic peaks were 3419 (O-H stretch); 3083 (aromatic C-H stretch); 2955, 2929, 2868 (aliphatic C-H stretch); 1696, 1657 (imides C=O stretch); 1595, 1578 (conjugated C=C stretch); 1339 (C-N stretch) 856 and 748 (C-H bend) cm^{-1} . The FT-IR spectra of dye 12 adsorbed on TiO_2 showed a broadening of all the peaks that are attributed to adsorption on the TiO_2 surface via the amino group as shown in figure 4.16.

The structural analysis of Dye 13 has been done by FTIR spectrophotometer using KBr pellet, the main characteristic peaks were 3419 (OH stretch); 1774, 1727 (anhydride C=O stretch); 1653 (imides C=O stretch); 1592 (conjugated C=C stretch); 1351 (C-N stretch); 1116 (C-O-C stretch); 861 and 770 (C-H bend) cm^{-1} , the FT-IR spectra of dye 13 adsorbed on TiO_2 surface showed the disappearing of 1774, 1727 peaks (anhydride C=O stretch) and appearing of an additional band of carboxylate stretching at 1324 cm^{-1} which indicate the breaking of the anhydride bond and binding to the TiO_2 surface chemically. As well as the broadening of all the singles that are attributed to adsorption on the TiO_2 surface as shown in figure 4.17.

The structural analysis of Dye 14 has been done by FTIR spectrophotometer using KBr pellet, the main characteristic peaks were broad carboxylic O-H stretch at 3434 cm^{-1} , aromatic C-H at 3035 cm^{-1} , aliphatic C-H stretch at 2917 and 2852 cm^{-1} , carboxylic acid C=O stretchings at 1765 and 1732 cm^{-1} , imide (N-C=O) stretchings at 1696 cm^{-1} and 1657 cm^{-1} , conjugated C=C stretch at 1596 cm^{-1} , C-N stretch at 1318 cm^{-1} , aromatic C-H bend at 810 cm^{-1} and 739 cm^{-1} . The FT-IR spectra of dye 14 adsorbed on TiO_2 surface showed the disappearing of carboxylic acid C=O stretch at 1765 and 1732 cm^{-1} which indicate the binding to the TiO_2 through the

carboxylic acid group, as well as shifting of the correspond peaks of (COO^-) to lower wavenumbers as shown in figure 4.18.

The structural analysis of Dye 15 has been done by FTIR spectrophotometer using KBr pellet, the main characteristic peaks were 3443 cm^{-1} (N-H stretch), $3176, 3070\text{ cm}^{-1}$ (aromatic C-H stretch), $2929, 2858\text{ cm}^{-1}$ (aliphatic C-H stretch), 1696 and 1631 cm^{-1} (imide C=O stretch), 1583 cm^{-1} (aromatic C=C stretch), 1343 cm^{-1} (N-H stretch) and 855 and 768 cm^{-1} (aromatic C-H bending). The FT-IR spectra of dye 15 adsorbed on TiO_2 was also done as shown in figure 4.19.

5.13 UV-Vis Absorption Studies of Dyes 9-15

The solid state UV/Vis spectra of Dyes 9, 12 and 13 were shown in figures 4.41, 4.42 and 4.43, and they showed three characteristic peaks at (250, 374 and 396 nm) dye 9, (467, 498 and 540 nm) dye 12, and (477, 499 and 556 nm) dye 13. The absorption peaks lost their fine vibronic structure and appeared to be broader when adsorbed on the TiO_2 films.

A red shift was observed in the absorption spectra of dye 12 adsorbed on TiO_2 film figure 4.42 this is probably because of the electron withdrawing effect of the Ti^{4+} ions on binding of the dye to the TiO_2 surface, relative to the protonated carboxylate precursor [67].

A blue shift was observed in the absorption spectra of dyes 9 and 13 adsorbed on TiO_2 film figure 4.41 and 4.43 due to a decrease in the effective π -conjugation length [68]. In addition the blue shift in the absorption spectra of dye 13 is attributed to the ring opening of anhydride group on perylene which was confirmed by FT-IR to form two

carboxylates, providing interactions with the TiO_2 film and this effect is the same in all perylenes [48].

Chapter 6

CONCLUSION

In this project, one novel bay-substituted perylene bisanhydride (4) and two bay-substituted perylene bisimides (6 and 8) have been designed and synthesized successfully. A swallow tail type electron donating substituent, 2-decyl-1-tetradecanoyl was used in the structure of the novel compounds 4, 6 and 8 at the bay positions (1 and 7).

The final compounds were purified and characterized by FTIR, elemental analysis, ^1H NMR and ^{13}C NMR analysis UV-vis and Emission measurements. The electrochemical properties of the compounds were investigated by cyclic voltammetry (CV). The thermal stability of the compounds was studied by differential scanning calorimetry (DSC) and thermogravimetric analysis (TGA). For comparison, photophysical, electrochemical and thermal properties of the intermediate products were carried out in parallel.

All compounds showed high thermal stability which is important for industrial applications. Compounds 4, 6 and 8 have shown J-aggregated featureless, very broad absorbance through the UV-vis-NIR region.

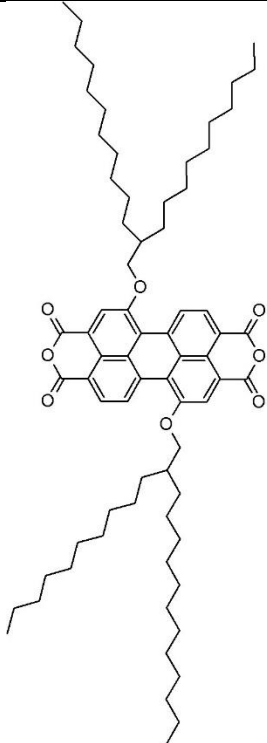
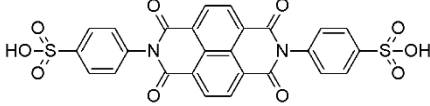
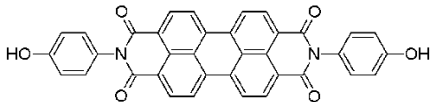
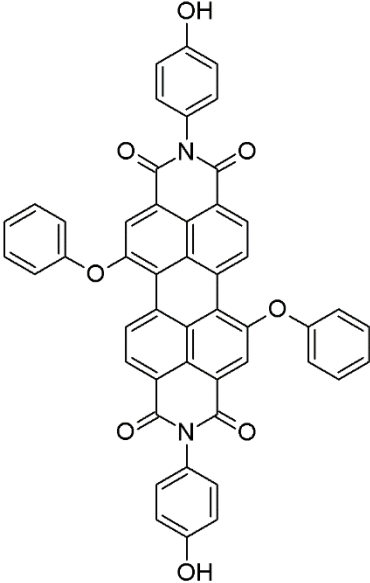
Strong fluorescence quenching attributed to intramolecular electron transfer from electron donor 2-decyl-1-tetradecanoyl substituent to PDI acceptor and scaffolds allow

π - π intermolecular interactions, inducing molecular aggregation. The particle aggregates average size should be less than 0.2 μm .

Interestingly, in their electrochemical studies the compounds 4, 6 and 8 have shown only a single and broad reversible reduction. Most probably, the oxidation step becomes easier therefore the two regular reduction steps of perylene bisimides become closer and finally overlapped. LUMO and HOMO energy levels of all compounds indicating that these are potentially suitable candidates for electron transport materials in photonic devices.

The DSSCs were prepared using different perylene diimide derivatives as sensitizers, the efficiencies of the solar cells related to dye structures, the absorption spectra of the dyes solution and dyes adsorbed onto transparent TiO_2 film, FT-IR for the dye molecules and (ATR-FT-IR) of the dyes adsorbed on the transparent TiO_2 film were measured and discussed within the previous chapters and their optoelectronic properties were summarized in Table 6.1.

Table 6.1: Structures and optoelectronic properties of dyes 9-15

| Dye | Structure | λ_{\max} nm | ϵ_{\max} L mol ⁻¹ cm ⁻¹ | V_{oc} V | I_{sc} mA cm ⁻² | $\eta\%$ $\times 10^{-2}$ |
|-----|---|------------------------|--|---------------|---------------------------------|------------------------------|
| 4 |  | 518 | 12500 | 0.23 | 0.03 | 4 |
| 9 |  | 380 | 13400 | 0.42 | 0.13 | 2 |
| 10 |  | 524 | 34400 | 0.30 | 0.14 | 1.3 |
| 11 |  | 495 | 20400 | 0.28 | 0.11 | 1 |

| | | | | | | |
|----|--|-----|-------|------|------|-----|
| 12 | | 526 | 65965 | 0.37 | 0.07 | 0.9 |
| 13 | | 518 | 71000 | 0.50 | 0.04 | 0.5 |
| 14 | | 523 | 17900 | 0.23 | 0.06 | 0.4 |
| 15 | | 377 | 33987 | 0.25 | 0.04 | 0.3 |

REFERENCES

- [1] M. T. Kibria, A. Ahammed, S. M. Sony, F. Hossain, and S. U. Islam, "A Review: Comparative studies on different generation solar cells technology," in *Proc. of 5th International Conference on Environmental Aspects of Bangladesh*, 2014, pp. 51–53.
- [2] P. C. Choubey, A. Oudhia, and R. Dewangan, "A review: Solar cell current scenario and future trends," *Recent Res. Sci. Technol.*, vol. 4, no. 8, 2012.
- [3] K. Kalyanasundaram, *Dye-sensitized solar cells*. CRC press, 2010.
- [4] M. Pakseresht, J. B. Bodapati, and H. Icil, "A new π -conjugated 1, 7-diphenoxy-perylene bisimide: synthesis, characterization, photophysical and electrochemical properties," *J. Photochem. Photobiol. A Chem.*, vol. 360, pp. 270–277, 2018.
- [5] S. Asir, C. Zanardi, R. Seeber, and H. Icil, "A novel unsymmetrically substituted chiral amphiphilic perylene diimide: Synthesis, photophysical and electrochemical properties both in solution and solid state," *J. Photochem. Photobiol. A Chem.*, vol. 318, pp. 104–113, 2016.
- [6] H. Icil, D. Uzun, and E. Arslan, "Synthesis and spectroscopic characterization of water soluble perylene tetracarboxylic diimide derivatives," *Spectrosc. Lett.*, vol. 34, no. 5, pp. 605–614, 2001.

- [7] H. Ahmed, “*Synthesis, characterization and spectroscopic properties of chiral perylene 3, 4-dicarboxylic-9, 10-((R)-(+)-1-Phenylethyl)-carboximide for solar cell applications,*” Eastern Mediterranean University (EMU)-Doğu Akdeniz Üniversitesi (DAÜ), 2013.
- [8] K. H. S. Mahmood, “*A Novel Naphthalene Polymer Based on the 1, 3, 5-Triazines,*” Eastern Mediterranean University EMU, 2015.
- [9] E. Kozma and M. Catellani, “Perylene diimides based materials for organic solar cells,” *Dye. Pigment.*, vol. 98, no. 1, pp. 160–179, 2013.
- [10] F. Würthner, V. Stepanenko, Z. Chen, C. R. Saha-Möller, N. Kocher, and D. Stalke, “Preparation and characterization of regioisomerically pure 1, 7-disubstituted perylene bisimide dyes,” *J. Org. Chem.*, vol. 69, no. 23, pp. 7933–7939, 2004.
- [11] C. Zafer *et al.*, “New perylene derivative dyes for dye-sensitized solar cells,” *Sol. energy Mater. Sol. cells*, vol. 91, no. 5, pp. 427–431, 2007.
- [12] P. R. Mohanta, J. Patel, J. Bhuvra, and M. Gandhi, “A Review on Solar Photovoltaics and Roof Top Application of It,” *Int. J. Adv. Res. Sci. Eng. Technol.*, vol. 2, pp. 2394–2444, 2015.
- [13] S. Sharma, K. K. Jain, A. Sharma, and others, “Solar cells: in research and applications—a review,” *Mater. Sci. Appl.*, vol. 6, no. 12, p. 1145, 2015.

- [14] A. Goetzberger, C. Hebling, and H.-W. Schock, "Photovoltaic materials, history, status and outlook," *Mater. Sci. Eng. R Reports*, vol. 40, no. 1, pp. 1–46, 2003.
- [15] O. A. Abdulrazzaq, V. Saini, S. Bourdo, E. Dervishi, and A. S. Biris, "Organic solar cells: a review of materials, limitations, and possibilities for improvement," *Part. Sci. Technol.*, vol. 31, no. 5, pp. 427–442, 2013.
- [16] T. L. Benanti and D. Venkataraman, "Organic solar cells: An overview focusing on active layer morphology," *Photosynth. Res.*, vol. 87, no. 1, pp. 73–81, 2006.
- [17] P. Peumans, A. Yakimov, and S. R. Forrest, "Small molecular weight organic thin-film photodetectors and solar cells," *J. Appl. Phys.*, vol. 93, no. 7, pp. 3693–3723, 2003.
- [18] S. Barth and H. Bässler, "Intrinsic photoconduction in PPV-type conjugated polymers," *Phys. Rev. Lett.*, vol. 79, no. 22, p. 4445, 1997.
- [19] D. Darwis, E. Sesa, D. Farhamza, and others, "The Fabrication of Bulk Heterojunction P3HT: PCBM Organic Photovoltaics," *MS&E*, vol. 367, no. 1, p. 12029, 2018.
- [20] A. Gaur and P. Kumar, "An improved circuit model for polymer solar cells," *Prog. Photovoltaics Res. Appl.*, vol. 22, no. 9, pp. 937–948, 2014.
- [21] A. J. Trindade and L. Pereira, "Bulk heterojunction organic solar cell area-

dependent parameter fluctuation,” *Int. J. Photoenergy*, vol. 2017, 2017.

- [22] B. Li, L. Wang, B. Kang, P. Wang, and Y. Qiu, “Review of recent progress in solid-state dye-sensitized solar cells,” *Sol. energy Mater. Sol. cells*, vol. 90, no. 5, pp. 549–573, 2006.
- [23] P. P. Kumavat, P. Sonar, and D. S. Dalal, “An overview on basics of organic and dye sensitized solar cells, their mechanism and recent improvements,” *Renew. Sustain. Energy Rev.*, vol. 78, pp. 1262–1287, 2017.
- [24] M. B. Cosar, “The development of bifacial dye sensitized solar cells based on binary ionic liquid electrolyte,” M Sc Thesis, Middle East Technical University, 2013.
- [25] Y. Zhou, M. Eck, and M. Krüger, “Organic-inorganic hybrid solar cells: state of the art, challenges and perspectives,” *Sol. Cells-New Asp. Solut.*, pp. 95–120, 2011.
- [26] D. Aldakov, F. Chandezon, R. De Bettignies, M. Firon, P. Reiss, and A. Pron, “Hybrid organic-inorganic nanomaterials: ligand effects,” *Eur. Phys. J. Appl. Phys.*, vol. 36, no. 3, pp. 261–265, 2006.
- [27] W. S. Yang *et al.*, “High-performance photovoltaic perovskite layers fabricated through intramolecular exchange,” *Science (80-.)*, vol. 348, no. 6240, pp. 1234–1237, 2015.

- [28] S. Pitchaiya *et al.*, “A review on the classification of organic/inorganic/carbonaceous hole transporting materials for perovskite solar cell application,” *Arab. J. Chem.*, vol. 13, no. 1, pp. 2526–2557, 2020.
- [29] W.-W. Liu, T.-H. Wu, M.-C. Liu, W.-J. Niu, and Y.-L. Chueh, “Recent Challenges in Perovskite Solar Cells Toward Enhanced Stability, Less Toxicity, and Large-Area Mass Production,” *Adv. Mater. Interfaces*, vol. 6, no. 9, p. 1801758, 2019.
- [30] M. R. Narayan, “Dye sensitized solar cells based on natural photosensitizers,” *Renew. Sustain. Energy Rev.*, vol. 16, no. 1, pp. 208–215, 2012.
- [31] T. Kawashima, T. Ezure, K. Okada, H. Matsui, K. Goto, and N. Tanabe, “FTO/ITO double-layered transparent conductive oxide for dye-sensitized solar cells,” *J. Photochem. Photobiol. A Chem.*, vol. 164, no. 1–3, pp. 199–202, 2004.
- [32] C. Sima, C. Grigoriu, and S. Antohe, “Comparison of the dye-sensitized solar cells performances based on transparent conductive ITO and FTO,” *Thin Solid Films*, vol. 519, no. 2, pp. 595–597, 2010.
- [33] N. N. Bwana, “Comparison of the performances of dye-sensitized solar cells based on different TiO₂ electrode nanostructures,” *J. Nanoparticle Res.*, vol. 11, no. 8, p. 1917, 2009.
- [34] M. Grätzel, “Conversion of sunlight to electric power by nanocrystalline dye-sensitized solar cells,” *J. Photochem. Photobiol. A Chem.*, vol. 164, no. 1–3, pp.

3–14, 2004.

- [35] B. Ohtani, O. O. Prieto-Mahaney, D. Li, and R. Abe, “What is Degussa (Evonik) P25? Crystalline composition analysis, reconstruction from isolated pure particles and photocatalytic activity test,” *J. Photochem. Photobiol. A Chem.*, vol. 216, no. 2–3, pp. 179–182, 2010.
- [36] P. Wang, S. M. Zakeeruddin, P. Comte, R. Charvet, R. Humphry-Baker, and M. Grätzel, “Enhance the performance of dye-sensitized solar cells by co-grafting amphiphilic sensitizer and hexadecylmalonic acid on TiO₂ nanocrystals,” *J. Phys. Chem. B*, vol. 107, no. 51, pp. 14336–14341, 2003.
- [37] T. Marinado, “Photoelectrochemical studies of dye-sensitized solar cells using organic dyes,” KTH, 2009.
- [38] S. Nakade *et al.*, “Enhancement of electron transport in nano-porous TiO₂ electrodes by dye adsorption,” *Electrochem. commun.*, vol. 5, no. 9, pp. 804–808, 2003.
- [39] F.-T. Kong, S.-Y. Dai, and K.-J. Wang, “Review of recent progress in dye-sensitized solar cells,” *Adv. Optoelectron.*, vol. 2007, 2007.
- [40] M. K. Nazeeruddin *et al.*, “Stepwise assembly of amphiphilic ruthenium sensitizers and their applications in dye-sensitized solar cell,” *Coord. Chem. Rev.*, vol. 248, no. 13–14, pp. 1317–1328, 2004.

- [41] M. Grätzel, "Solar energy conversion by dye-sensitized photovoltaic cells," *Inorg. Chem.*, vol. 44, no. 20, pp. 6841–6851, 2005.
- [42] A. Mishra, M. K. R. Fischer, and P. Bäuerle, "Metal-free organic dyes for dye-sensitized solar cells: From structure: Property relationships to design rules," *Angew. Chemie Int. Ed.*, vol. 48, no. 14, pp. 2474–2499, 2009.
- [43] Y. Numata, I. Ashraful, Y. Shirai, and L. Han, "Preparation of donor--acceptor type organic dyes bearing various electron-withdrawing groups for dye-sensitized solar cell application," *Chem. Commun.*, vol. 47, no. 21, pp. 6159–6161, 2011.
- [44] T. Kitamura *et al.*, "Phenyl-conjugated oligoene sensitizers for TiO₂ solar cells," *Chem. Mater.*, vol. 16, no. 9, pp. 1806–1812, 2004.
- [45] Z.-S. Wang, Y. Cui, Y. Dan-oh, C. Kasada, A. Shinpo, and K. Hara, "Thiophene-functionalized coumarin dye for efficient dye-sensitized solar cells: electron lifetime improved by coadsorption of deoxycholic acid," *J. Phys. Chem. C*, vol. 111, no. 19, pp. 7224–7230, 2007.
- [46] N. Koumura, Z.-S. Wang, S. Mori, M. Miyashita, E. Suzuki, and K. Hara, "Alkyl-functionalized organic dyes for efficient molecular photovoltaics," *J. Am. Chem. Soc.*, vol. 128, no. 44, pp. 14256–14257, 2006.
- [47] S. Hwang *et al.*, "A highly efficient organic sensitizer for dye-sensitized solar cells," *Chem. Commun.*, no. 46, pp. 4887–4889, 2007.

- [48] T. Edvinsson *et al.*, “Intramolecular charge-transfer tuning of perylenes: spectroscopic features and performance in dye-sensitized solar cells,” *J. Phys. Chem. C*, vol. 111, no. 42, pp. 15137–15140, 2007.
- [49] C. Li *et al.*, “An improved perylene sensitizer for solar cell applications,” *ChemSusChem*, vol. 1, no. 7, pp. 615–618, 2008.
- [50] Y. Shibano, T. Umeyama, Y. Matano, and H. Imahori, “Electron-donating perylene tetracarboxylic acids for dye-sensitized solar cells,” *Org. Lett.*, vol. 9, no. 10, pp. 1971–1974, 2007.
- [51] F. Gao *et al.*, “Enhance the optical absorptivity of nanocrystalline TiO₂ film with high molar extinction coefficient ruthenium sensitizers for high performance dye-sensitized solar cells,” *J. Am. Chem. Soc.*, vol. 130, no. 32, pp. 10720–10728, 2008.
- [52] J. Wu *et al.*, “Electrolytes in dye-sensitized solar cells,” *Chem. Rev.*, vol. 115, no. 5, pp. 2136–2173, 2015.
- [53] A. Kay and M. Grätzel, “Low cost photovoltaic modules based on dye sensitized nanocrystalline titanium dioxide and carbon powder,” *Sol. Energy Mater. Sol. Cells*, vol. 44, no. 1, pp. 99–117, 1996.
- [54] P. Wang, C. Klein, R. Humphry-Baker, S. M. Zakeeruddin, and M. Grätzel, “Stable \geq 8% efficient nanocrystalline dye-sensitized solar cell based on an electrolyte of low volatility,” *Appl. Phys. Lett.*, vol. 86, no. 12, p. 123508, 2005.

- [55] A. Hauch and A. Georg, "Diffusion in the electrolyte and charge-transfer reaction at the platinum electrode in dye-sensitized solar cells," *Electrochim. Acta*, vol. 46, no. 22, pp. 3457–3466, 2001.
- [56] N. Papageorgiou, W. F. Maier, and M. Grätzel, "An iodine/triiodide reduction electrocatalyst for aqueous and organic media," *J. Electrochem. Soc.*, vol. 144, no. 3, p. 876, 1997.
- [57] A. Olea, G. Ponce, and P. J. Sebastian, "Electron transfer via organic dyes for solar conversion," *Sol. Energy Mater. Sol. Cells*, vol. 59, no. 1–2, pp. 137–143, 1999.
- [58] A. Listorti, B. O'regan, and J. R. Durrant, "Electron transfer dynamics in dye-sensitized solar cells," *Chem. Mater.*, vol. 23, no. 15, pp. 3381–3399, 2011.
- [59] V. Kamm *et al.*, "Organic Solar Cells: Polythiophene: Perylene Diimide Solar Cells--the Impact of Alkyl-Substitution on the Photovoltaic Performance (Adv. Energy Mater. 2/2011)," *Adv. Energy Mater.*, vol. 1, no. 2, p. 137, 2011.
- [60] A. Nowak-Król and F. Würthner, "Progress in the synthesis of perylene bisimide dyes," *Org. Chem. Front.*, vol. 6, no. 8, pp. 1272–1318, 2019.
- [61] B. Al-Khateeb *et al.*, "Swallow tail bay-substituted novel perylene bisimides: Synthesis, characterization, photophysical and electrochemical properties and DFT studies," *J. Photochem. Photobiol. A Chem.*, vol. 393, p. 112432, 2020.

- [62] H. Tian, T. Xu, Y. Zhao, and K. Chen, "Two-path photo-induced electron transfer in naphthalimide-based model compound," *J. Chem. Soc. Perkin Trans.* 2, no. 3, pp. 545–550, 1999.
- [63] E. Yenel, "*Sepiyolit temelli iskelet yapısına sahip yüksek verimli yeni nesil perovskit güneş hücrelerinin üretimi*," Selçuk Üniversitesi Fen Bilimleri Enstitüsü, 2018.
- [64] M. K. Nazeeruddin *et al.*, "Conversion of light to electricity by cis-X₂bis (2, 2'-bipyridyl-4, 4'-dicarboxylate) ruthenium (II) charge-transfer sensitizers (X= Cl-, Br-, I-, CN-, and SCN-) on nanocrystalline titanium dioxide electrodes," *J. Am. Chem. Soc.*, vol. 115, no. 14, pp. 6382–6390, 1993.
- [65] C. Noumising Sao, "*Dye-sensitized solar cells based on perylene derivatives*," 2009.
- [66] A. T. R. Williams, S. A. Winfield, and J. N. Miller, "Relative fluorescence quantum yields using a computer-controlled luminescence spectrometer," *Analyst*, vol. 108, no. 1290, pp. 1067–1071, 1983.
- [67] C. Sahin, C. Varlikli, C. Zafer, Q. Shi, and R. E. Douthwaite, "A new 1 H-pyridin-(2E)-ylidene ruthenium complex as sensitizer for a dye-sensitized solar cell," *J. Coord. Chem.*, vol. 66, no. 8, pp. 1384–1395, 2013.
- [68] U. Cappel, "*Characterisation of organic dyes for solid state dye-sensitized solar cells*," Acta Universitatis Upsaliensis, 2011.